WDM and Galaxy Formation

N. Menci
Osservatorio Astronomico di Roma - INAF

Outline

“Ab Initio” Galaxy Formation in DM dominated Universe
- Power Spectrum
- Free Streaming Scale
- Connecting baryon physics to DM haloes: semi-analytic models

Galaxy Formation in Cold Dark Matter:
- Basic properties
- The small-scale crisis: Galaxies
- Feedback scale
- Is baryon physics a solution ?

Galaxy Formation in Warm Dark Matter scenarios
- Galaxy and AGN luminosity functions
- The luminosity function of satellites
- Hints from abundance matching: the V_{max}-M_* relation
- The star formation properties of satellites

Limits to Warm Dark Matter candidate mass
- High-redhsift galaxy counts
- Luminosity function of ultra-faint galaxies at z=2
- Dwarf galaxies in clusters down to M_{UV}=-10

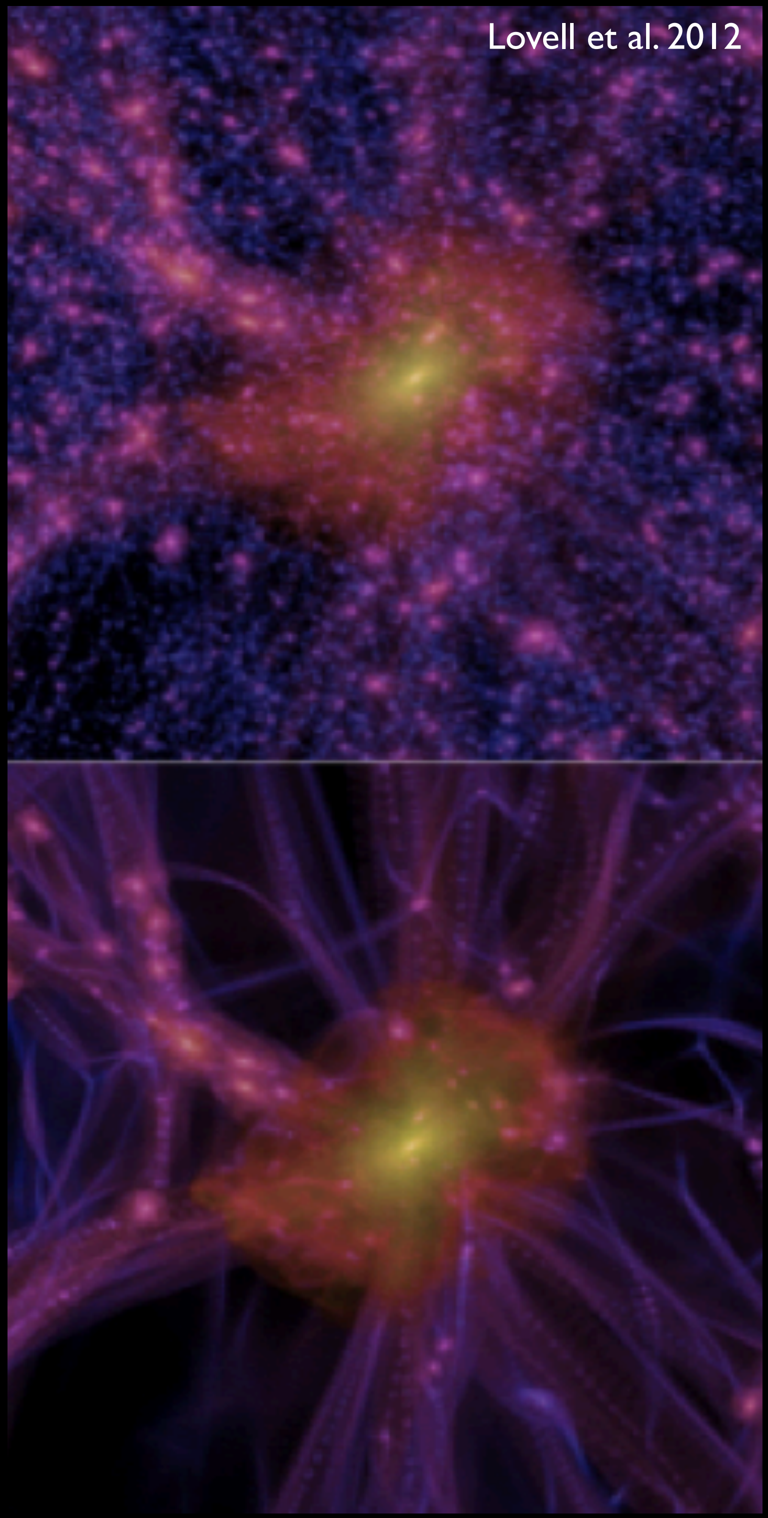

Cosmic Structures form from the collapse of overdense regions in the DM primordial density field, and grow by gravitational instability

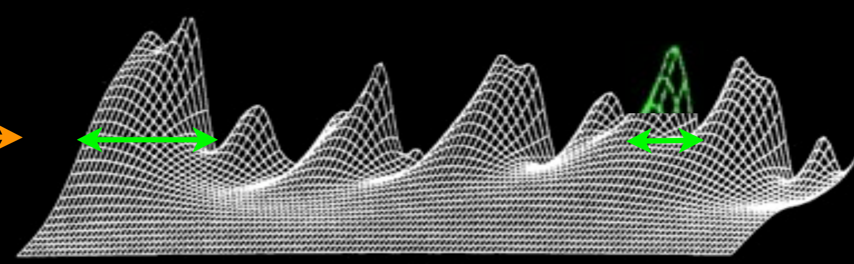

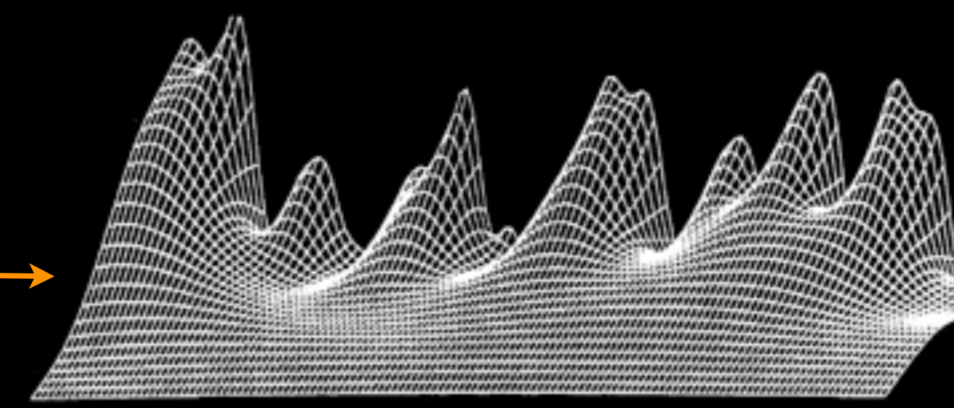

R=2π/k

$$M = \frac{4\pi}{3}\rho R^3$$

$$\langle \delta_M^2 \rangle = \sigma^2(M)\, g(t)$$

Gaussian Random field

$$\delta = \frac{\delta\rho}{\rho}$$

$$p(\delta_k) = \frac{1}{\sqrt{2\pi}\,\sigma_k}\, e^{-\frac{\delta_k^2}{2\sigma_k^2}}$$

Mean (square) value of perturbations of size R(~1/k) enclosing a mass M

$$P(k) = \frac{1}{V}\langle|\delta_k|^2\rangle$$

$$\sigma_M^2 = \frac{1}{(2\pi)^3 V}\int^{M\leftrightarrow k} dk\, k^2\, P(k)$$

$$\sigma_M^2 \leftrightarrow P(k)$$

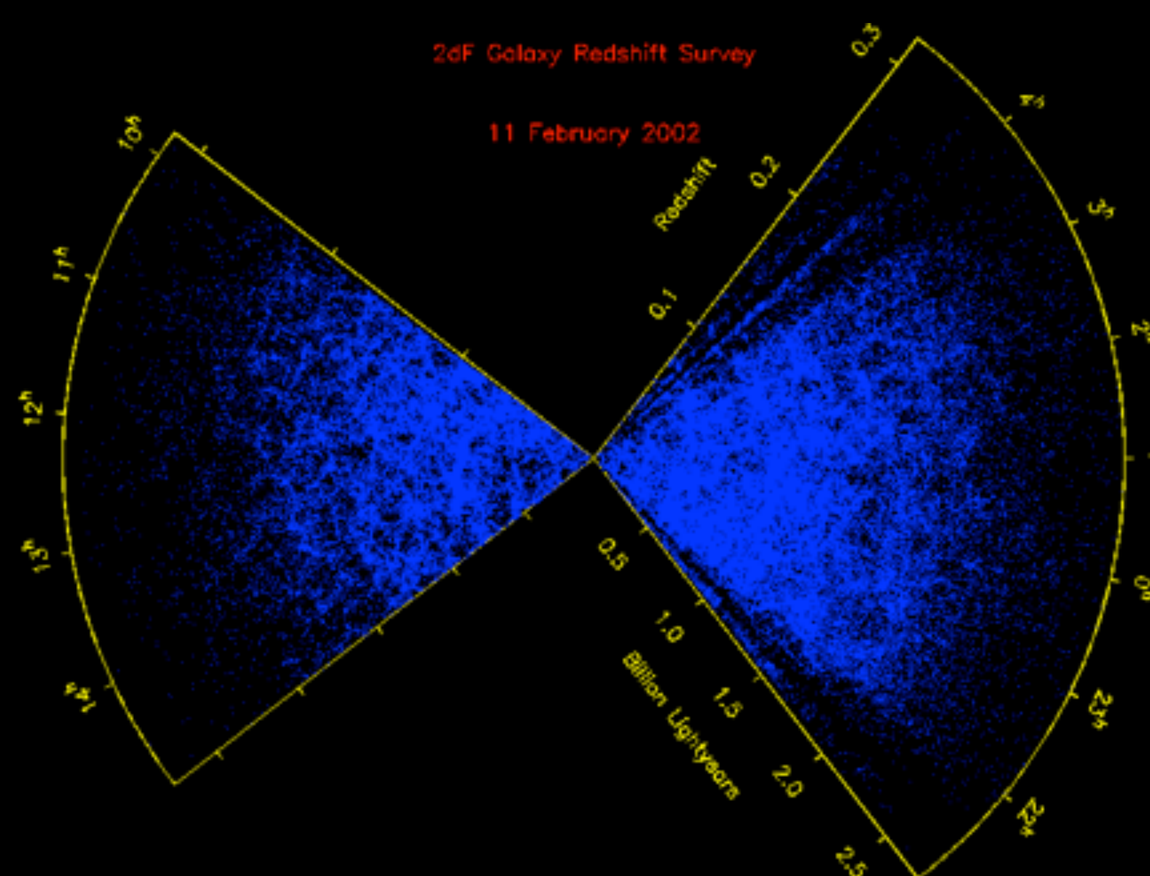

Cosmic Structures form from the collapse of overdense regions in the DM primordial density field, and grow by gravitational instability

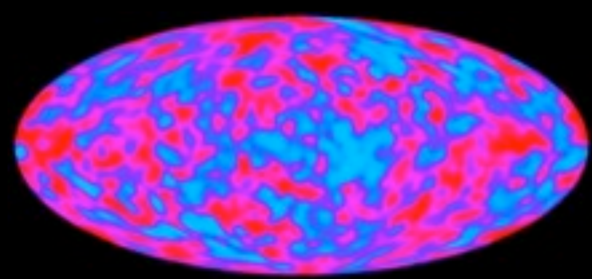

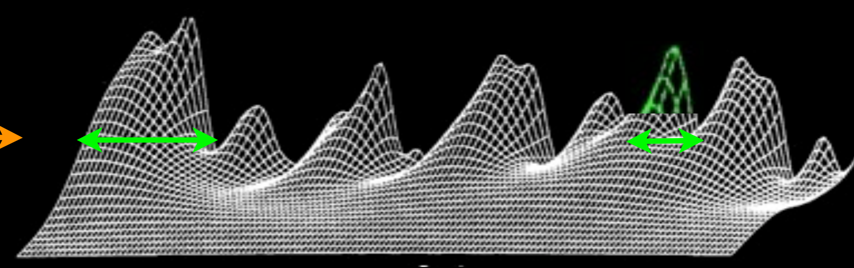

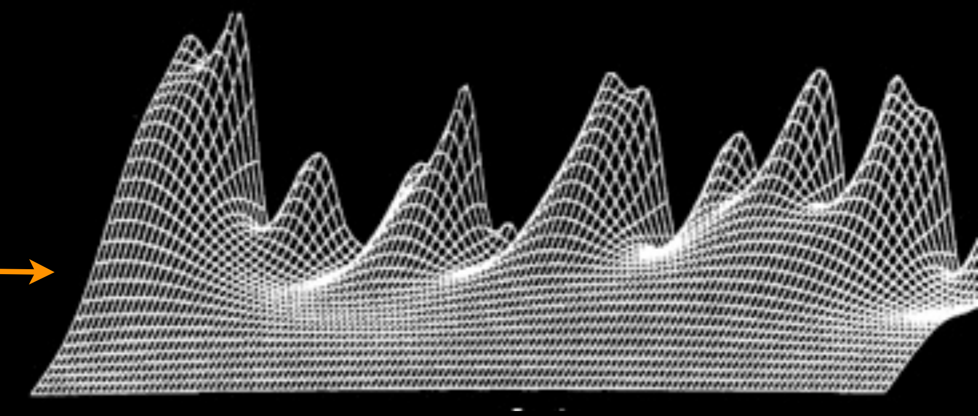

R=2π/k

$$M = \frac{4\,\pi}{3}\,\rho\,R^3$$

$$\langle \delta_M^2 \rangle = \sigma^2(M)\,g(t)$$

Gaussian Random field

$$\delta = \frac{\delta\rho}{\rho}$$

$$p(\delta_k) = \frac{1}{\sqrt{2\pi}\,\sigma_k}\,e^{-\frac{\delta_k^2}{2\,\sigma_k^2}}$$

Mean (square) value of perturbations of size R(~1/k) enclosing a mass M

$$P(k) = \frac{1}{V}\,\langle|\delta_k|^2\rangle$$

$$\sigma_M^2 = \frac{1}{(2\pi)^3\,V}\int^{M\leftrightarrow k} dk\,k^2\,P(k)$$

$$\sigma_M^2 \leftrightarrow P(k)$$

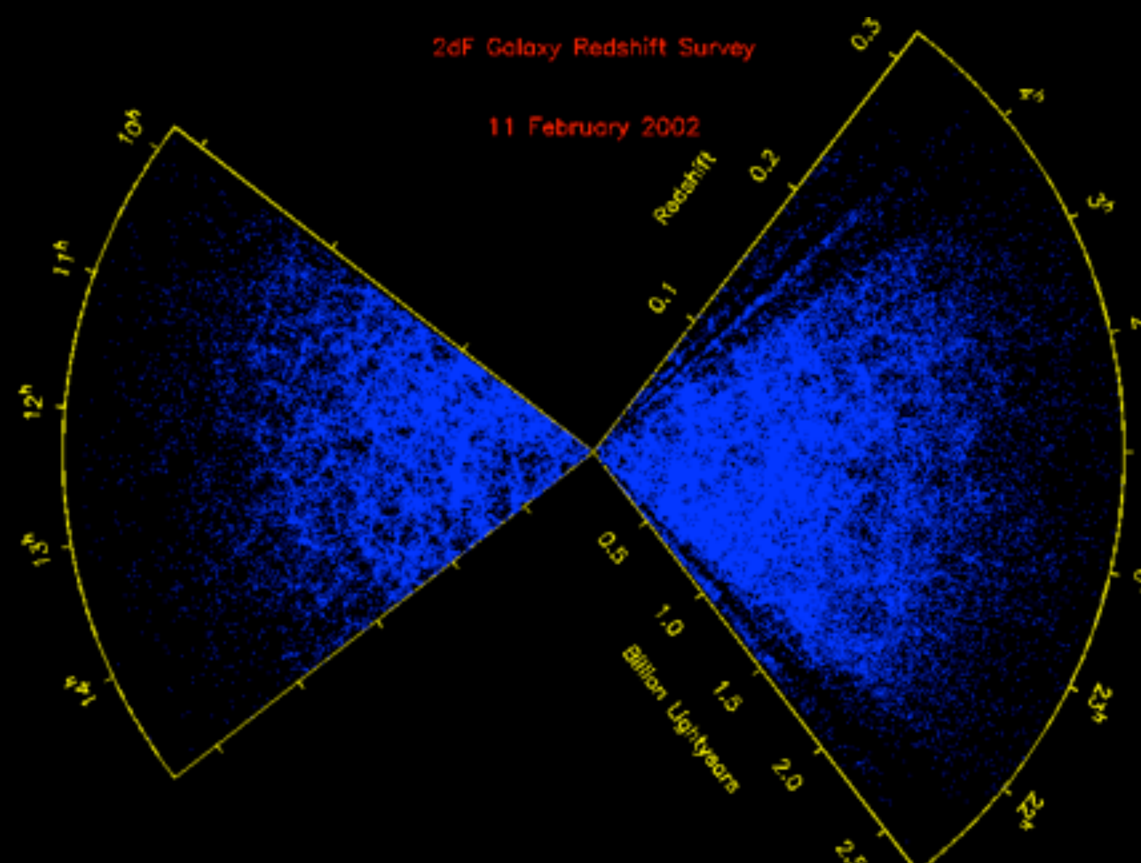

The Variance of the perturbation field

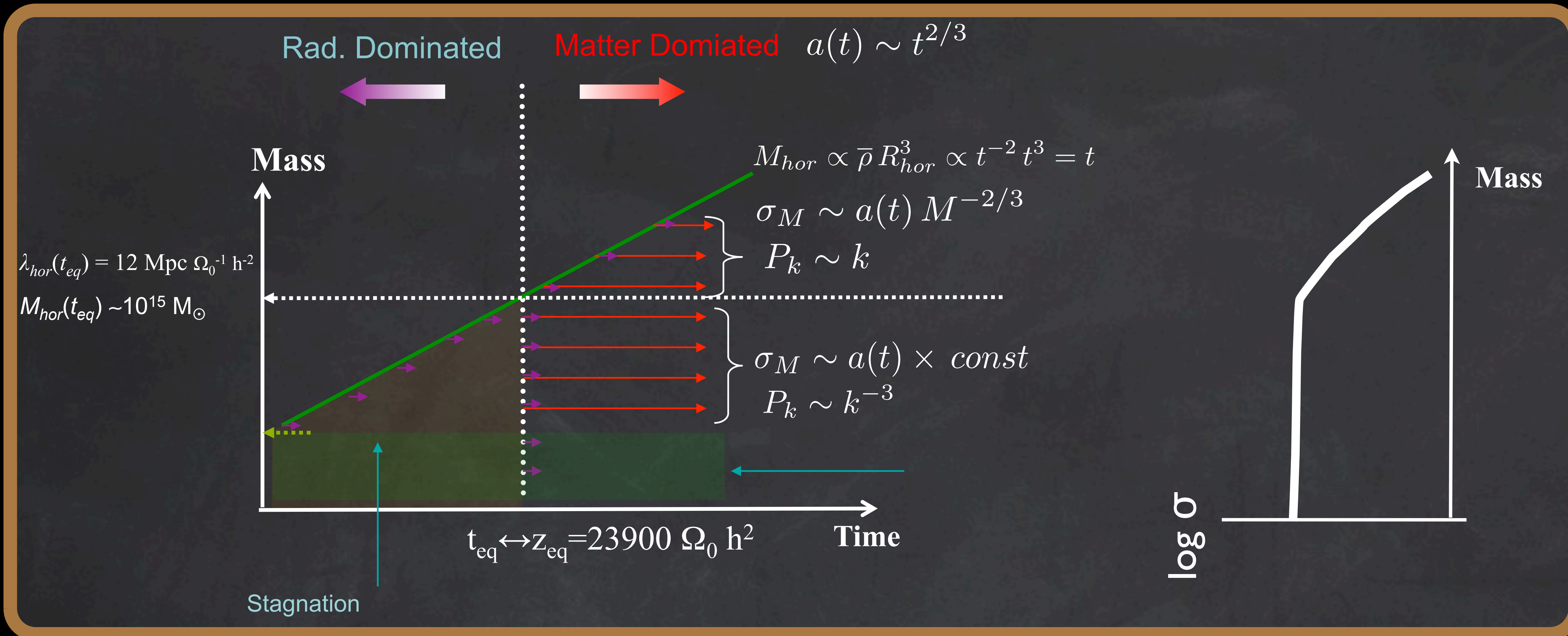

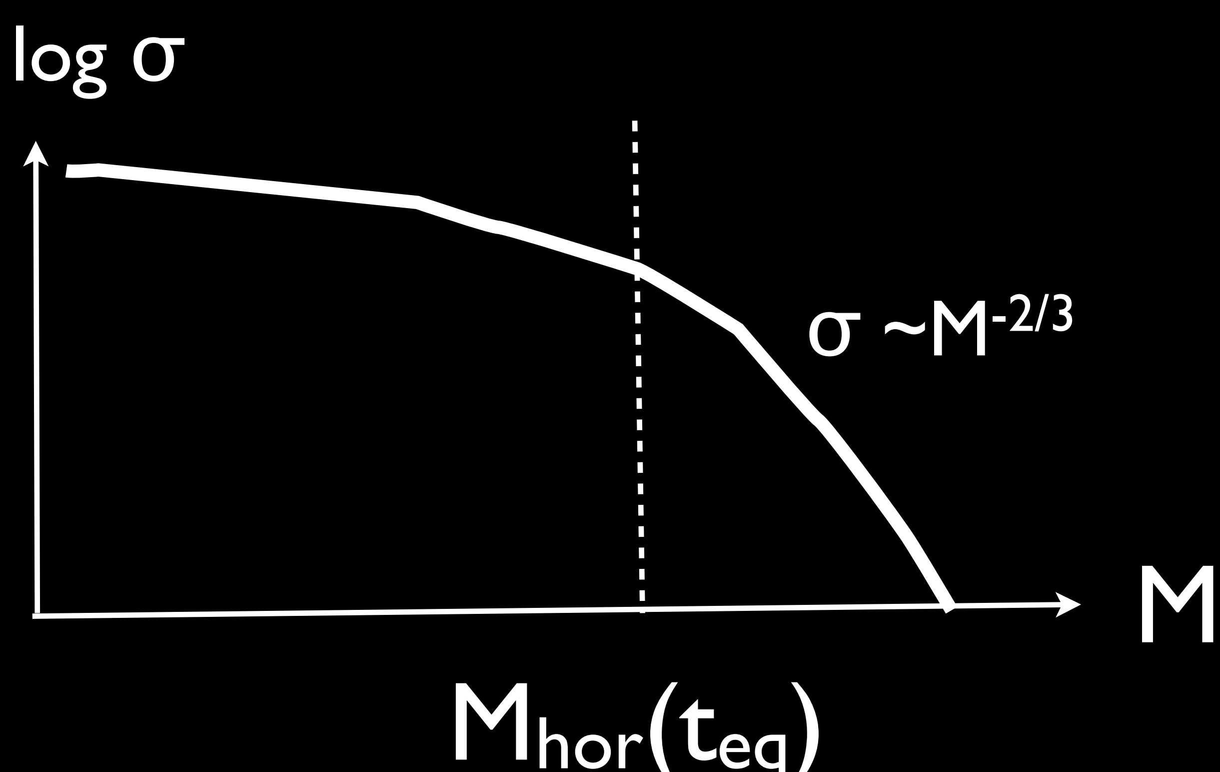

Perturbations involving scales larger than that of the horizon at the equivalence start to grow later

$R_{hor}=2c\ t_{hor}=13\ h^{-2}$ Mpc
=110 Mpc for $\sigma_0=0.3$ $h=0.7$

In terms of wavenumber k→Power Spectrum

$$\sigma_M^2 = \frac{1}{(2\pi)^3 V}\int^{M\leftrightarrow k} dk\, k^2\, P(k)$$

$$P(k) = \langle|\delta_k|^2\rangle$$

$$\sigma_M \propto M^{-2/3} \qquad P(k) \propto k$$

$$\sigma_M = const \qquad P(k) \propto k^{-3}$$

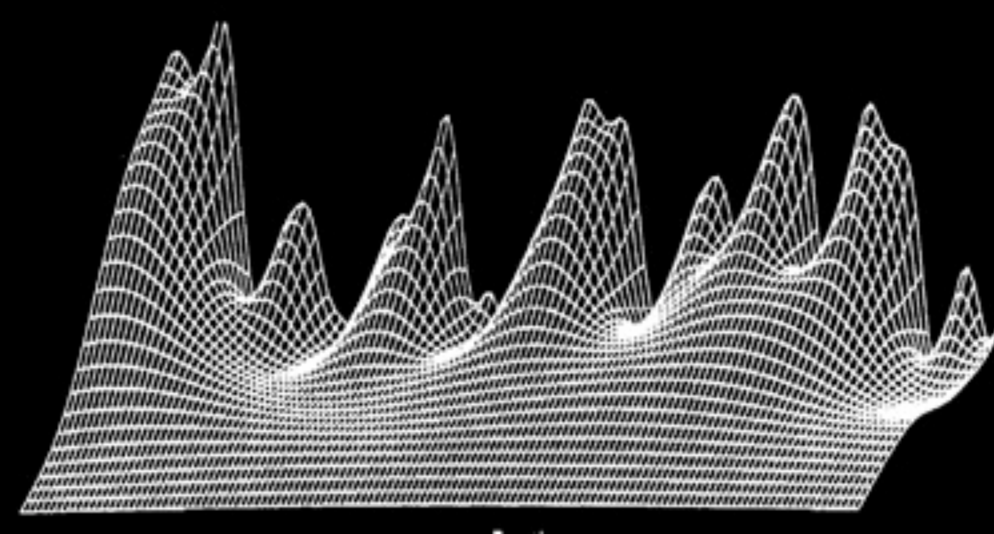

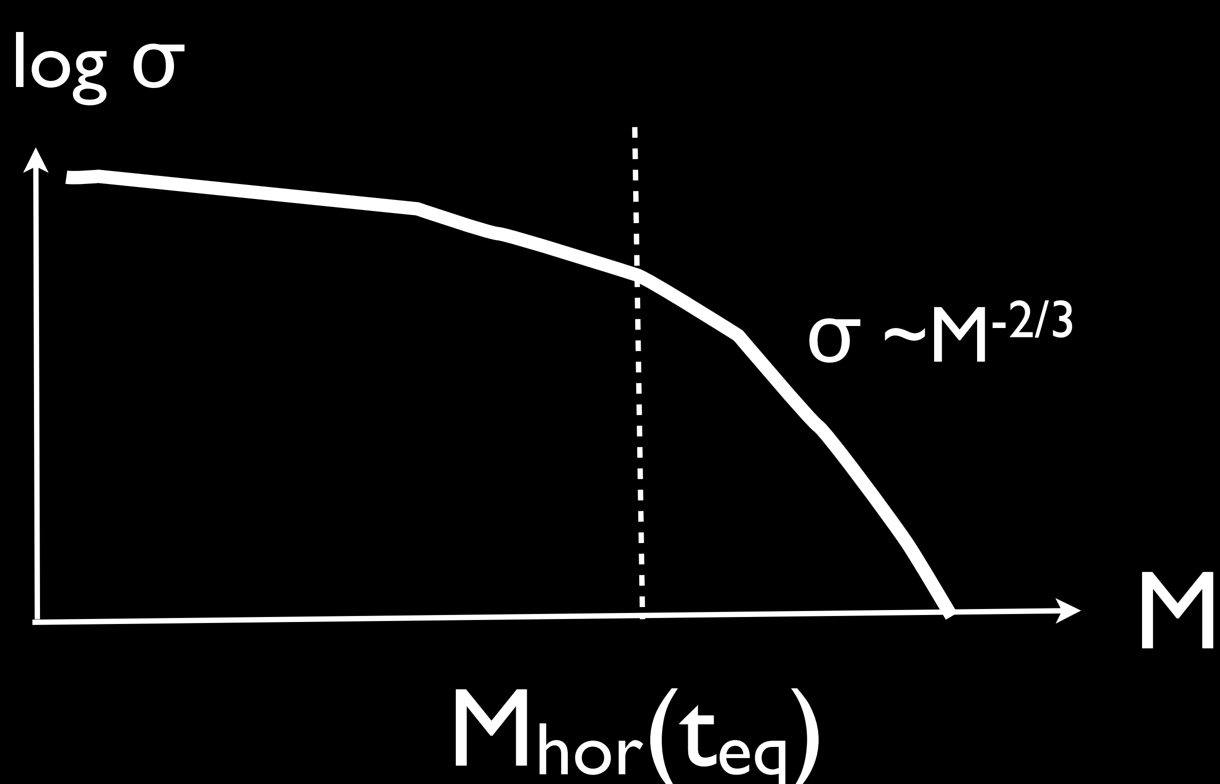

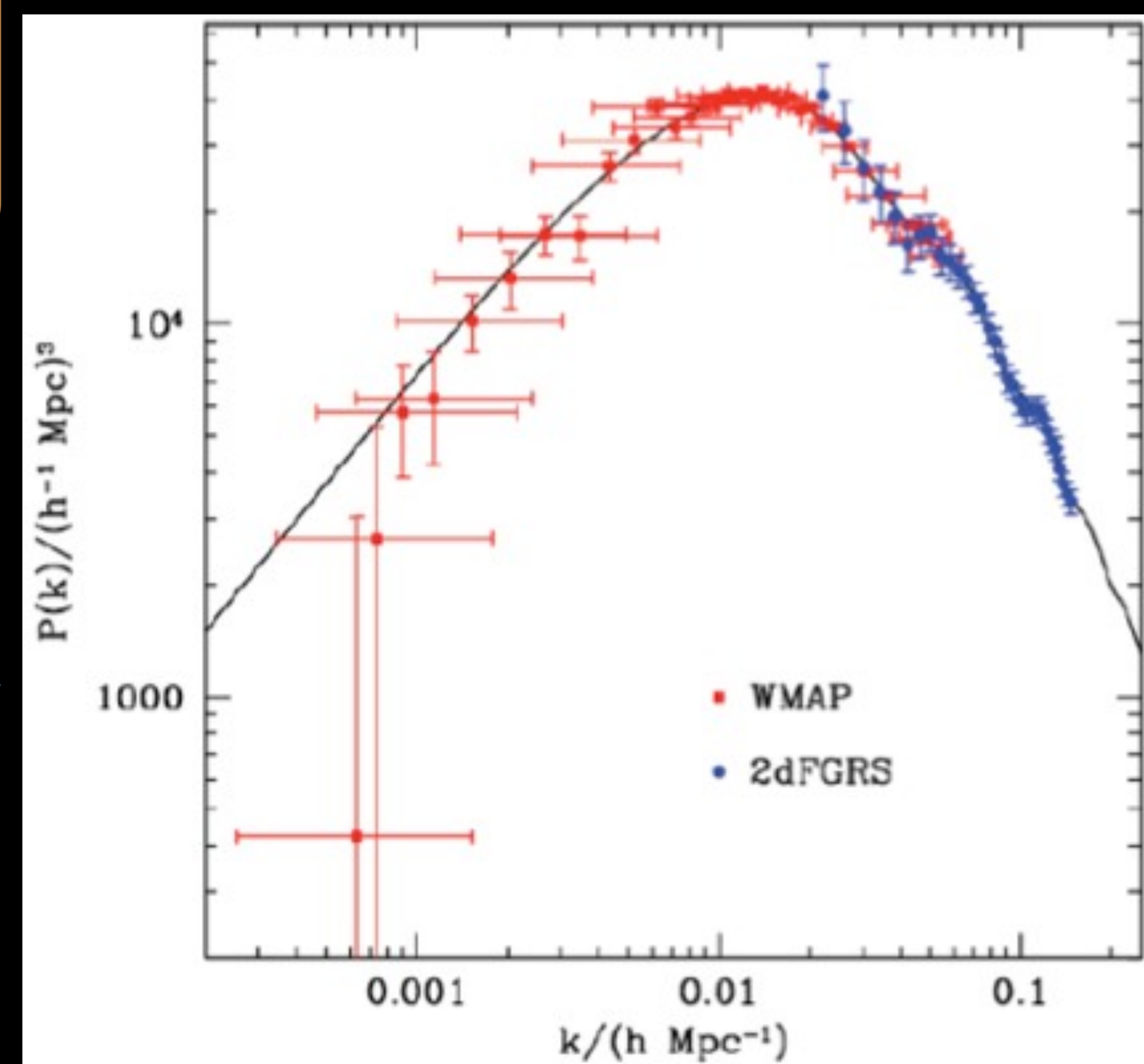

Dissipation, free-streaming scale

$$r_{fs} = \int_0^t \frac{v(t)}{R(t)}$$

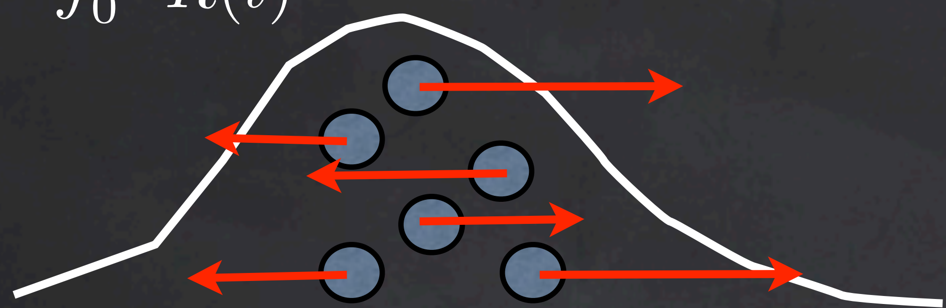

$$\sigma_\chi \propto a^{-1}\, m_\chi^{-1/2}$$

$$M_{fs} = 4 \times 10^{15} \left(\frac{m_\nu}{30\ \mathrm{eV}}\right)^{-2} M_\odot$$

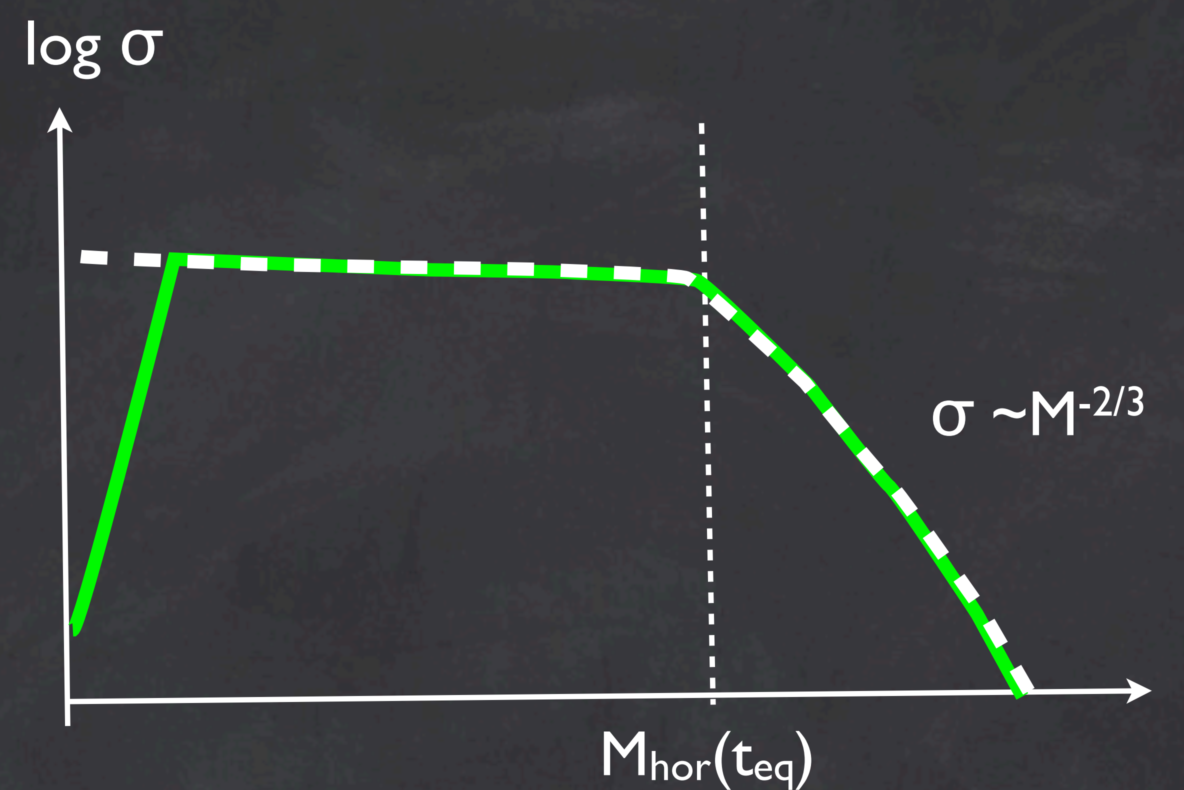

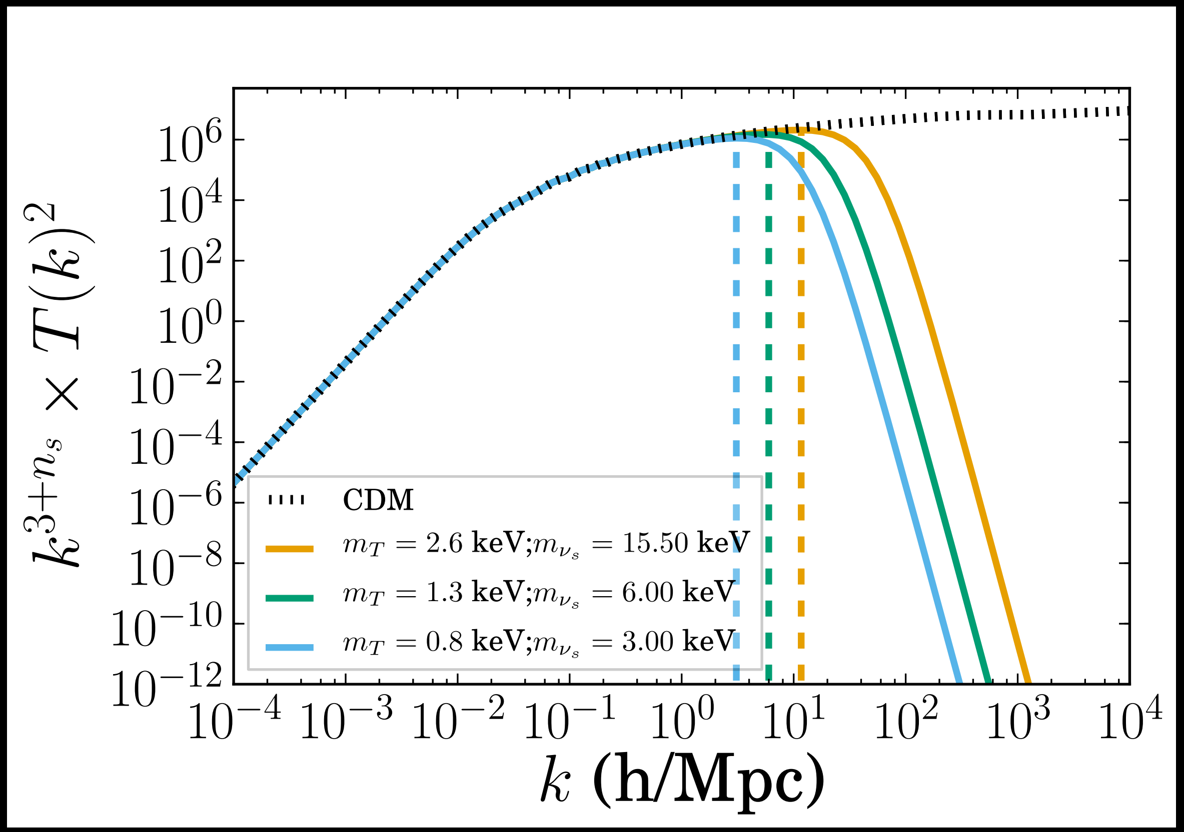

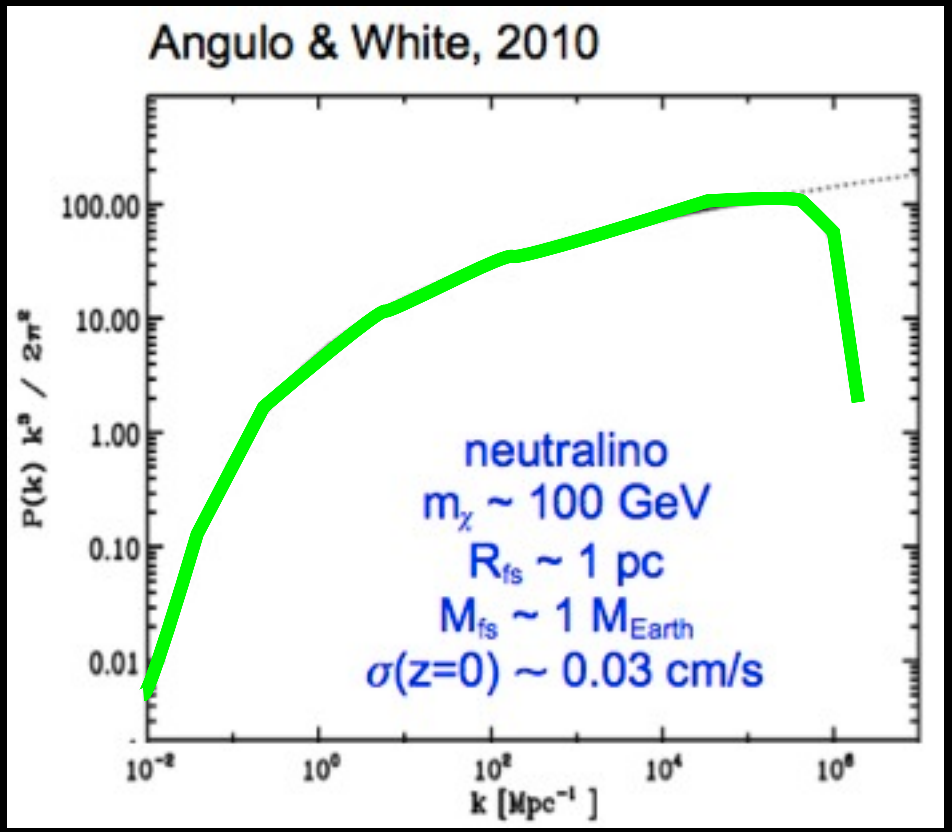

Dissipation, free-streaming scale

$$r_{fs} = \int_0^t \frac{v(t)}{R(t)}$$

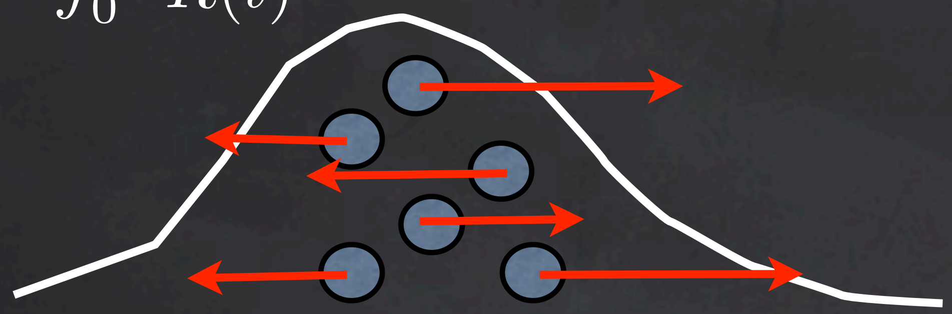

$$\sigma_\chi \propto a^{-1}\, m_\chi^{-1/2}$$

$$M_{fs} = 4 \times 10^{15} \left(\frac{m_\nu}{30\ \text{eV}} \right)^{-2} M_\odot$$

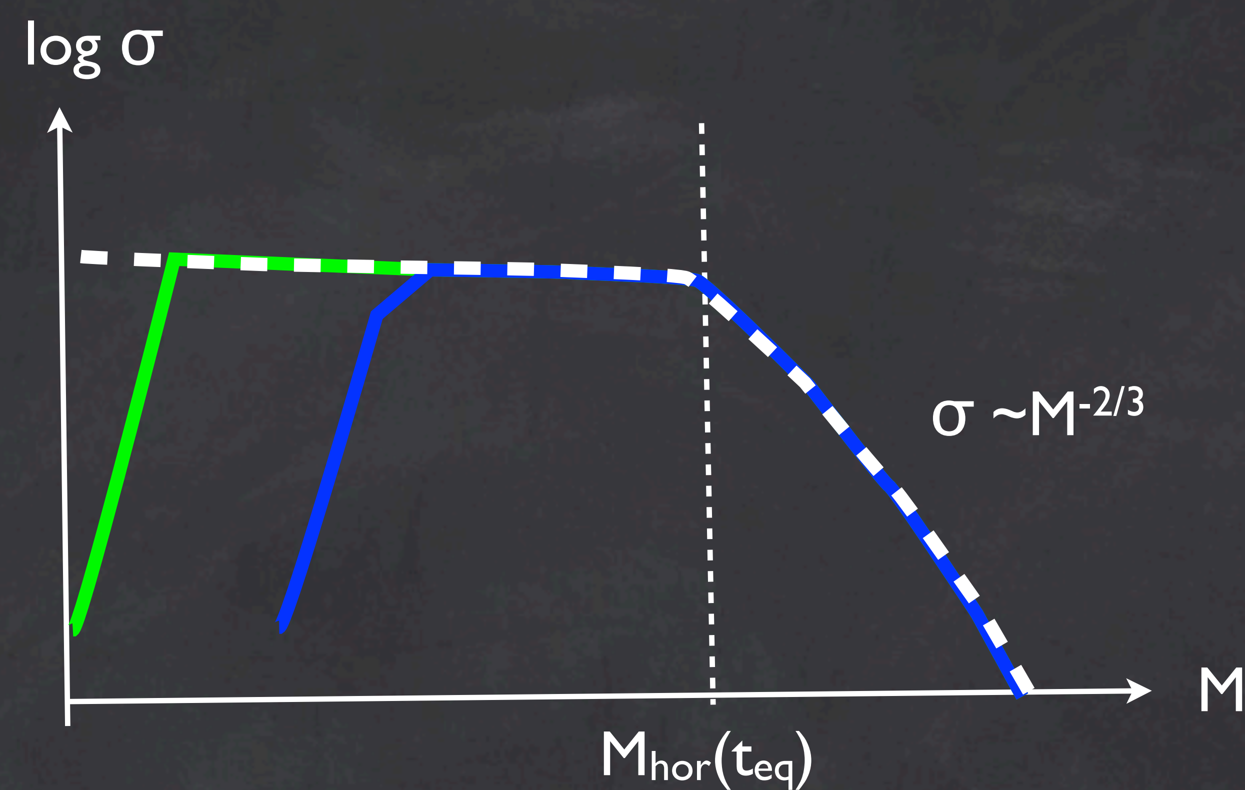

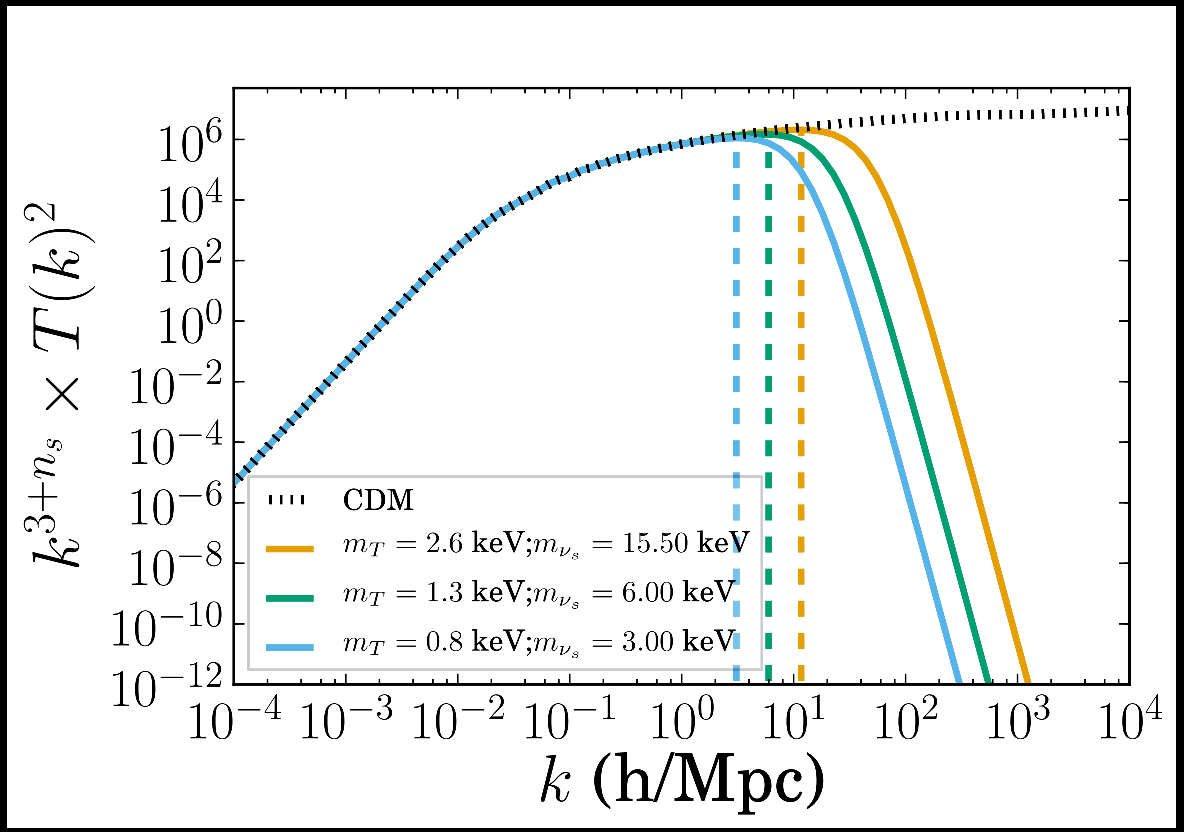

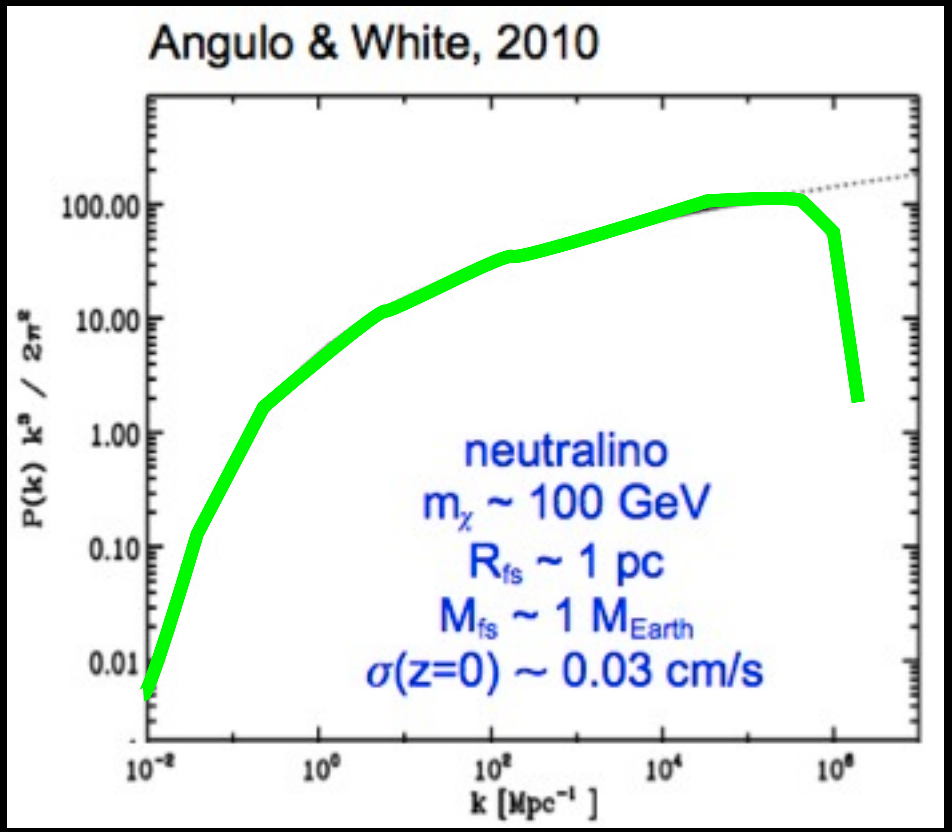

Varying the particle mass

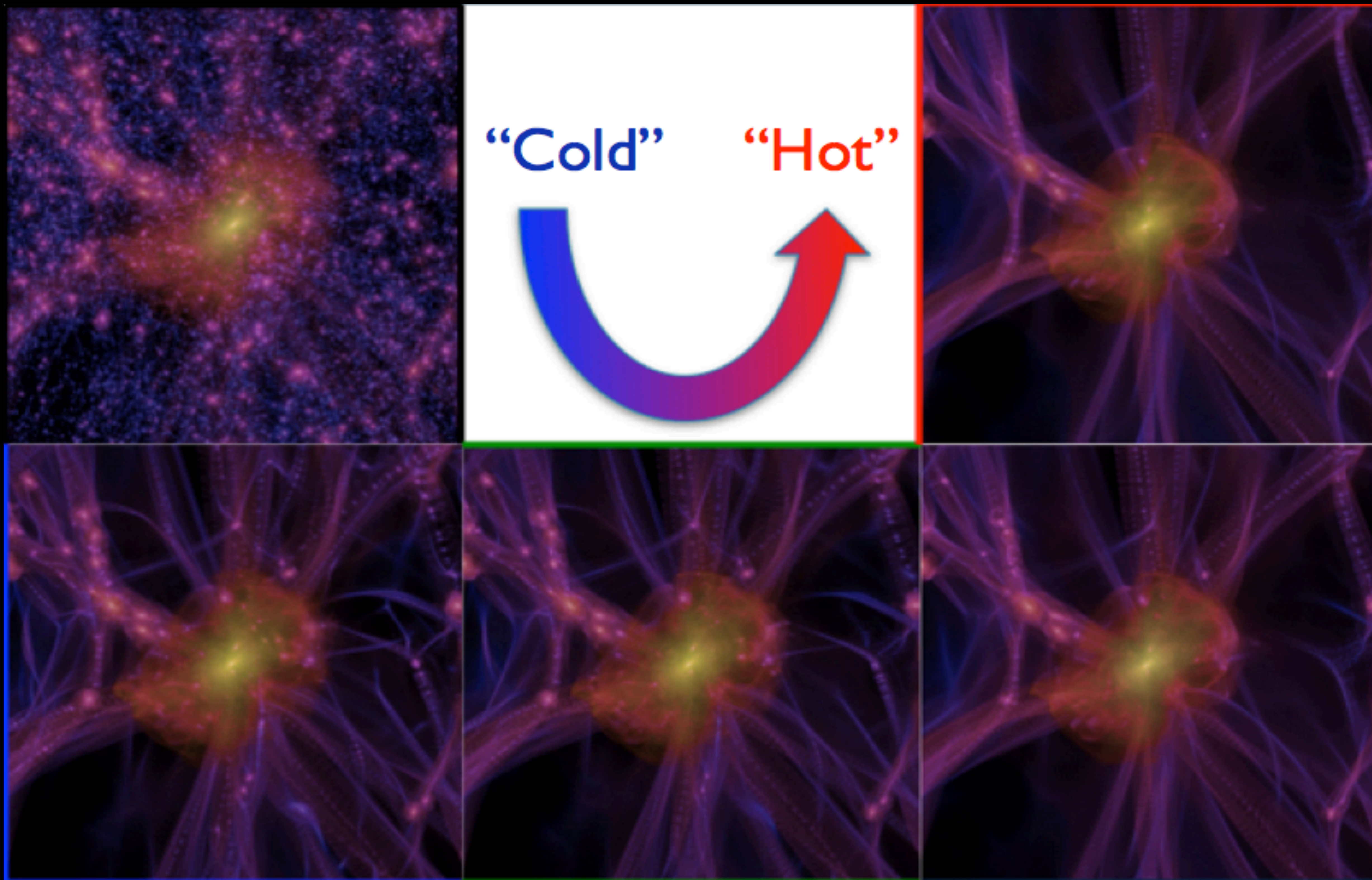

Lovell et al. 2012

Testing the DARK MATTER scenarios against observations: the evolution of galaxies

Requires modelling of baryon physics inside evolving DM potential wells

- gas physis (cooling, heating)
- disk formation
- star formation
- evolution of the stellar population
- injection of energy into the gas
  from SNae

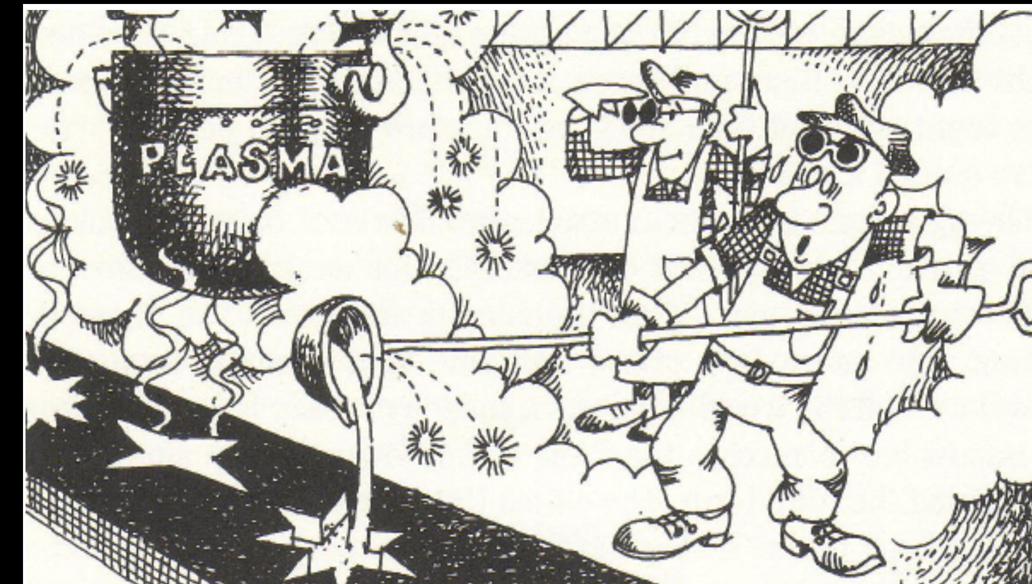

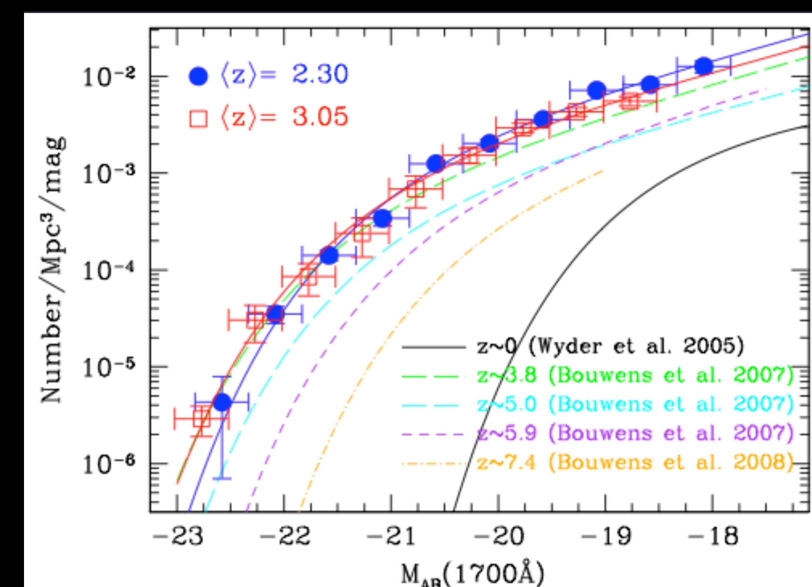

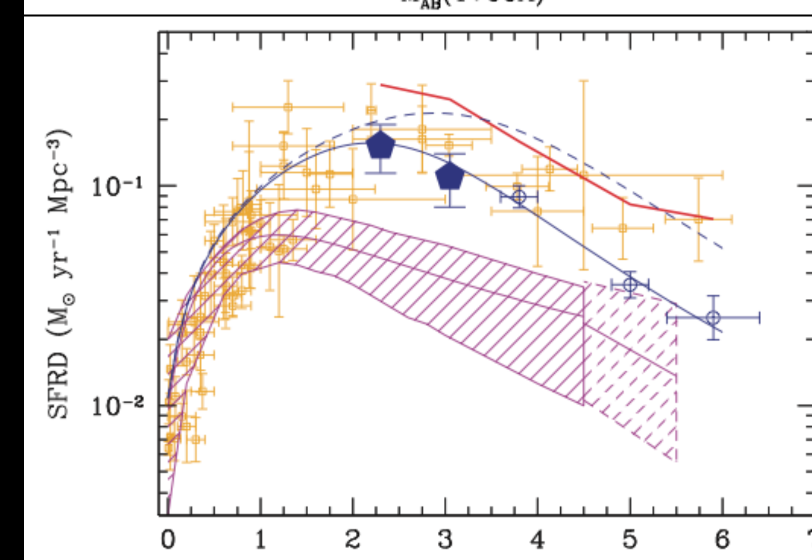

Testing the DARK MATTER scenarios against observations: the evolution of galaxies

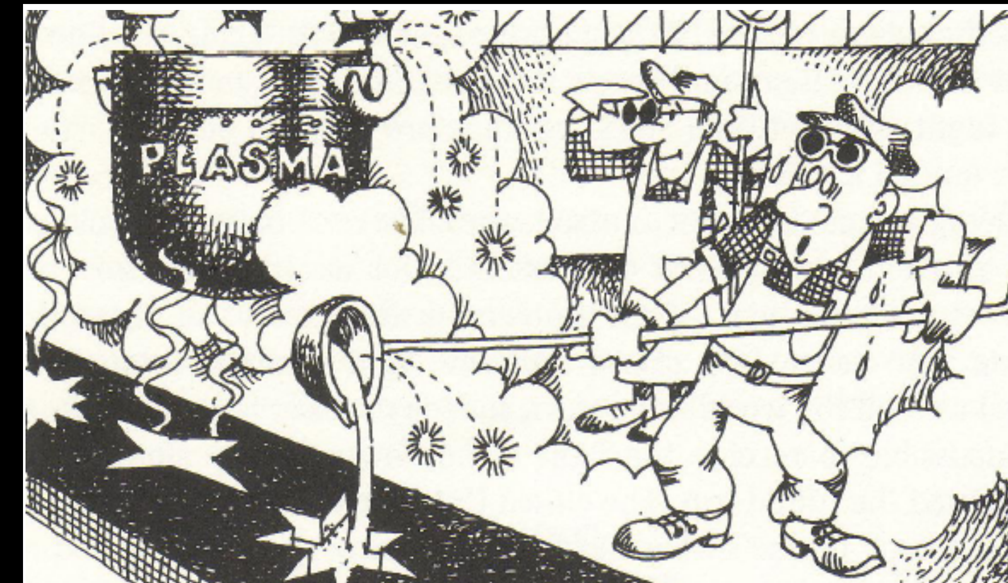

Requires modelling of baryon physics inside evolving DM potential wells

- gas physis (cooling, heating)
- disk formation
- star formation
- evolution of the stellar population
- injection of energy into the gas from SNae

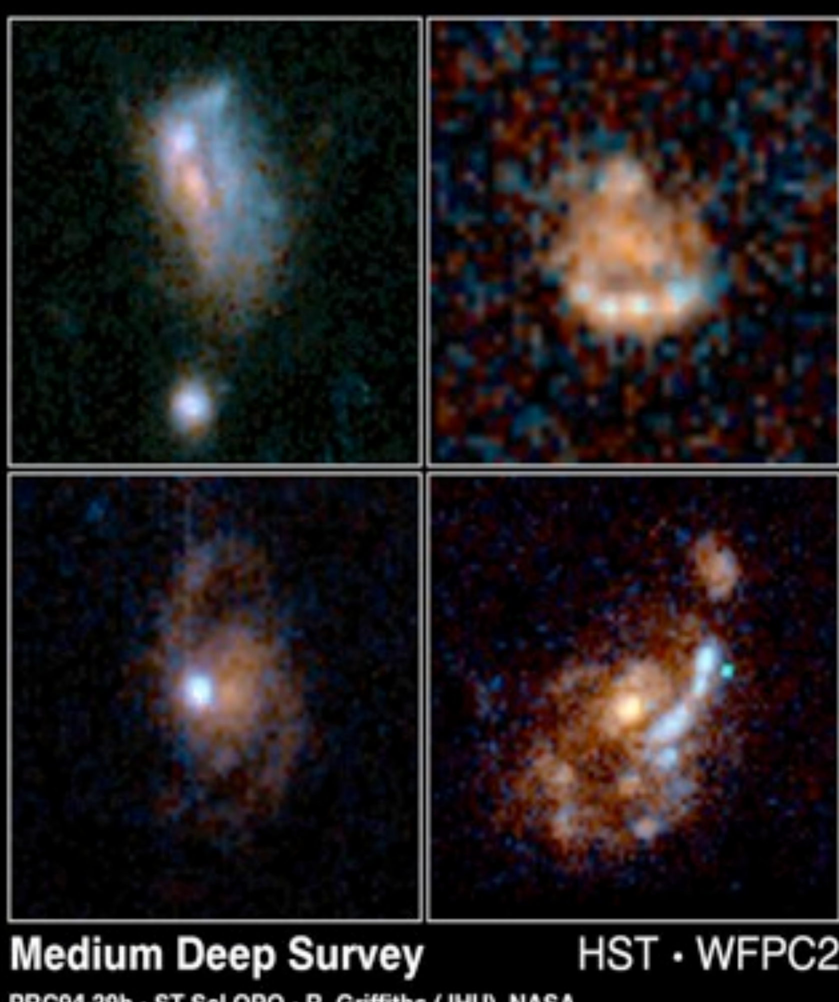

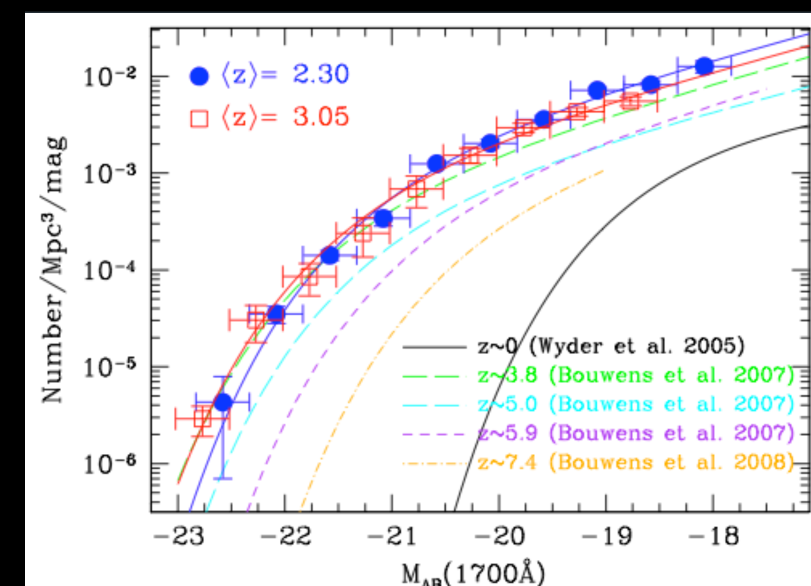

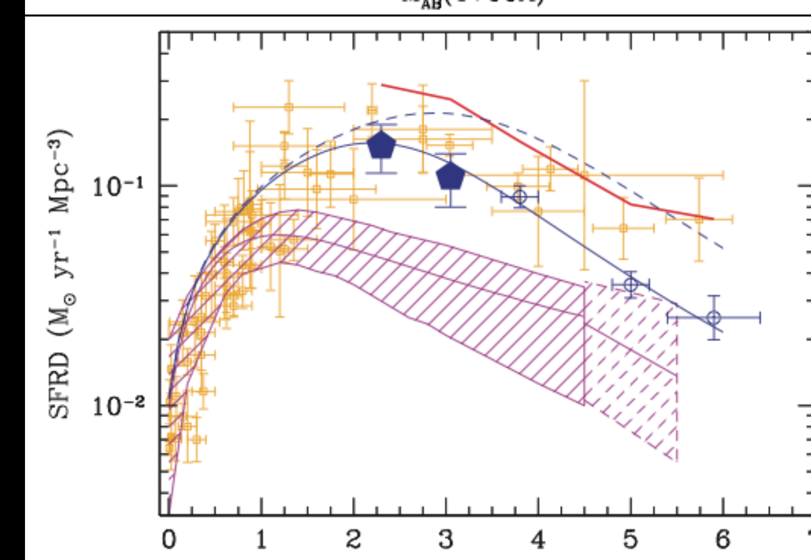

Galaxy Formation in a Cosmological Context

Hydrodynamcal
N-body simulations

Pros

include hydrodynamics of gas
contain spatial information

Cons

numerically expensive
(limited exploration of parameter space)
requires sub-grid physics

Semi-Analytic Models
Monte-Carlo realization of collapse and merging histories

Pros

Physics of baryons linked to DM halos through scaling laws, allows a fast spanning of parameter space

Cons

Simplified description of gas physics
Do not contain spatial informations

Galaxy Formation in a Cosmological Context

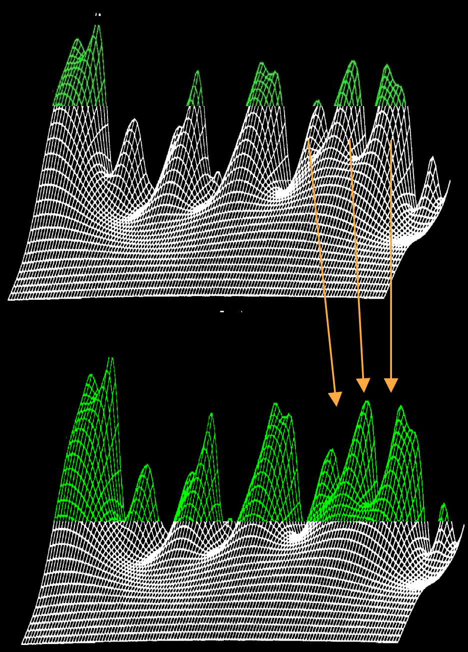

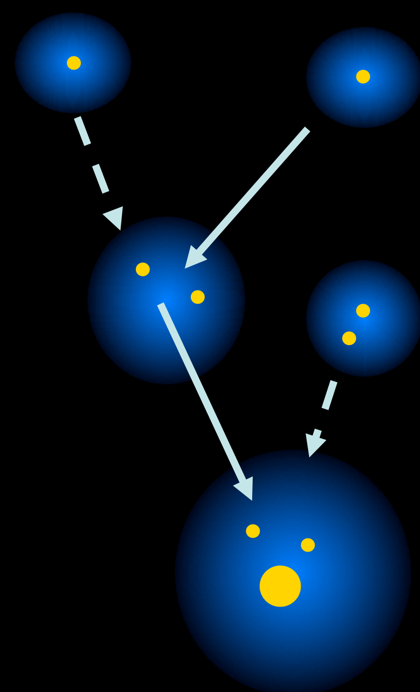

Semi-Analytic Models
Monte-Carlo realization of collapse and merging histories

Pros

Physics of baryons linked to DM halos through scaling laws, allows a fast spanning of parameter space

Cons

Simplified description of gas physics
Do not contain spatial informations

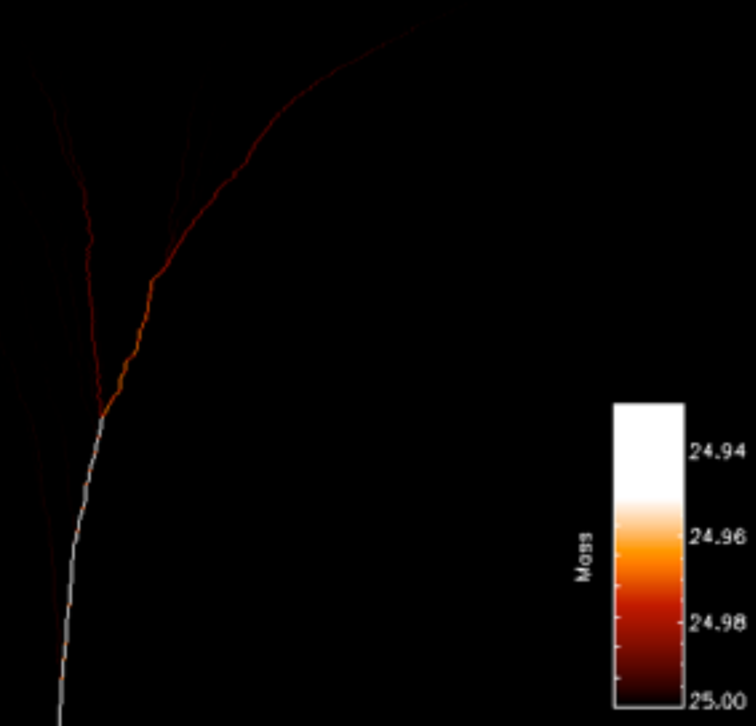

Sub-Halo dymanics:
dynamical friction, binary aggregation

Halo Properties
Density Profiles
Virial Temperature

Gas Properties
Profiles
Cooling - Heating Processes
Collapse, disk formation

Star Formation Rate

Gas Heating (feedback)
SNae
UV background

Evolution of stellar populations

Growth of Supermassive BHs
Evolution of AGNs

Properties of merging trees

Simulation
by Governato 04

Initial (z≈4-6) merging events involve small clumps with comparable size

Rapid merging, frequent encounters

Last major merging at z≈3 for M≈3 10^{12} $M_\odot$

At later times, merging rate declines

Accretion of smaller lumps onto the main progenitor

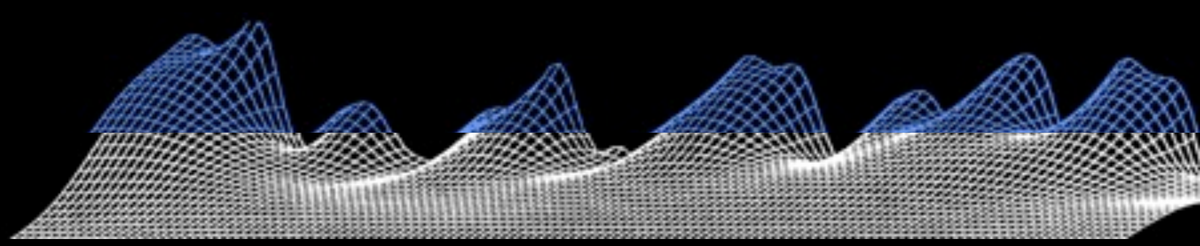

NM et al. 06

Baryonic Processes

Frequent galaxy encounters

Rapid cooling (high gas density)

Starbursts with large fraction of Gas converted into stars

$z \gtrsim 2$

Decline of cooling rate

Drop of encounter rate

Quiescent and declining star formation

$z \lesssim 2$

z

Properties of merging trees

Simulation
by Governato 04

Initial ($z \approx 4$-6) merging events involve small clumps with comparable size

Rapid merging, frequent encounters

Last major merging at $z \approx 3$ for $M \approx 3 10^{12}\ M_{\odot}$

At later times, merging rate declines

Accretion of smaller lumps onto the main progenitor

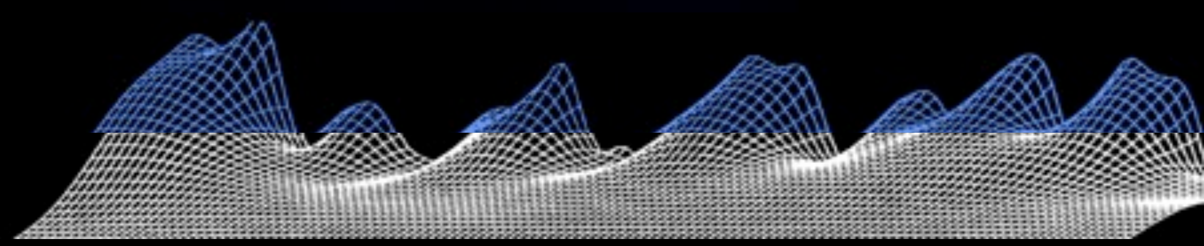

Baryonic Processes

NM et al. 06

Frequent galaxy encounters

Rapid cooling (high gas density)

Starbursts with large fraction of Gas converted into stars

$z \gtrsim 2$

Decline of cooling rate

Drop of encounter rate

Quiescent and declining star formation

$z \lesssim 2$

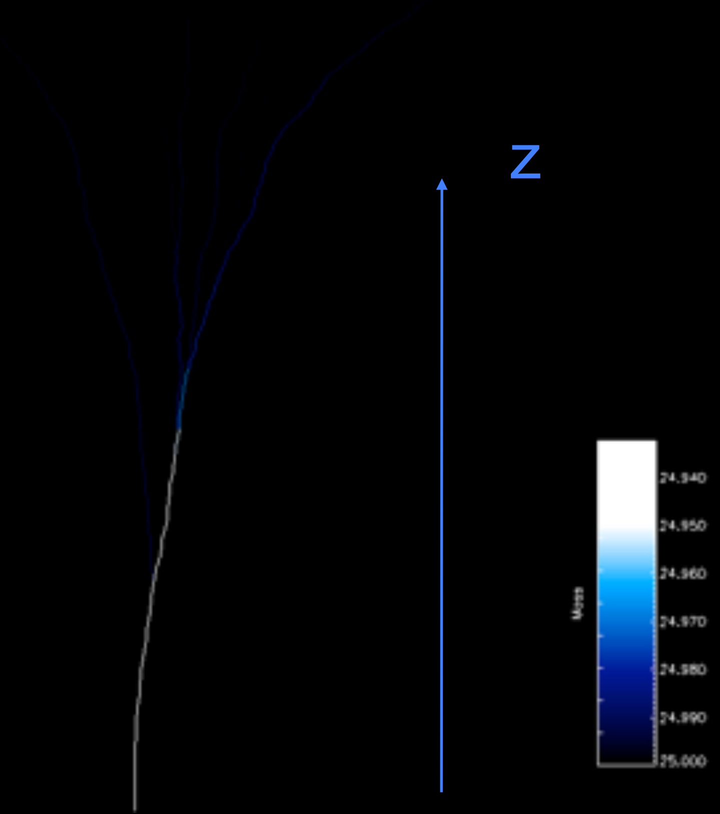

Properties of merging trees

Simulation
by Governato 04

Initial ($z \approx 4$-6) merging events involve small clumps with comparable size

Rapid merging, frequent encounters

Last major merging at $z \approx 3$ for $M \approx 3\,10^{12}\ M_\odot$

At later times, merging rate declines

Accretion of smaller lumps onto the main progenitor

Phase 1

Zhao et al. 2003
Diemand et al. 2007
Hoffman et al. 2007
Ascasibar & Gottloeber 2008

Phase 2

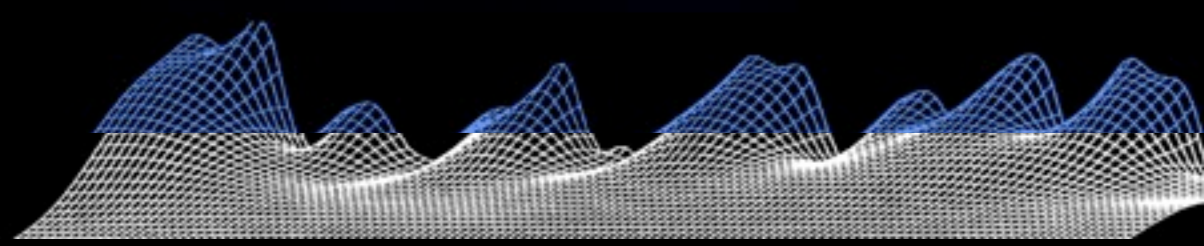

NM et al. 06

Baryonic Processes

Frequent galaxy encounters

Rapid cooling (high gas density)

Starbursts with large fraction of Gas converted into stars

$$z \gtrsim 2$$

Decline of cooling rate

Drop of encounter rate

Quiescent and declining star formation

$$z \lesssim 2$$

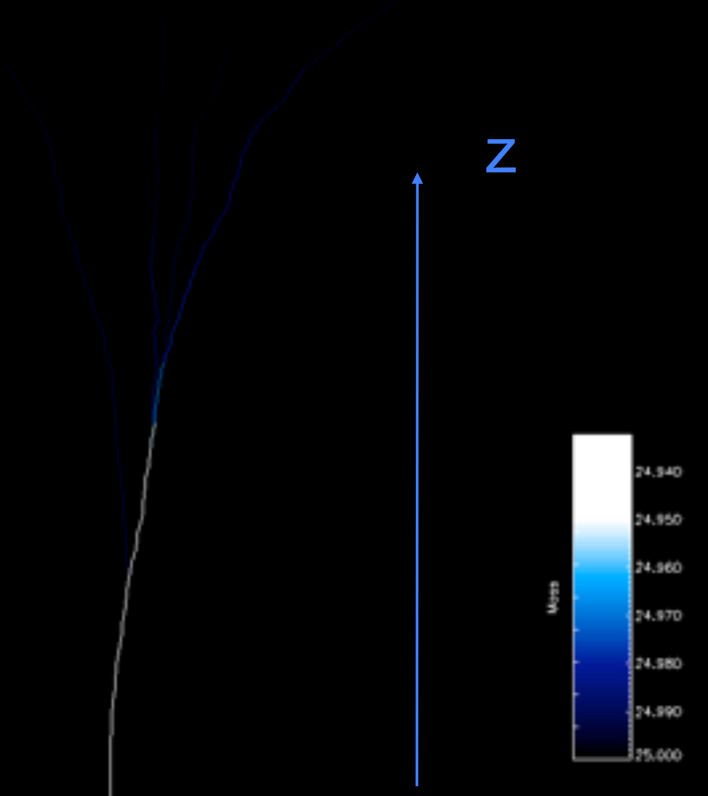

Properties of merging trees

Simulation
by Governato 04

Initial ($z \approx 4$-6) merging events involve small clumps with comparable size

Rapid merging, frequent encounters

Last major merging at $z \approx 3$ for $M \approx 3 \, 10^{12}$ $M_\odot$

At later times, merging rate declines

Accretion of smaller lumps onto the main progenitor

Phase 1

Zhao et al. 2003
Diemand et al. 2007
Hoffman et al. 2007
Ascasibar & Gottloeber 2008

Phase 2

Baryonic Processes

Frequent galaxy encounters

Rapid cooling (high gas density)

Starbursts with large fraction of Gas converted into stars

$\Bigg\} \; z \gtrsim 2$

Decline of cooling rate

Drop of encounter rate

Quiescent and declining star formation

$\Bigg\} \; z \lesssim 2$

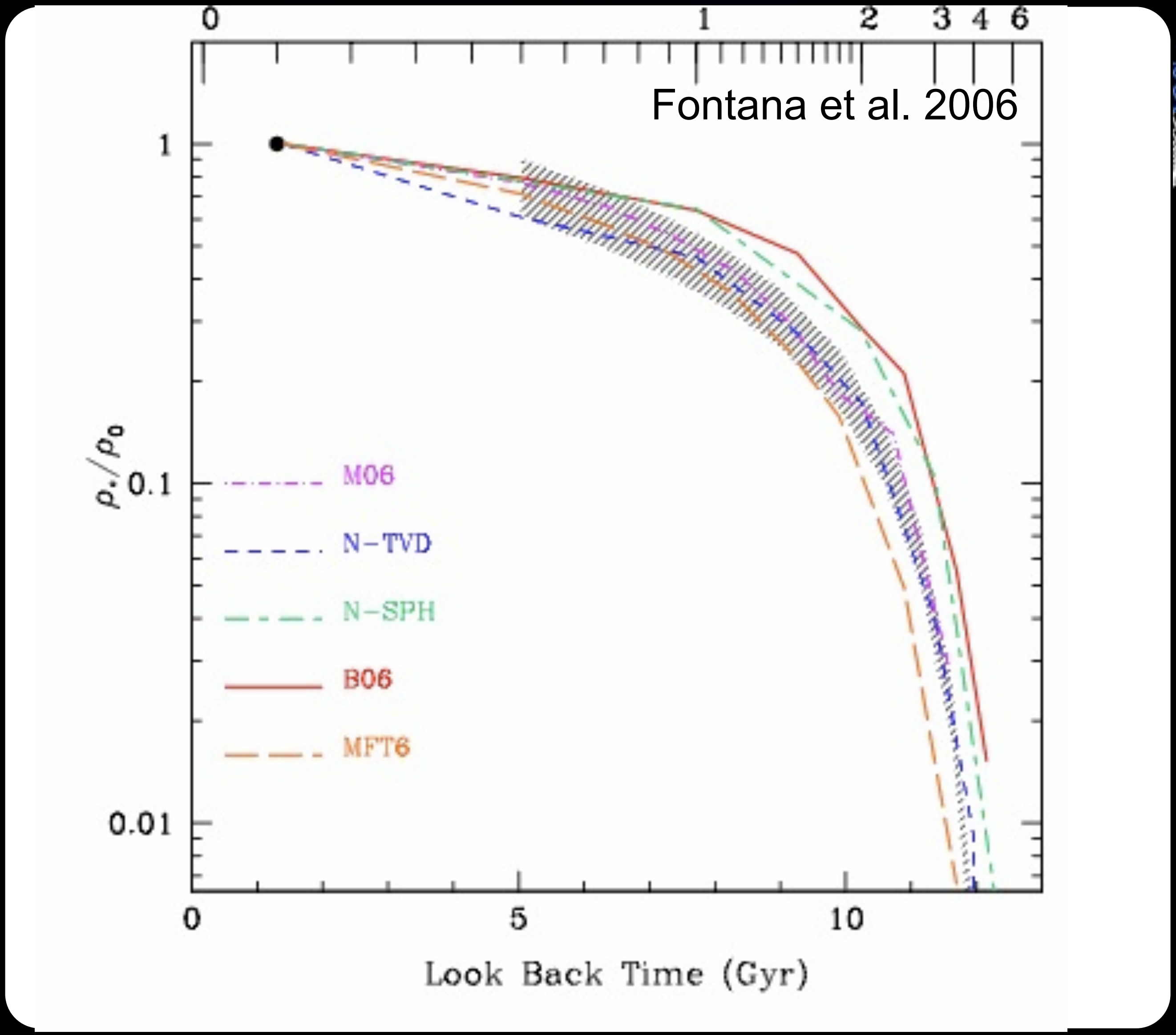

Galaxy Formation models in CDM scenario

Local properties:
gas content
luminosity distribution
disk sizes
distribution of the stellar mass content

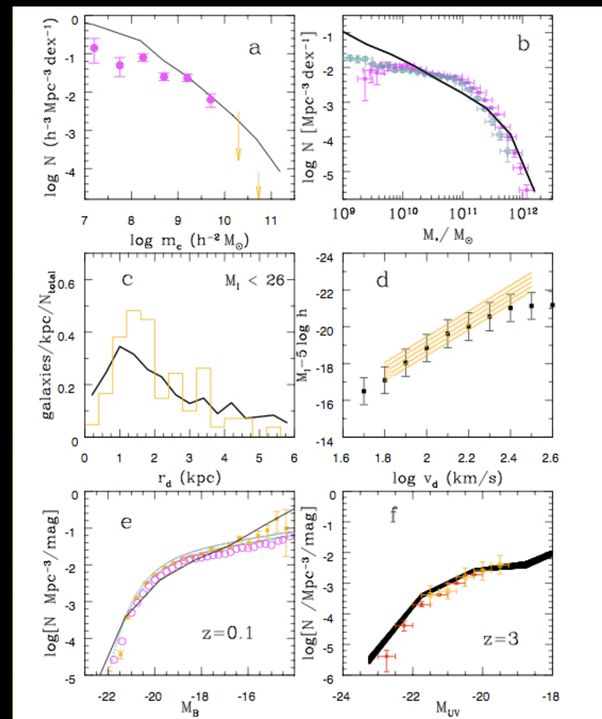

NM et al. 2006

properties of distant galaxies:
luminosity distribution
evolution of the star formation rate

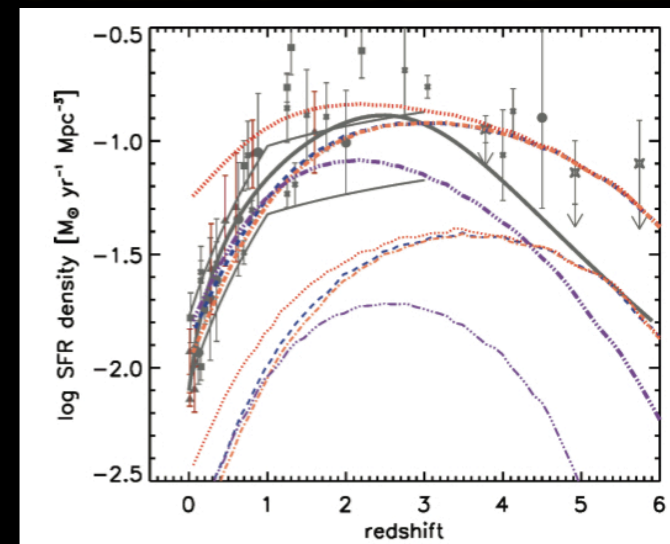

Somerville et al. 2010

NM et al. 2006

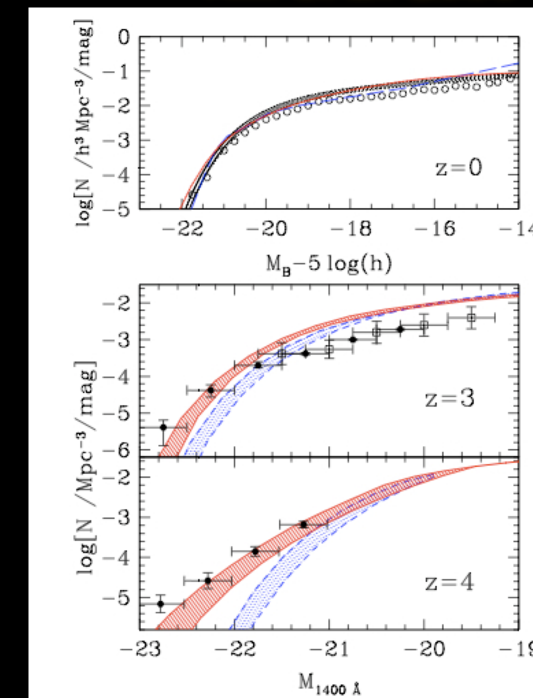

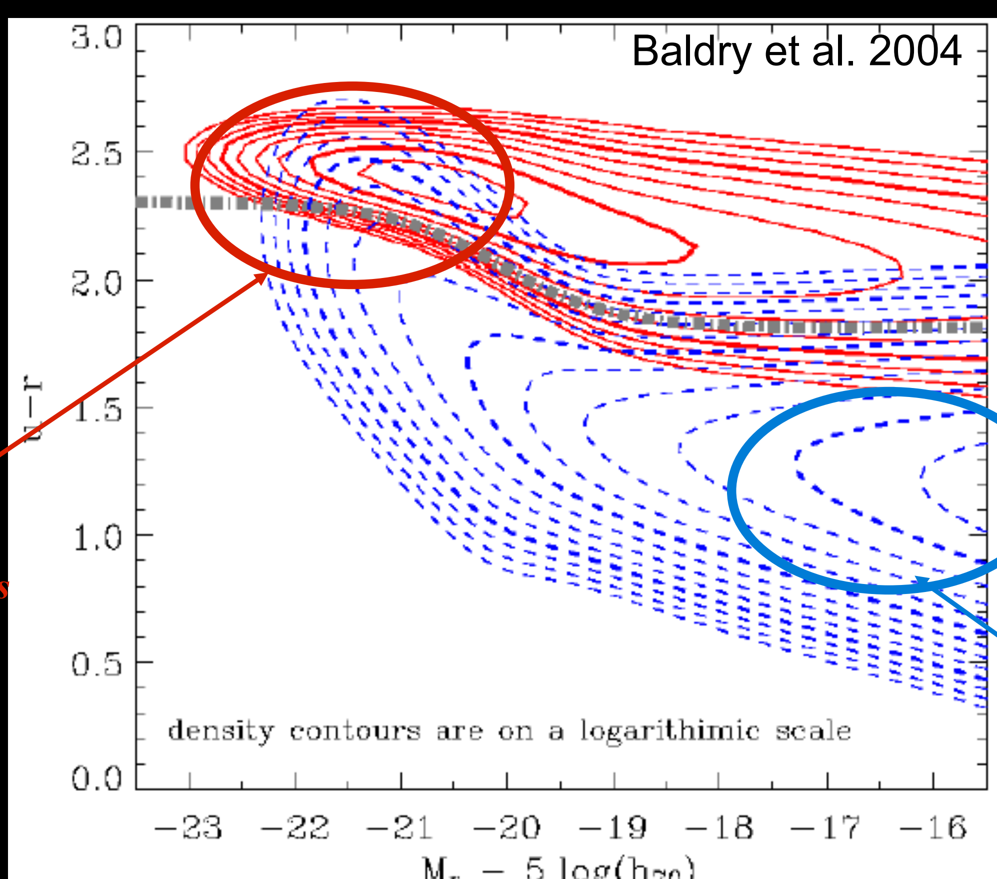

Color Distributions: bimodal distribution (early type vs late type)

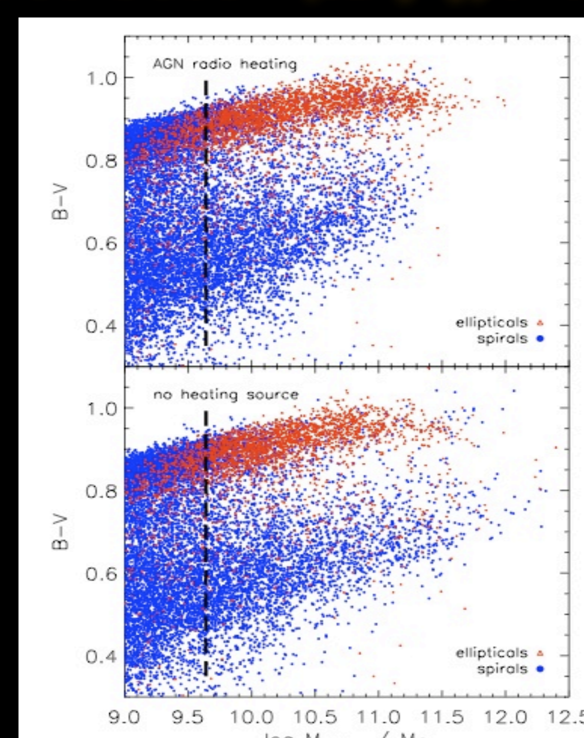

Croton et al. 2006

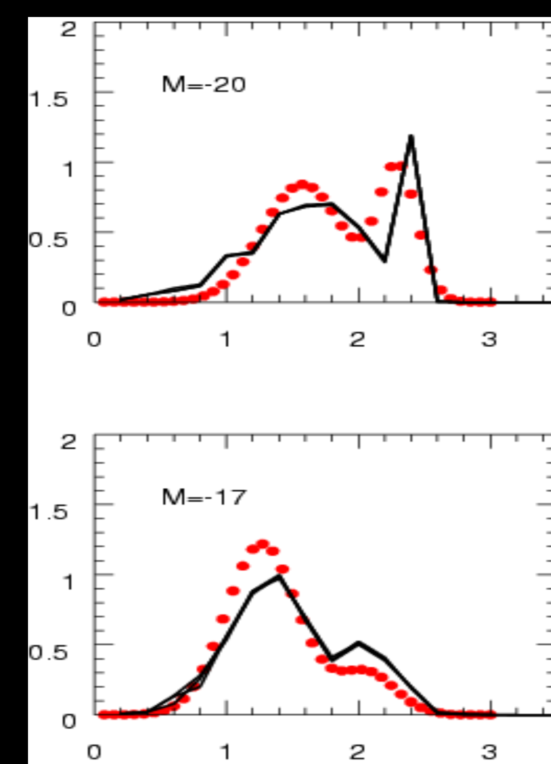

NM et al. 2008

Critical Issues

Overabundance of low-mass objects

i) abundance of satellite DM haloes
ii) density profiles
iii) abundance of faint galaxies
iv) the M_*-M_{halo} relation
v) star formation histories of satellites

1) Dependence on specific theoretical model
2) Dependence on star formation and feedback effects
3) Solutions in WDM scenario

Critical Issues

Overabundance of low-mass objects

i) abundance of satellite DM haloes
ii) density profiles
iii) abundance of faint galaxies
iv) the M_*-M_{halo} relation
v) star formation histories of satellites

CDM Substructure in simulated cluster and galaxy haloes look similar.

Expected number of satellites in Milky Way- like galaxies in CDM largely exceeds the observed abundance.

Kravtsov, Klypin, Gnedin 2004

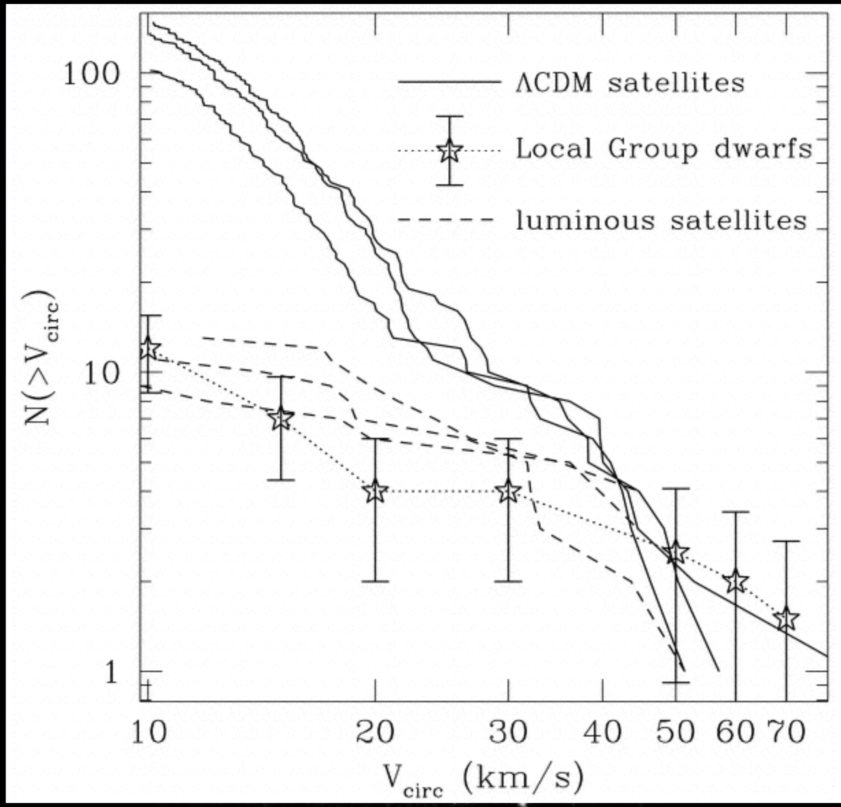

Via Lactea simulation of a Milky Way - like galaxy
Diemand et al. 2008

Critical Issues

Overabundance of low-mass objects

i) abundance of satellite DM haloes
ii) density profiles
iii) abundance of faint galaxies
iv) the M_*-M_{halo} relation
v) star formation histories of satellites

Moore et al. 2002

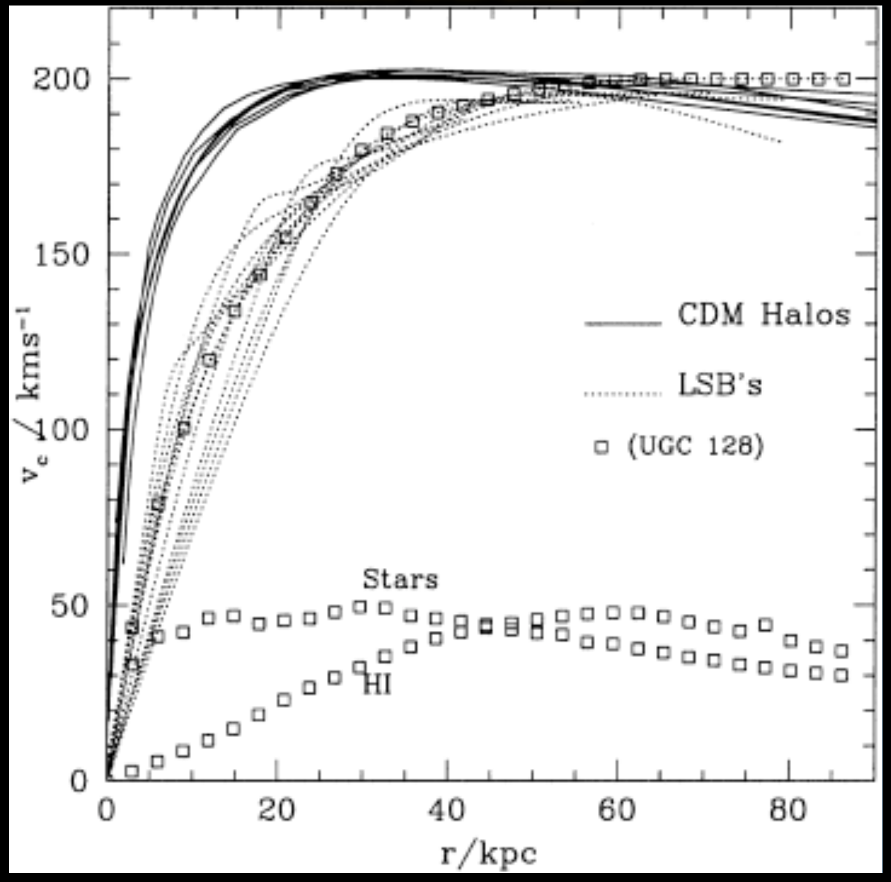

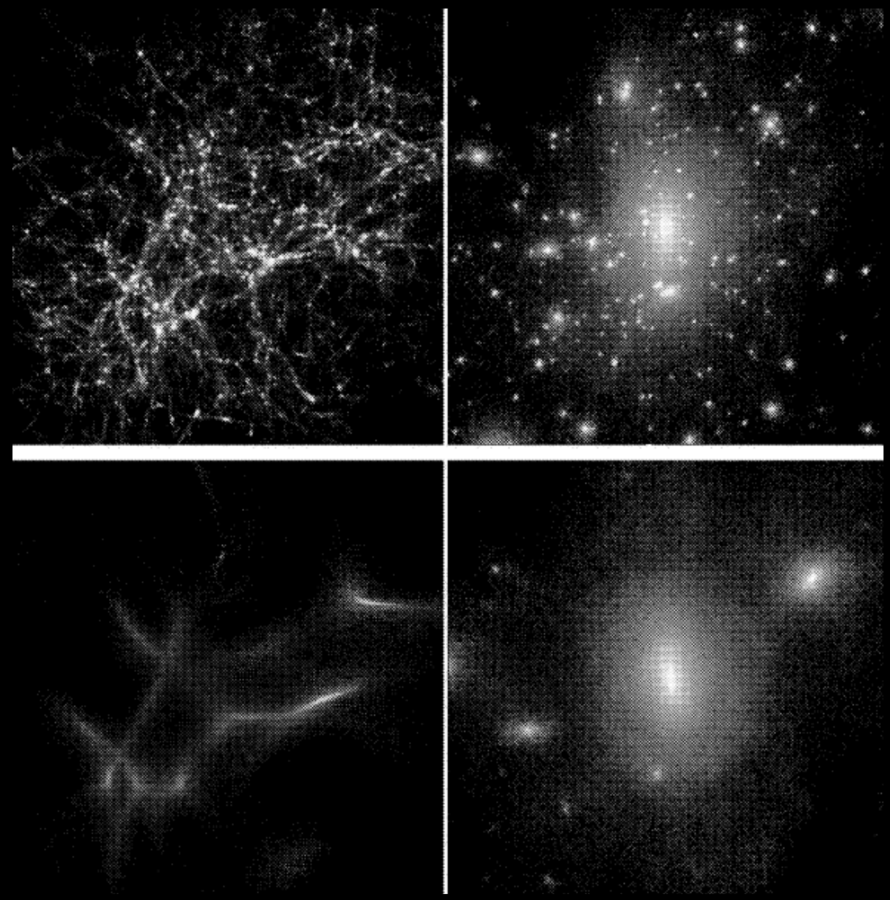

Most observed dwarf galaxies consist of a rotating stellar disk embedded in a massive dark-matter halo with a near-constant-density core. Models based on the dominance of CDM, however, invariably form galaxies with dense spheroidal stellar bulges and steep central dark-matter profiles, because low-angular- momentum baryons and dark matter sink to the centres of galaxies through accretion and repeated mergers.

Critical Issues

Overabundance of low-mass objects

i) abundance of satellite DM haloes
ii) density profiles
iii) abundance of faint galaxies
iv) the M*-M$_{halo}$ relation
v) star formation histories of satellites

In all first-generation SAM the number density of faint (low-mass) galaxies was over-predicted

Bower et al. 2006

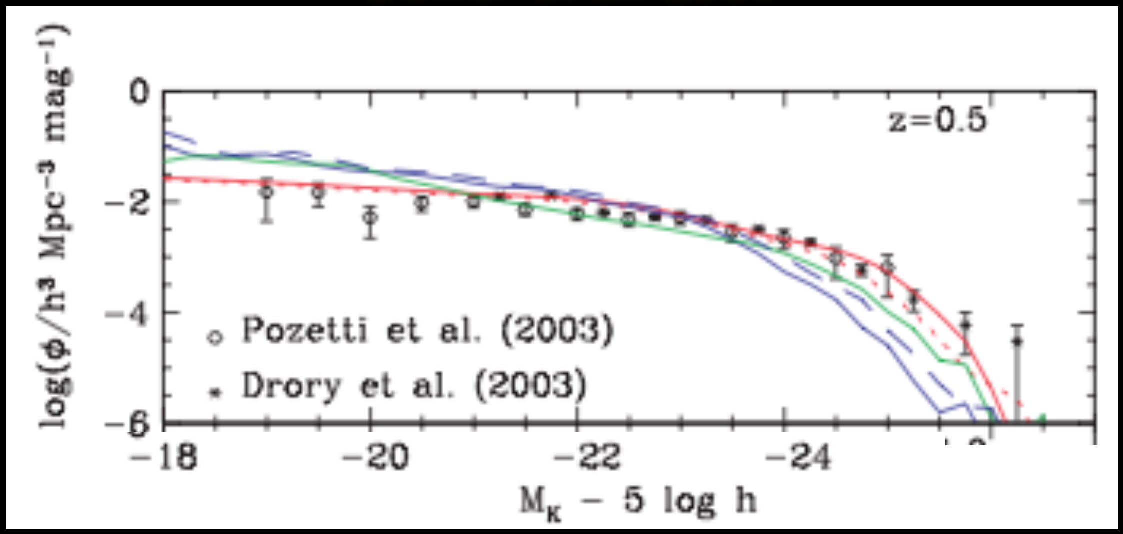

The K-Band Luminosity Function
Somerville et al. SAM

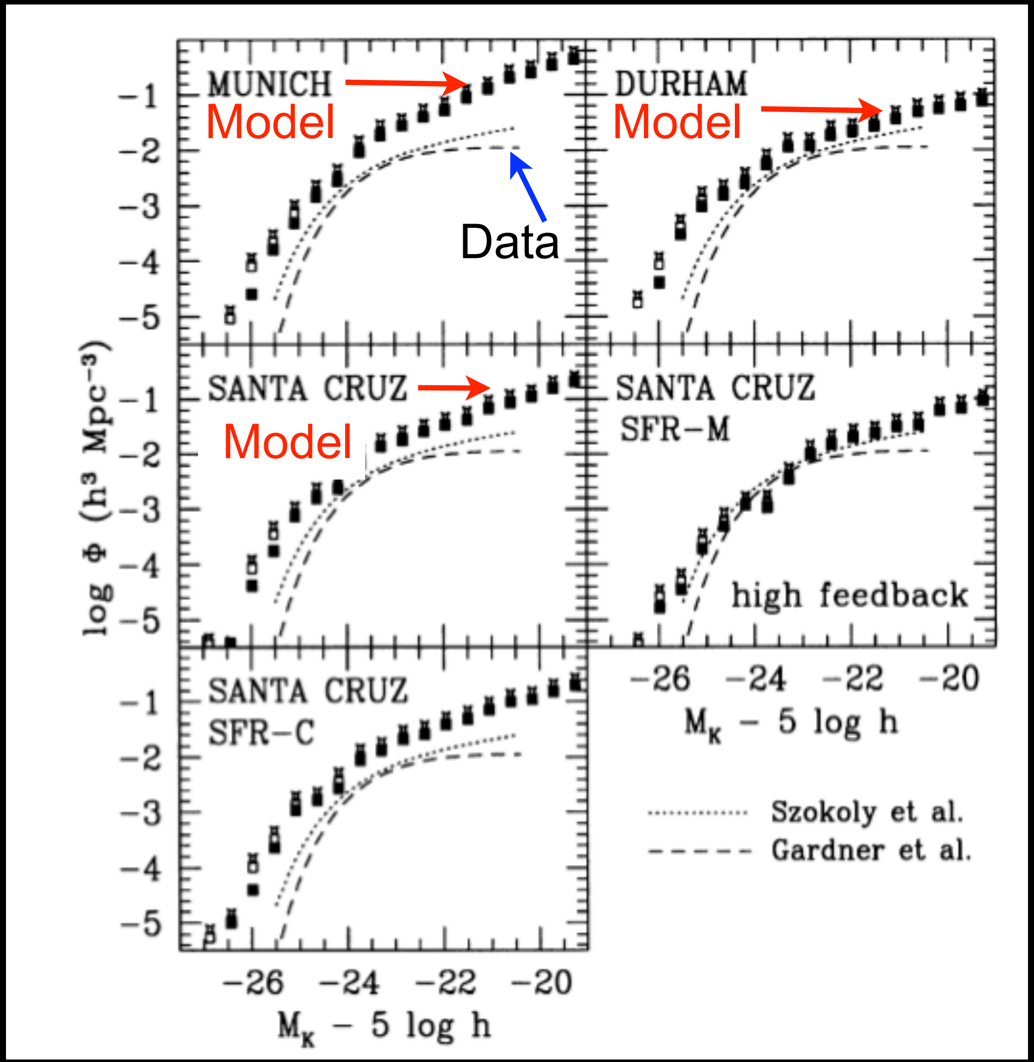

A first-order solution: feedback and UV background

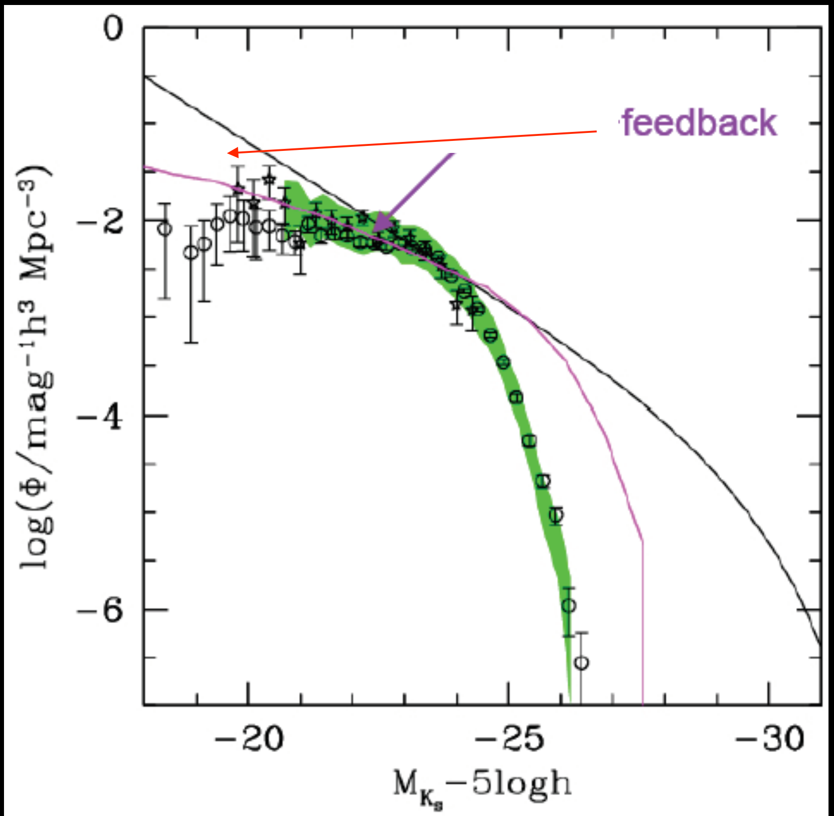

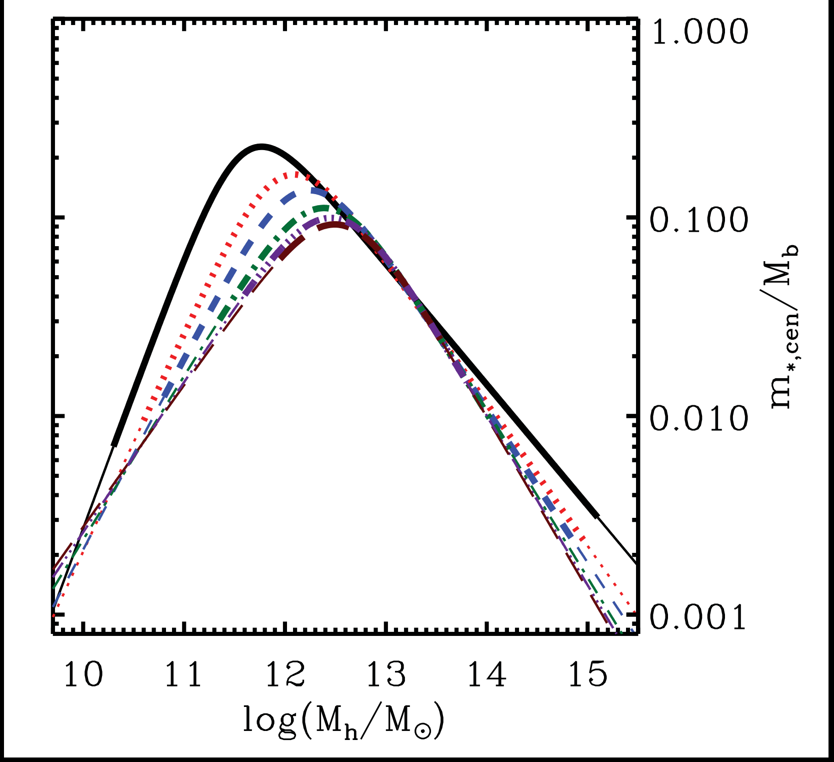

Moster et al. 2014

The origin of the problem:
The DM halo Mass function has a steep log slope $N \sim M^{-1.8}$
While the Observed Galaxy Luminosity Function
has a much flattter slope $N \sim L^{-1.2}$

A Possible Solution:
Suppress luminosity (star formation) in low-mass haloes $L/M \sim M^{\beta}$ $\beta = 1\text{-}3$
Heat - Expell Gas from shallow potential wells
- Enhanced SN feedback
- UV background

$$E_{SN} \approx 10^{51}\, \eta_0 \eta_{IMF}\, \Delta M_* erg/s$$

$$v_{SN} = \sqrt{E_{SN}/M_{gas}} \approx 100 \quad km/s$$

At Z=0 the mass scale at which SN can effectively espell gas from DM potential wells

$$M_{SN} \sim 10^{10}\, M_{\odot}$$

at low z, at higher redshift the density is higher an M_{SN} increases

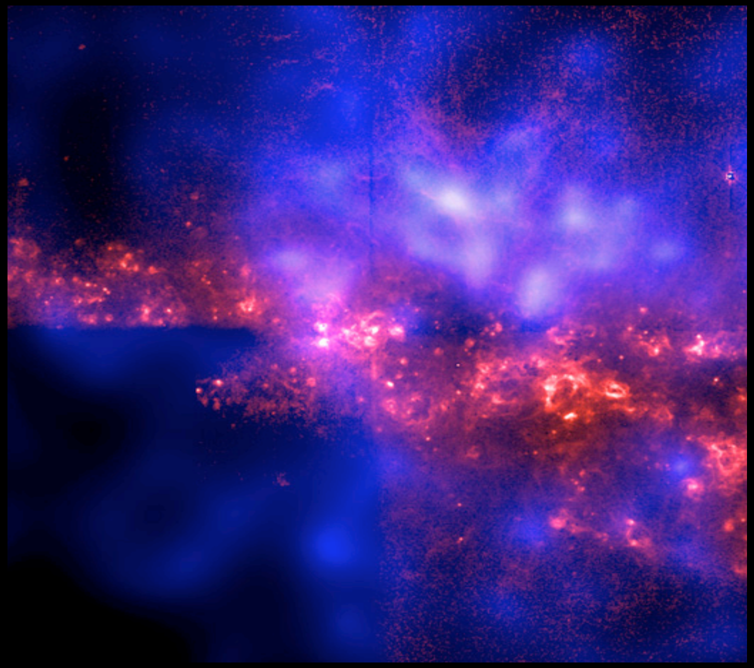

Feedback and UV background

i) the abundance of satellites

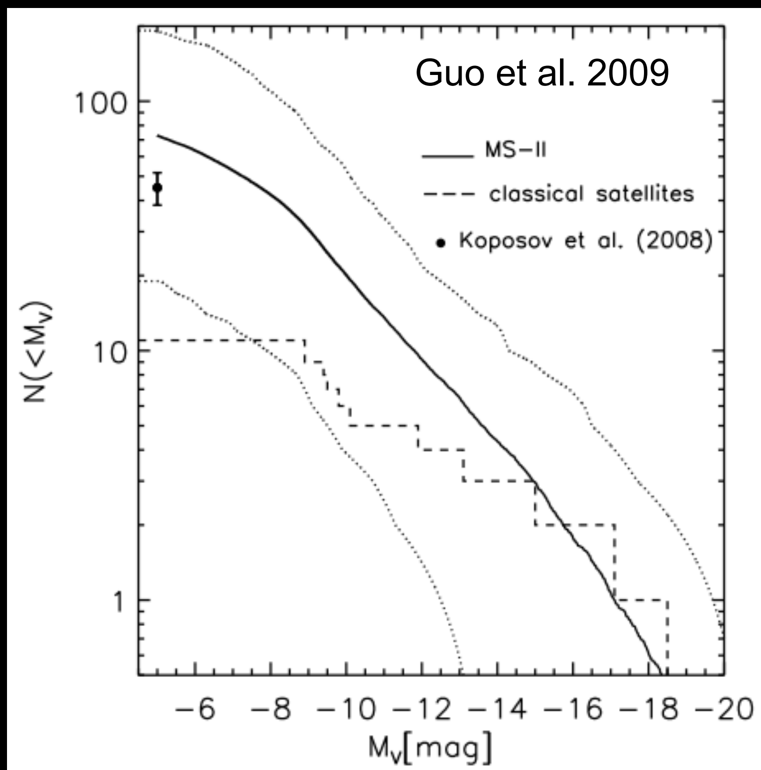

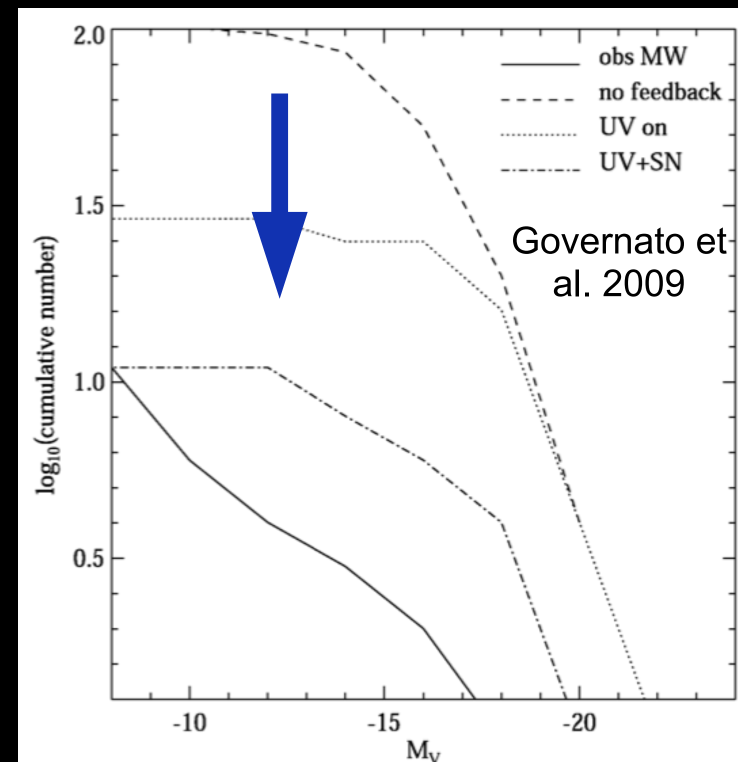

Brooks & Zolotov 2014

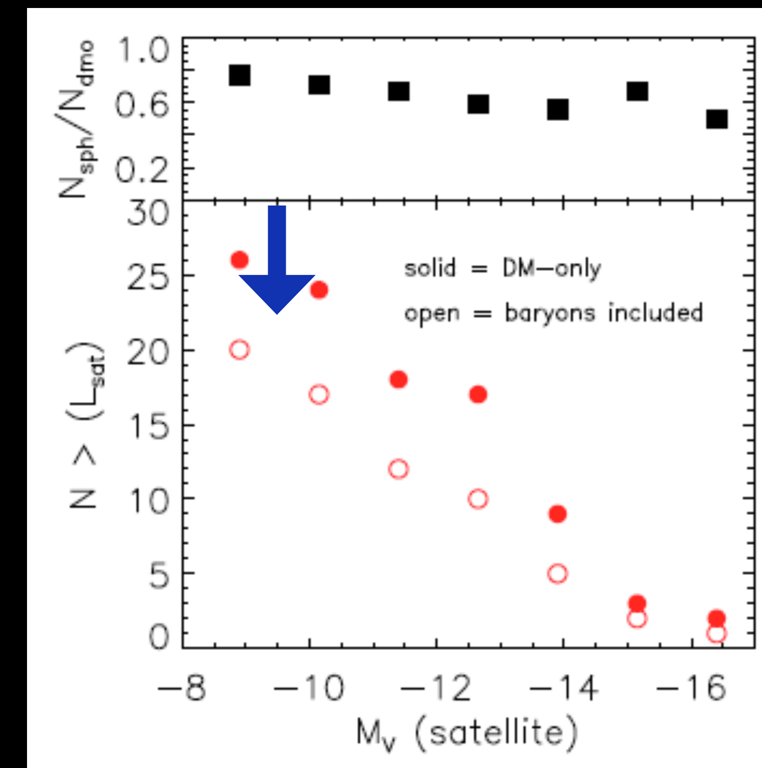

ii) the abundance of faint galaxies

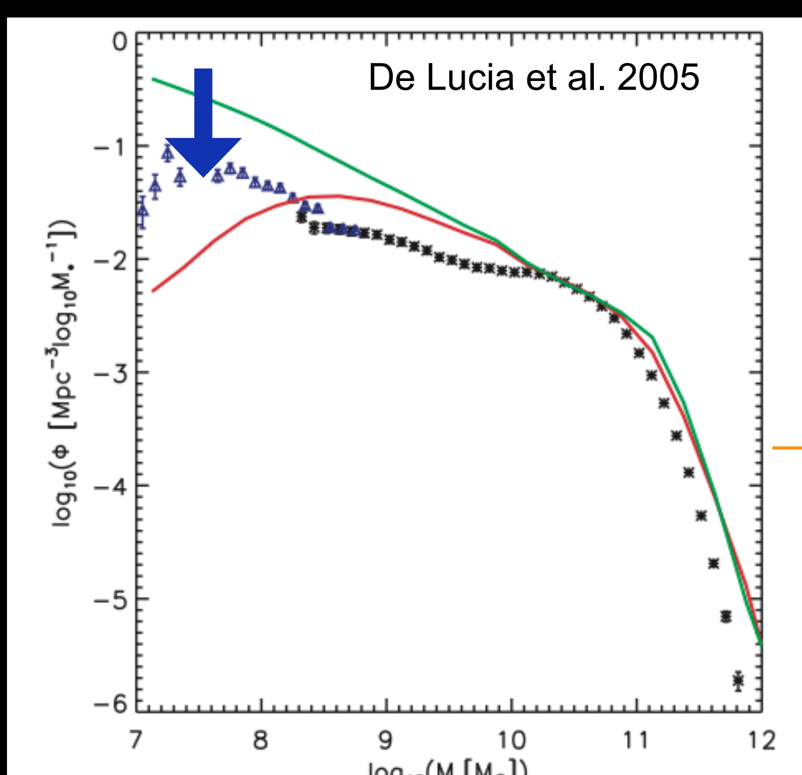

Refined treatment of Gas and Stellar Stripping

Enhanced (tuned) feedback dependence on the circular velocity of the DM halo

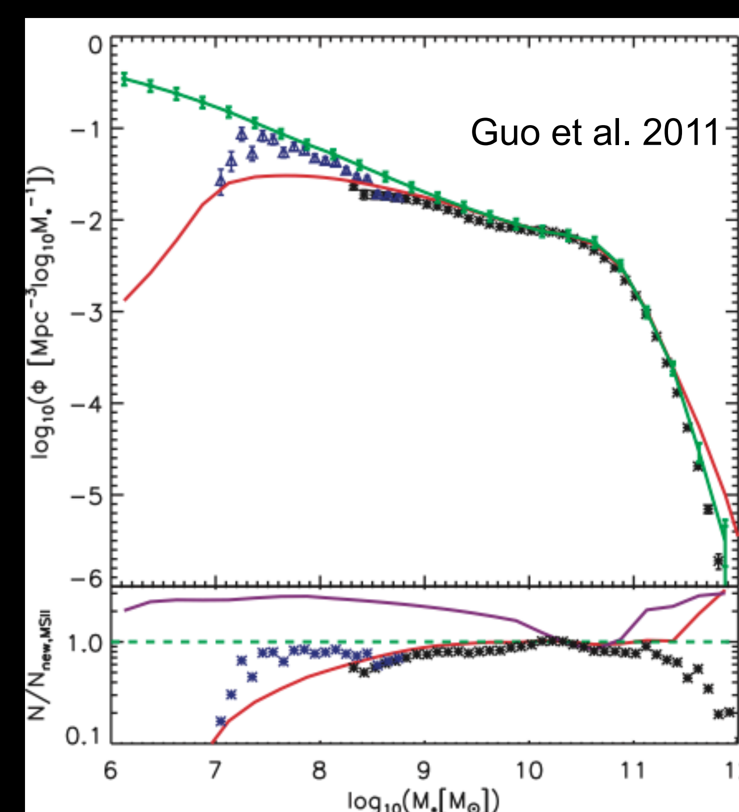

Feedback and UV background

i) the abundance of satellites

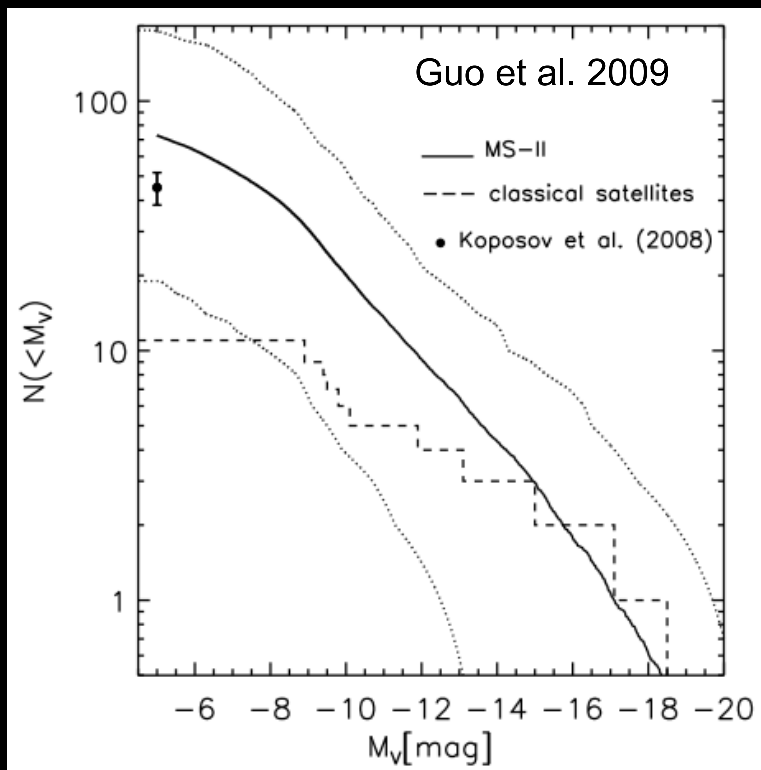

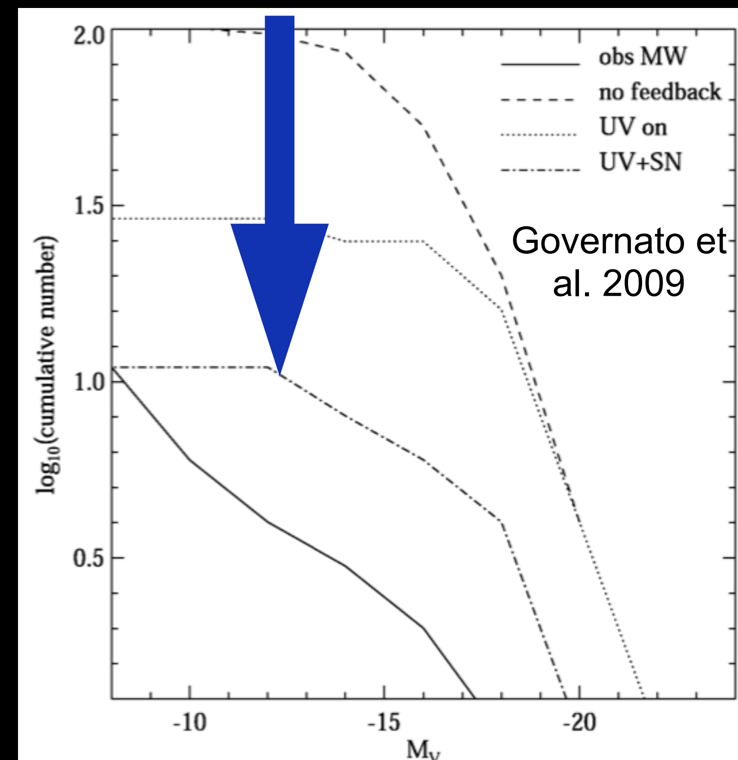

Brooks & Zolotov 2014

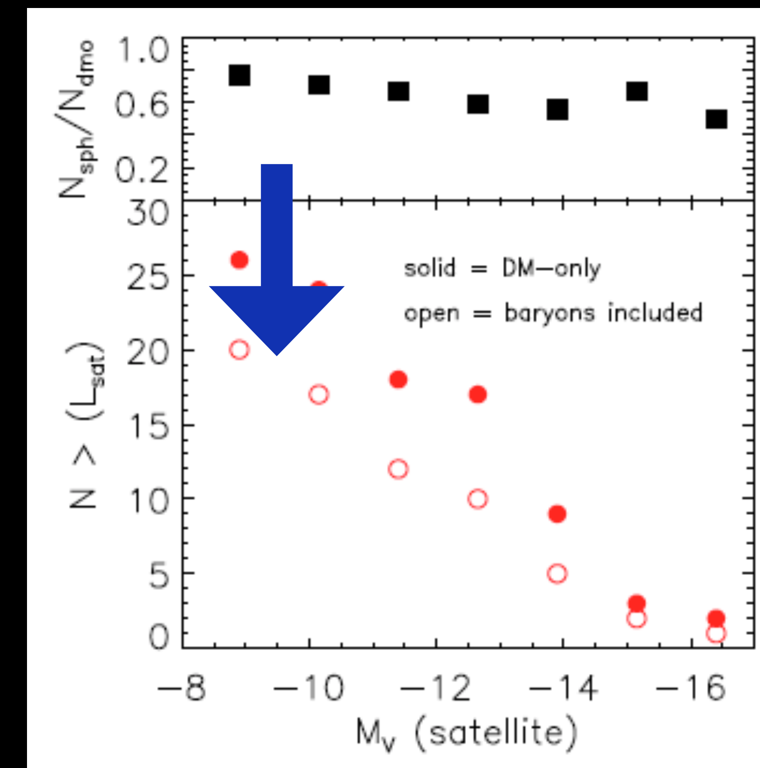

ii) the abundance of faint galaxies

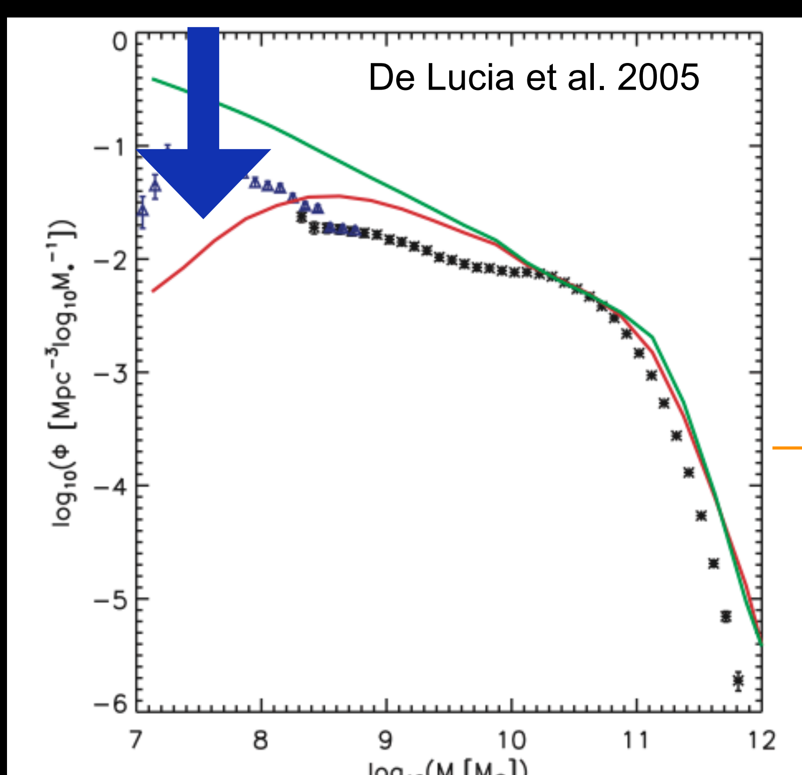

Refined treatment of Gas and Stellar Stripping

Enhanced (tuned) feedback dependence on the circular velocity of the DM halo

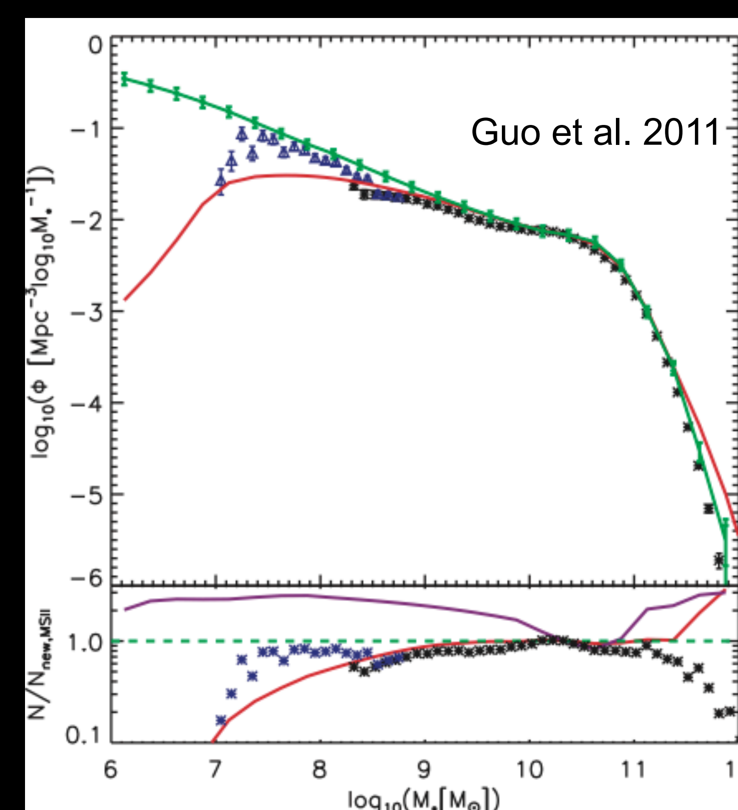

Feedback and UV background
iii) the density profiles

A proposed solution at low redshift

"... The rapid fluctuations caused by episodic feedback progressively pump energy into the DM particle orbits, so that they no longer penetrate to the centre of the halo" (Weinberg et al. 2013, Governato et al. 2012)

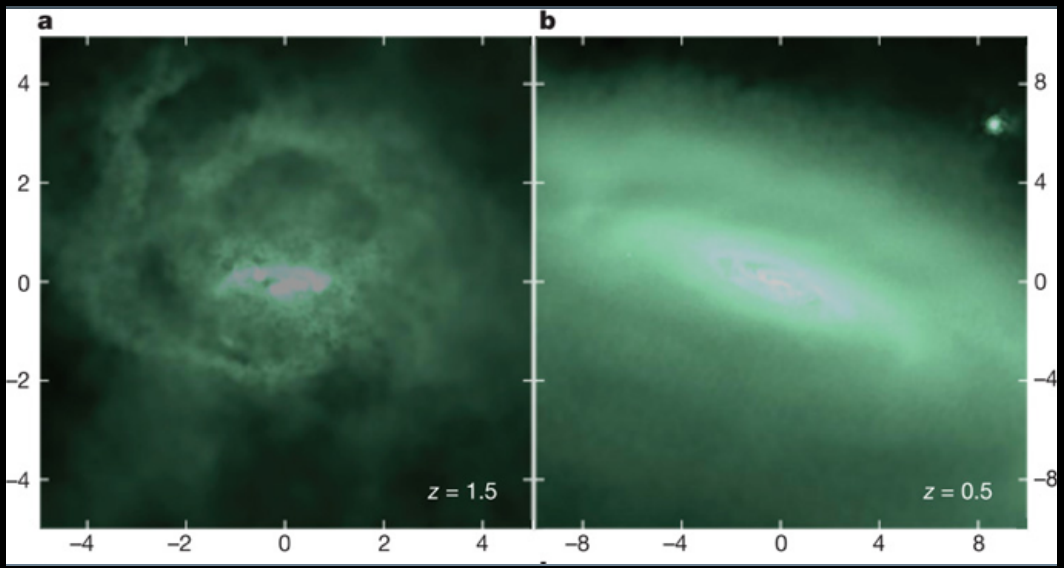

Governato et al. 2012

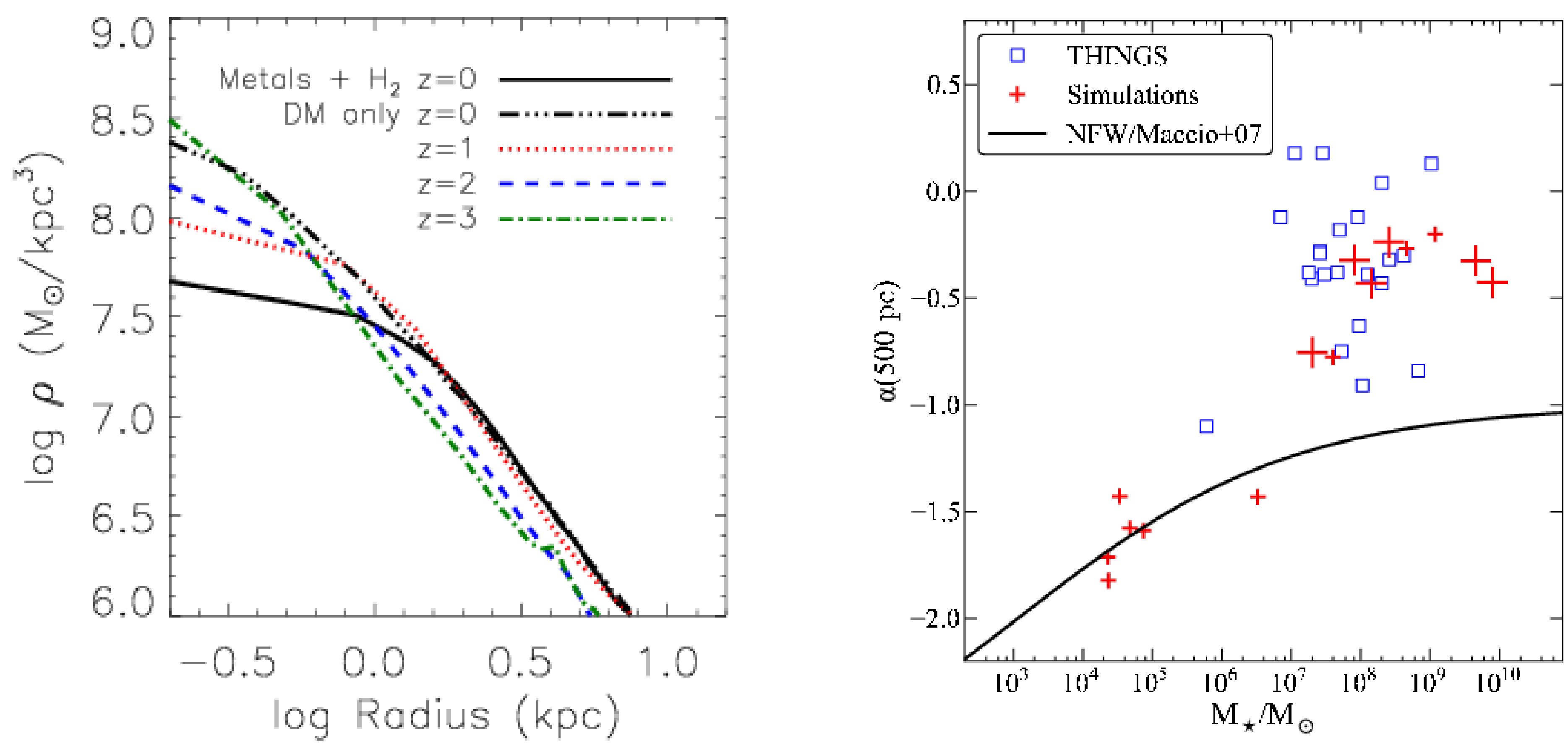

Fig. 3. Baryonic effects on CDM halo profiles in cosmological simulations, from Governato et al. (2012). *(Left)* The upper, dot-dash curve shows the cuspy dark matter density profile resulting from from a collisionless N-body simulation. Other curves show the evolution of the dark matter profile in a simulation from the same initial conditions that includes gas dynamics, star formation, and efficient feedback. By $z = 0$ (solid curve) the perturbations from the fluctuating baryonic potential have flattened the inner profile to a nearly constant density core. *(Right)* Logarithmic slope of the dark matter profile α measured at 0.5 kpc, as a function of galaxy stellar mass. Crosses show results from multiple hydrodynamic simulations. Squares show measurements from rotation curves of observed galaxies. The black curve shows the expectation for pure dark matter simulations, computed from NFW profiles with the appropriate concentration. For $M_* > 10^7 M_\odot$, baryonic effects reduce the halo profile slopes to agree with observations.

The problem persists at high redshifts

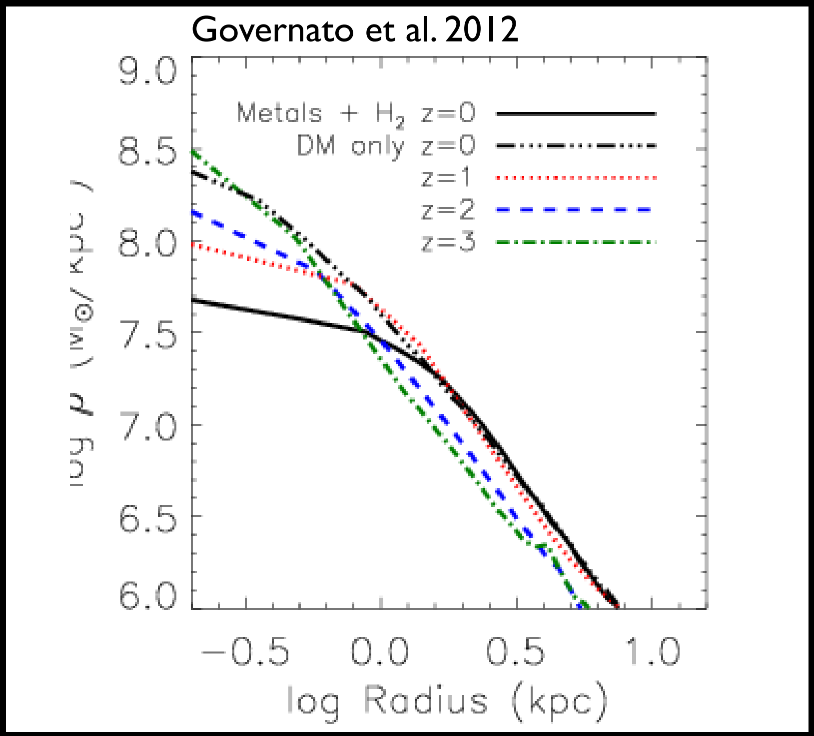

Even with strong feedback, for z≳1 in CDM

- Steeper central profiles are expected
- Steeper luminosity functions are expected

Stellar Mass Functions Guo et al. 2011

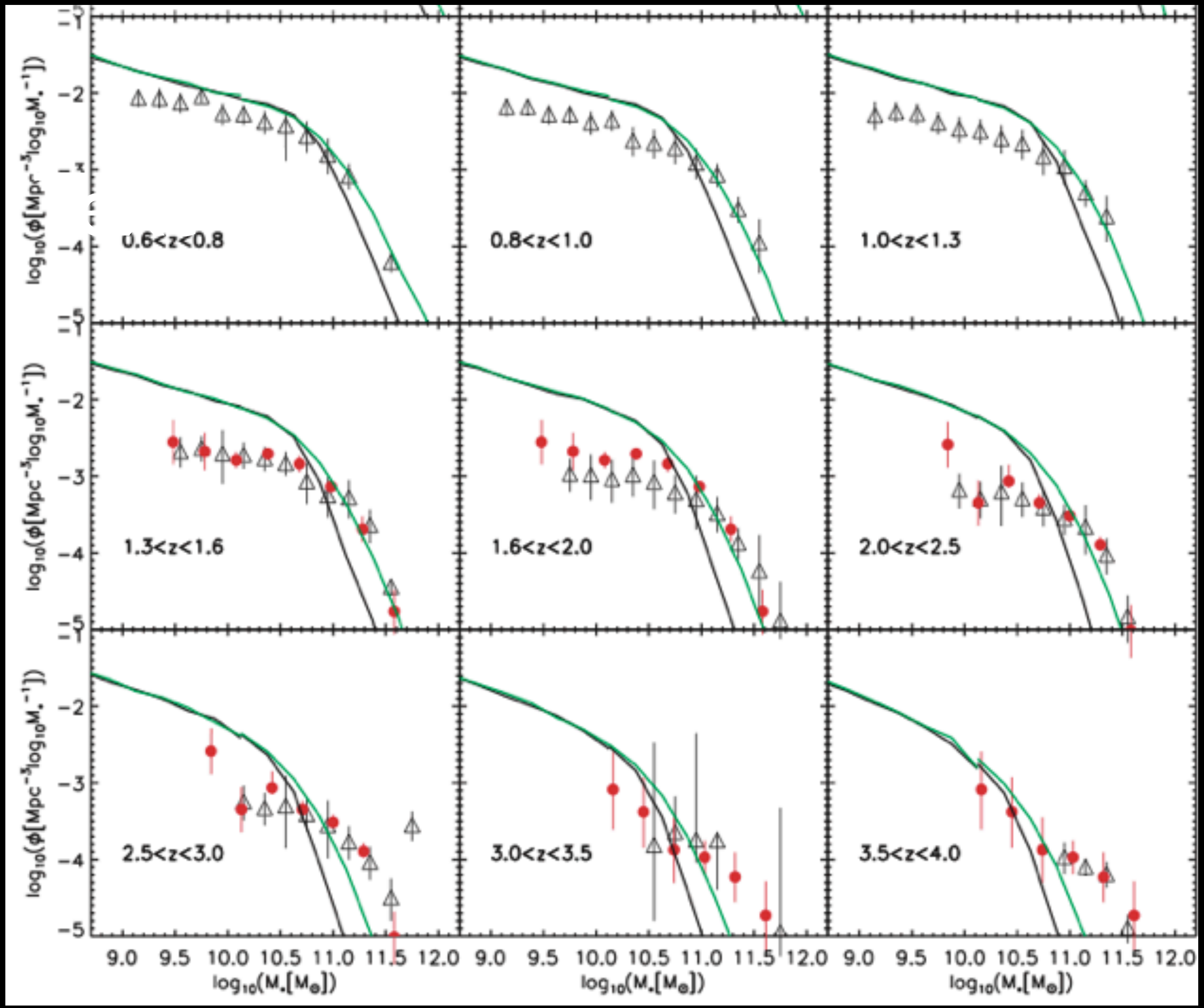

UV Luminosity Function z>4 Lo Faro et al. 2009

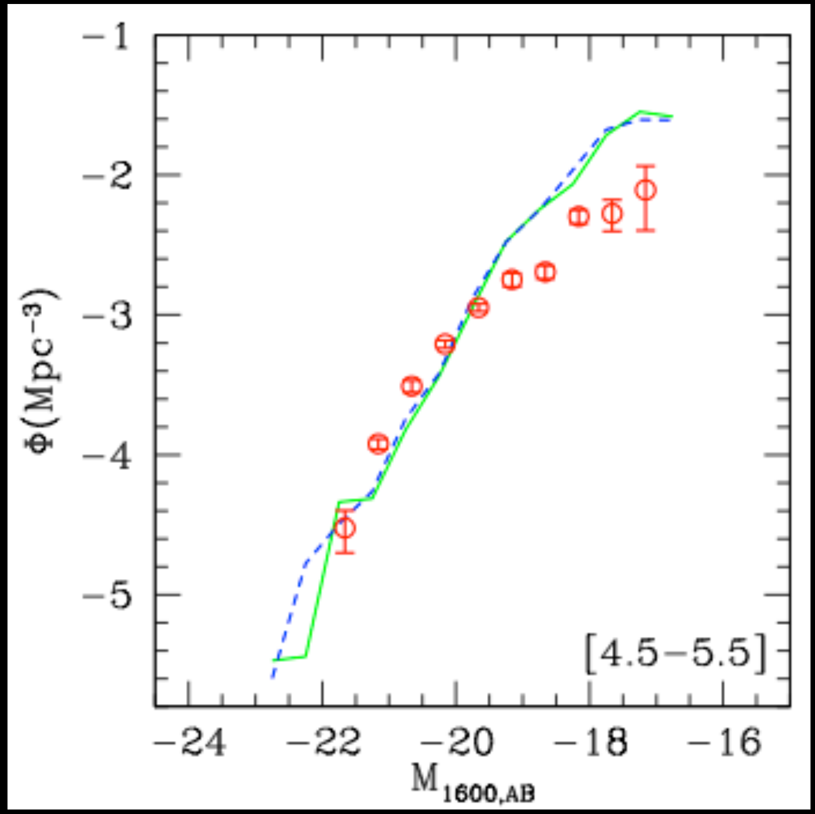

The problem persists at high redshifts

Corresponds to a mass scale affected by non-gravitational SN energy injection

$$M \approx (v_{esc}^2/G)\, r$$

$$r \propto (M/\rho)^{1/3}$$

$$\rho = 180\,\rho_u = 180\,\rho_u\,(1+z)^3$$

$$M \approx A\, v_{esc}^3\,(1+z)^{-3/2}$$

$$A \equiv \sqrt{3/G^3\,4\pi\,\rho_u}$$

$$v_{esc} = v_{SN} \rightarrow \quad M_{SN} \approx A\, v_{SN}^3\,(1+z)^{-3/2}$$

at $z \approx 0$ $\quad M_{SN} \sim 10^{10}\, M_\odot$

At high-z
larger densities imply
larger escape velocity
even for low-mass galaxies
feedback increasingly
ineffective

Lo Faro et al. 2009

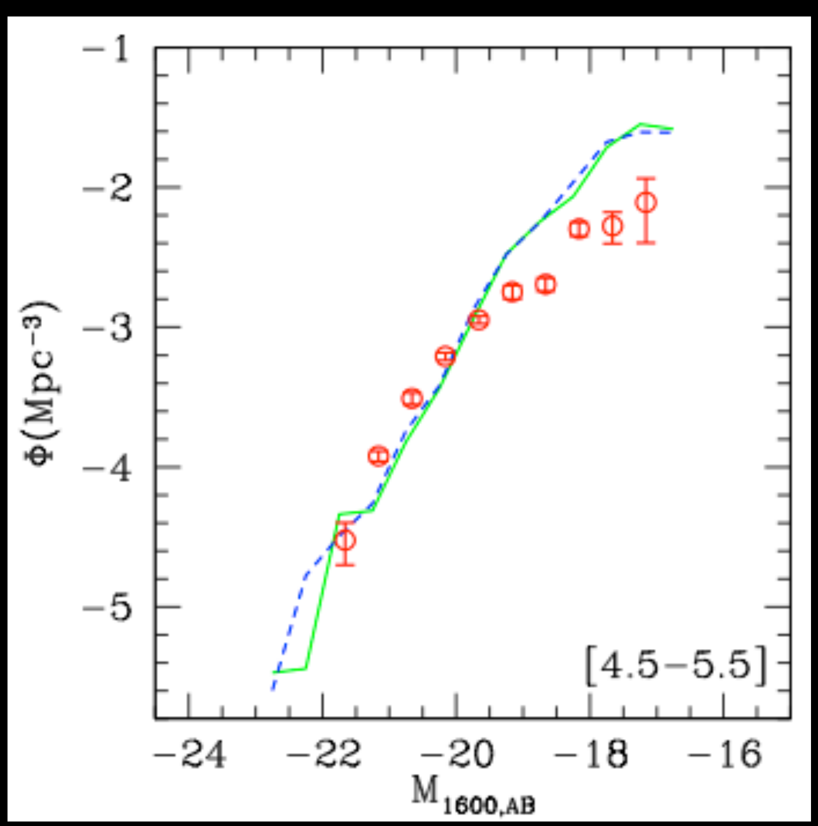

Guo et al. 2011

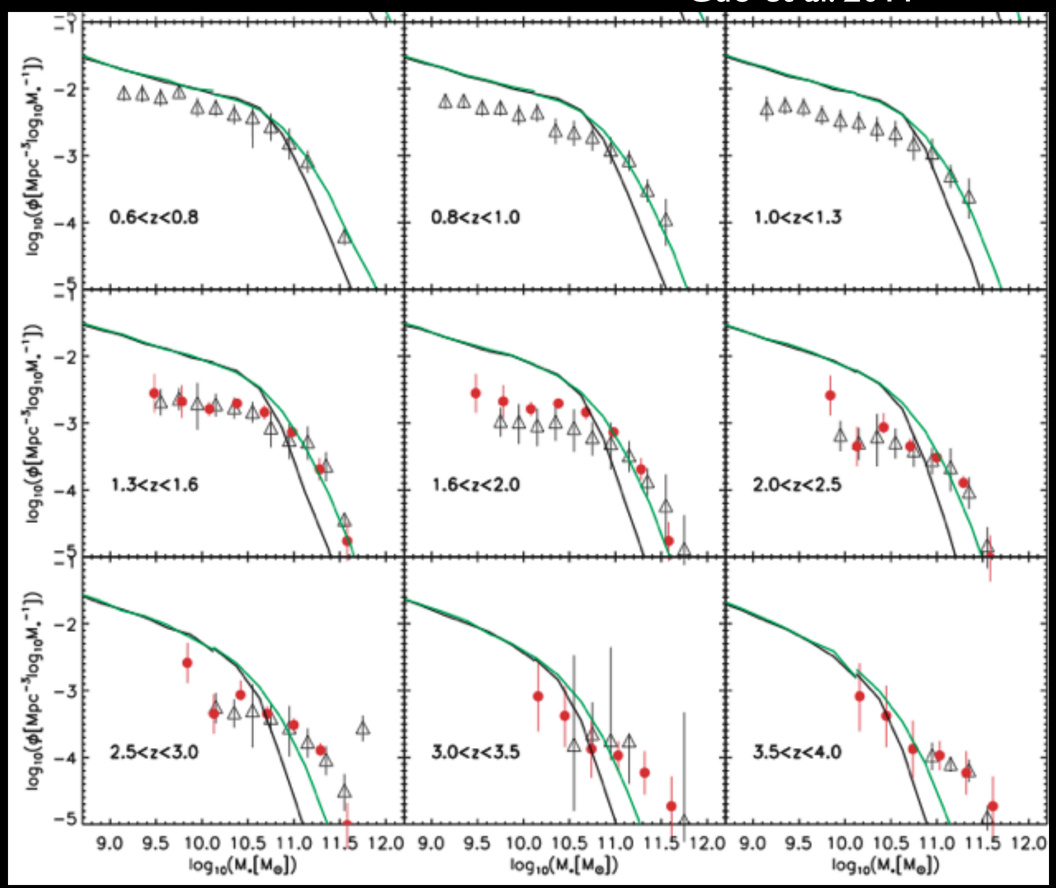

In addition, enhancing the feedback results into inefficient star formationfor given DM halo (suppress L/M).

This seems at variance with observed M_{star}-M relation

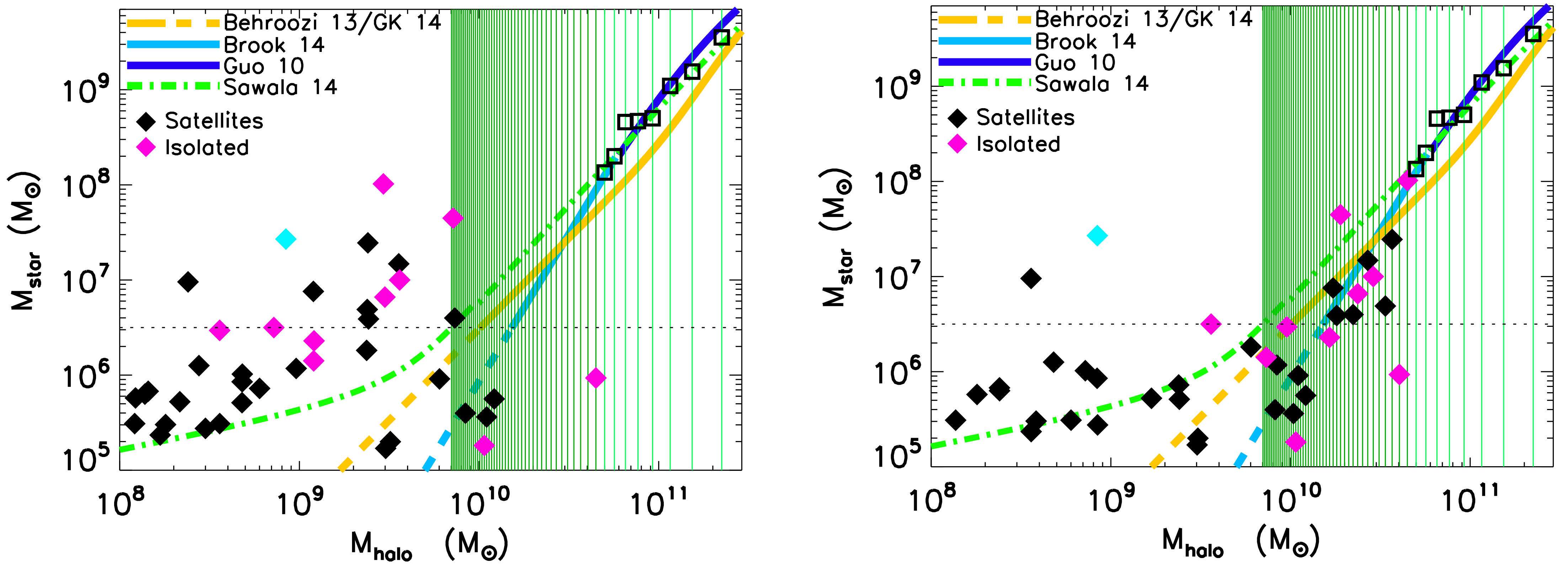

Figure 2. The relation between observed stellar mass and derived halo mass for LG galaxies. The halo mass has been found by fitting kinematical data and assuming two different halo profiles. The results for an NFW profile are shown in the left-hand panel, while the mass-dependent DC14 halo profile has been used in the right-hand panel. Satellites and isolated galaxies are shown in different colours, with Sagittarius dwarf irregular, highly affected by tides, shown in cyan. Several abundance matching predictions are indicated, in particular the Brook et al. (2014) one has been constrained using the LG mass function, and it is shown as dashed line below the observational completeness limit of the LG.

Critical Issues after Including Feedback

Overabundance of low-mass objects

i) abundance of satellite DM haloes
ii) density profiles → Steepen for z>1
iii) abundance of faint galaxies → Persists at high redshift
iv) the M_*-M_{halo} relation → Stems from supressed L/M *(too big to fail problem)*
v) star formation histories of satellites

Galaxy formation in WDM Cosmology

Problem Persists at high redshifts

Too many low-mass structures

Need to suppress Power Spectrum at small scales ?

can WDM solve all problems simultaneously ?

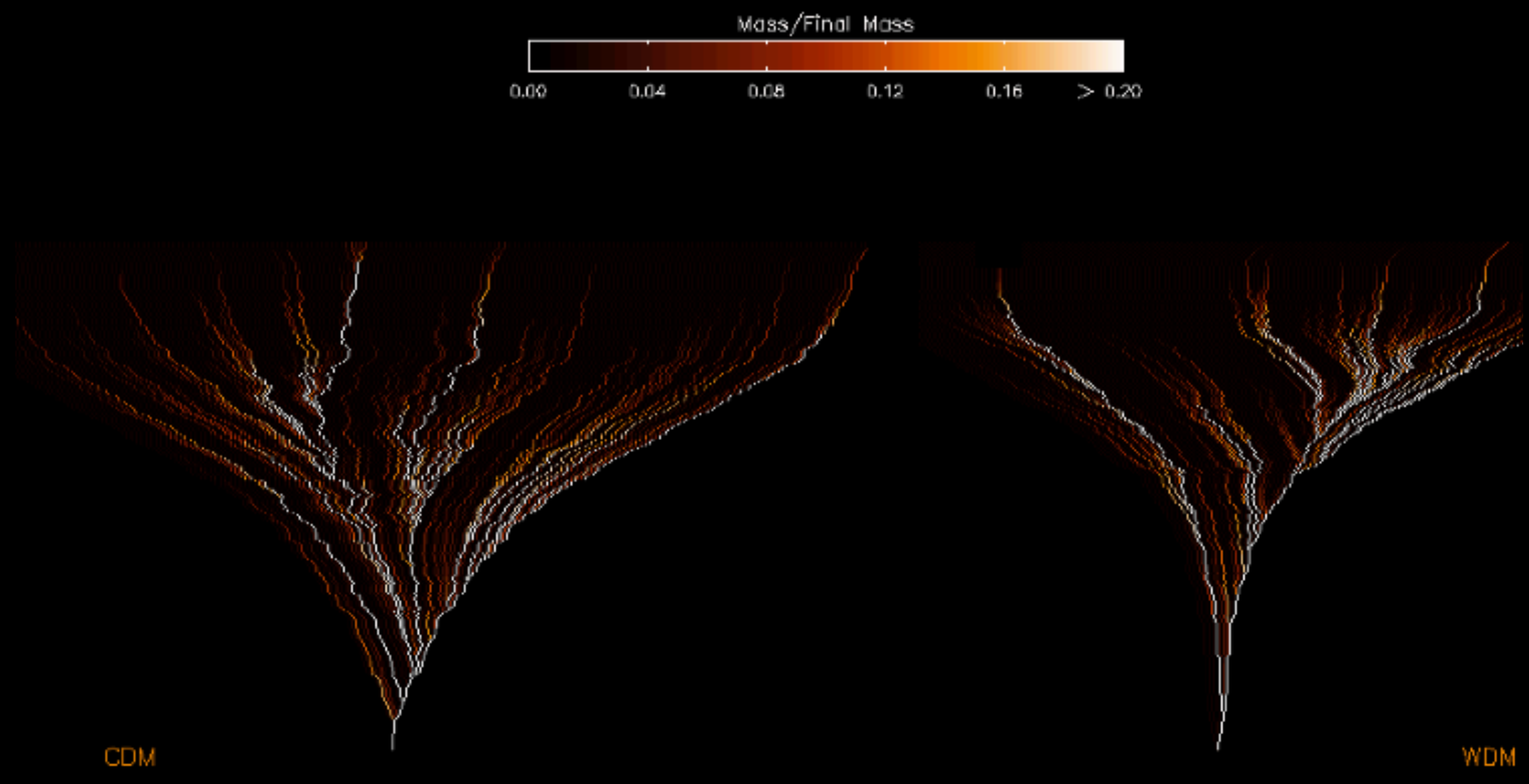

Galaxy formation in WDM Cosmology

Problem Persists at high redshifts

Too many low-mass structures

Need to suppress Power Spectrum at small scales ?

can WDM solve all problems simultaneously ?

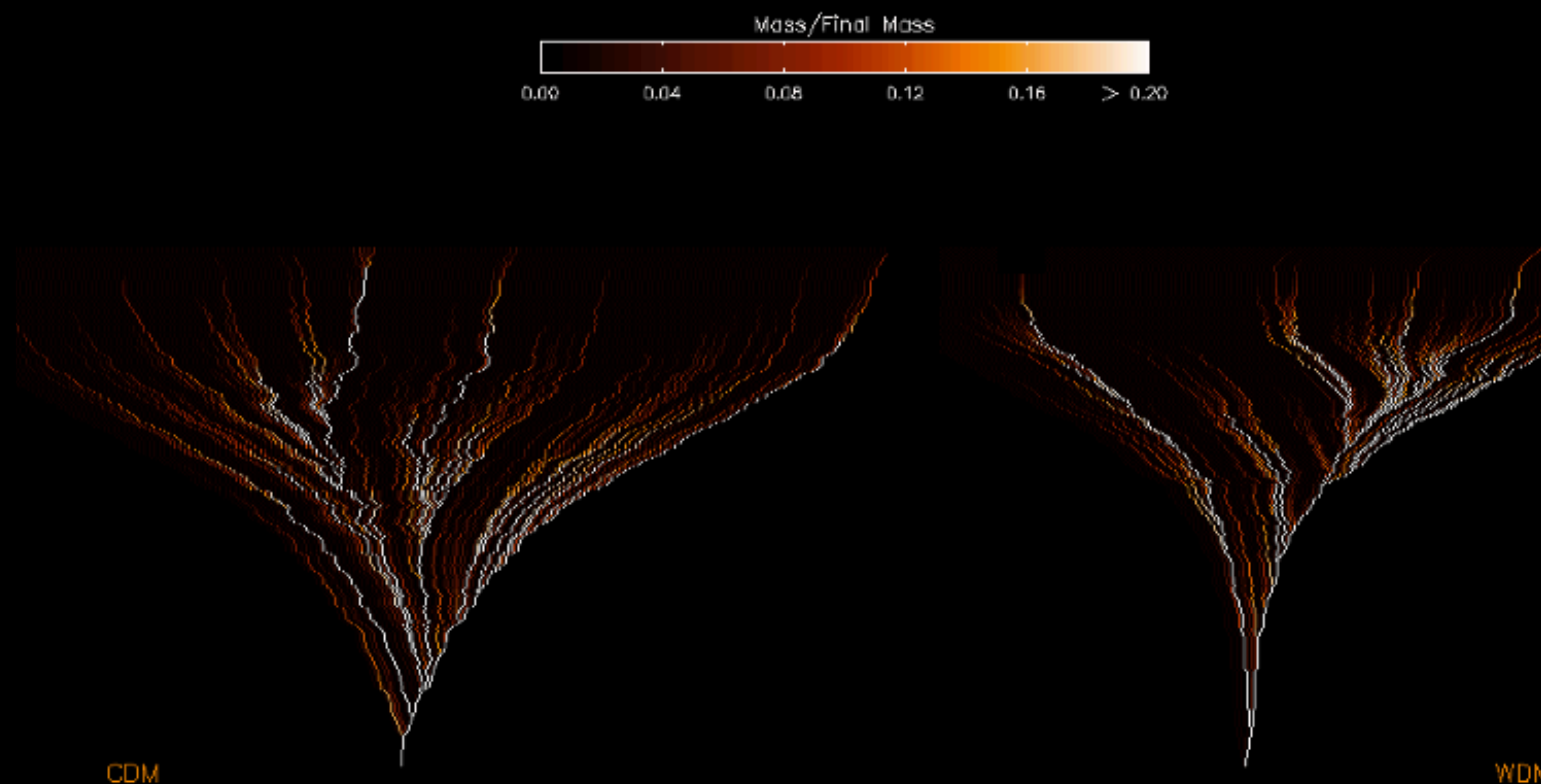

Rome PANDA model

NM, A. Lamstra

Implementing WDM power spectrum in the galaxy formation model

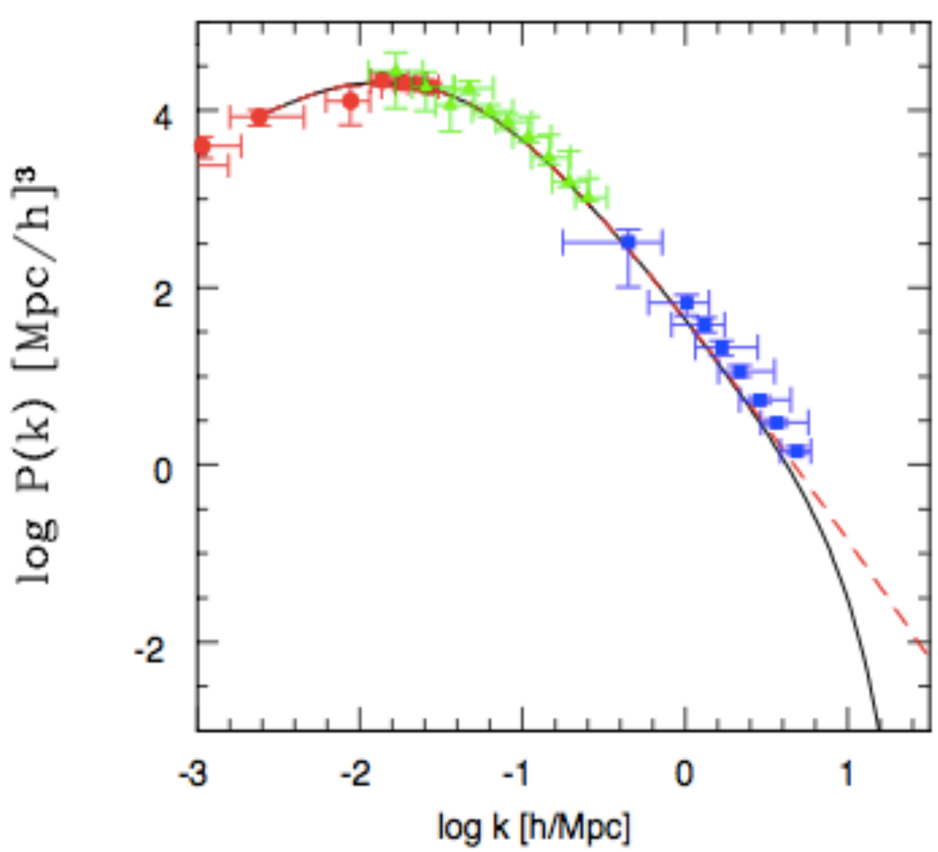

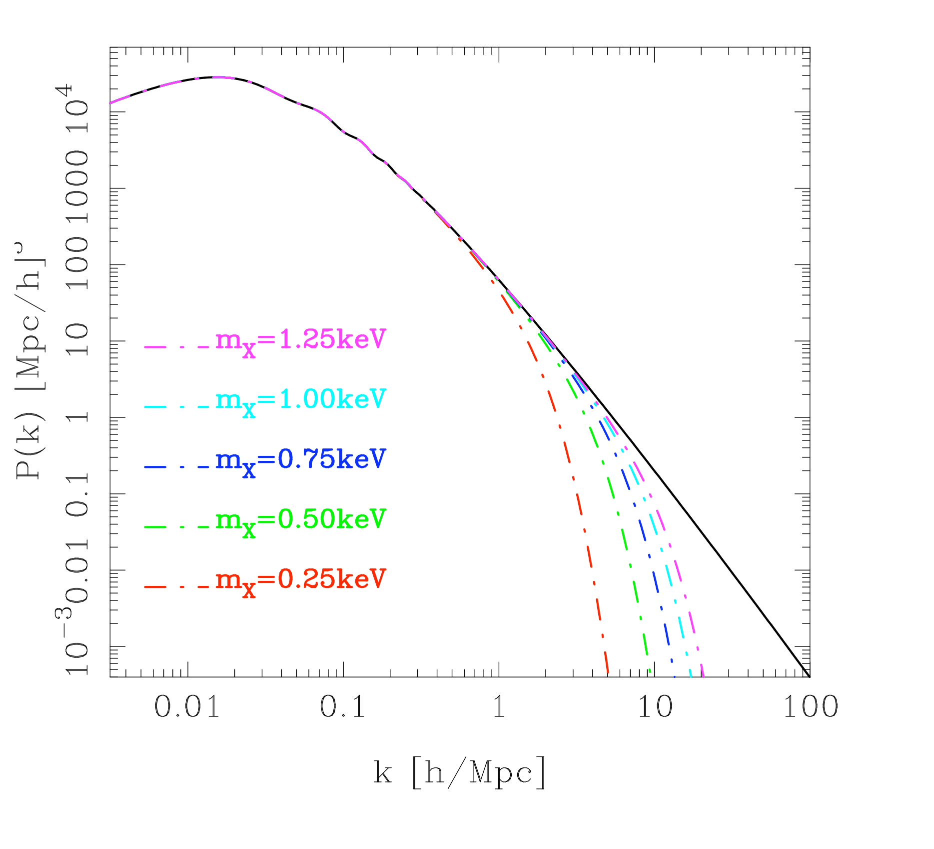

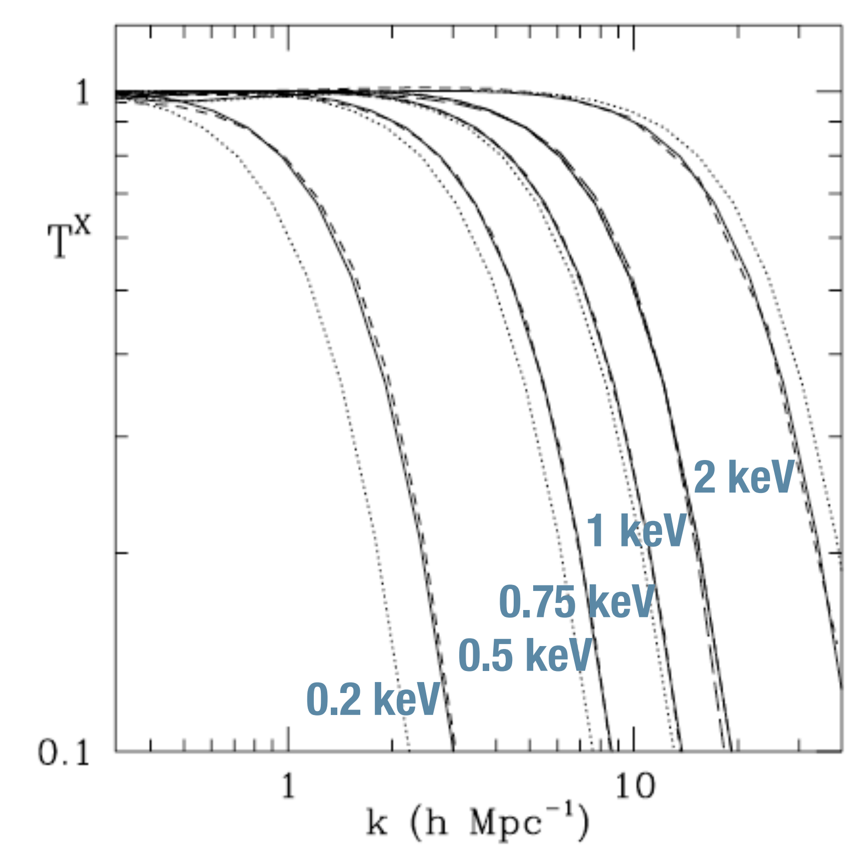

Effect on power-spectrum of assuming (thermal relic) particles with mass m_X.

To comply with existing observations the mass m_X must be in the keV range

$$r_{fs} \approx 0.2 \left[\frac{\Omega_X\, h^2}{0.15}\right]^{1/3} \left[\frac{m_X}{rmkeV}\right]^{-4/3} \mathrm{Mpc} \qquad \frac{P_{WDM}(k)}{P_{CDM}(k)} = \left[1 + (\alpha\, k)^{2\,\mu}\right]^{-5\,\mu}$$

$$\alpha = 0.049 \left[\frac{\Omega_X}{0.25}\right]^{0.11} \left[\frac{m_X}{\mathrm{keV}}\right]^{-1.11} \left[\frac{h}{0.7}\right]^{1.22} h^{-1}\ \mathrm{Mpc}$$

Implementing WDM power spectrum in the galaxy formation model

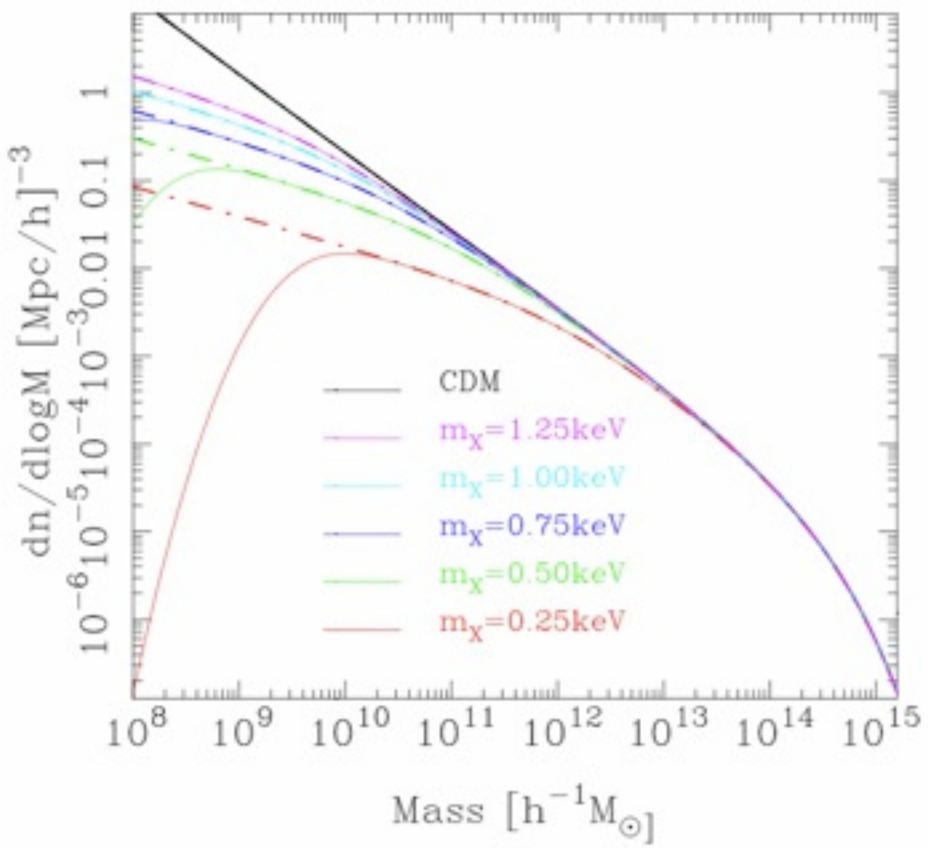

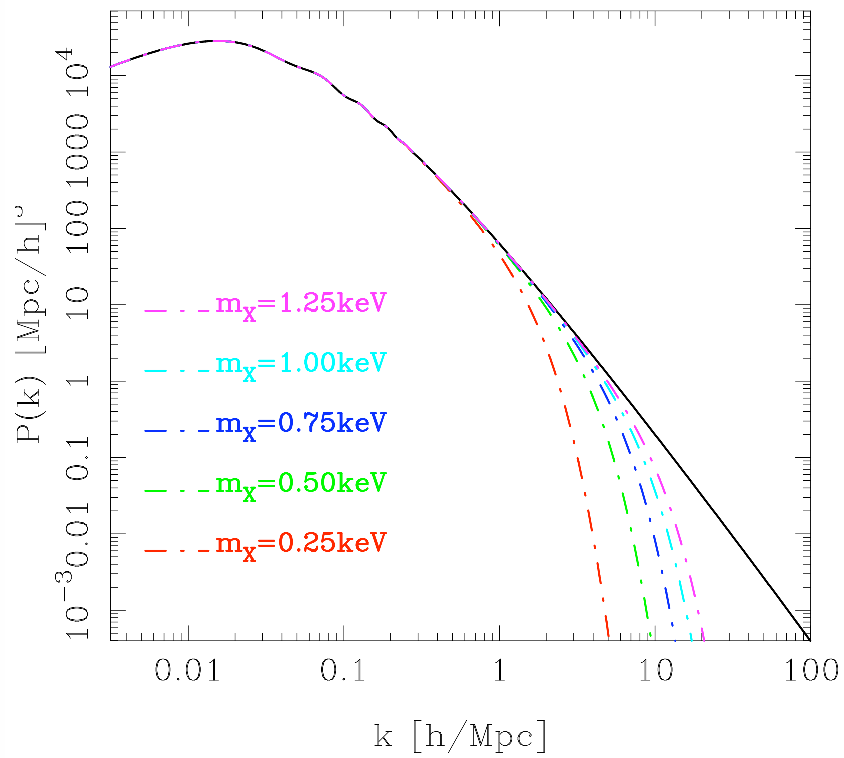

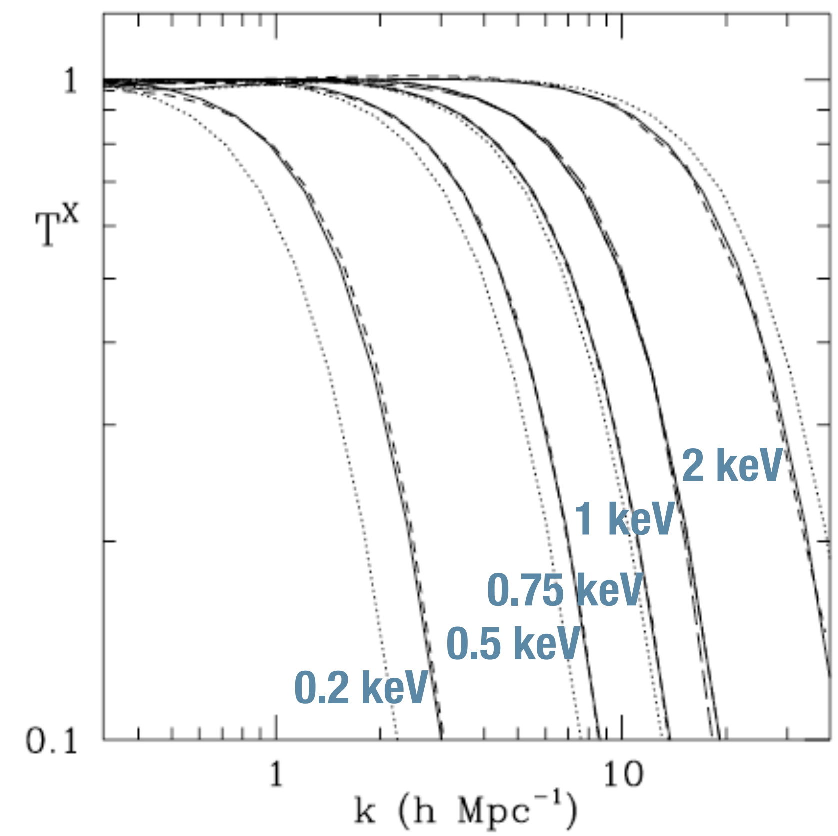

Effect on power-spectrum of assuming (thermal relic) particles with mass m_X.

To comply with existing observations the mass m_X must be in the keV range

$$r_{fs} \approx 0.2 \left[\frac{\Omega_X h^2}{0.15}\right]^{1/3} \left[\frac{m_X}{rmkeV}\right]^{-4/3} \mathrm{Mpc} \qquad \frac{P_{WDM}(k)}{P_{CDM}(k)} = \left[1 + (\alpha\, k)^{2\,\mu}\right]^{-5\,\mu}$$

$$\alpha = 0.049 \left[\frac{\Omega_X}{0.25}\right]^{0.11} \left[\frac{m_X}{\mathrm{keV}}\right]^{-1.11} \left[\frac{h}{0.7}\right]^{1.22} h^{-1}\ \mathrm{Mpc}$$

Implementing WDM power spectrum in the galaxy formation model

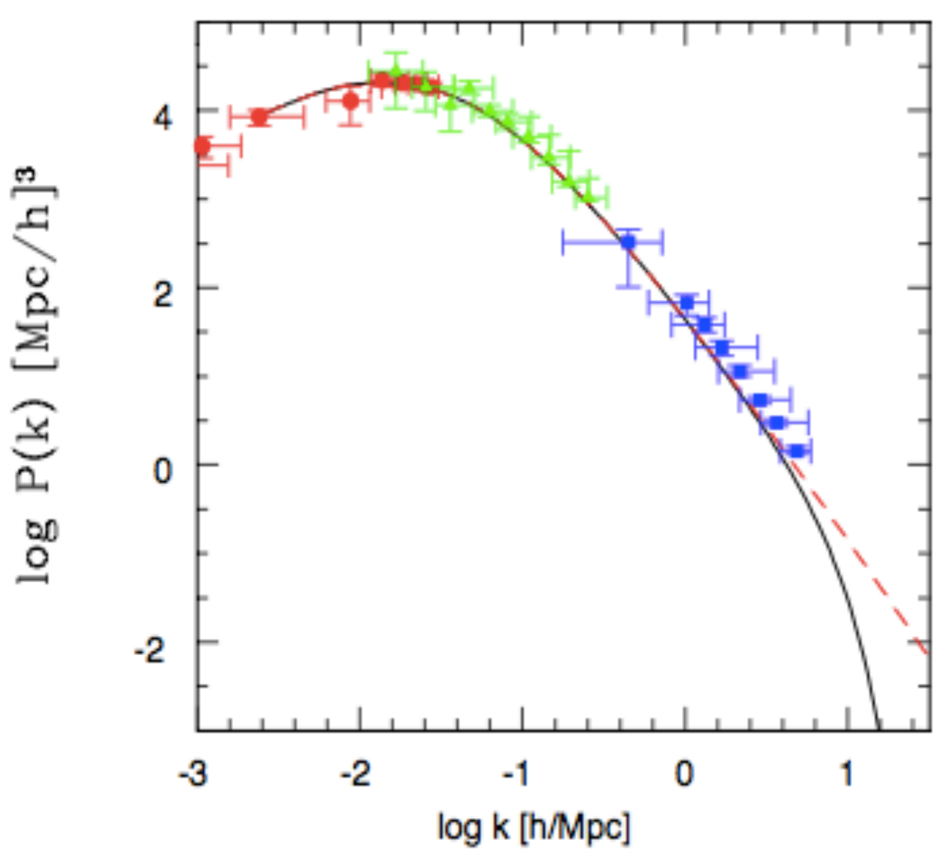

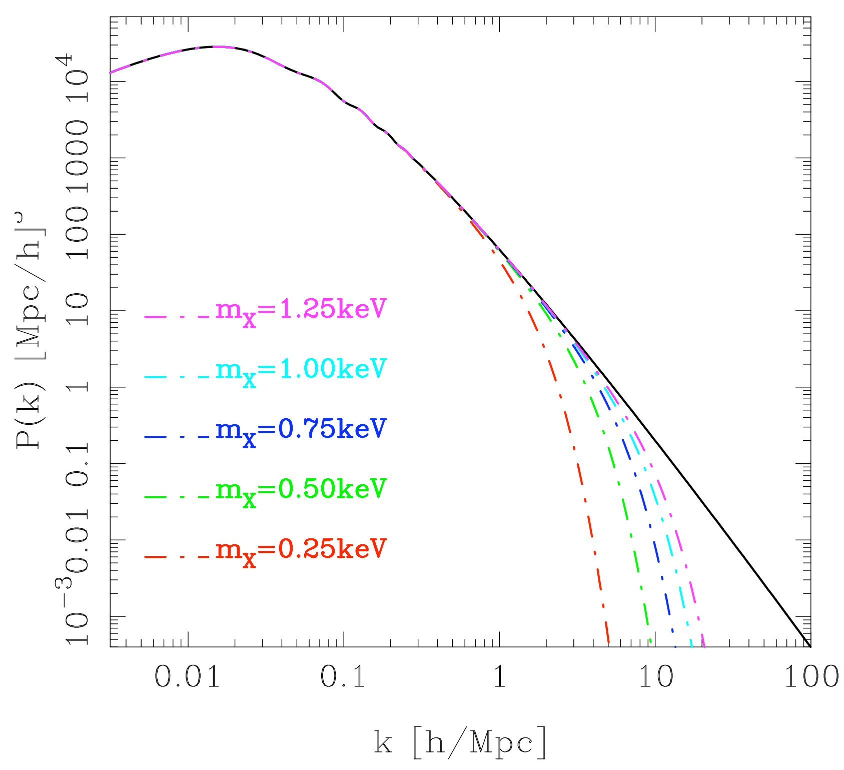

In terms of thermal relic mass

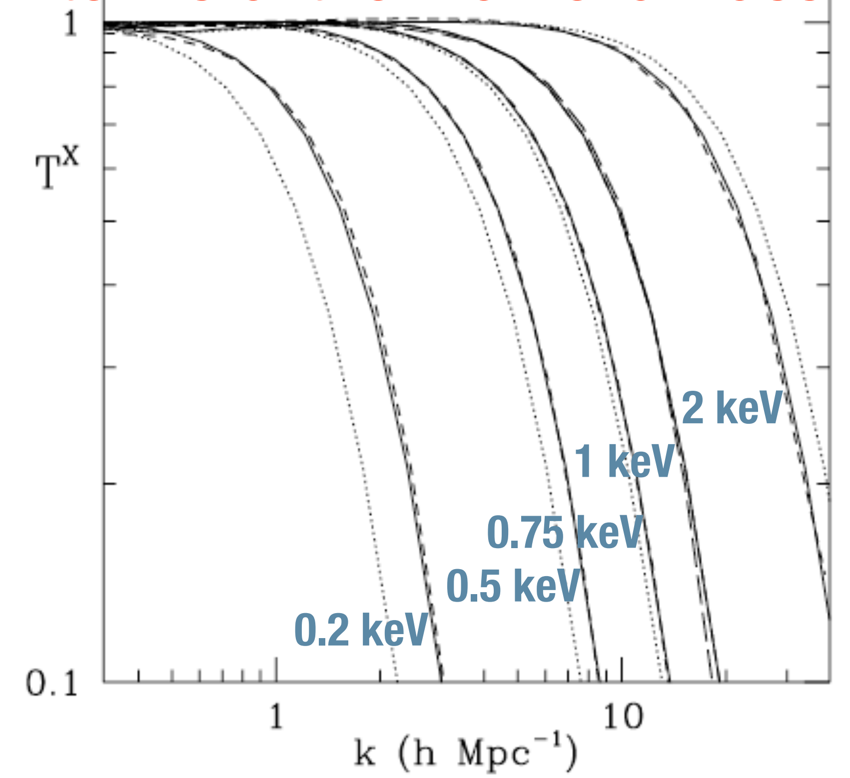

Effect on power-spectrum of assuming (thermal relic) particles wit

To comply with existing observations the mass m_X must be in the k

$$r_{fs} \approx 0.2 \left[\frac{\Omega_X\, h^2}{0.15}\right]^{1/3} \left[\frac{m_X}{rmkeV}\right]^{-4/3} \mathrm{Mpc} \qquad \frac{P_{WDM}(k)}{P_{CDM}(k)} = \left[1 + (\alpha\, k)^{2\,\mu}\right]$$

$$\alpha = 0.049 \left[\frac{\Omega_X}{0.25}\right]^{0.11} \left[\frac{m_X}{\mathrm{keV}}\right]^{-1.11} \left[\frac{h}{0.7}\right]^{1.22} h^{-1}\ \mathrm{Mpc}$$

In terms of resonantly produced sterile neutrinos

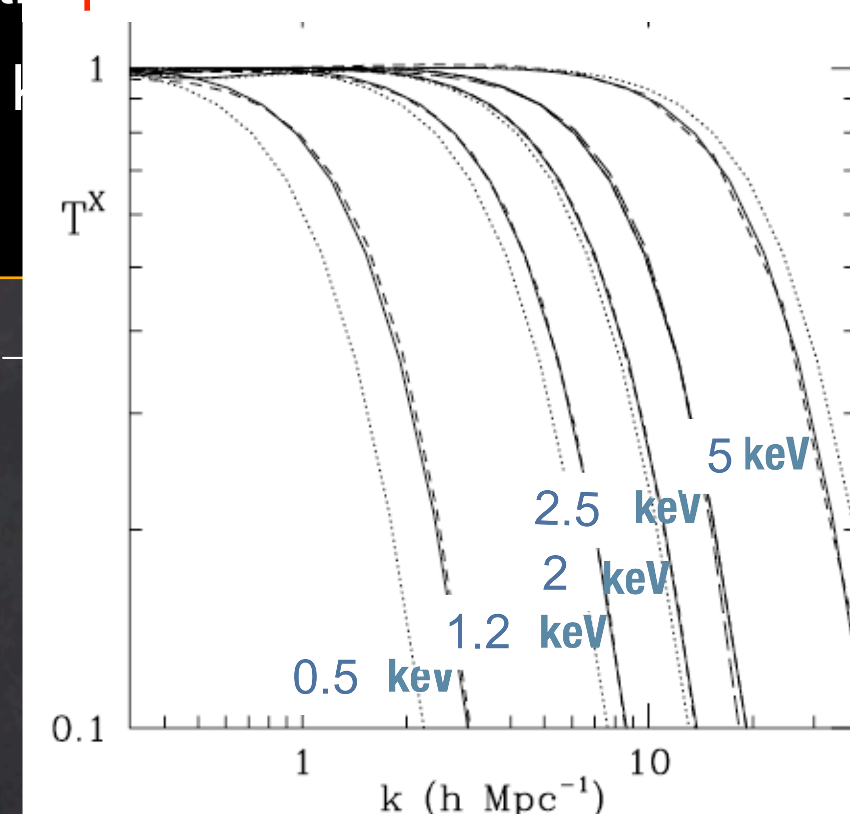

Implementing WDM power spectrum in the galaxy formation model

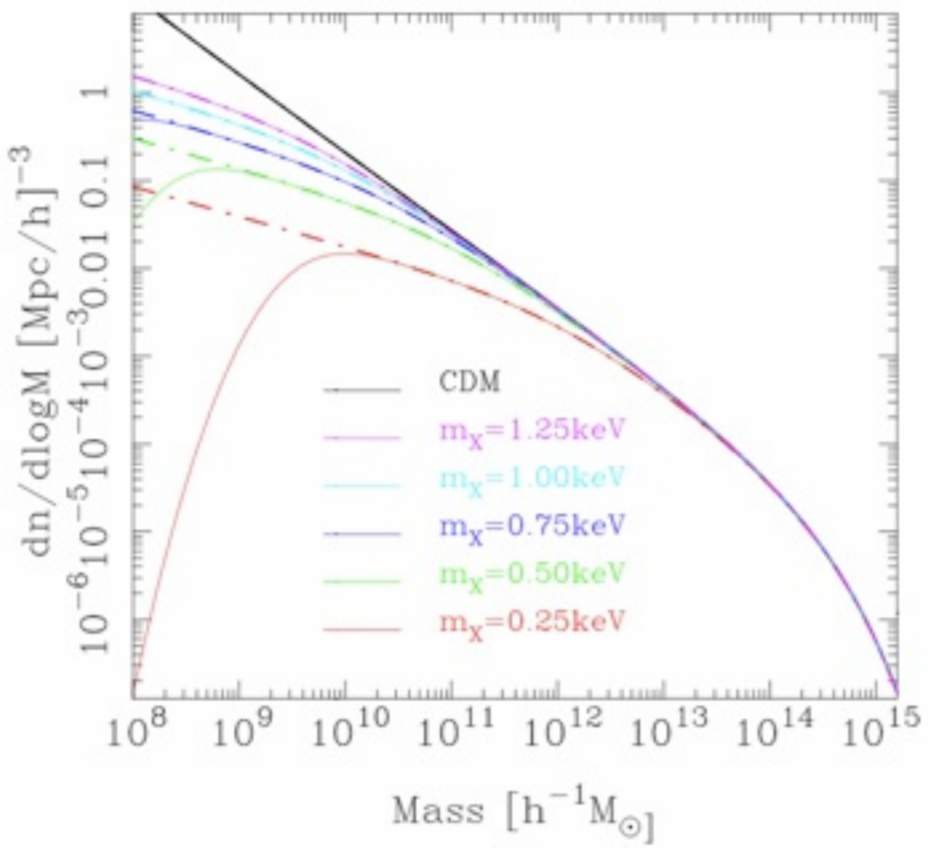

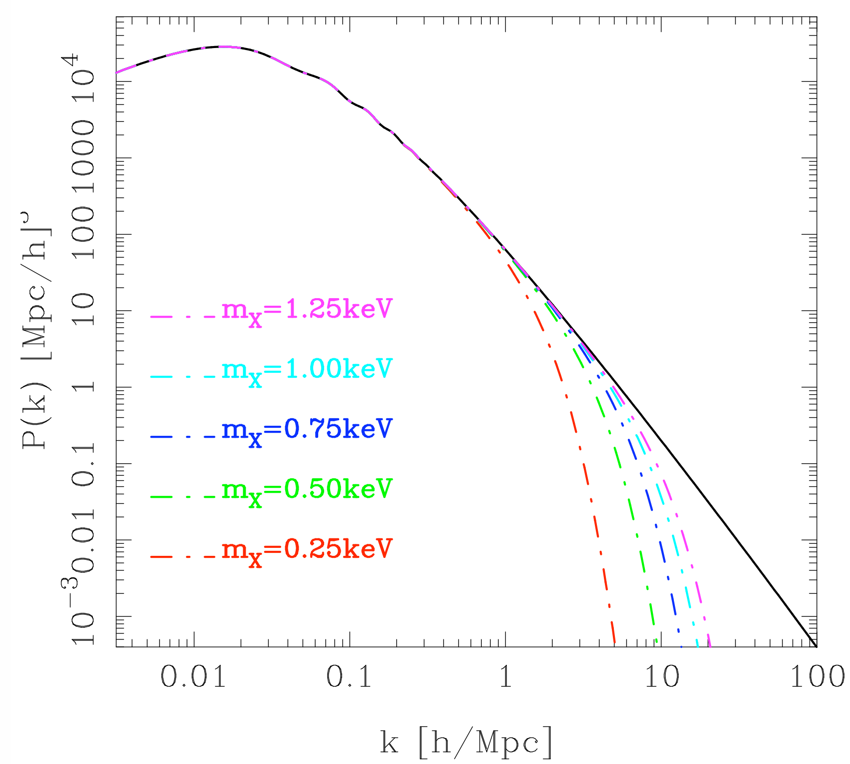

In terms of thermal relic mass

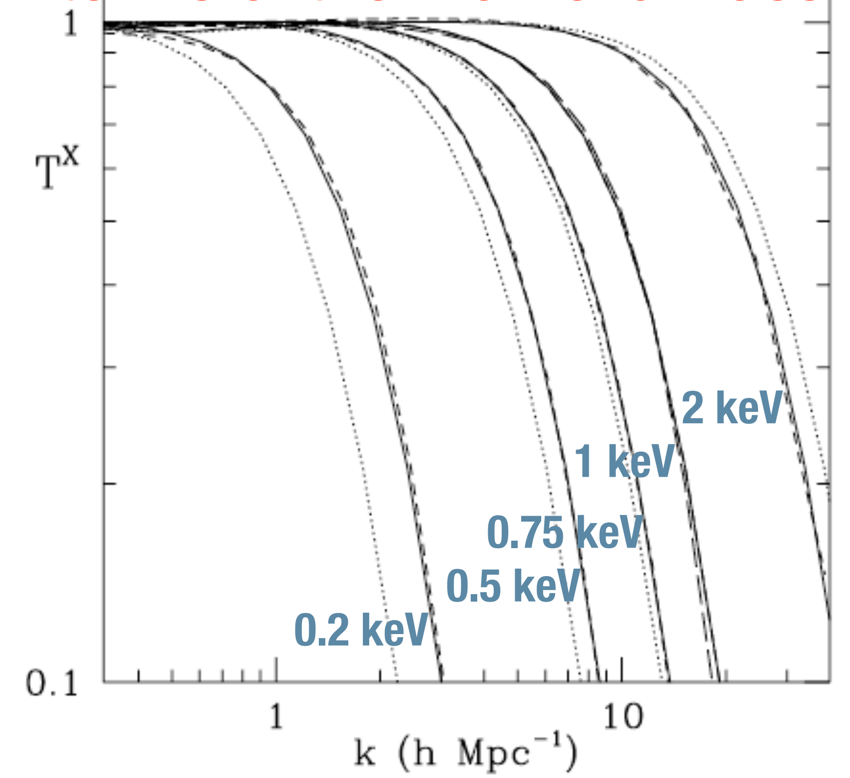

Effect on power-spectrum of assuming (thermal relic) particles wit

To comply with existing observations the mass m_X must be in the k

In terms of resonantly produced sterile neutrinos

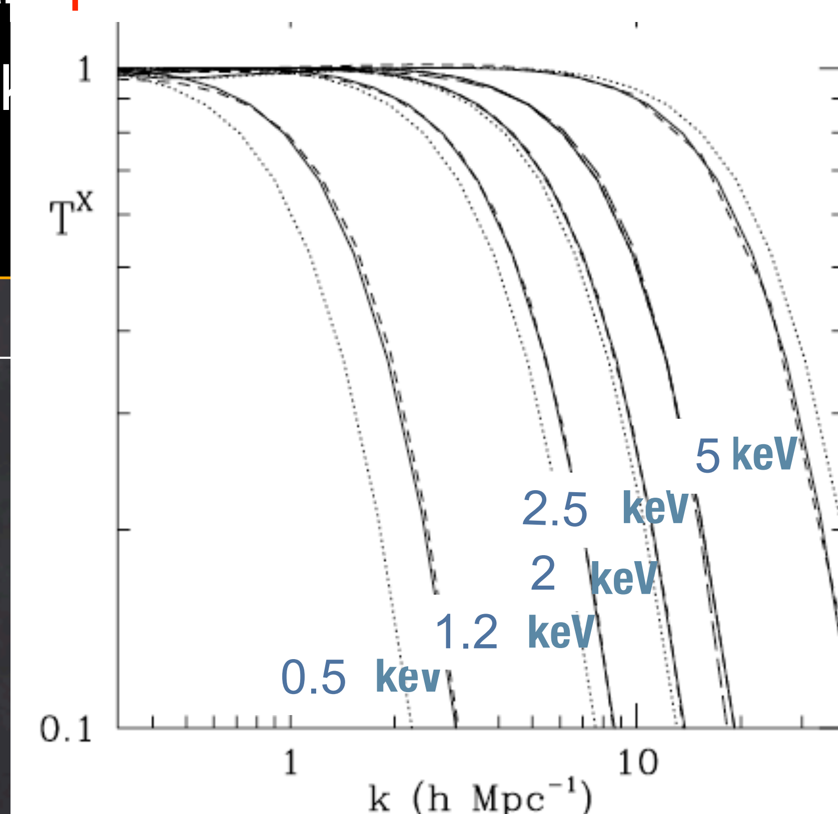

$$r_{fs} \approx 0.2 \left[\frac{\Omega_X h^2}{0.15}\right]^{1/3} \left[\frac{m_X}{rmkeV}\right]^{-4/3} \text{Mpc}$$

$$\frac{P_{WDM}(k)}{P_{CDM}(k)} = \left[1 + (\alpha\, k)^{2\,\mu}\right]$$

$$\alpha = 0.049 \left[\frac{\Omega_X}{0.25}\right]^{0.11} \left[\frac{m_X}{\text{keV}}\right]^{-1.11} \left[\frac{h}{0.7}\right]^{1.22} h^{-1}\ \text{Mpc}$$

Implementing WDM power spectrum in the galaxy formation model

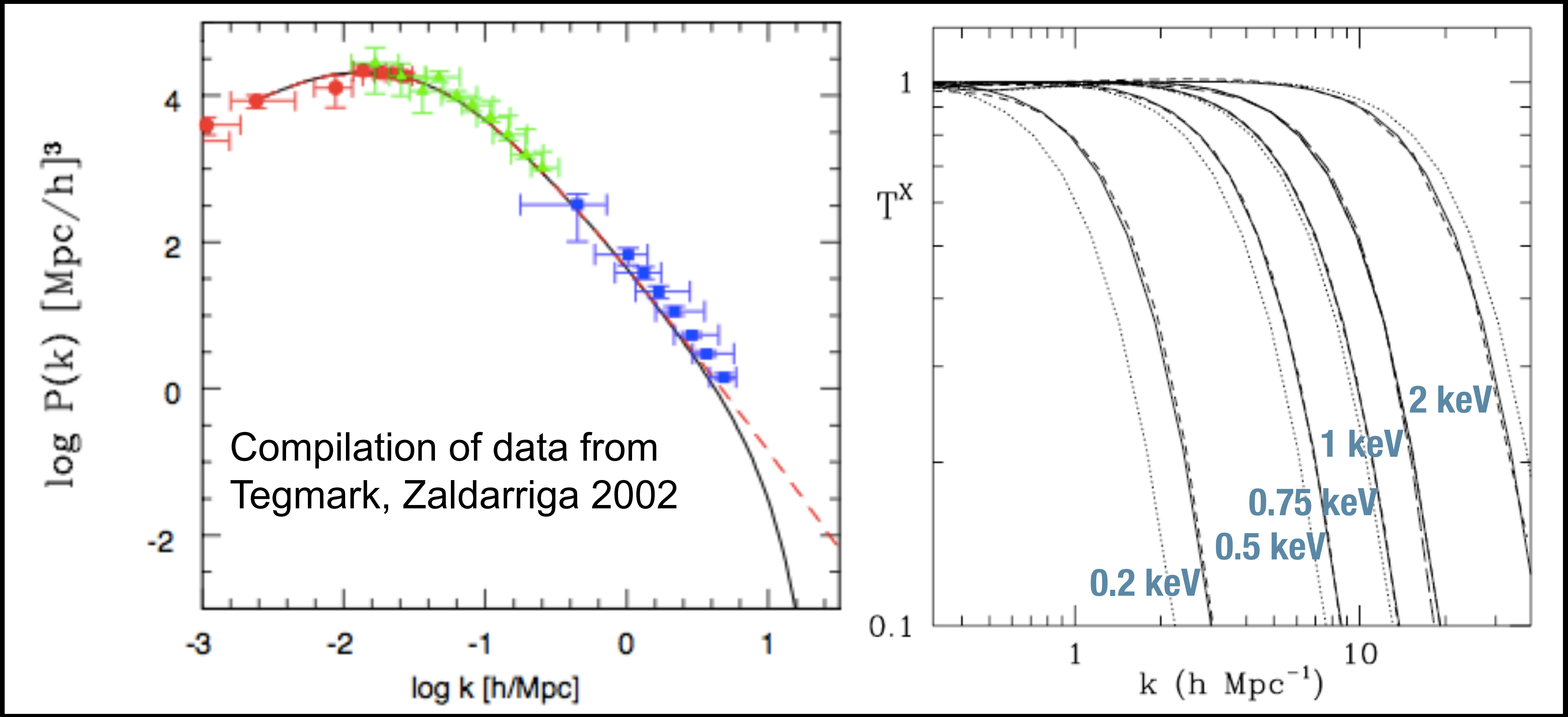

$$r_{fs} \approx 0.2 \left[\frac{\Omega_X\, h^2}{0.15}\right]^{1/3} \left[\frac{m_X}{rmkeV}\right]^{-4/3} \mathrm{Mpc} \qquad \frac{P_{WDM}(k)}{P_{CDM}(k)} = \left[1 + (\alpha\, k)^{2\,\mu}\right]^{-5\,\mu}$$

$$\alpha = 0.049 \left[\frac{\Omega_X}{0.25}\right]^{0.11} \left[\frac{m_X}{\mathrm{keV}}\right]^{-1.11} \left[\frac{h}{0.7}\right]^{1.22} h^{-1}\ \mathrm{Mpc}$$

Implementing WDM power spectrum in the galaxy formation model

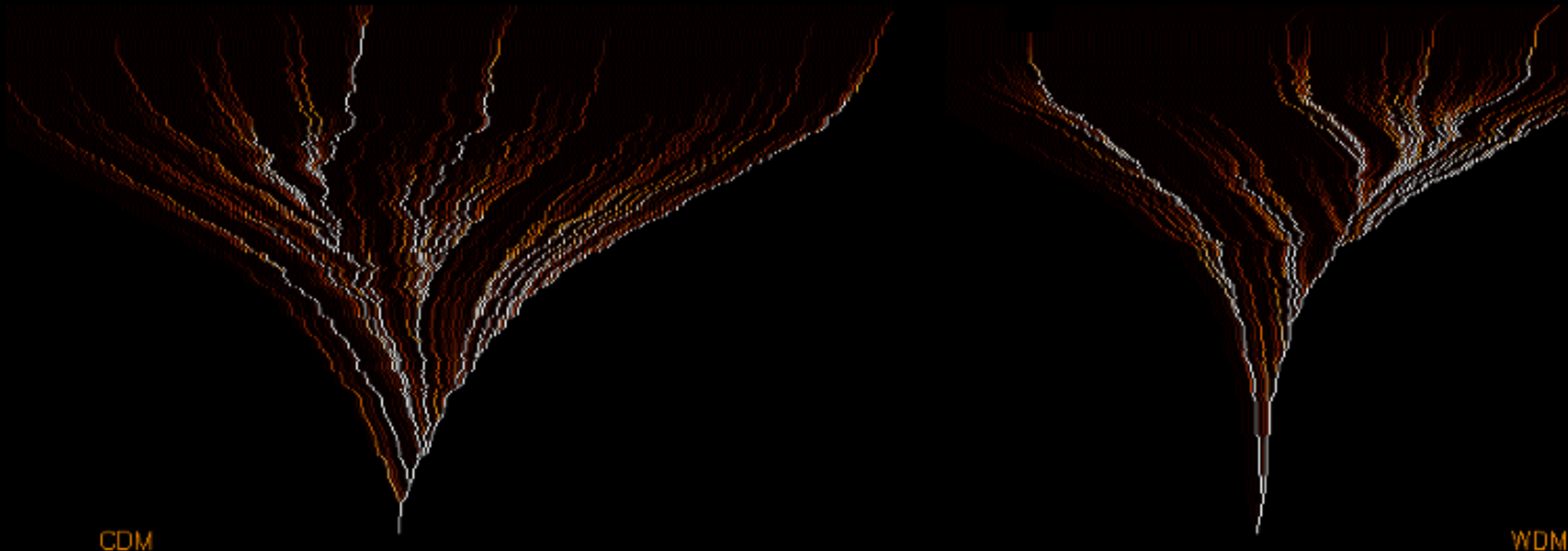

$$r_{fs} \approx 0.2 \left[\frac{\Omega_X\, h^2}{0.15}\right]^{1/3} \left[\frac{m_X}{rmkeV}\right]^{-4/3} \mathrm{Mpc} \qquad \frac{P_{WDM}(k)}{P_{CDM}(k)} = \left[1 + (\alpha\, k)^{2\,\mu}\right]^{-5\,\mu}$$

$$\alpha = 0.049 \left[\frac{\Omega_X}{0.25}\right]^{0.11} \left[\frac{m_X}{\mathrm{keV}}\right]^{-1.11} \left[\frac{h}{0.7}\right]^{1.22} h^{-1}\ \mathrm{Mpc}$$

Implementing WDM power spectrum in the galaxy formation model

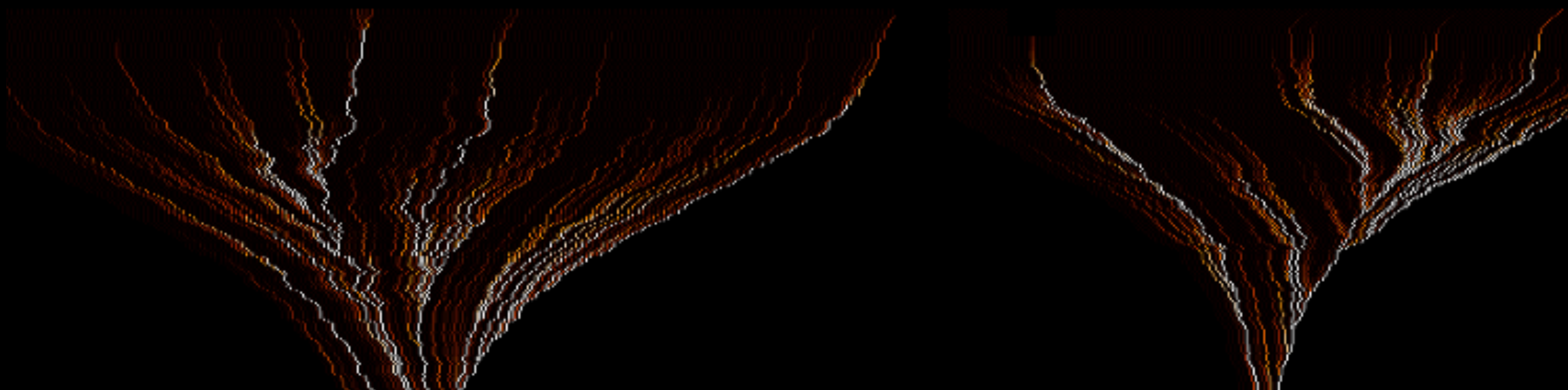

Halo Properties	Gas Properties	Star Formation	Gas Heating (feedback)	Evolution of stellar populations
Density Profiles Virial Temperature	Profiles Cooling - Heating Collapse Disk formation		SNae UV background	

WDM

Galaxy formation in WDM implies computing how modifications of the power spectrum propagate to the above processes

$$r_{fs} \approx 0.2 \left[\frac{\Omega_X\, h^2}{0.15}\right]^{1/3} \left[\frac{m_X}{rmkeV}\right]^{-4/3} \mathrm{Mpc} \qquad \frac{P_{WDM}(k)}{P_{CDM}(k)} = \left[1 + (\alpha\, k)^{2\,\mu}\right]^{-5\,\mu}$$

$$\alpha = 0.049 \left[\frac{\Omega_X}{0.25}\right]^{0.11} \left[\frac{m_X}{\mathrm{keV}}\right]^{-1.11} \left[\frac{h}{0.7}\right]^{1.22} h^{-1}\ \mathrm{Mpc}$$

WDM particle mass ~ kev

Galaxy Formation in WDM cosmology (m_{WDM}~1 keV)

NM et al. 2012-2013

Evolution

local lum. and stell. mass distributions

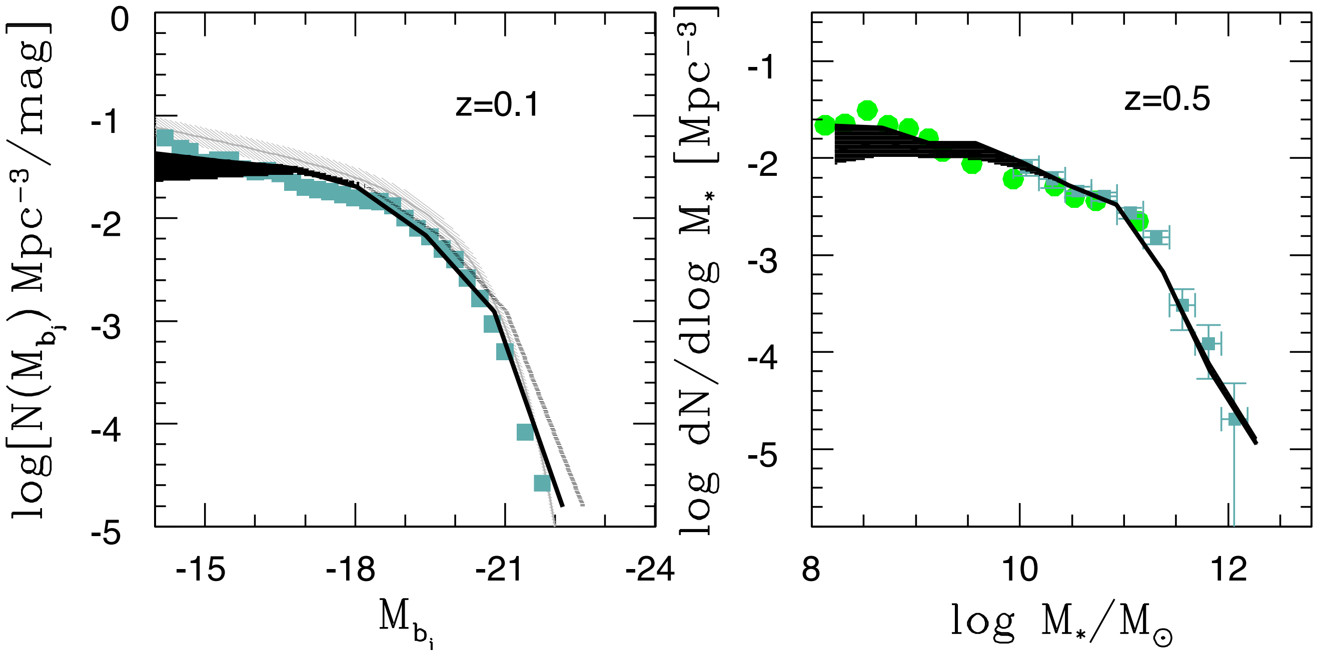

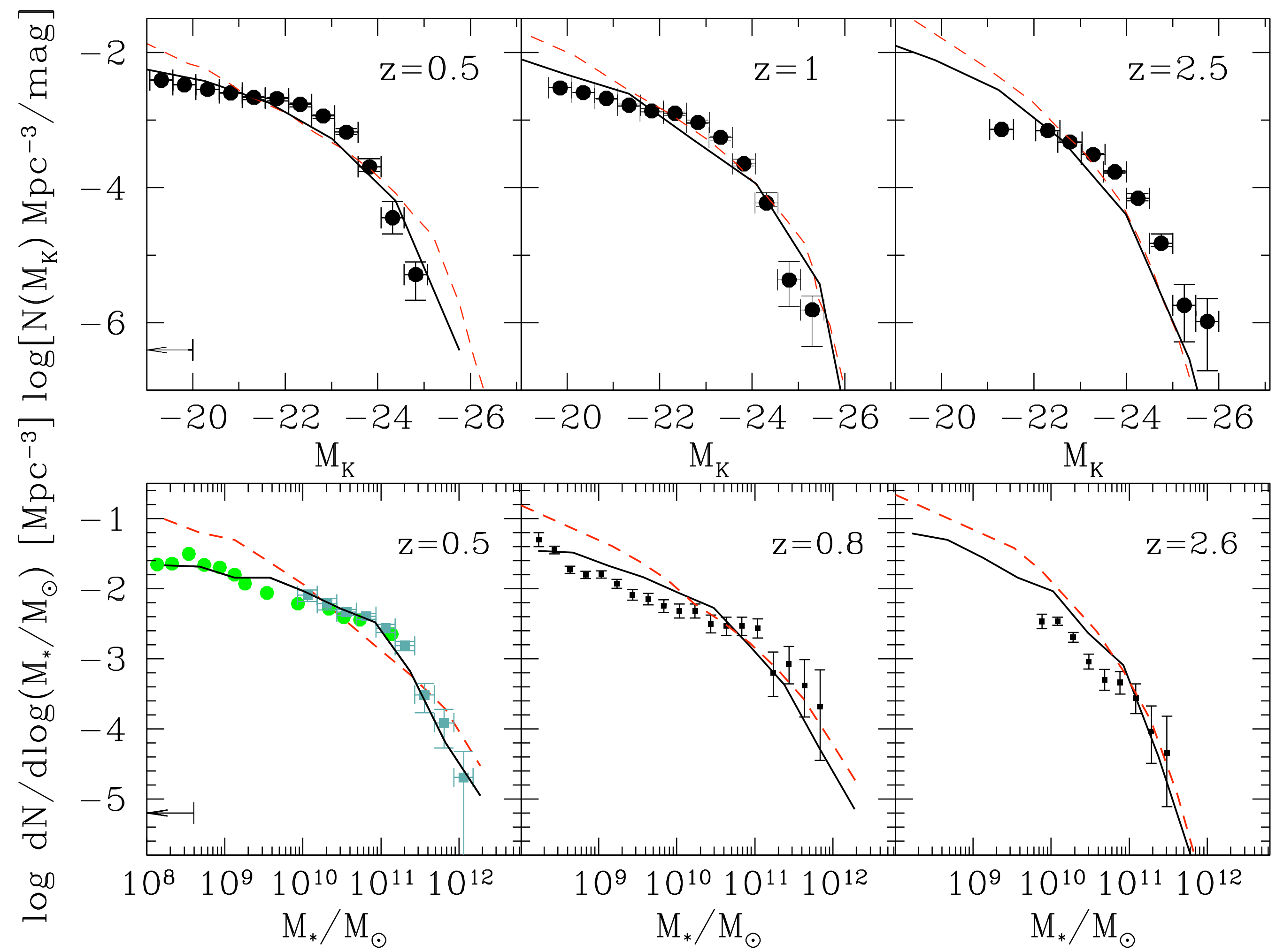

High-z (z=4) lum. distributions

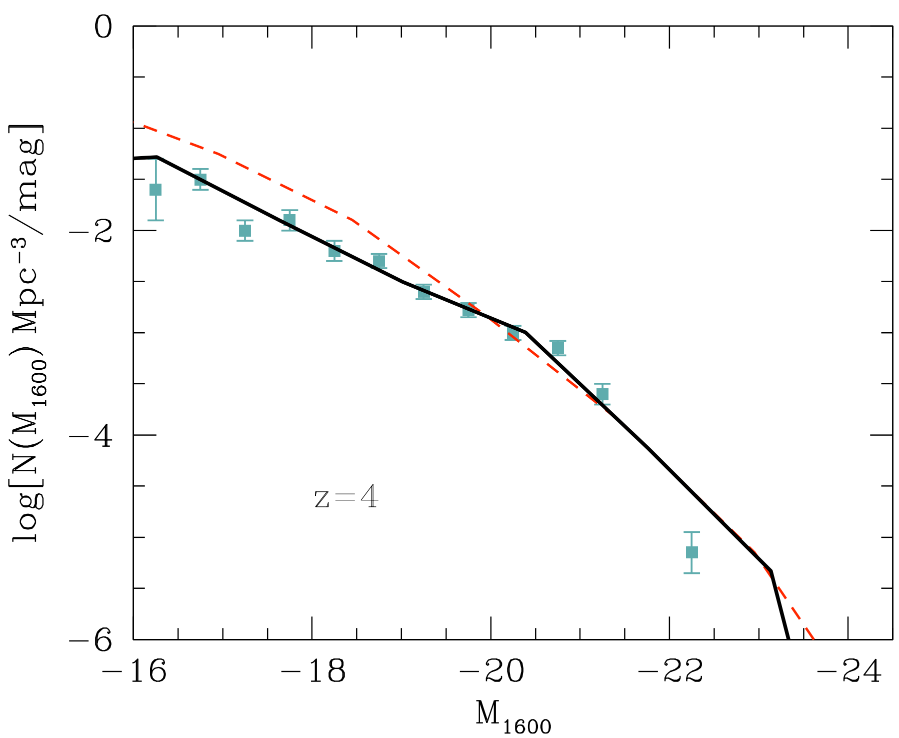

color distributions

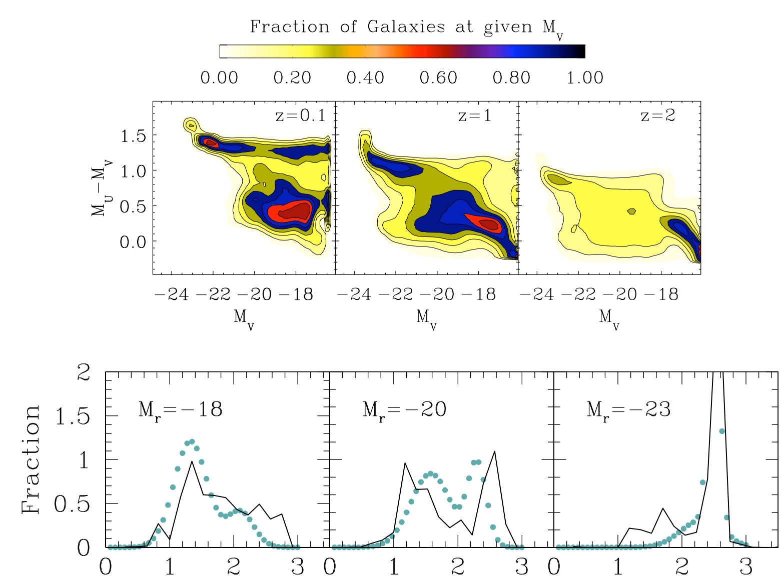

Density profiles & Rotation curves in WDM

Density Profiles

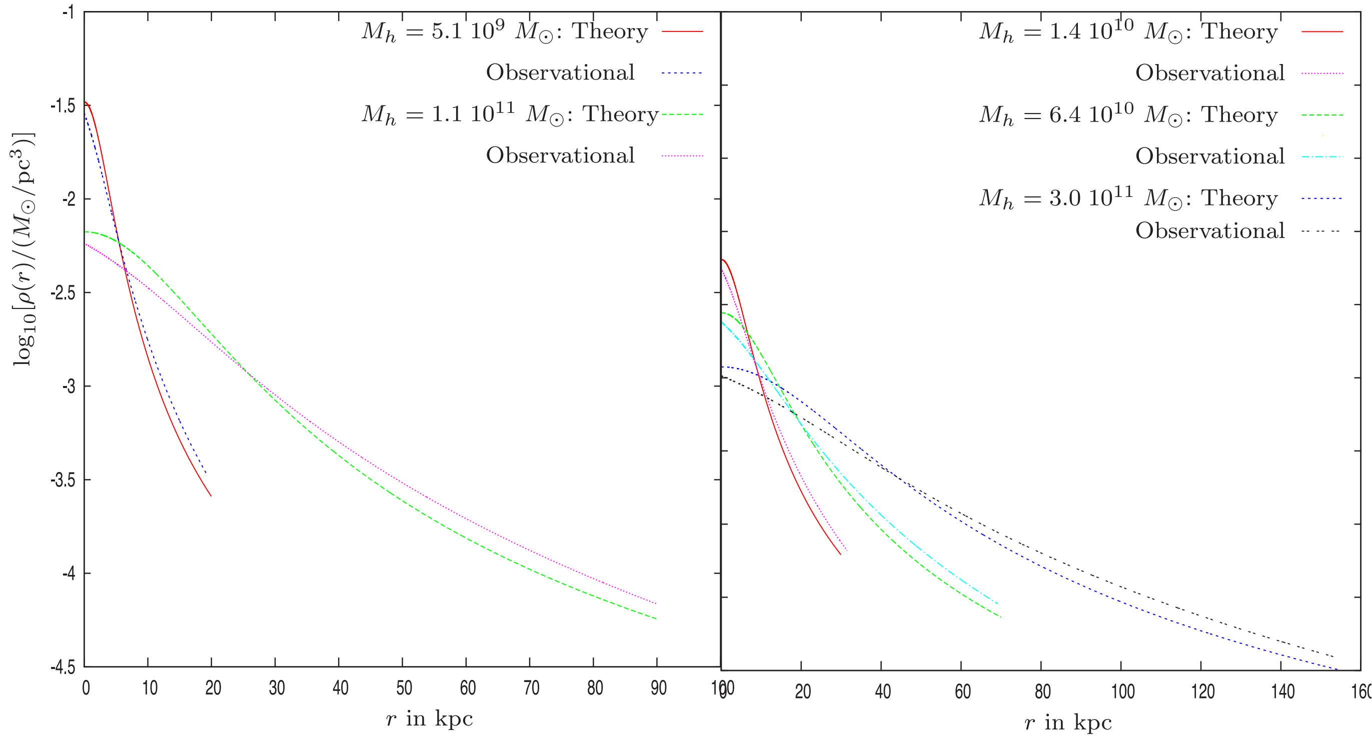

Rotation Curves

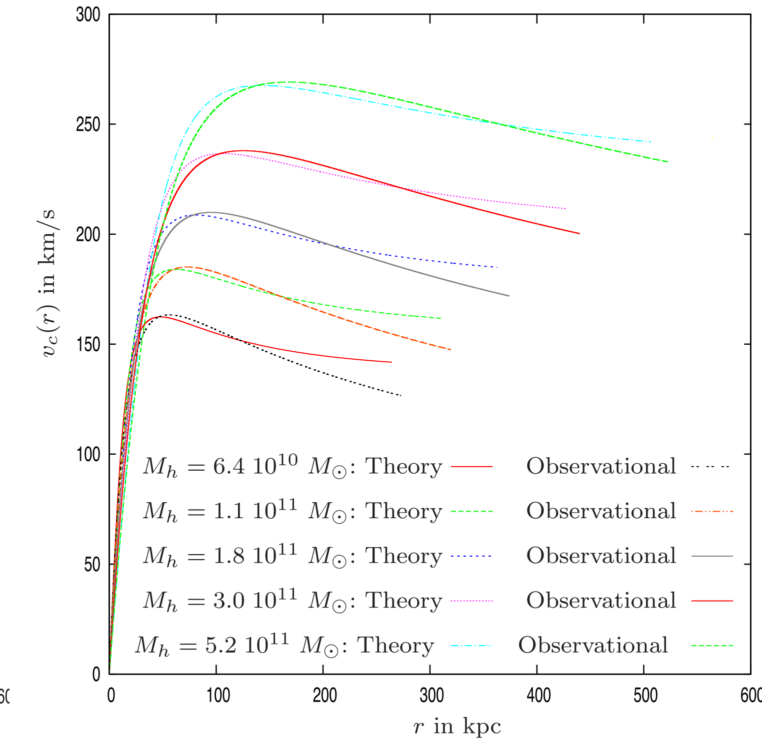

De Vega, Salucci, Sanchez 2014, Fermionic WDM

Abundance of low-mass Milky-Way satellites

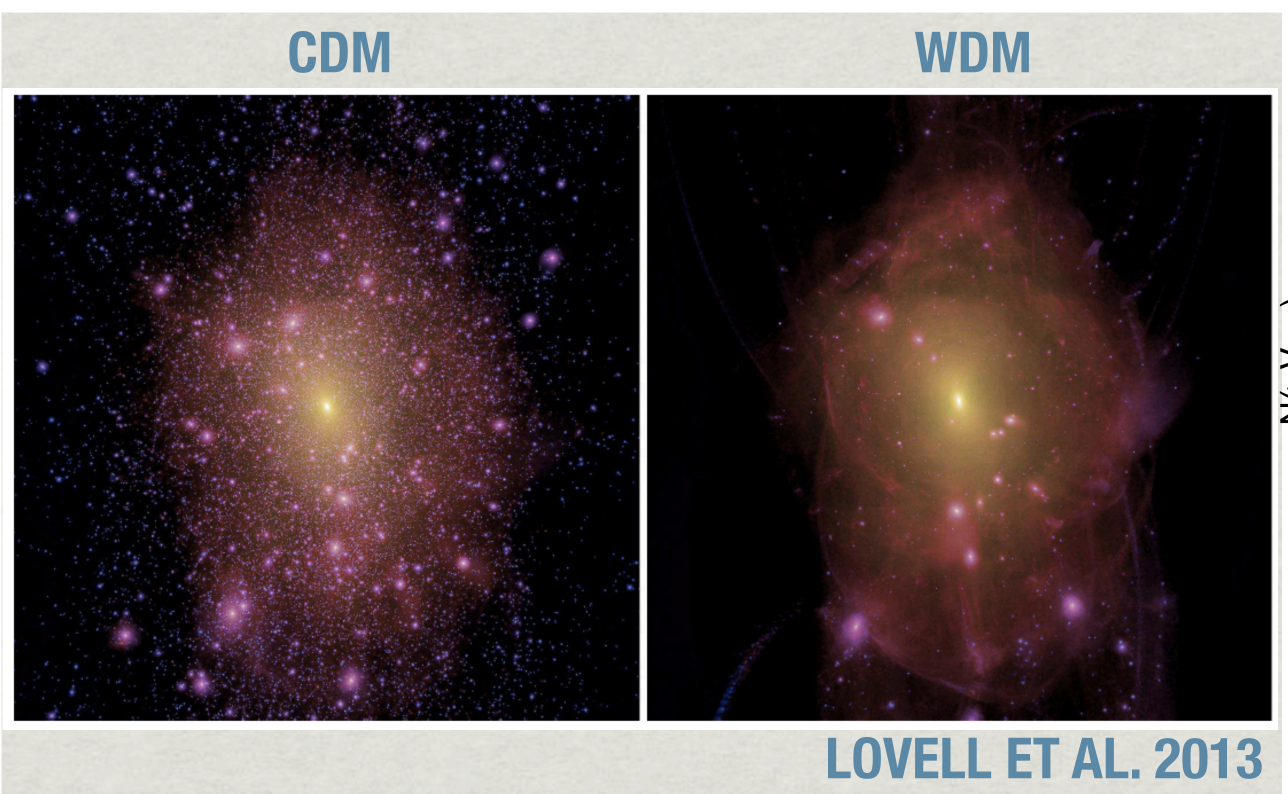

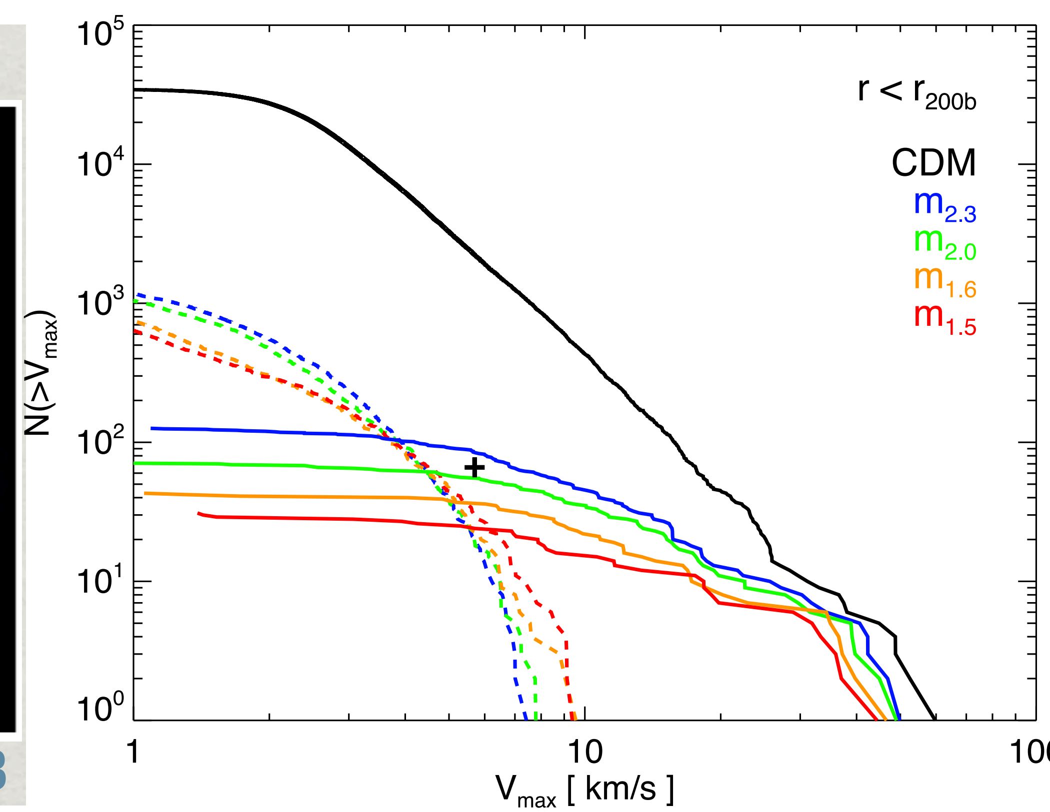

Luminosity Function of Satellite Galaxies, Beyond the Milky-Way

Is Milky Way representative of $M_{halo} \approx 10^{12}\ M_\odot$?

Compare with a wide set of satellites/host halos through the satellite luminosity function

ACS F814W imaging of the COSMOS field,

identify satellites as much as a thousand times fainter than their host galaxies and as close as 0.3 (1.4) arcsec (kpc)and as close as 0.3 (1.4) arcsec (kpc)

Hundreds of hosts

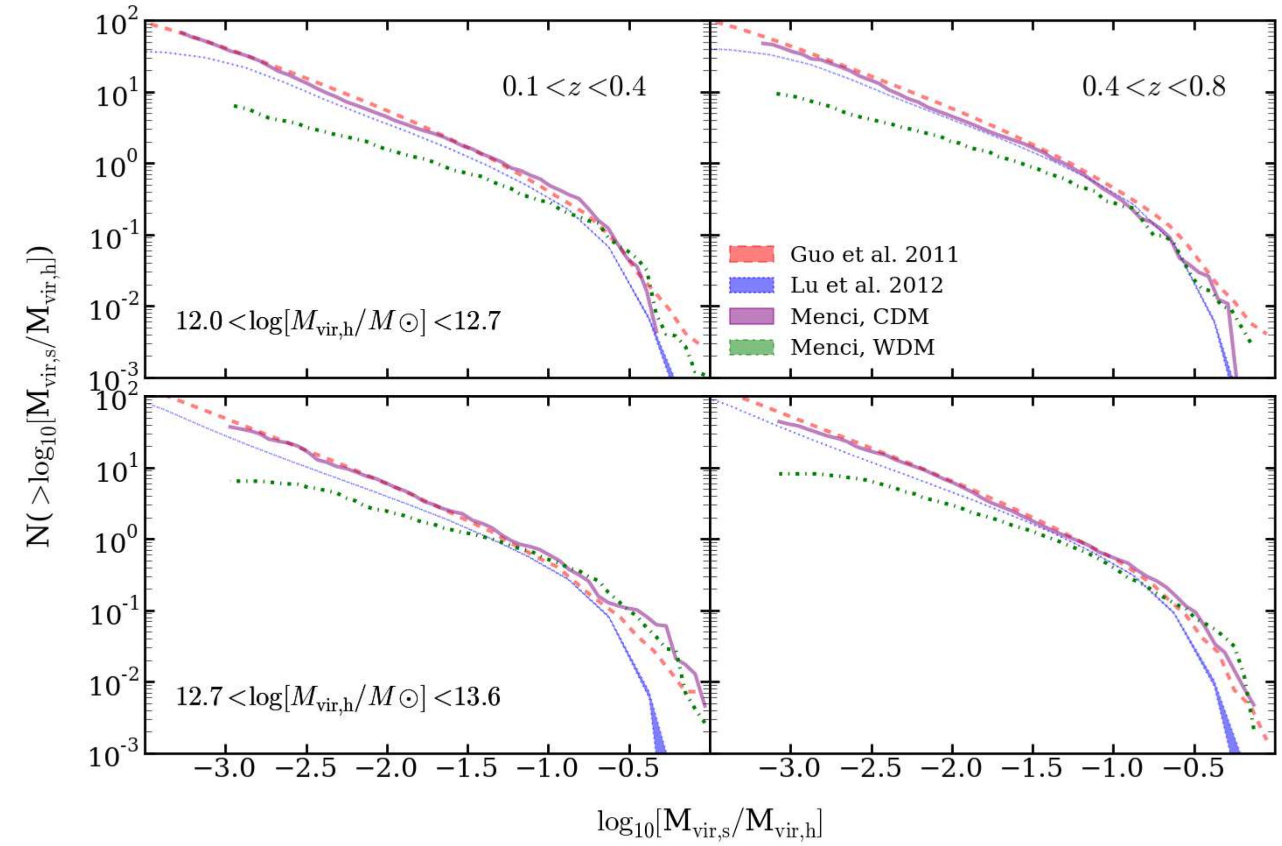

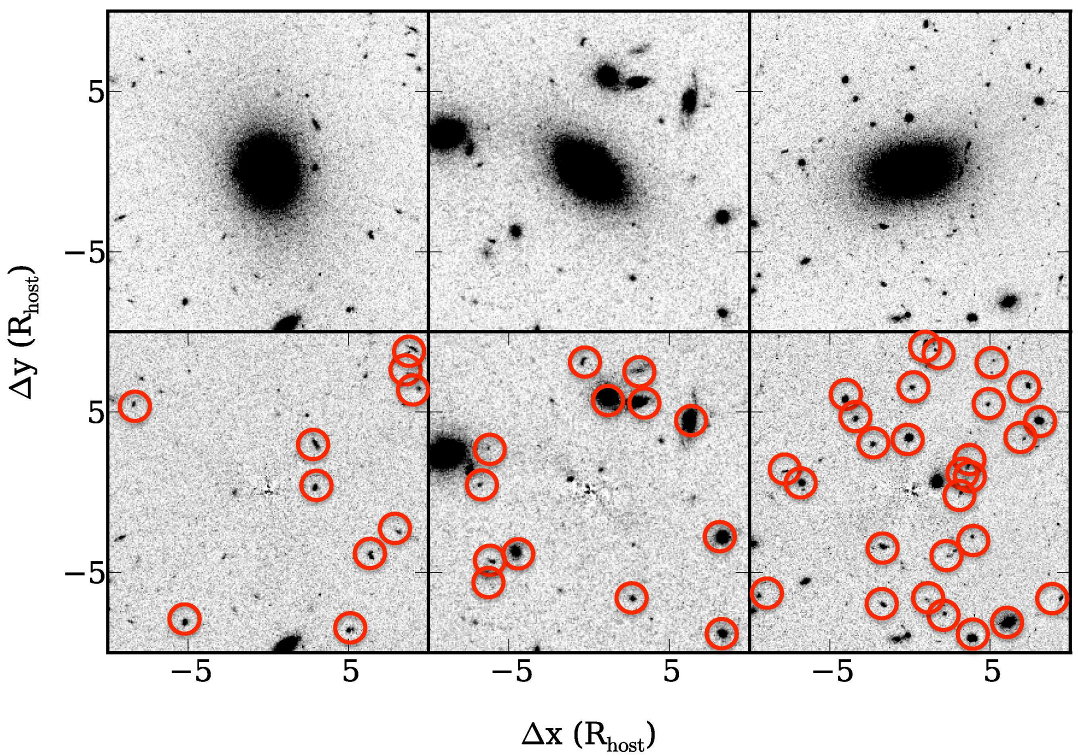

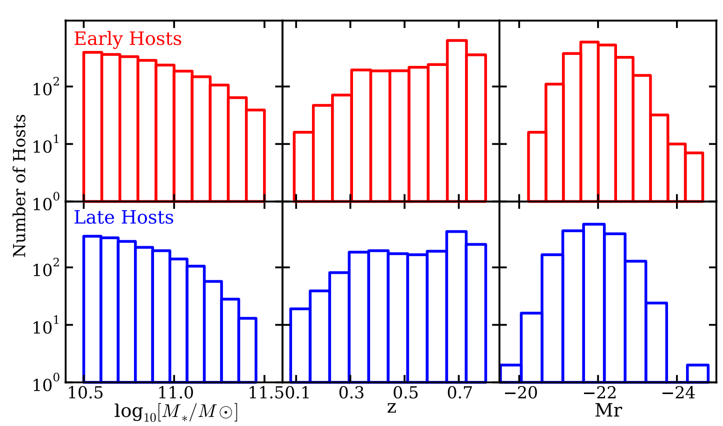

The luminosity distribution of Satellite Galaxies
Nierenberg, Treu, NM 2013

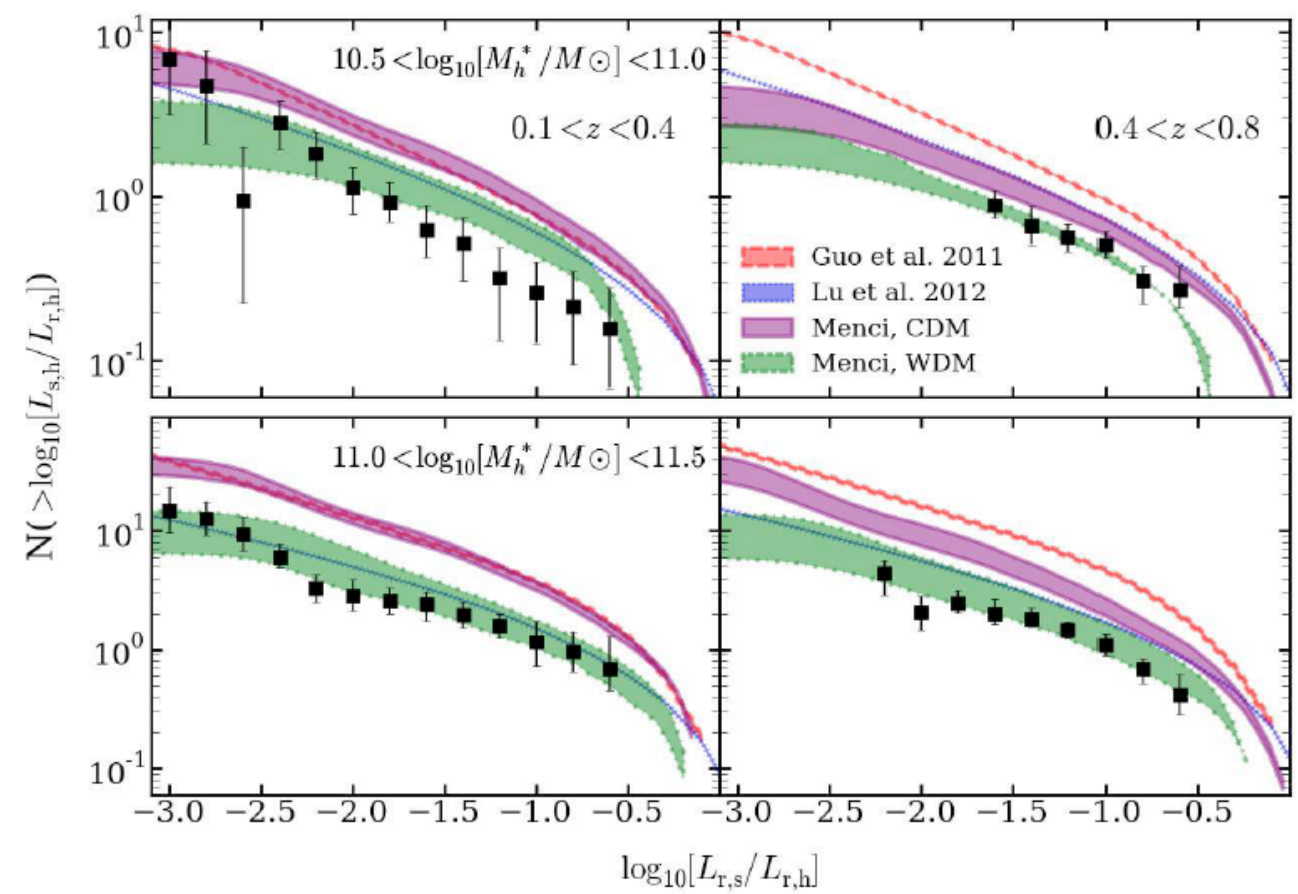

Disentangling feedback effects from WDM

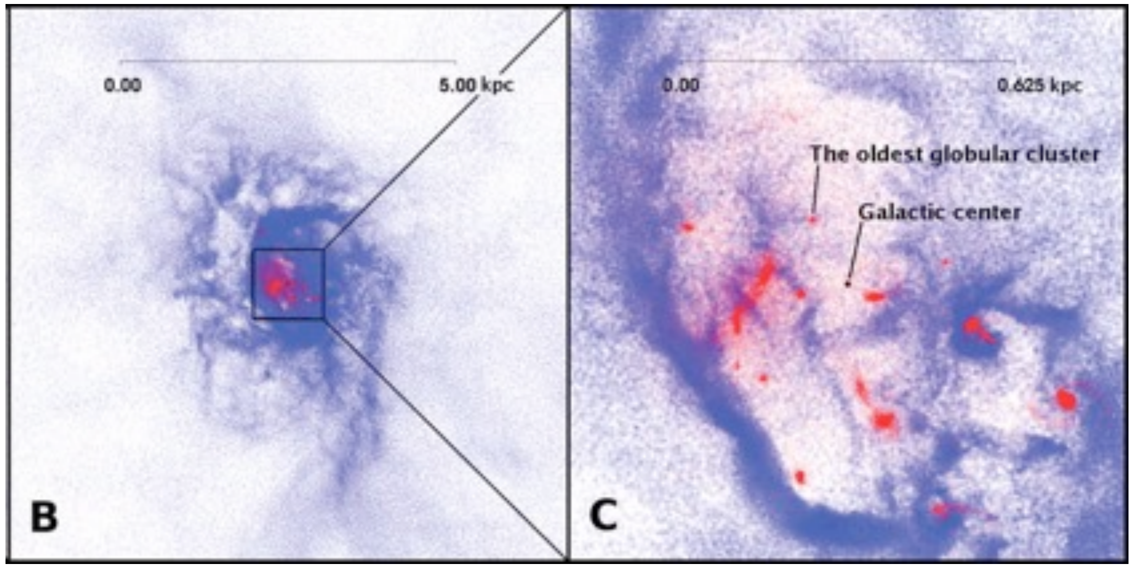

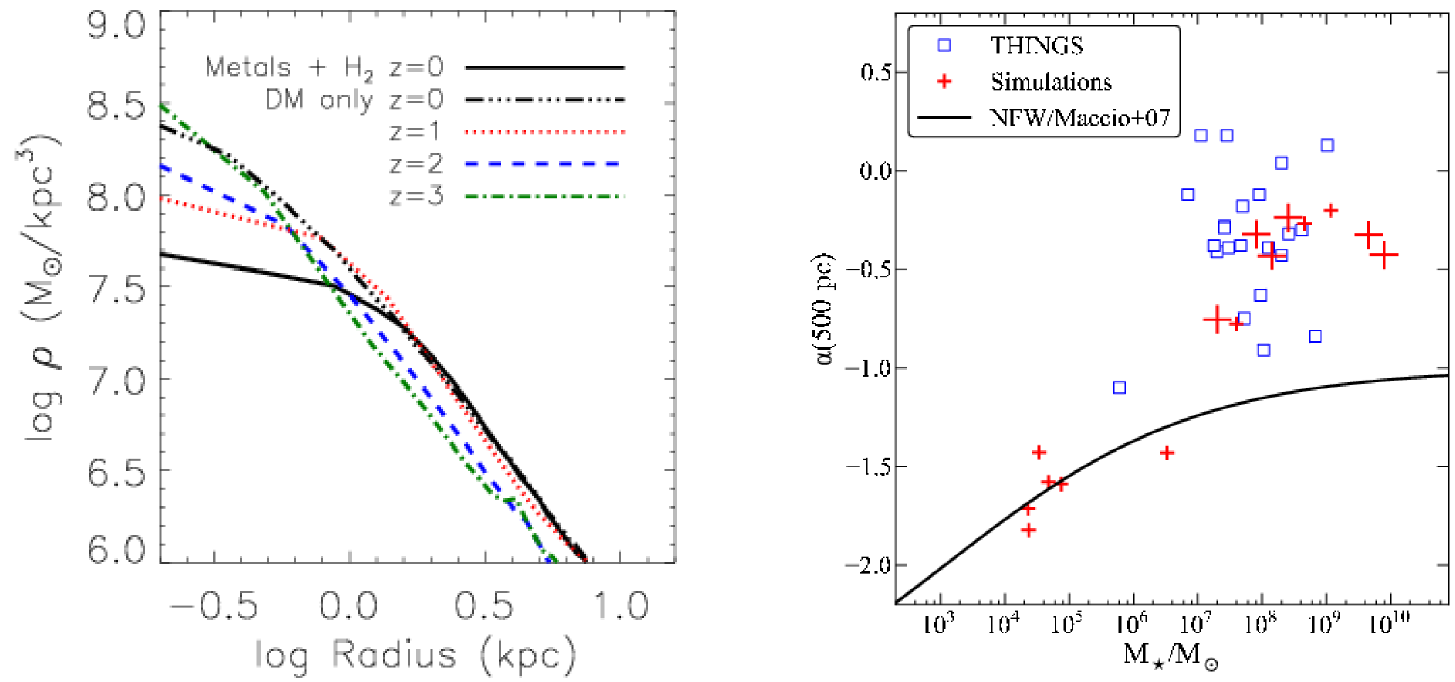

Fig. 3. Baryonic effects on CDM halo profiles in cosmological simulations, from Governato et al. (2012). *(Left)* The upper, dot-dash curve shows the cuspy dark matter density profile resulting from from a collisionless N-body simulation. Other curves show the evolution of the dark matter profile in a simulation from the same initial conditions that includes gas dynamics, star formation, and efficient feedback. By $z = 0$ (solid curve) the perturbations from the fluctuating baryonic potential have flattened the inner profile to a nearly constant density core. *(Right)* Logarithmic slope of the dark matter profile α measured at 0.5 kpc, as a function of galaxy stellar mass. Crosses show results from multiple hydrodynamic simulations. Squares show measurements from rotation curves of observed galaxies. The black curve shows the expectation for pure dark matter simulations, computed from NFW profiles with the appropriate concentration. For $M_* > 10^7 M_\odot$, baryonic effects reduce the halo profile slopes to agree with observations.

In the outer region profiles with feedback are close to CDM NFW

Feedback acts in the inner regions

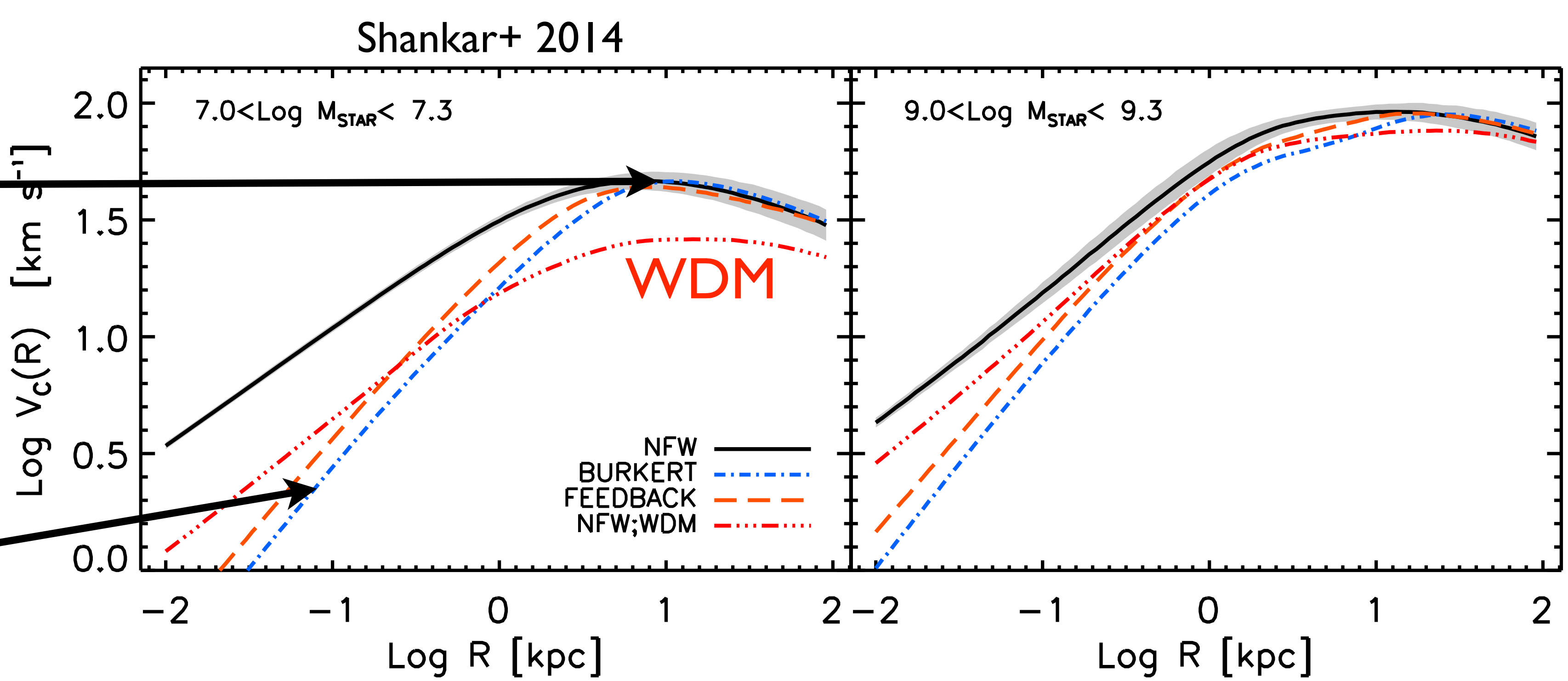

Abundance of galaxies as a function of their velocity width (gas rotation velocity)

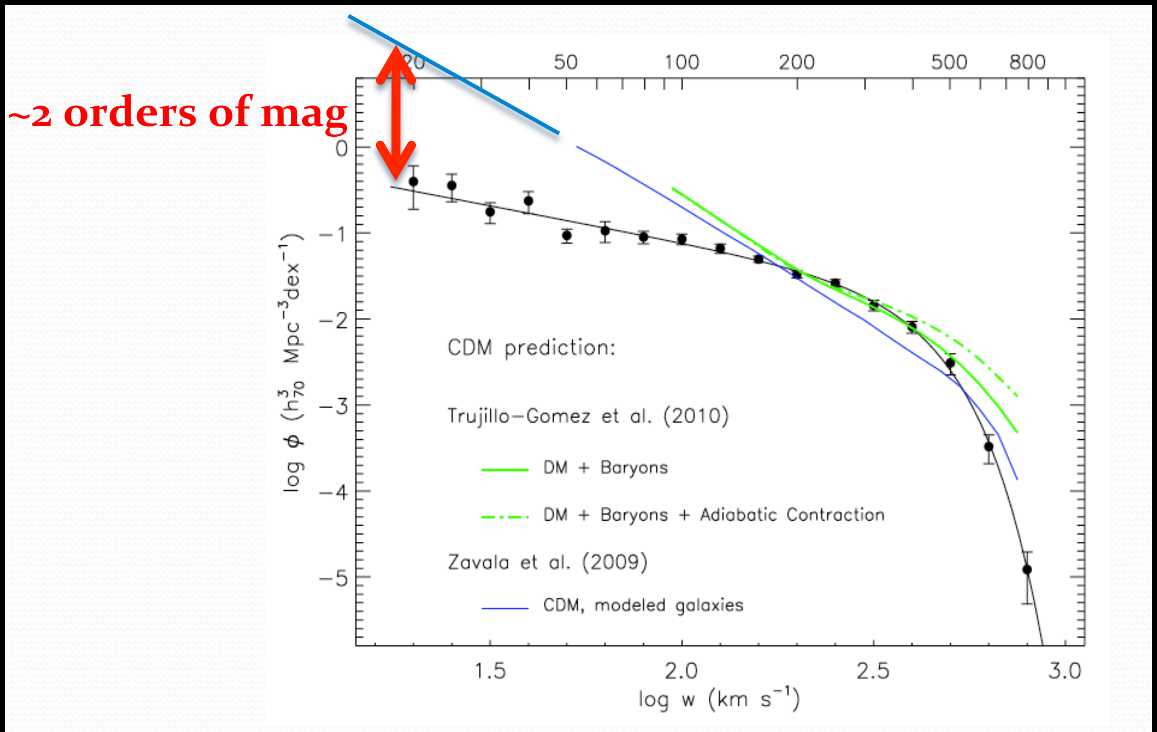

Papastergis+ (2011)

21-cm survey done with Arecibo Telescope: 3000 deg^2; 11000 detections
measures: redshift, velocity width, integrated flux
No spatial resolution (size, inclination, shape)

Directly measures
the depth of the potential well:
less prone to physics of gas (feedback)

Solutions within CDM scenario ?
- large fraction of galaxies with low gas content (below the sensitivity)
-large fraction of galaxies with rising rotation curve

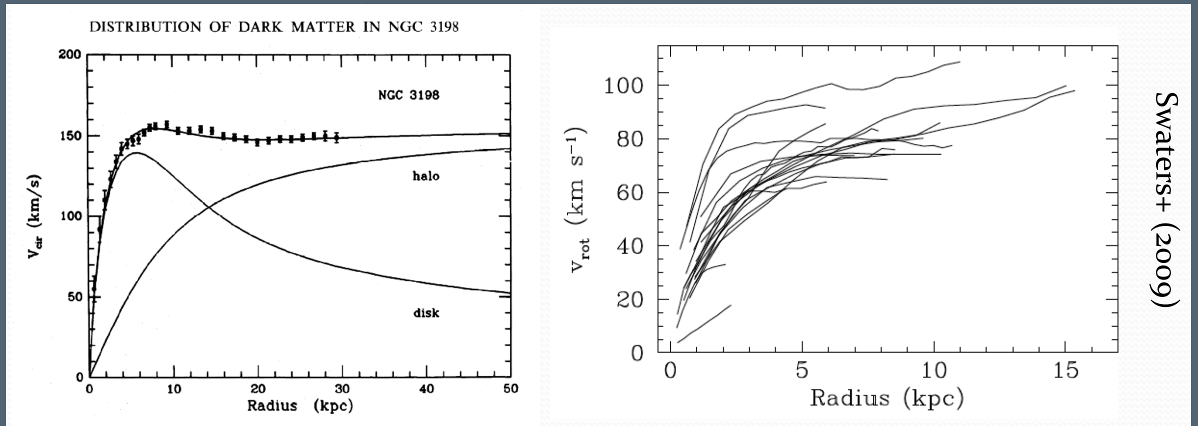

'flat' rotation curve

'rising' rotation curves

Abundance of galaxies as a function of their velocity width (gas rotation velocity)

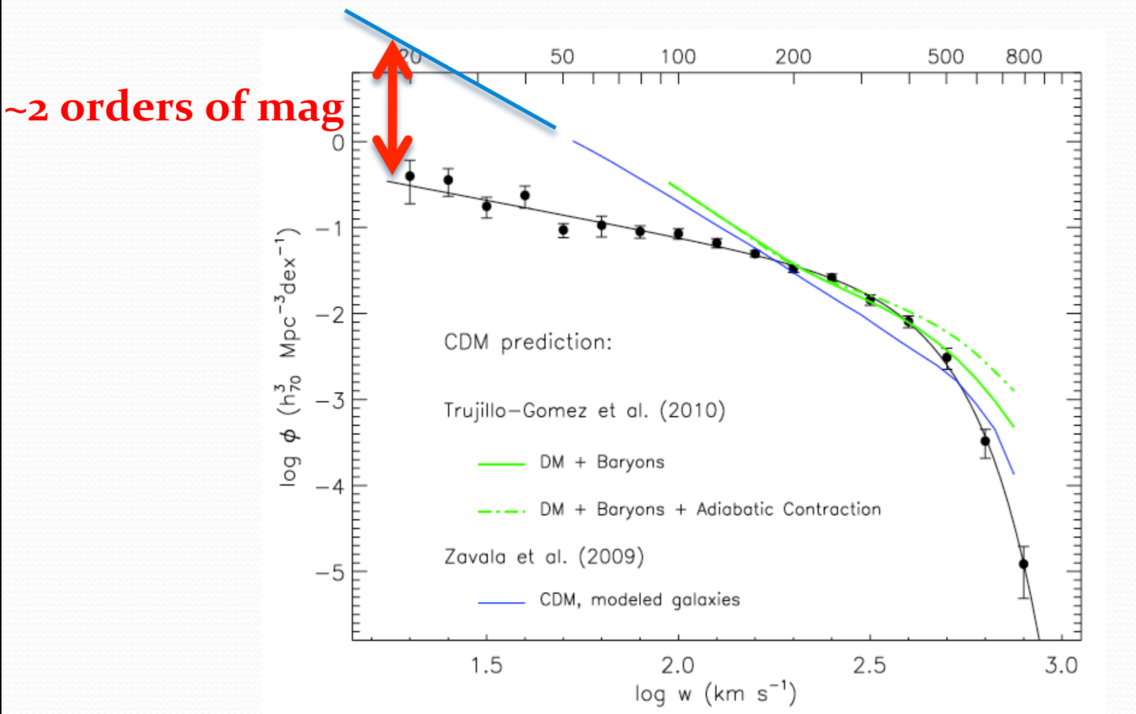

Papastergis+ (2011)

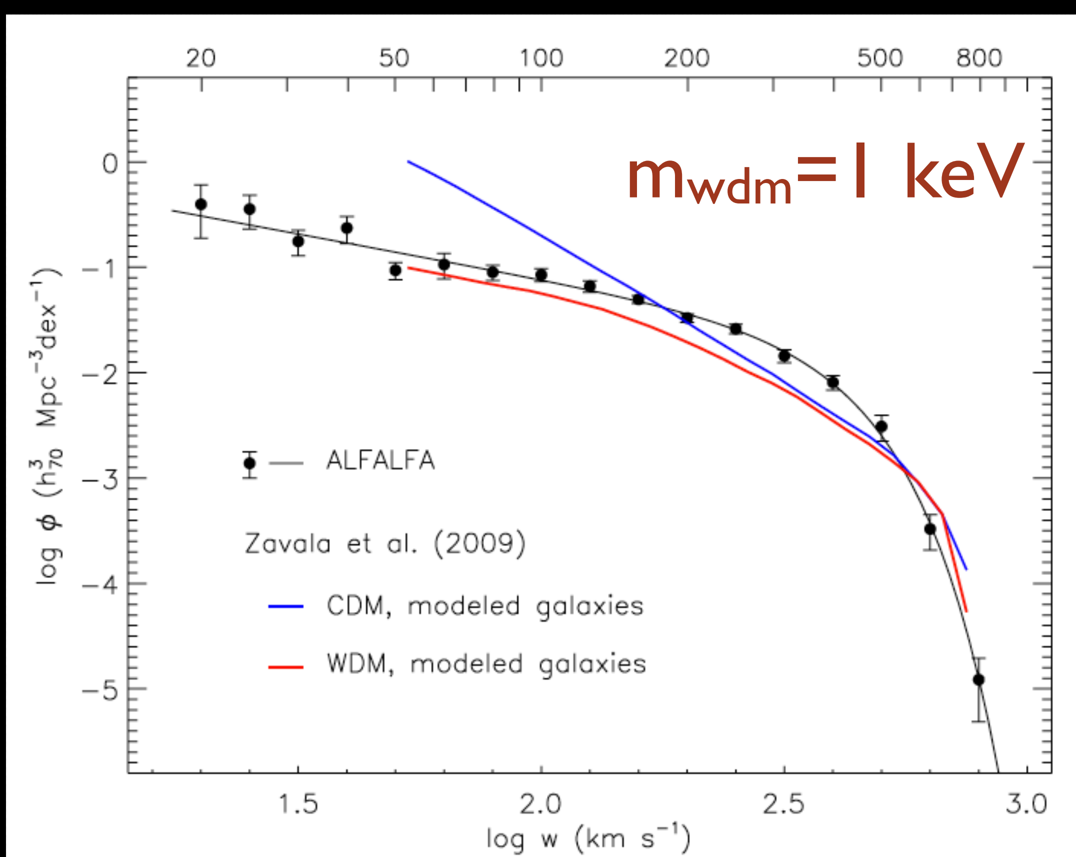

Papastergis+ (2011)

modeling: Zavala+ (2009)

21-cm survey done with Arecibo Telescope: 3000 deg^2; 11000 detections
measures: redshift, velocity width, integrated flux
No spatial resolution (size, inclination, shape)

Directly measures
the depth of the potential well:
less prone to physics of gas (feedback)

WDM naturally yields a flat distribution
Zavala et al. 2009

Abundance of galaxies as a function of their velocity width (gas rotation velocity)

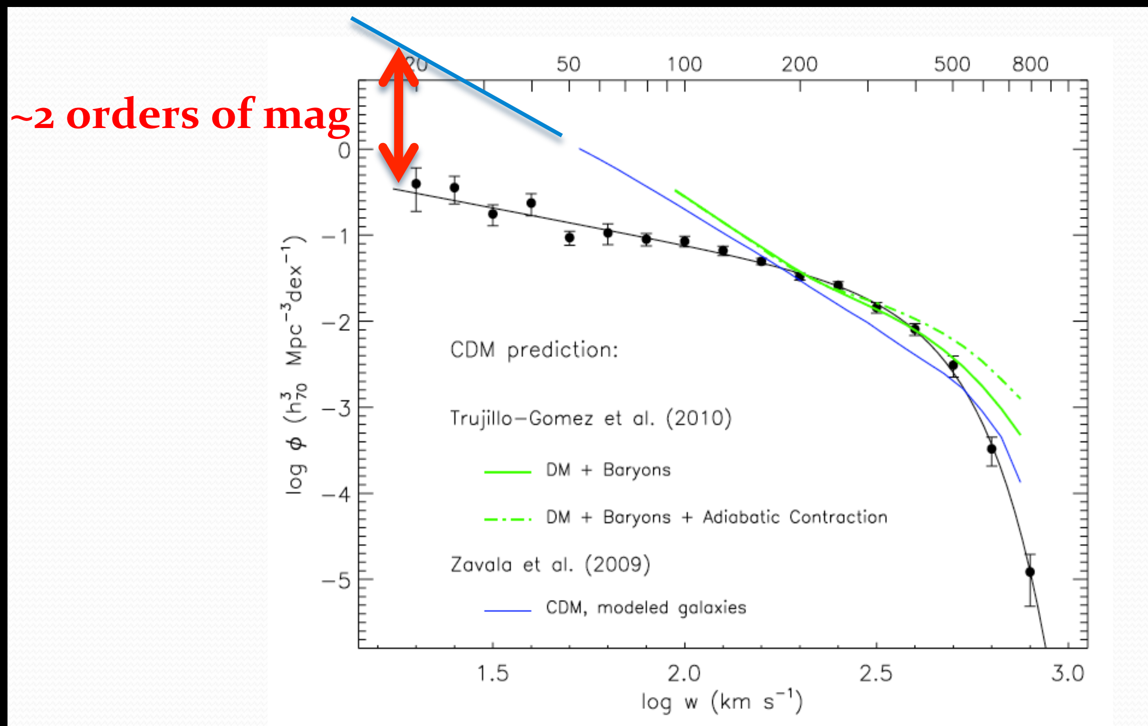

Papastergis+ (2011)

21-cm survey done with Arecibo Telescope: 3000 deg^2; 11000 detections

measures: redshift, velocity width, integrated flux

No spatial resolution (size, inclination, shape)

To match the observatons, observed rotation velocities should correspond to huge host DM halos with large V_{halo} so as to suppress the V_{rot}/V_{halo} ratio at low V_{rot}

$$\frac{dN}{dV_{rot}} = \frac{dN}{dV_{Halo}} \frac{dV_{Halo}}{dV_{rot}}$$

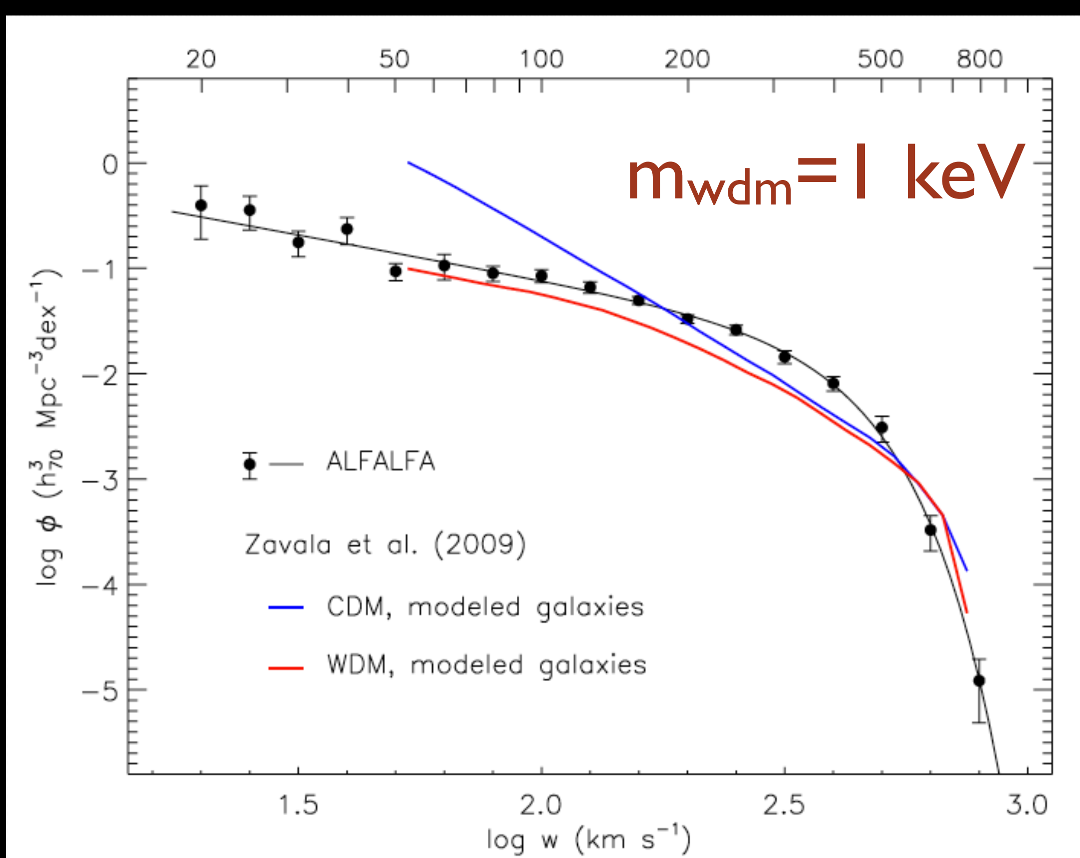

Papastergis+ (2011)

modeling: Zavala+ (2009)

Papastergis et al. 2015

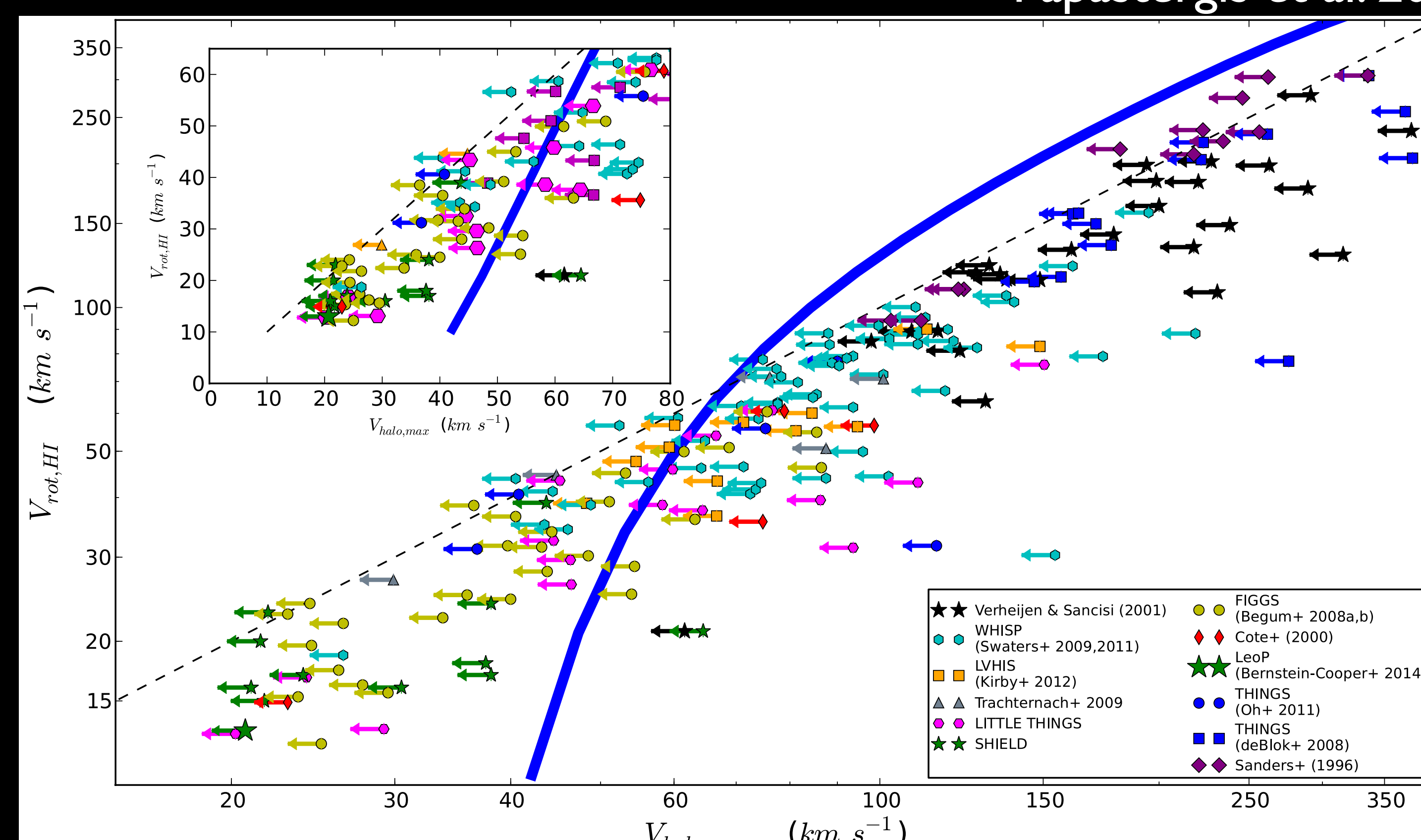

Effect of observ. uncert. on the VFs

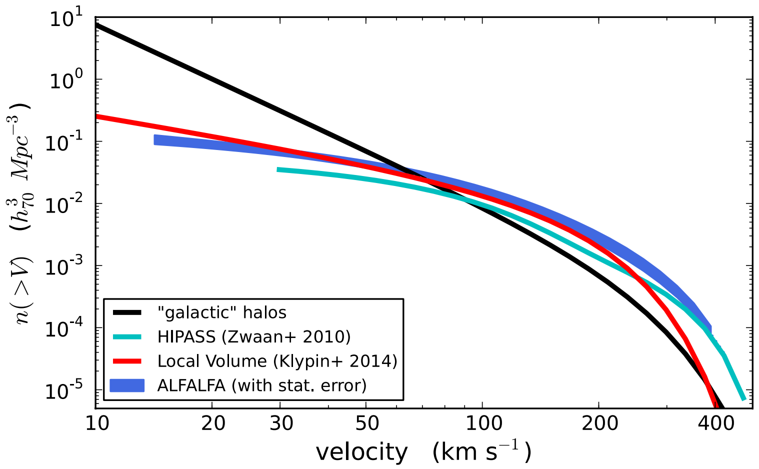

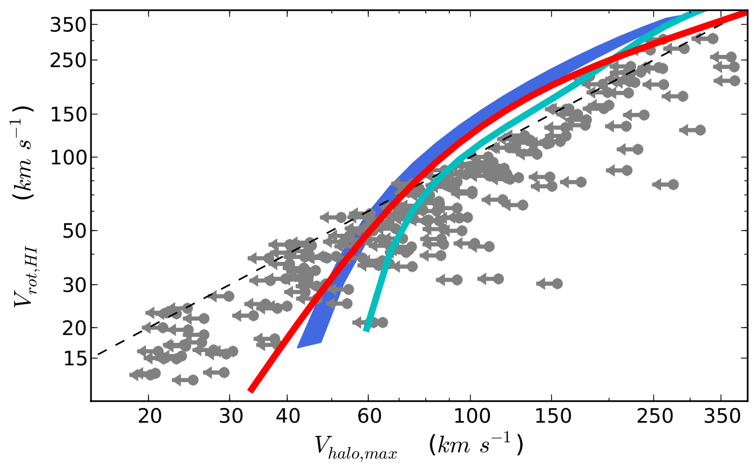

Effect of incompleteness in the the VFs

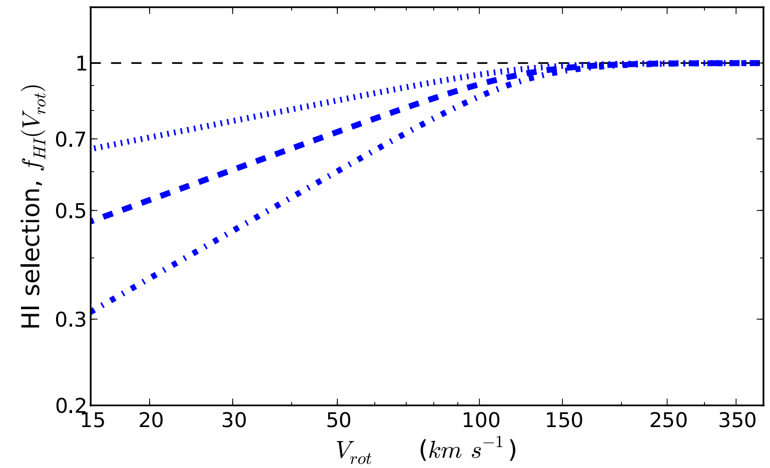

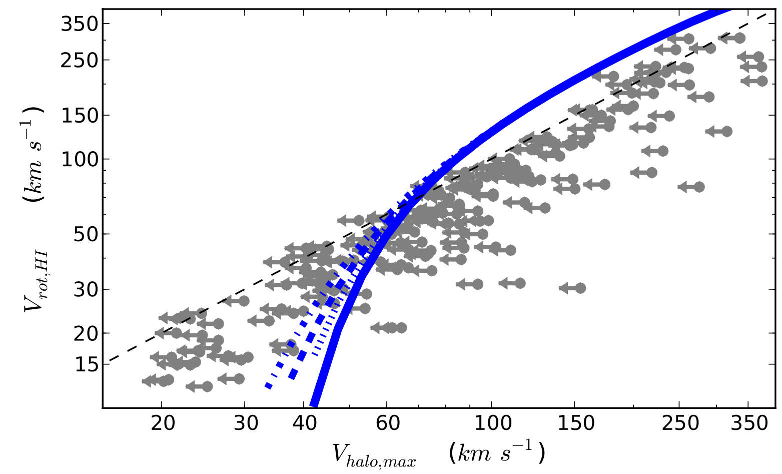

Effect of epxansio due to feedback

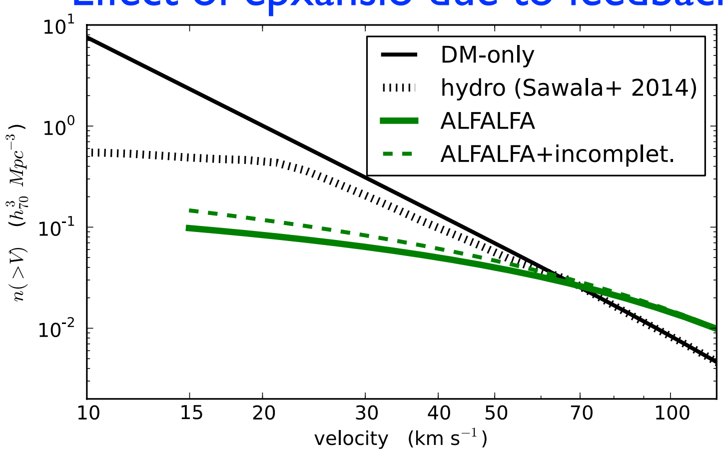

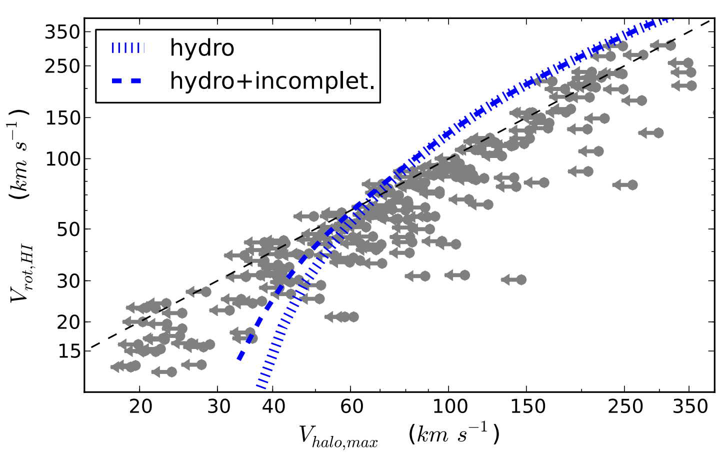

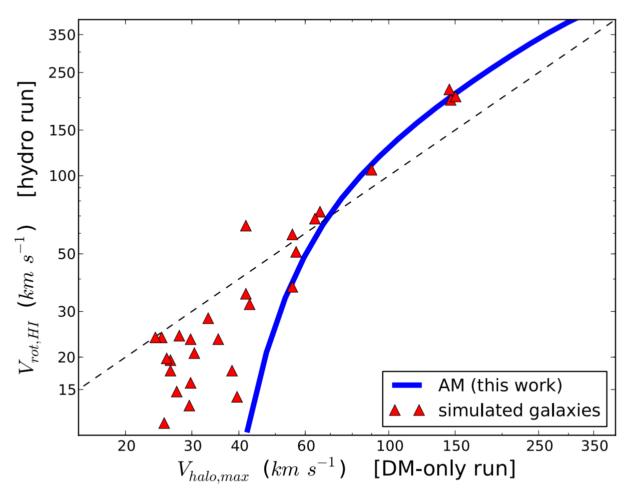

Papastergis et al. 2015

Matching the V_{max}-M_* relation

A semi-empirical approach (Shankar 2013; Papastergis et al. 2014)

1. select a sample of DM haloes
2. associate to each halo a galaxy of a given stellar mass according to an abundance matching relation
3. compute rotation velocity curves for each DM halo (for WDM adopt the $c(M_h)$ relation by Schneider et al 2012 for 1 keV thermal relic DM)
4. infer predicted V_{MAX}-Vh relation (computed at maximum of the rotation curve)

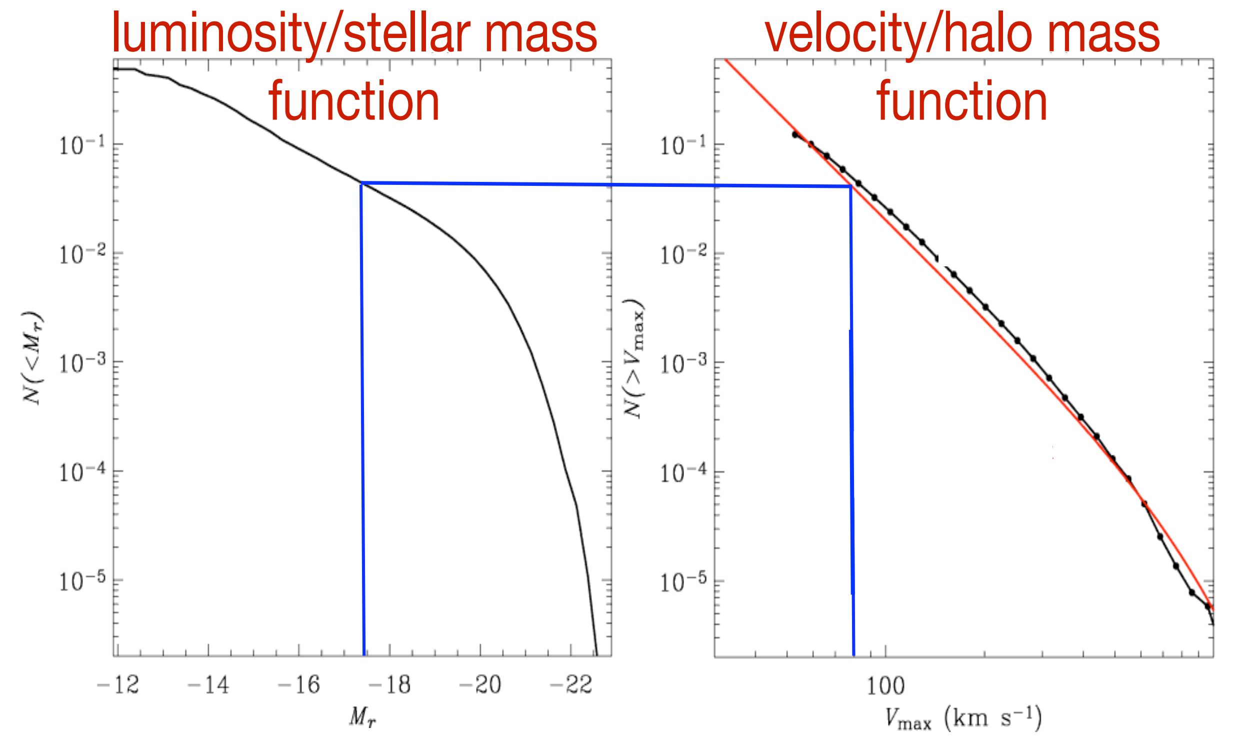

Matching the V_{max}-M_* relation

A semi-empirical approach (Shankar 2013; Papastergis et al. 2014)

1. select a sample of DM haloes
2. associate to each halo a galaxy of a given stellar mass according to an abundance matching relation
3. compute rotation velocity curves for each DM halo (for WDM adopt the $c(M_h)$ relation by Schneider et al 2012 for 1 keV thermal relic DM)
4. infer predicted V_{MAX}-Vh relation (computed at maximum of the rotation curve)

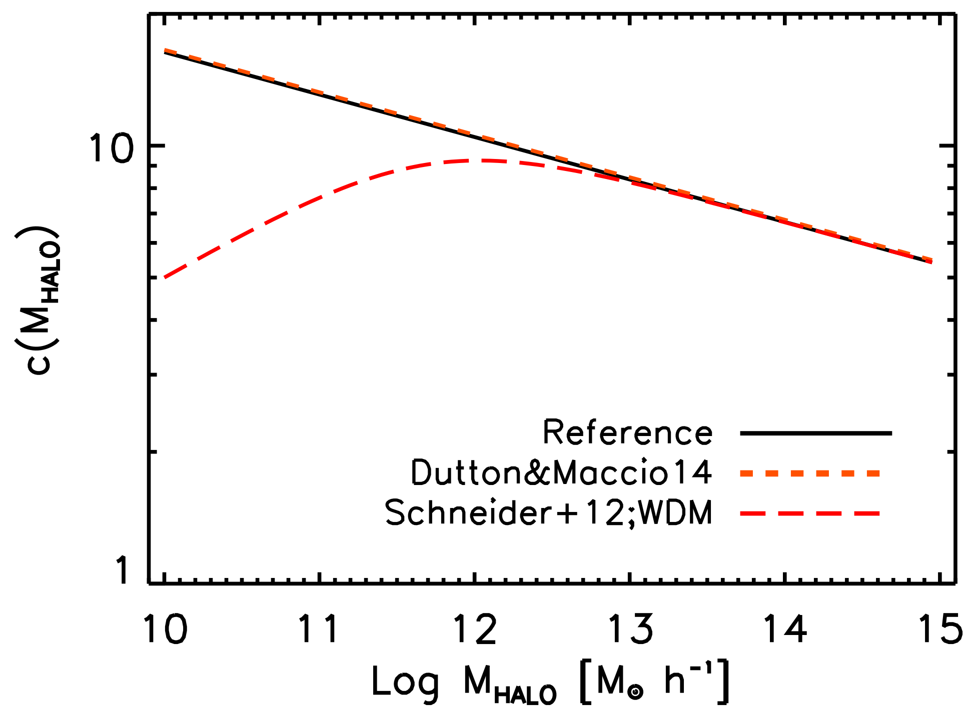

Matching the V_{max}-M_* relation

A semi-empirical approach (Shankar 2013; Papastergis et al. 2014)

1. select a sample of DM haloes
2. associate to each halo a galaxy of a given stellar mass according to an abundance matching relation
3. compute rotation velocity curves for each DM halo (for WDM adopt the $c(M_h)$ relation by Schneider et al 2012 for 1 keV thermal relic DM)
4. infer predicted V_{MAX}-Vh relation (computed at maximum of the rotation curve)

Feedback profile from Di Cintio et al. 2014
hydro-simulations baryons+stellar feedback

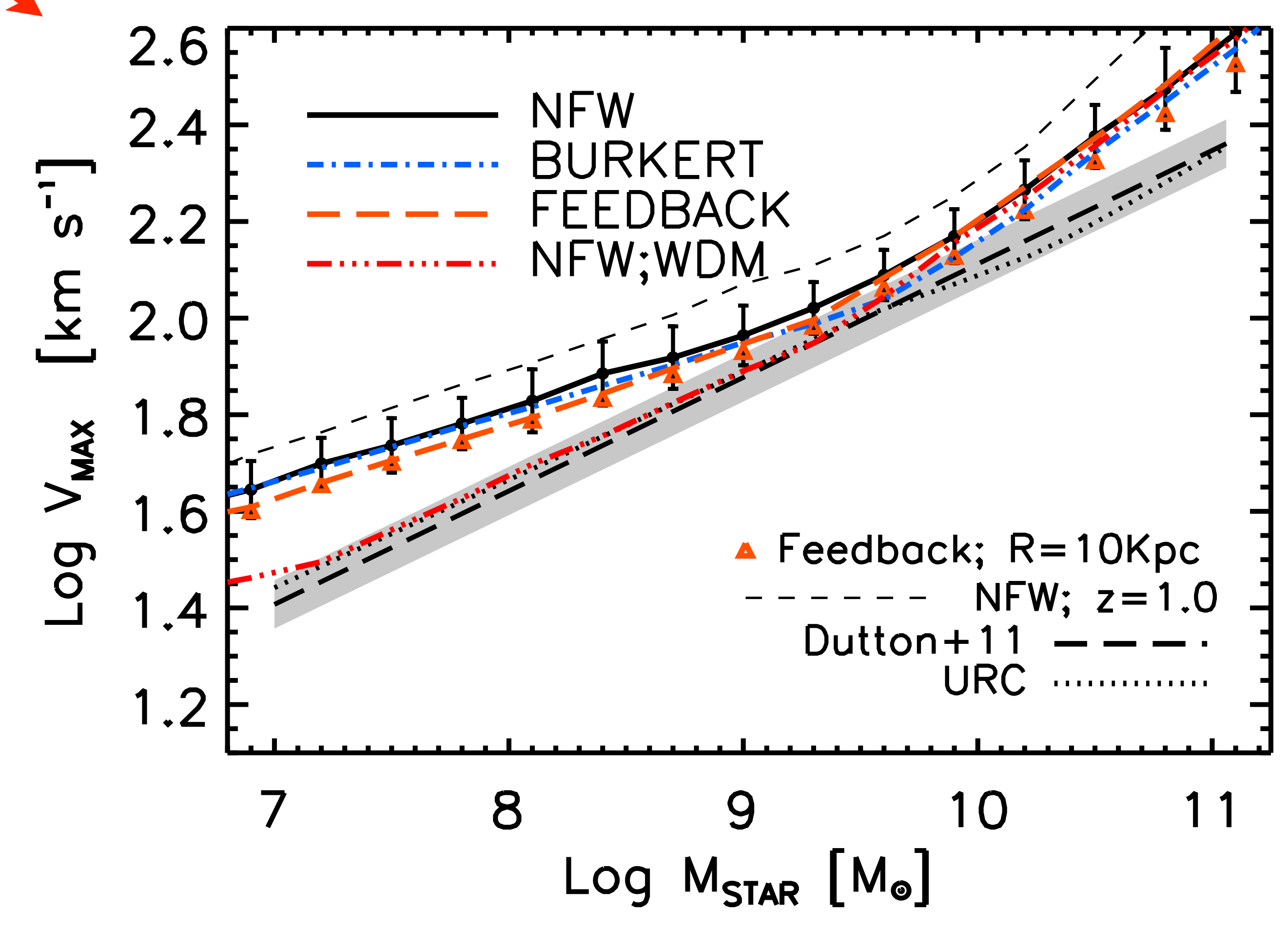

Solution in CDM scenario

most low-mass haloes do not contain galaxies due to the effect or UV background, feedback and reionization(assuming no self-shielding and H_2 cooling)

Sawala et al. 2015

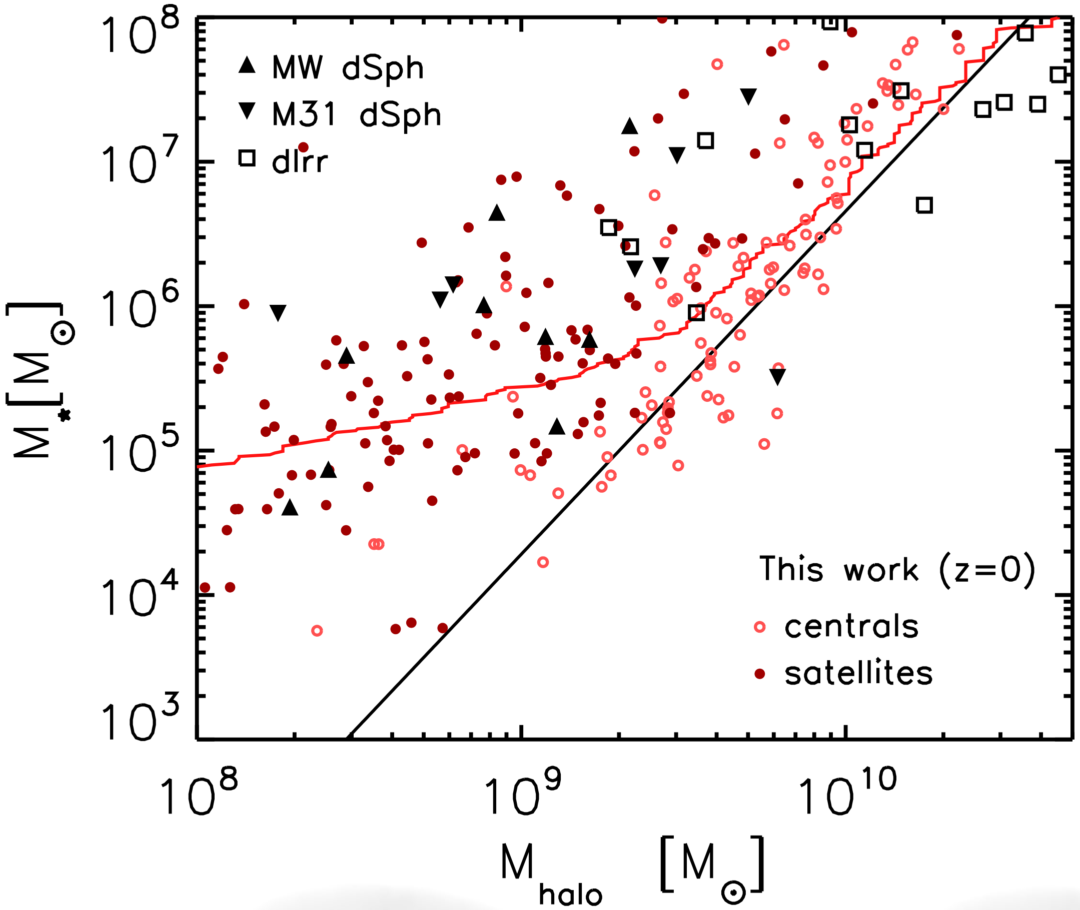

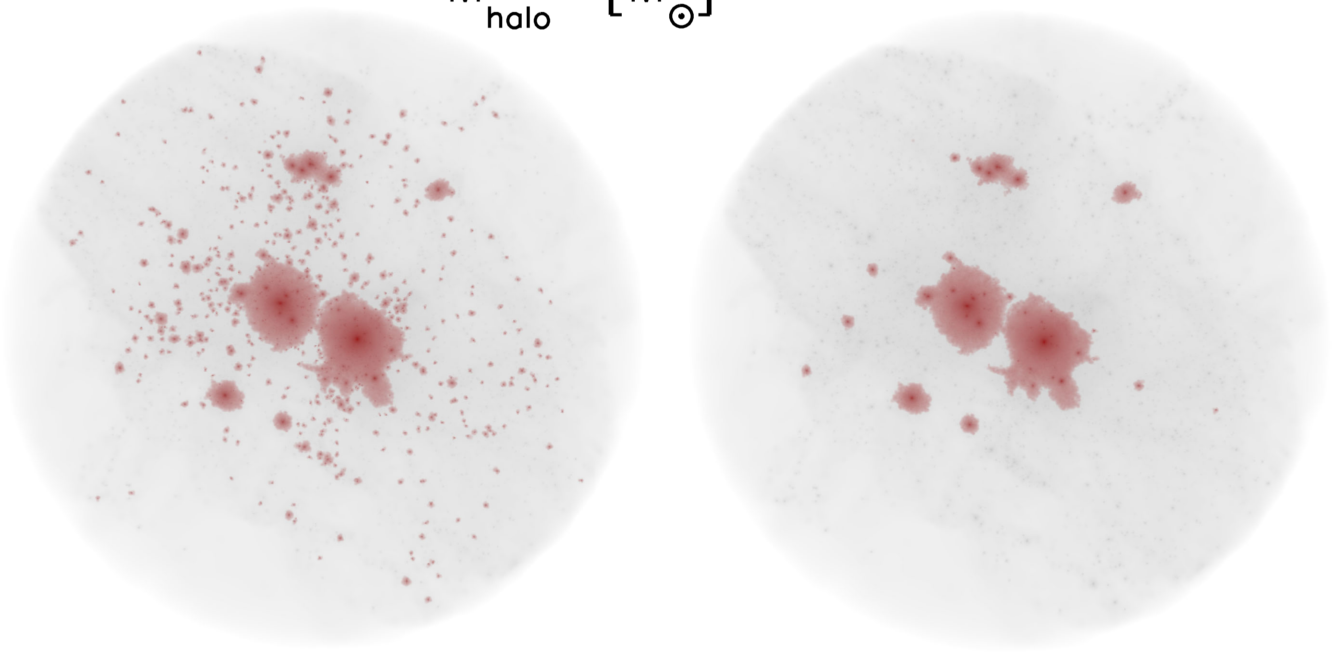

Figure 1. Projected density distribution of dark matter within 2 Mpc around the simulated Milky Way – M31 barycentre at $z = 0$ from one of our simulation volumes. Highlighted in red on top of the total mass distribution are particles in haloes above 5×10^7 $M_\odot$ (left-hand panel), and particles in just those haloes that contain stars (right-hand panel).

Milky-Way like haloes should contain thousands of dark halos (with no stars or gas)

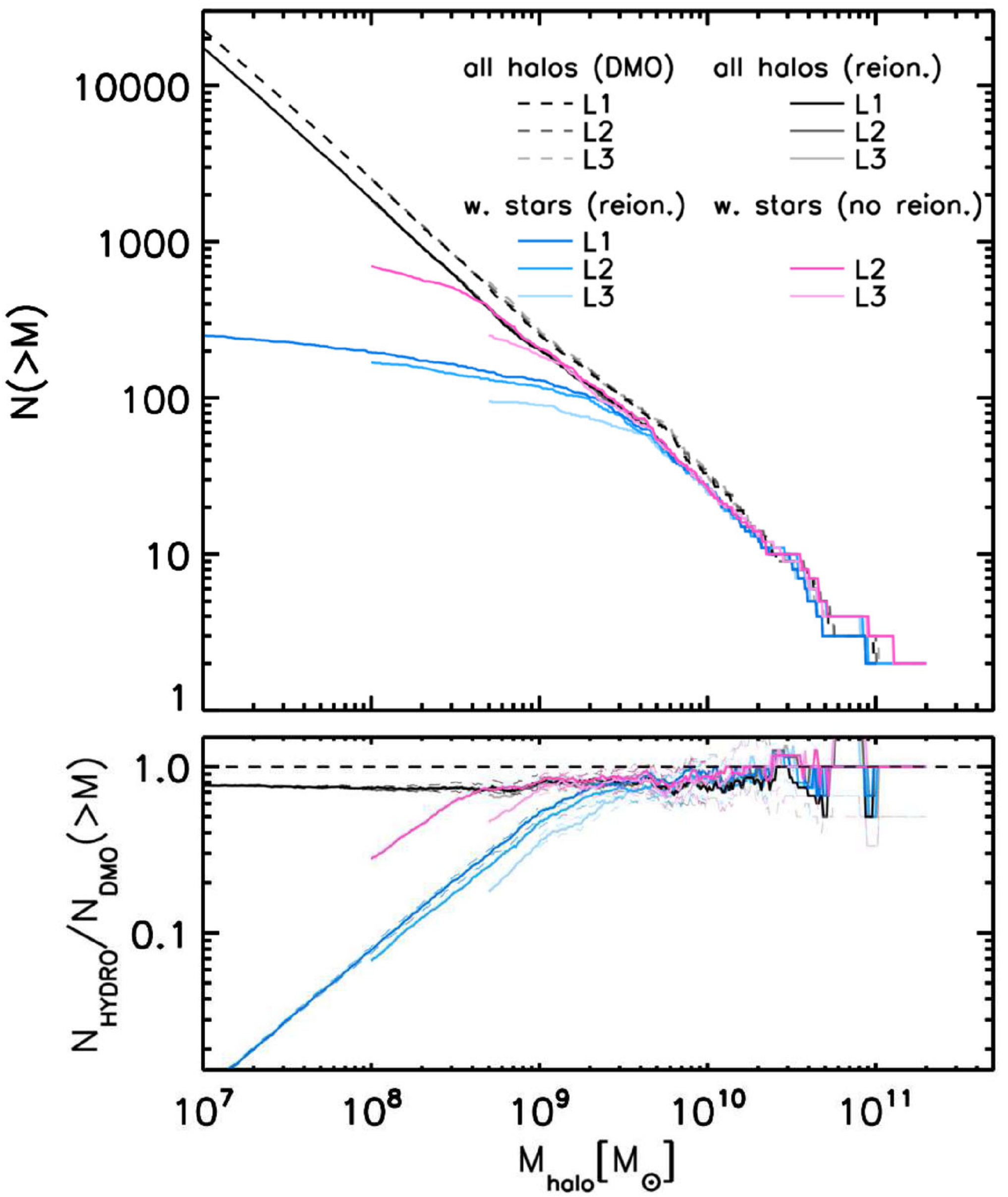

Critical Issues

Overabundance of low-mass objects

i) abundance of satellite DM haloes
ii) density profiles
iii) abundance of faint galaxies
iv) the M_*-M_{halo} relation
v) star formation histories of satellites

SATELLITE GALAXIES

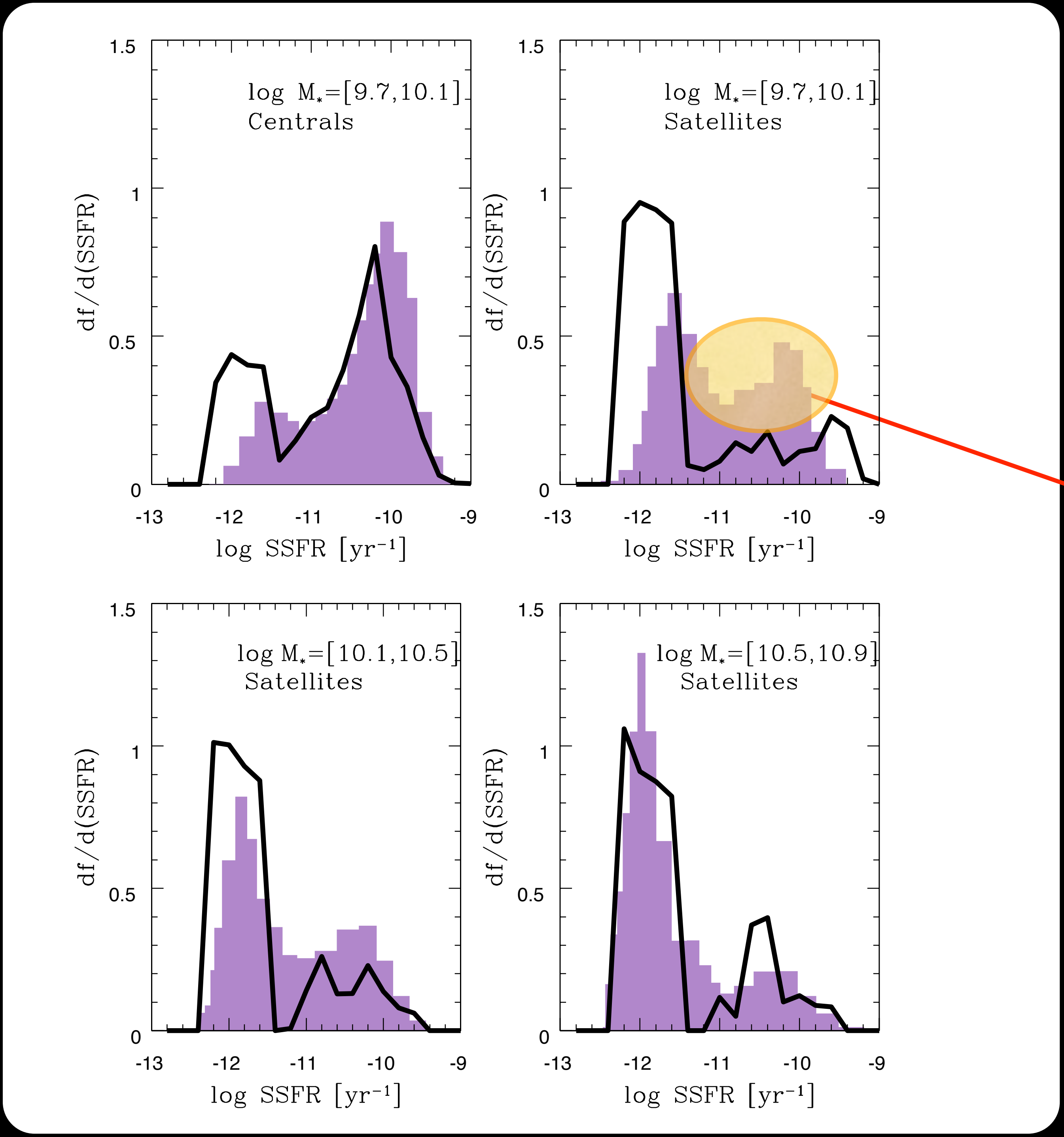

NM 2014;
Data from Wetzel et al. 2013

Specific Star Formation Rate SSFR
measures the current star formation activity with respect to the past

$$SSFR = \dot{M}_*/M*$$

Population of active satellites missing in CDM models
Model satellites undergo passive evolution

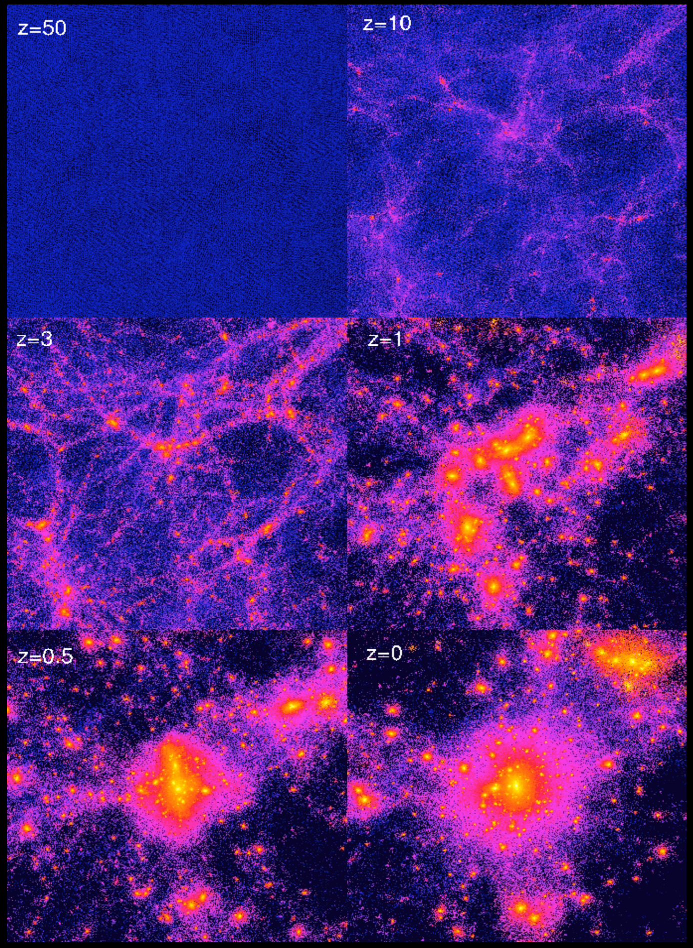

THE FRACTION OF QUIESCENT SATELLITE GALAXIES

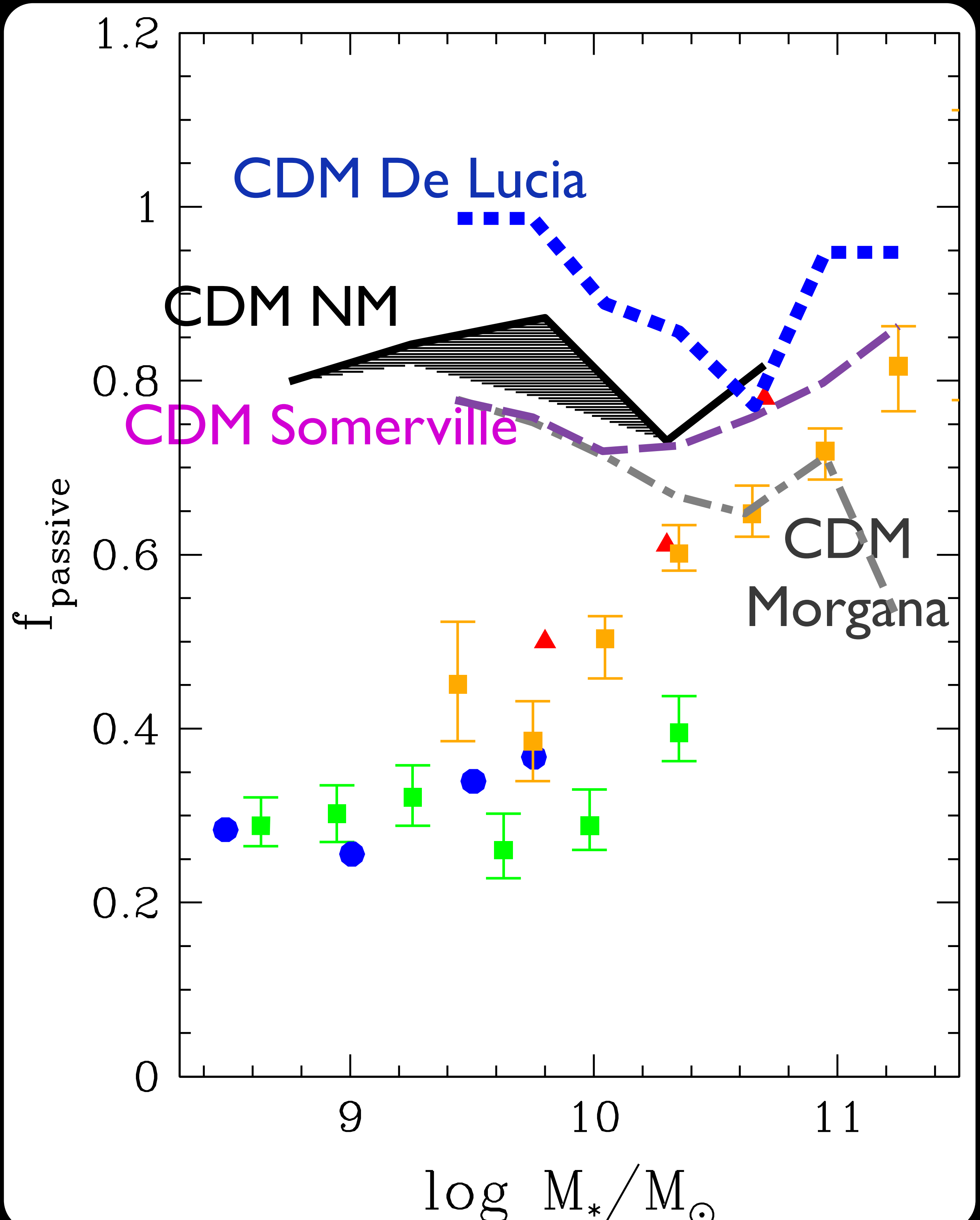

NM 2014;
Data from Wetzel et al. 2013
Kimm et al. 2014
Phillips 2014
Geha 2012

Quiescent Fraction

Measures the fract.ion of quescent satellites

Threshold SSFR<10^{-11} yrs
corresponds to minimum in the SSFR distribution
correspond to Δt=3 t_H
(to form M_* it would need 3t_H at current SF rate)

$$SSFR = \dot{M}_*/M* = 10^{-11}\ \mathrm{yrs} \rightarrow M_* = 3\,t_H\,\dot{M}_*$$

Result robust with respect to different CDM models with different feedback modelling

Due to the large number of dense DM clumps collapsed at high redshifts
gas rapidly converted into stars at high-redshifts

- Cold gas converted into stars at high z
- Hot gas stripped when they were incorporated into larger DM haloes

No further star formation at low redhsift

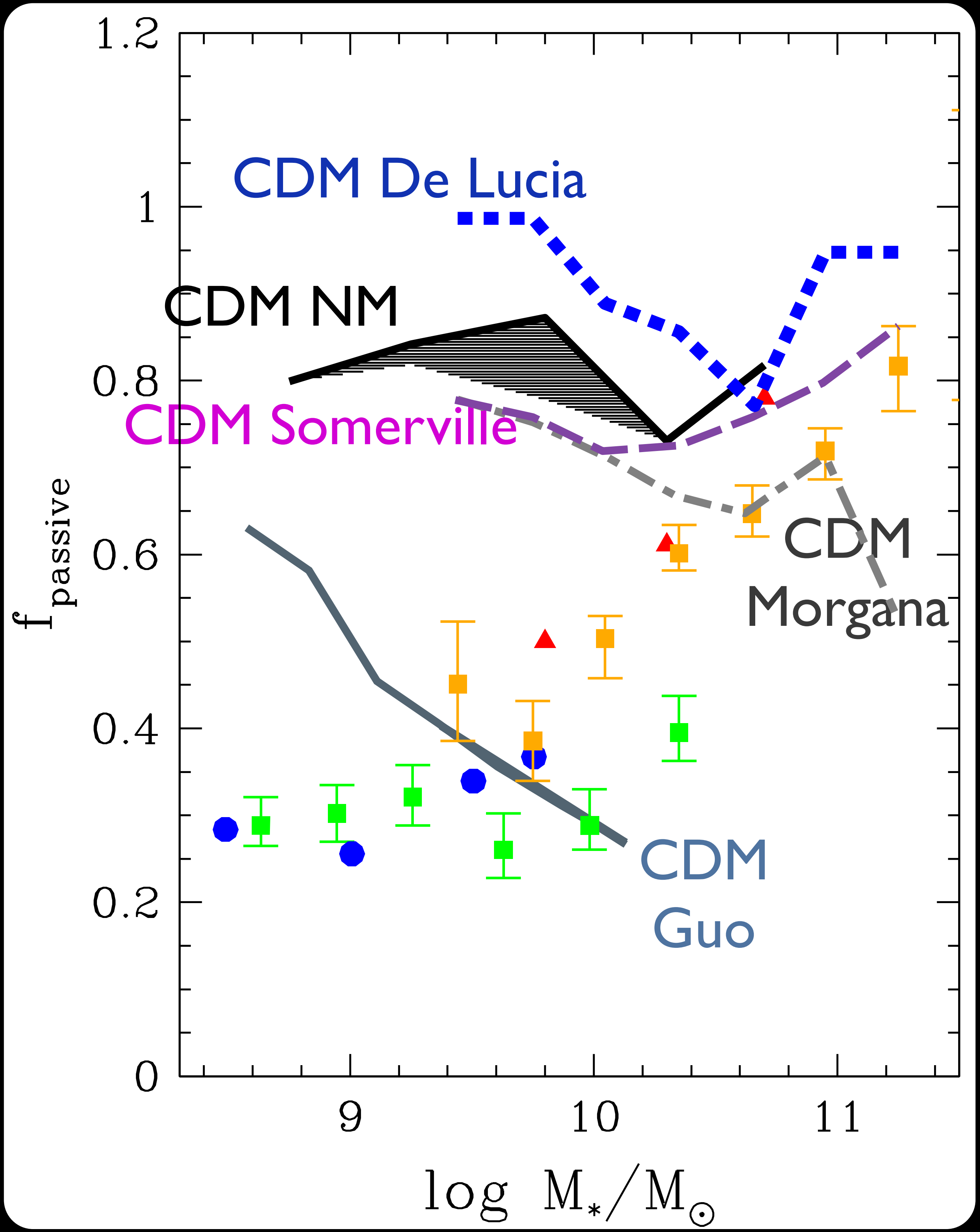

NM 2014;
Data from Wetzel et al. 2013
Kimm et al. 2014
Phillips 2014
Geha 2012

THE FRACTION OF QUIESCENT SATELLITE GALAXIES

Quiescent Fraction

Measures the fract.ion of quescent satellites

Threshold SSFR<10^{-11} yrs
corresponds to minimum in the SSFR distribution
correspond to $\Delta t=3\ t_H$
(to form M_* it would need $3t_H$ at current SF rate)

$$SSFR = \dot{M}_*/M* = 10^{-11}\ \mathrm{yrs} \rightarrow M_* = 3\,t_H\,\dot{M}_*$$

Result robust with respect to different CDM models with different feedback modelling

Due to the large number of dense DM clumps collapsed at high redshifts
gas rapidly converted into stars at high-redshifts

- Cold gas converted into stars at high z
- Hot gas stripped when they were incorporated into larger DM haloes

No further star formation at low redhsift

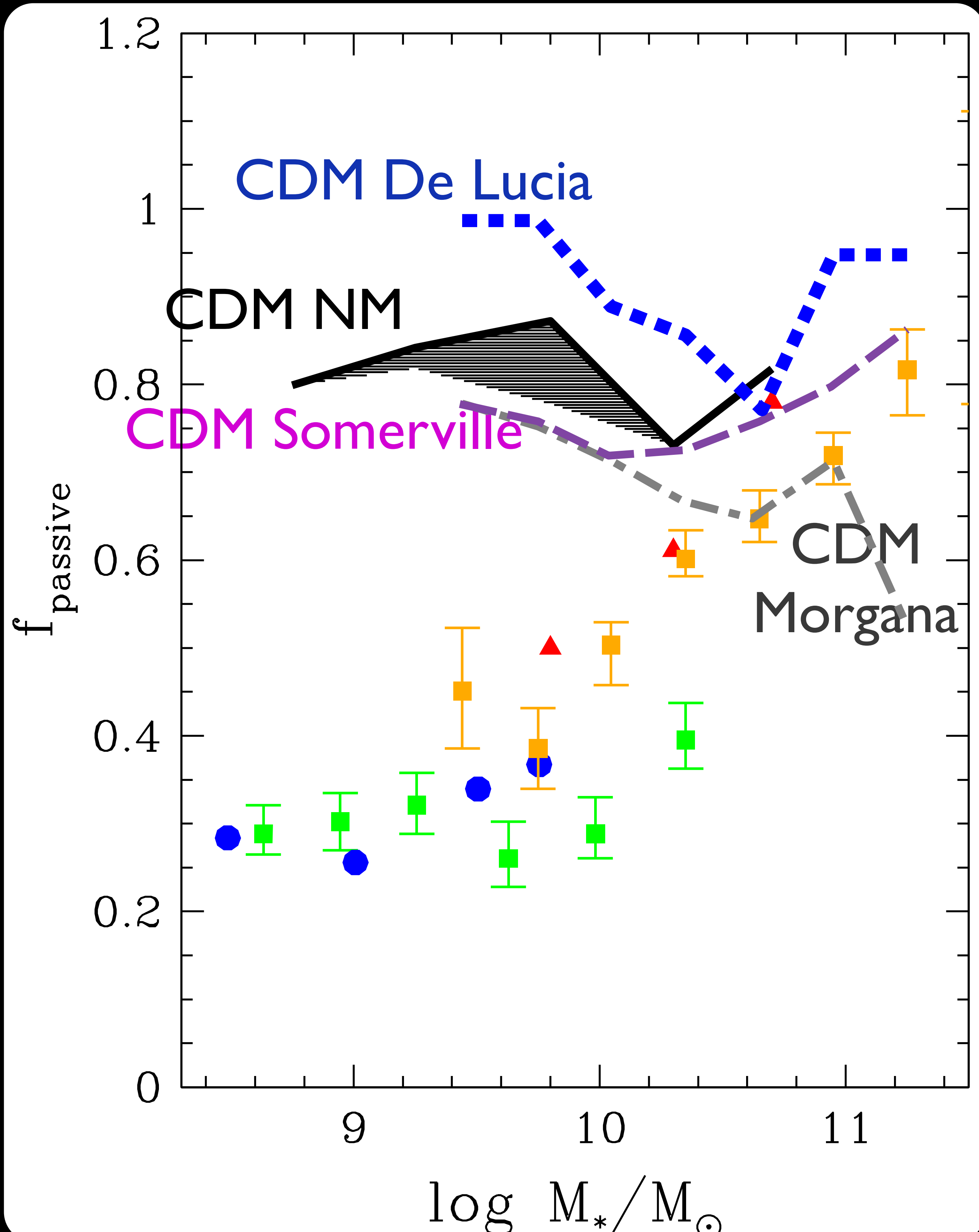

NM 2014;
Data from Wetzel et al. 2013
Kimm et al. 2014
Phillips 2014
Geha 2012

THE FRACTION OF QUIESCENT SATELLITE GALAXIES

Quiescent Fraction

Measures the fract.ion of quescent satellites

Threshold SSFR<10^{-11} yrs
corresponds to minimum in the SSFR distribution
correspond to $\Delta t=3\ t_H$
(to form M_* it would need $3t_H$ at current SF rate)

$$SSFR = \dot{M}_*/M* = 10^{-11}\ \mathrm{yrs} \rightarrow M_* = 3\, t_H\, \dot{M}_*$$

Result robust with respect to different CDM models with different feedback modelling

Due to the large number of dense DM clumps collapsed at high redshifts
gas rapidly converted into stars at high-redshifts

- Cold gas converted into stars at high z
- Hot gas stripped when they were incorporated into larger DM haloes

No further star formation at low redhsift

THE FRACTION OF QUIESCENT SATELLITE GALAXIES

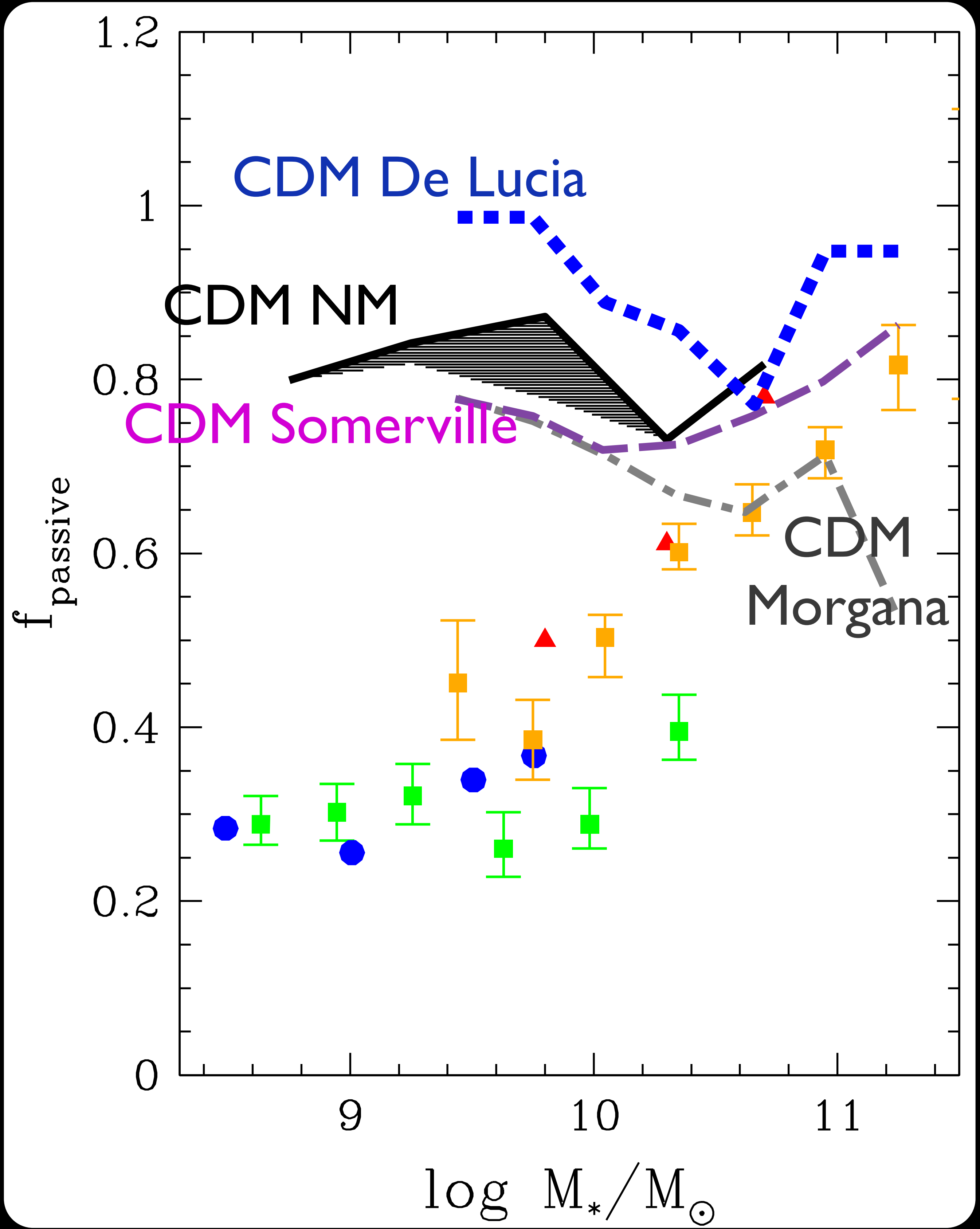

NM 2014;
Data from Wetzel et al. 2013
Kimm et al. 2014
Phillips 2014
Geha 2012

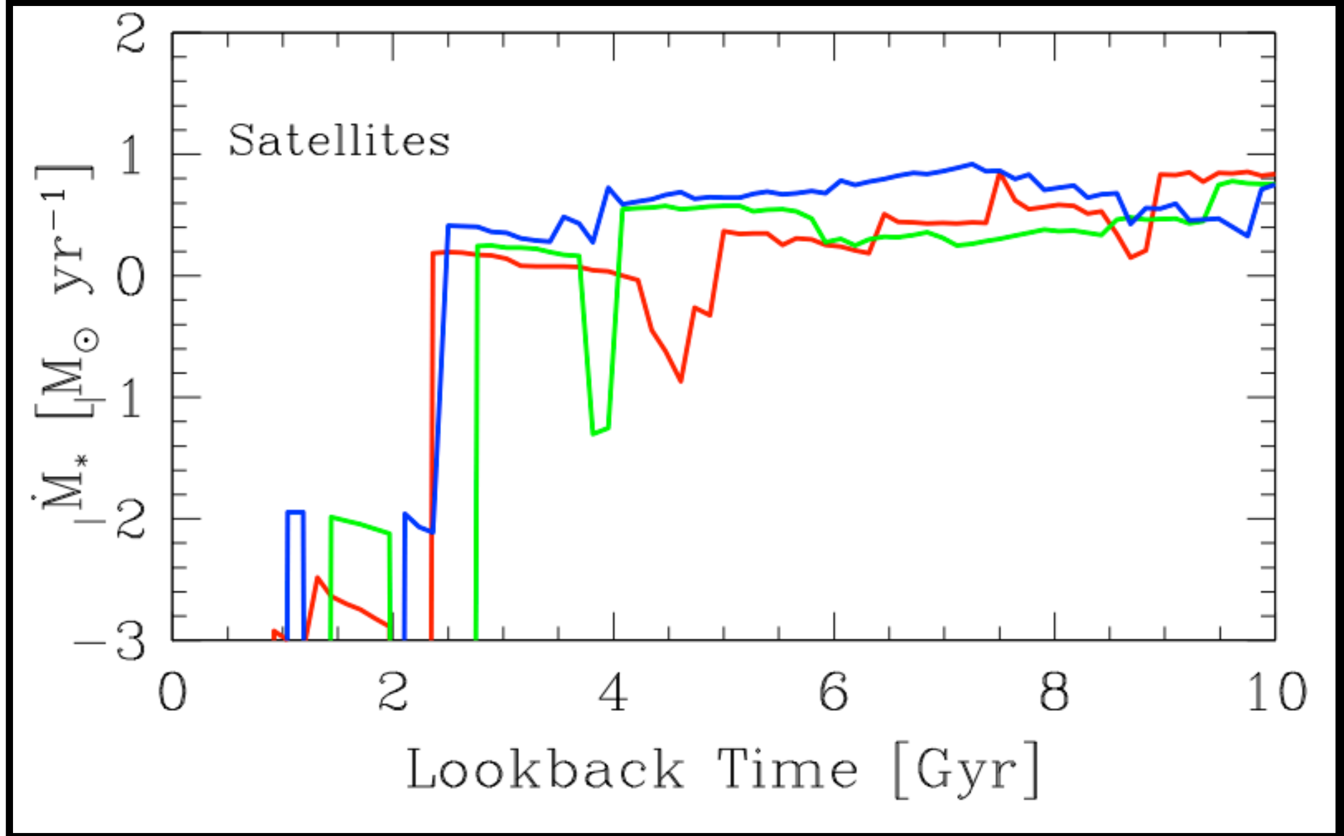

Result robust with respect to different CDM models with different feedback modelling

Due to the large number of dense DM clumps collapsed at high redshifts gas rapidly converted into stars at high-redshifts

- Cold gas converted into stars at high z
- Hot gas stripped when they were incorporated into larger DM haloes

No further star formation at low redhsift

THE FRACTION OF QUIESCENT SATELLITE GALAXIES

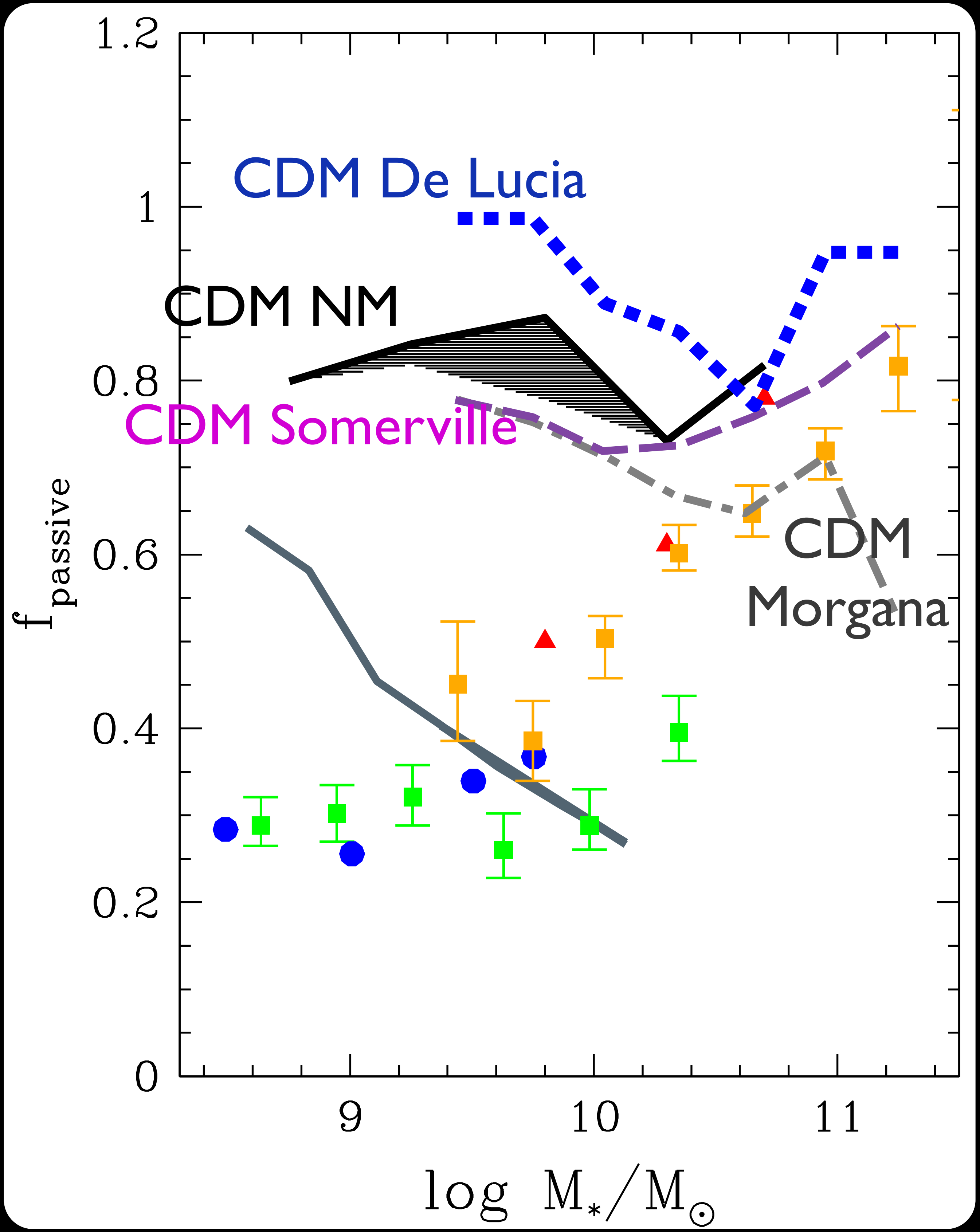

NM 2014;
Data from Wetzel et al. 2013
Kimm et al. 2014
Phillips 2014
Geha 2012

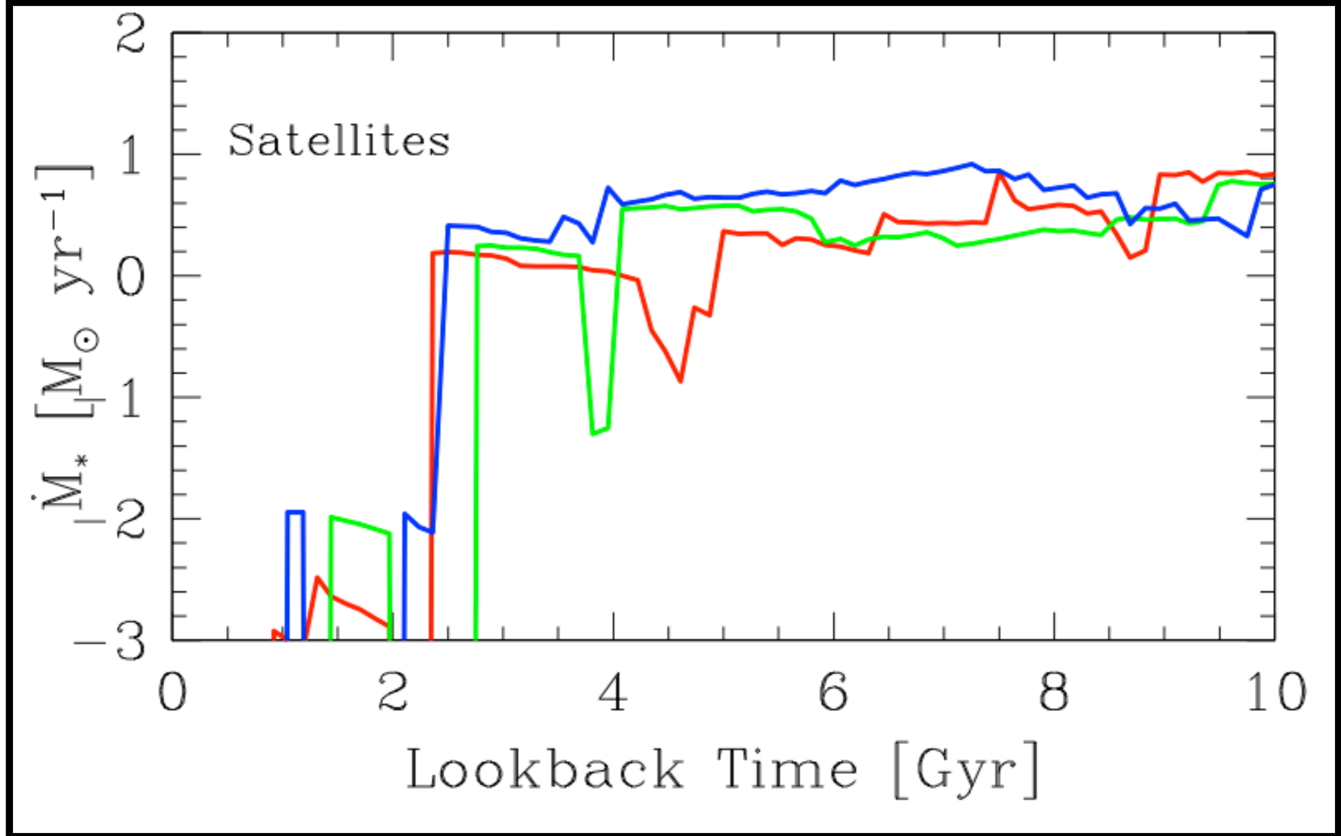

Result robust with respect to different CDM models with different feedback modelling

Due to the large number of dense DM clumps collapsed at high redshifts
gas rapidly converted into stars at high-redshifts

- Cold gas converted into stars at high z
- Hot gas stripped when they were incorporated into larger DM haloes

No further star formation at low redhsift

THE FRACTION OF QUIESCENT SATELLITE GALAXIES

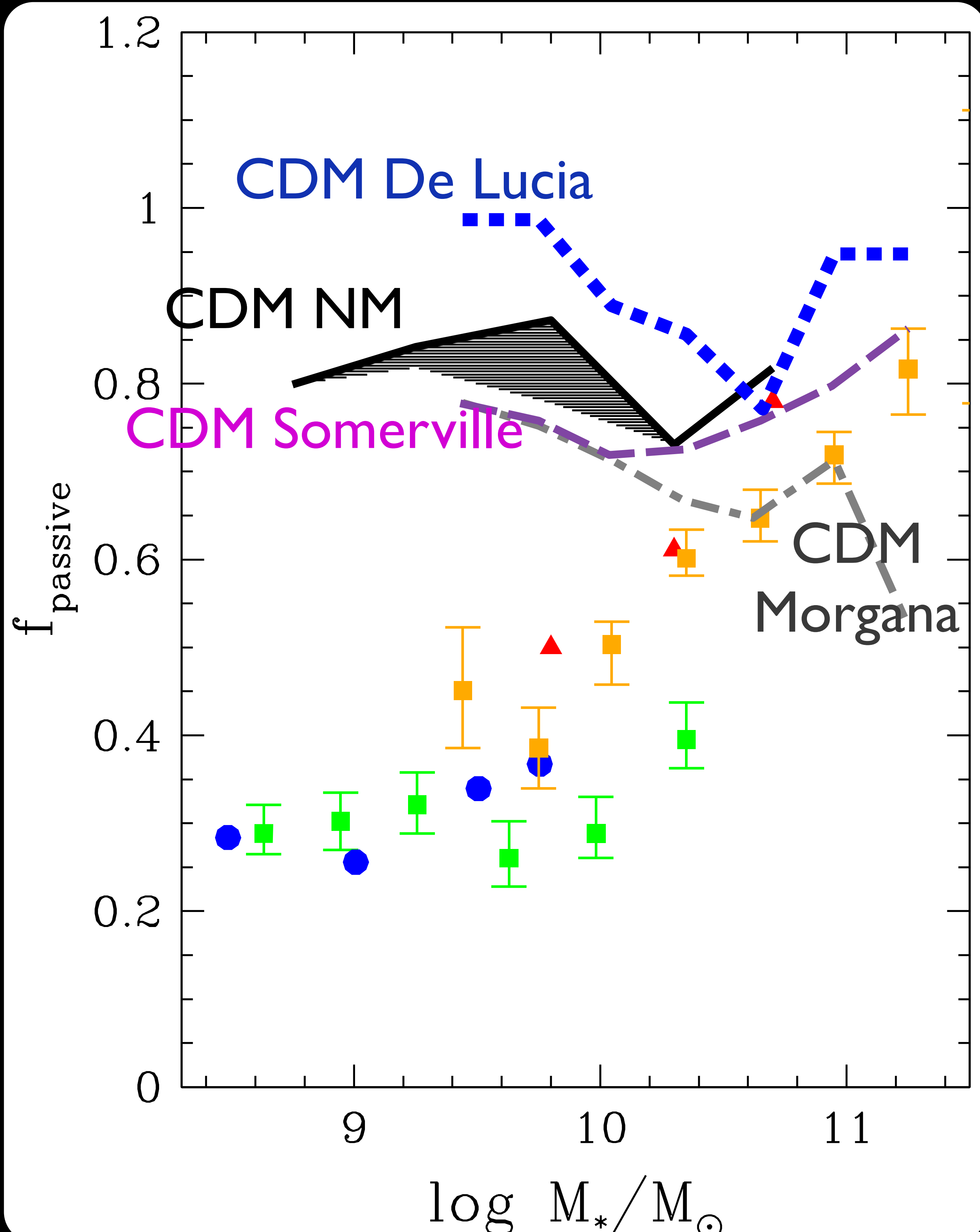

NM 2014;
Data from Wetzel et al. 2013
Kimm et al. 2014
Phillips 2014
Geha 2012

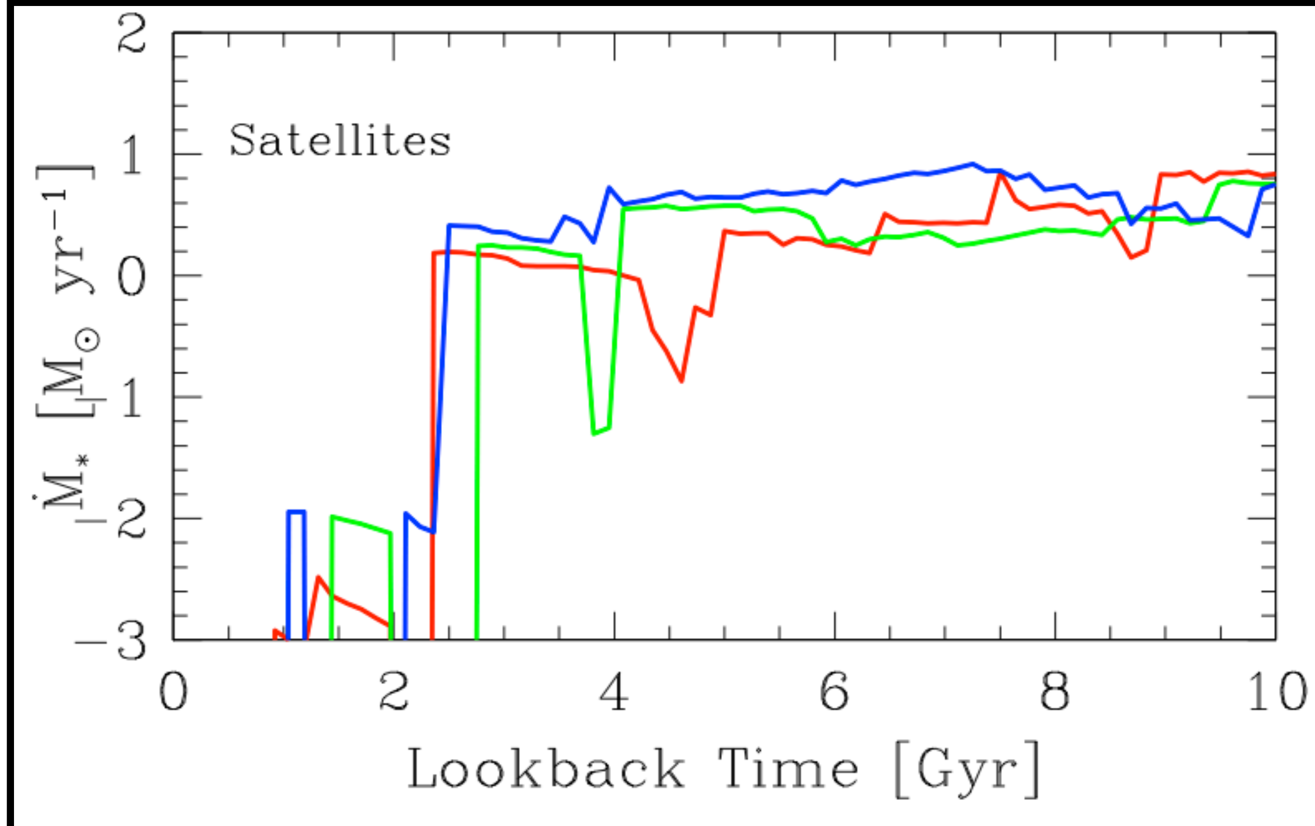

Result robust with respect to different CDM models with different feedback modelling

Due to the large number of dense DM clumps collapsed at high redshifts
gas rapidly converted into stars at high-redshifts

- Cold gas converted into stars at high z
- Hot gas stripped when they were incorporated into larger DM haloes

No further star formation at low redhsift

THE FRACTION OF QUIESCENT SATELLITE GALAXIES

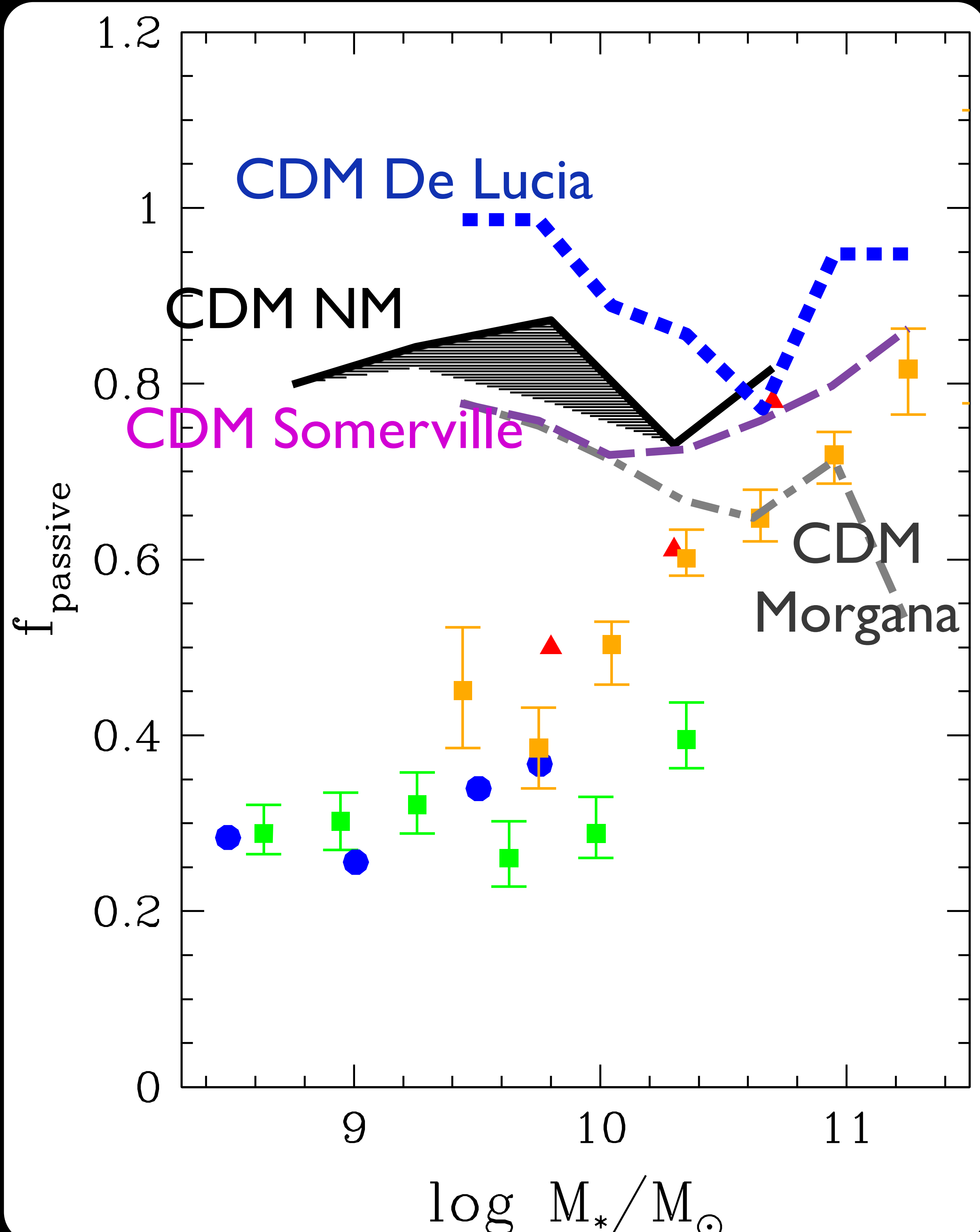

NM 2014;
Data from Wetzel et al. 2013
Kimm et al. 2014
Phillips 2014
Geha 2012

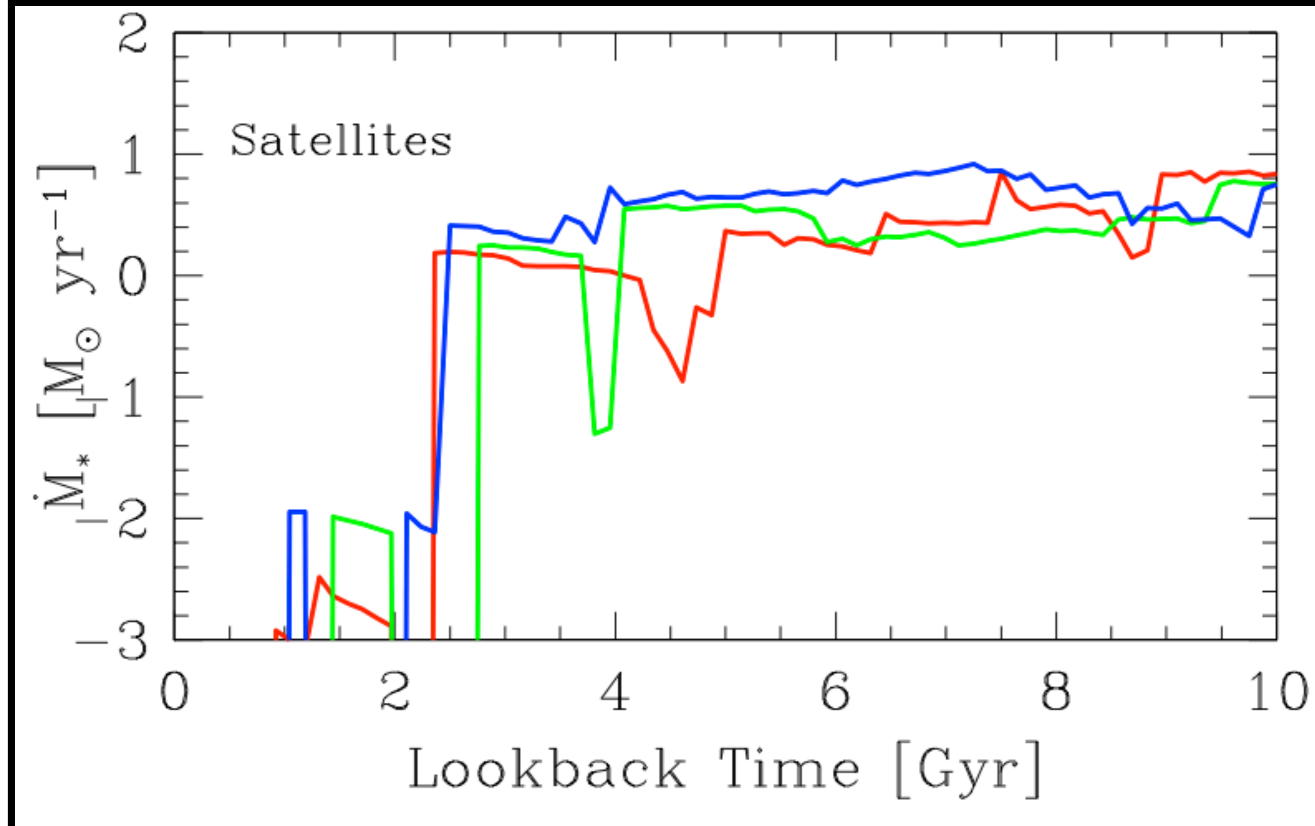

Result robust with respect to different CDM models with different feedback modelling

Due to the large number of dense DM clumps collapsed at high redshifts
gas rapidly converted into stars at high-redshifts

- Cold gas converted into stars at high z
- Hot gas stripped when they were incorporated into larger DM haloes

No further star formation at low redhsift

Star Formation histories of satellites in WDM

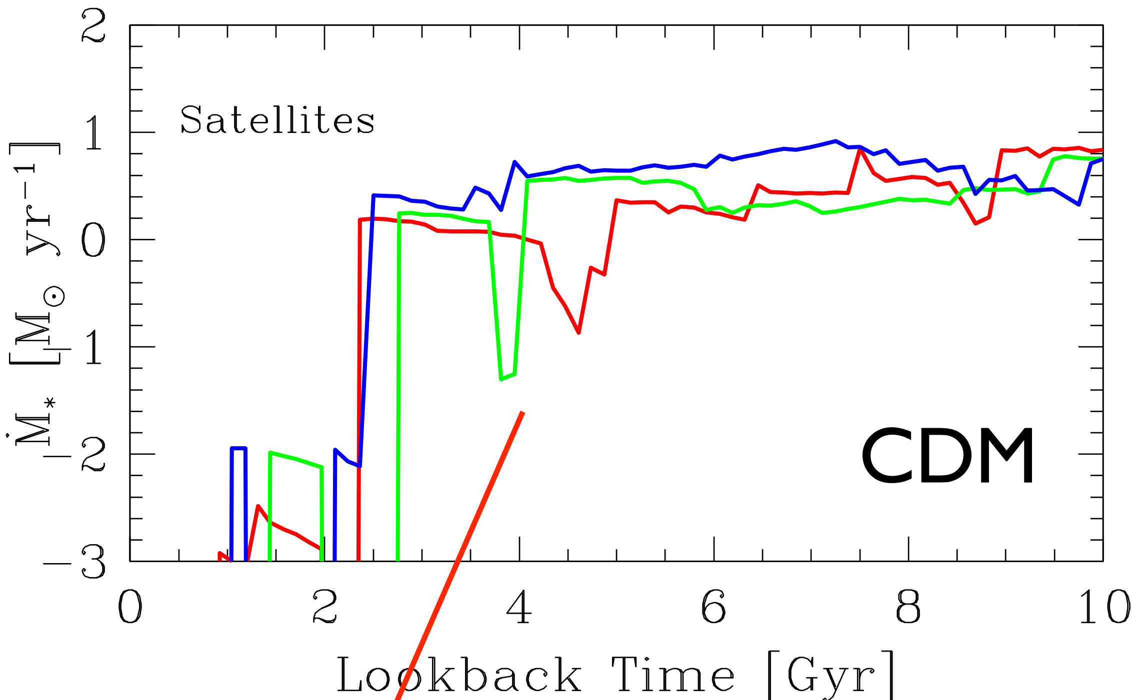

Passive Satellites in CDM at low redshift
- Cold gas converted into stars at high z
- Hot gas stripped when they were incorporated into larger DM haloesNo further star formation

CDM

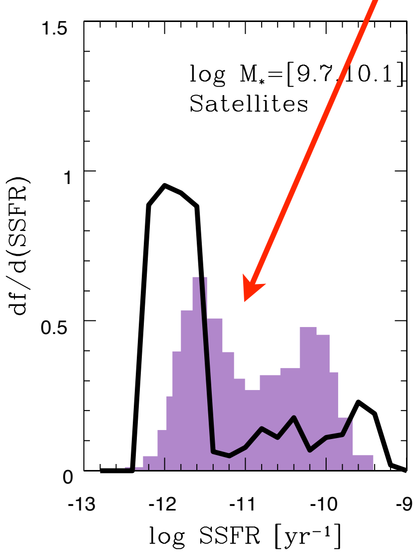

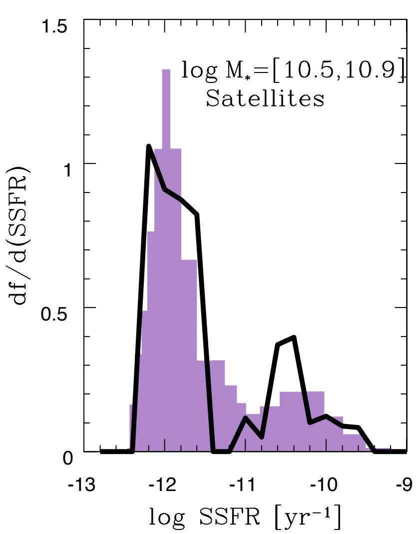

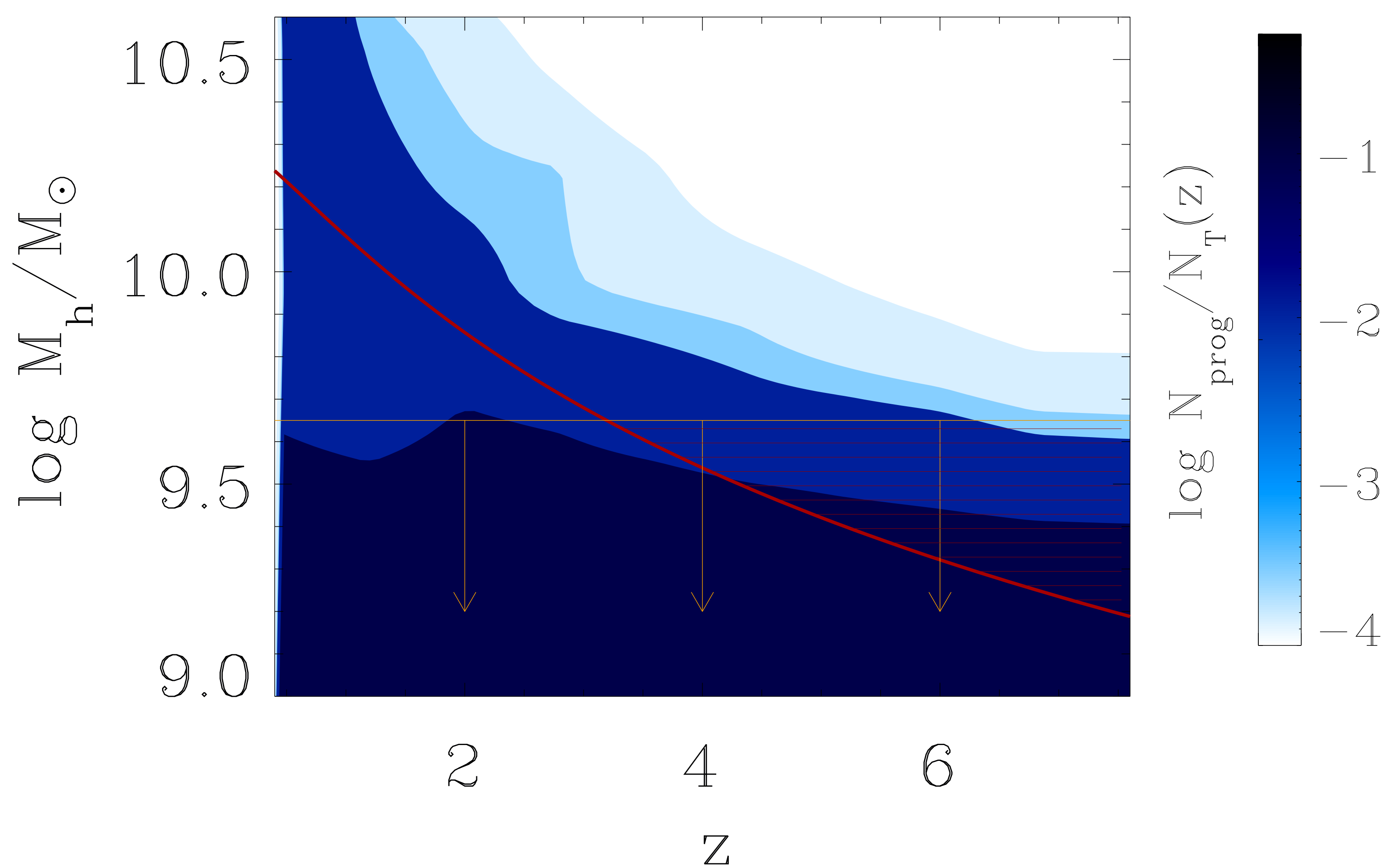

Star Formation histories of satellites in WDM

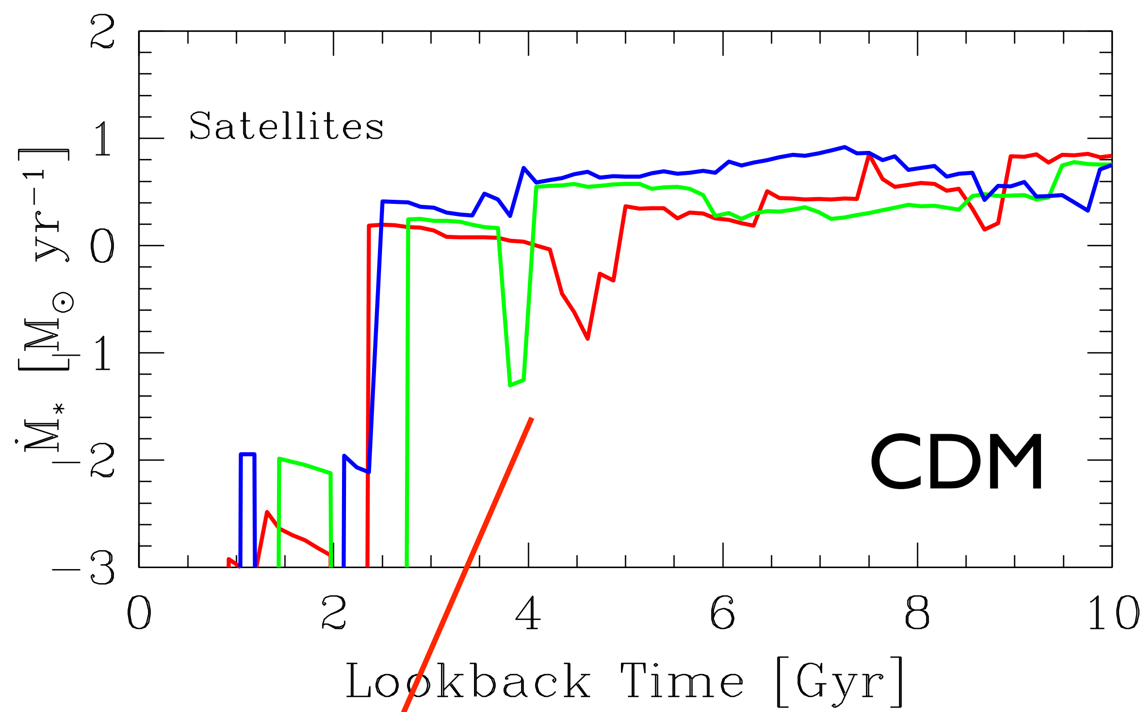

Passive Satellites in CDM at low redshift

- Cold gas converted into stars at high z
- Hot gas stripped when they were incorporated into larger DM haloesNo further star formation

CDM

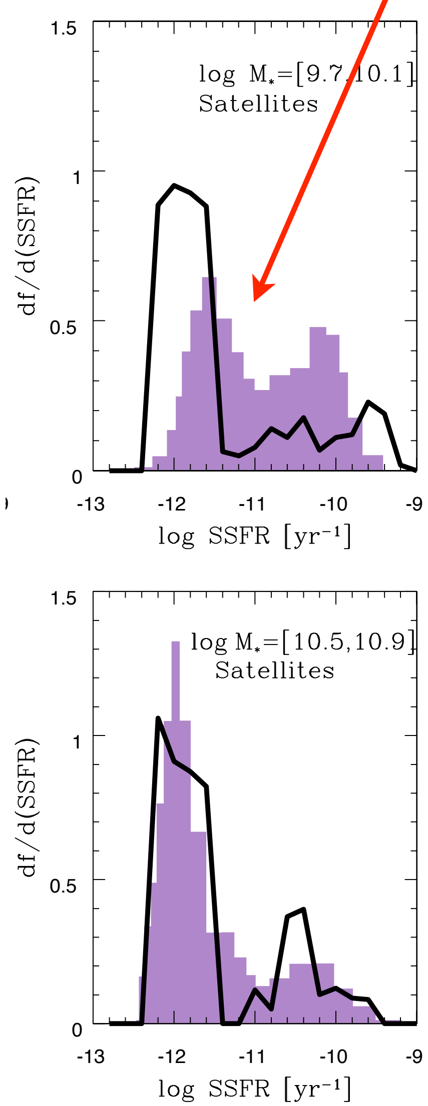

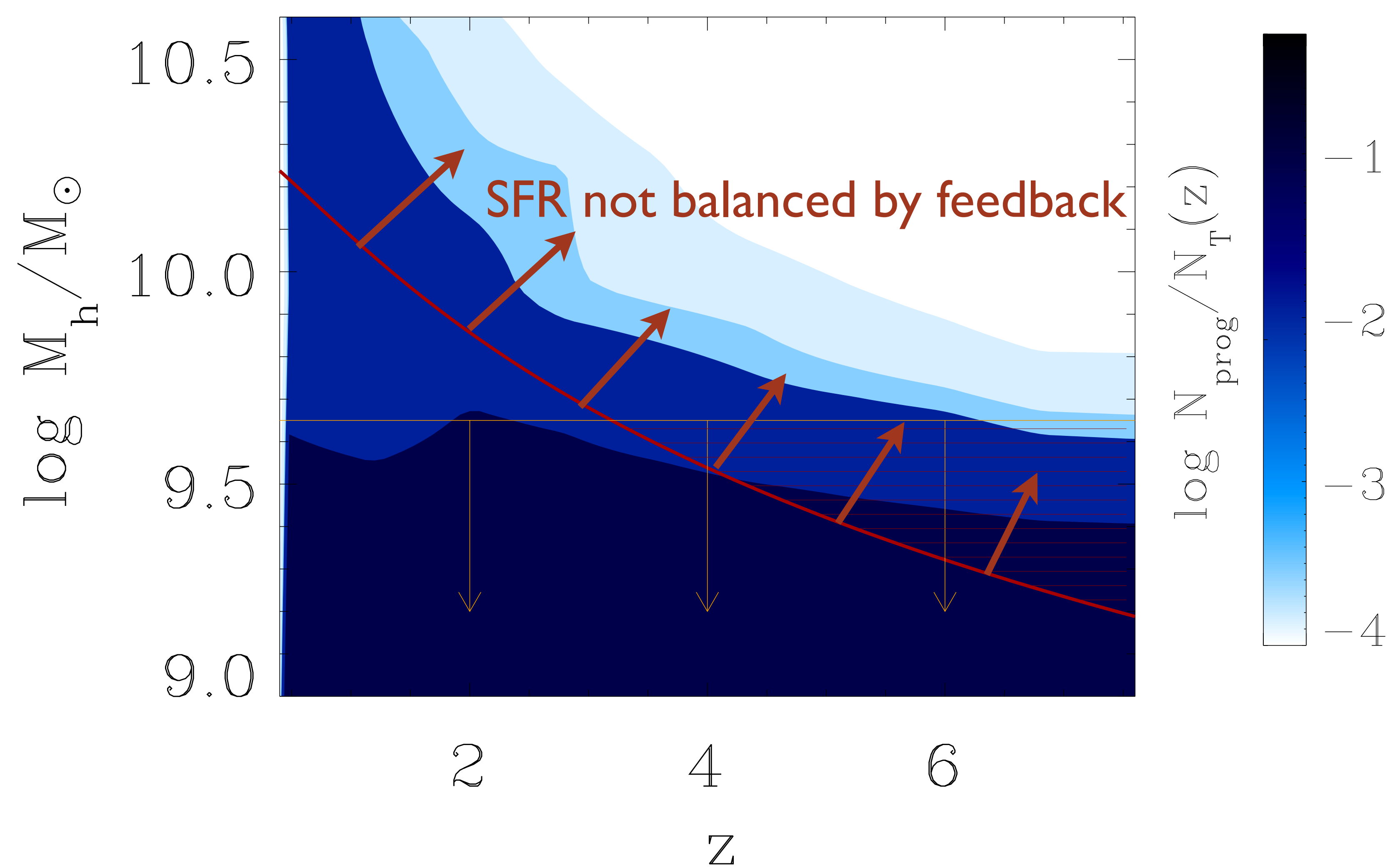

Star Formation histories of satellites in WDM

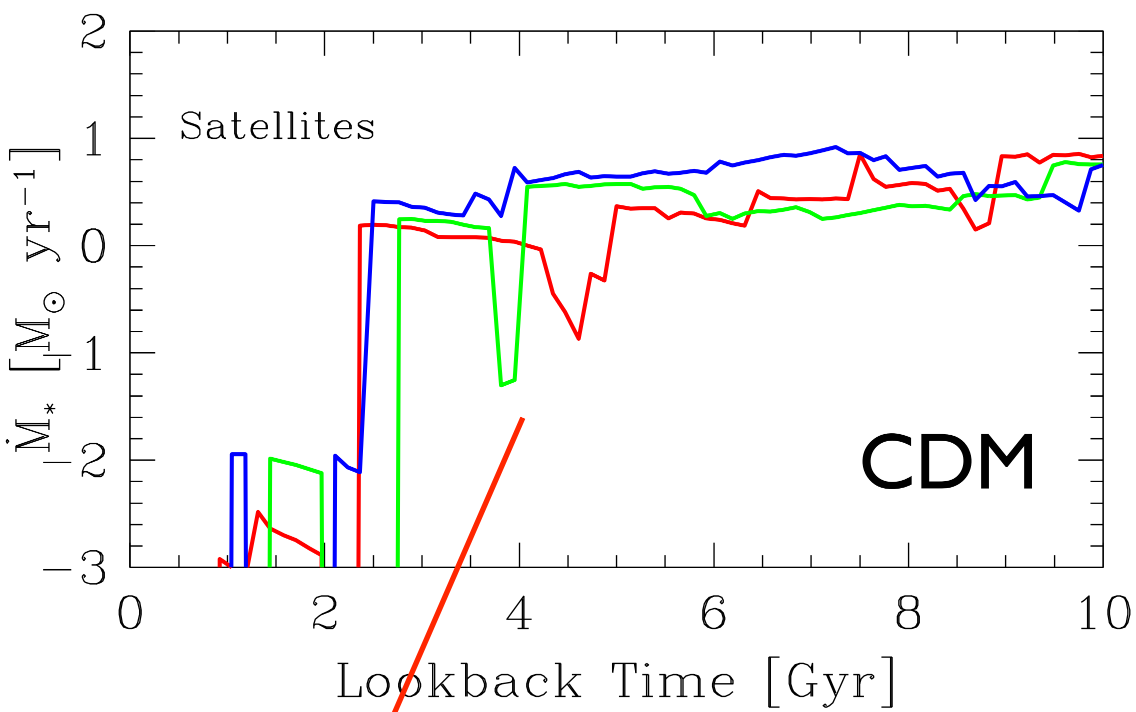

Passive Satellites in CDM at low redshift

- Cold gas converted into stars at high z
- Hot gas stripped when they were incorporated into larger DM haloesNo further star formation

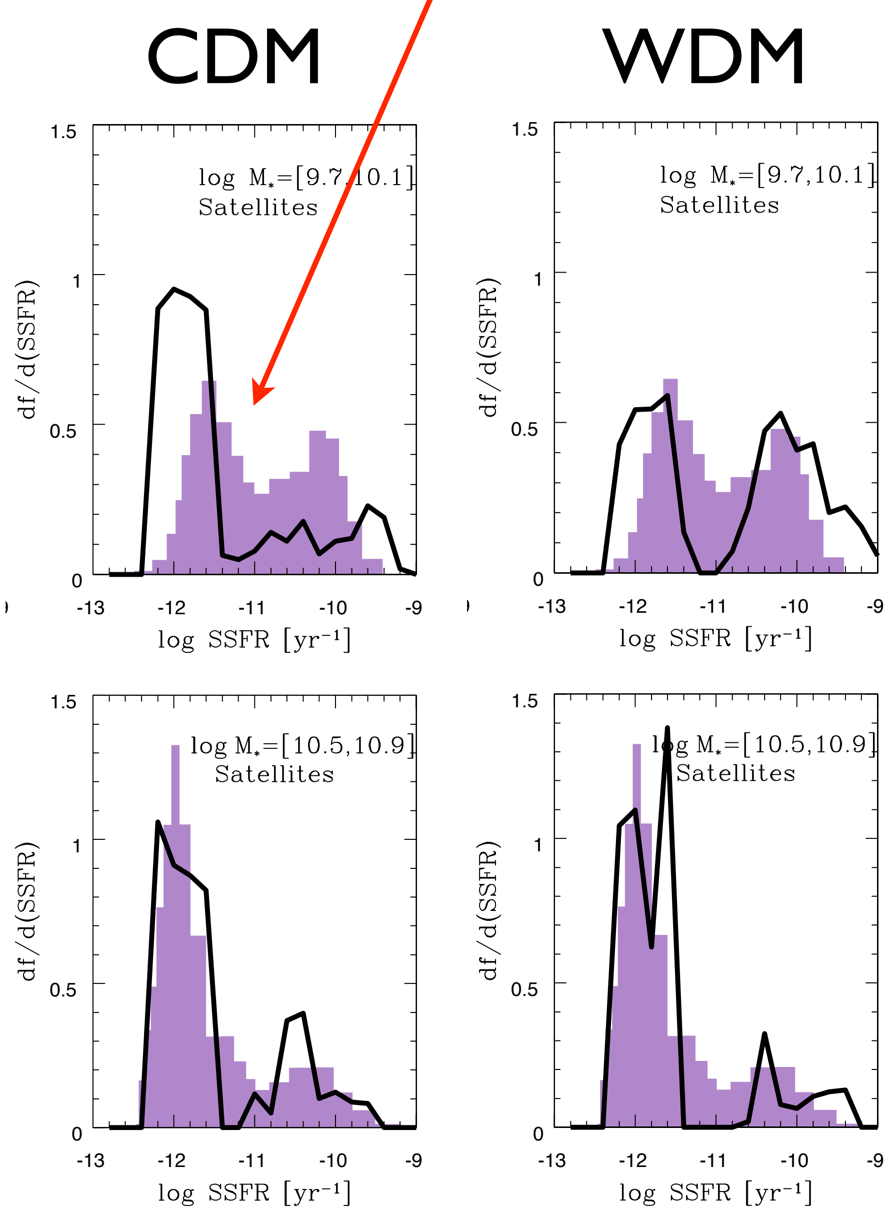

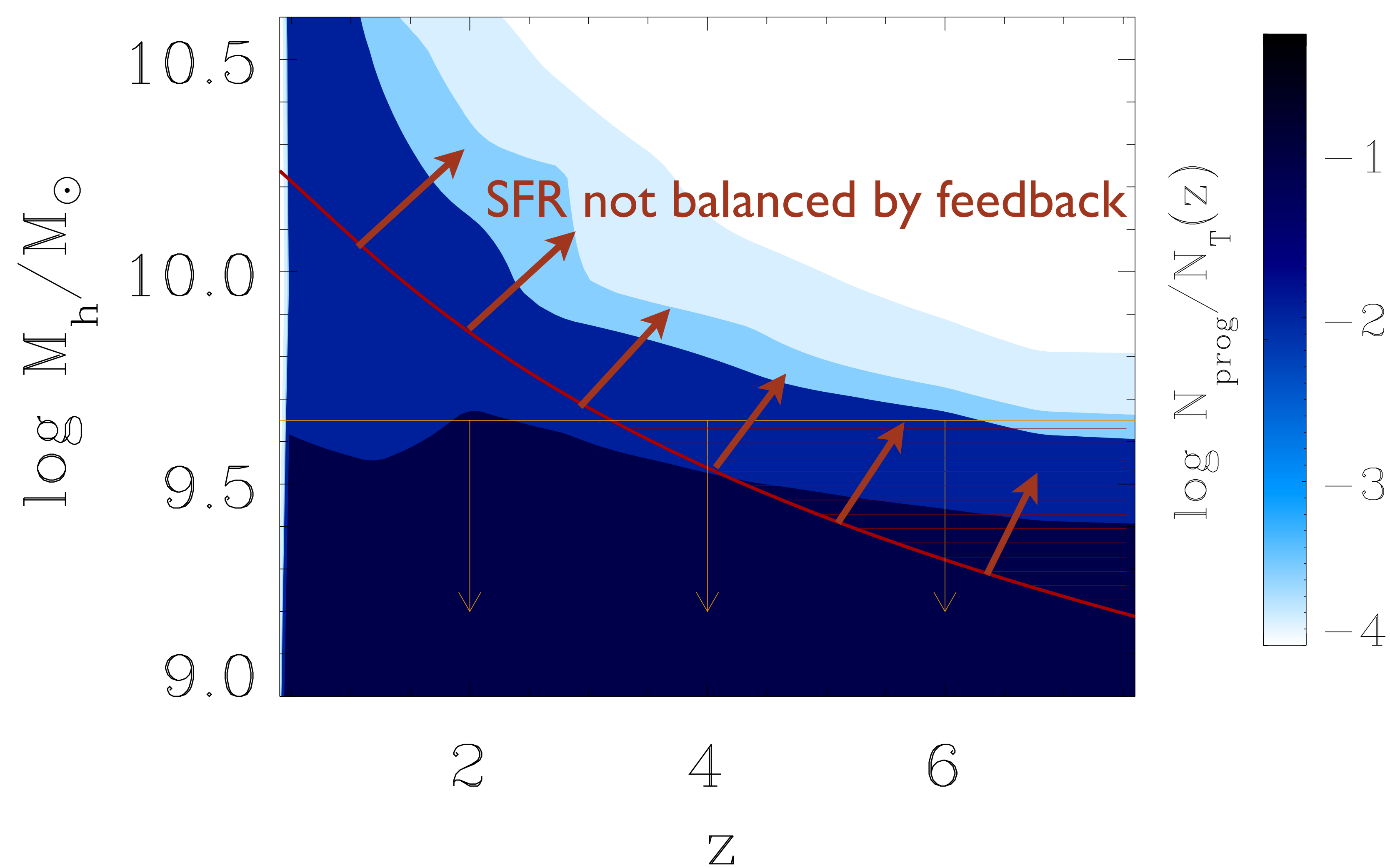

Star Formation histories of satellites in WDM

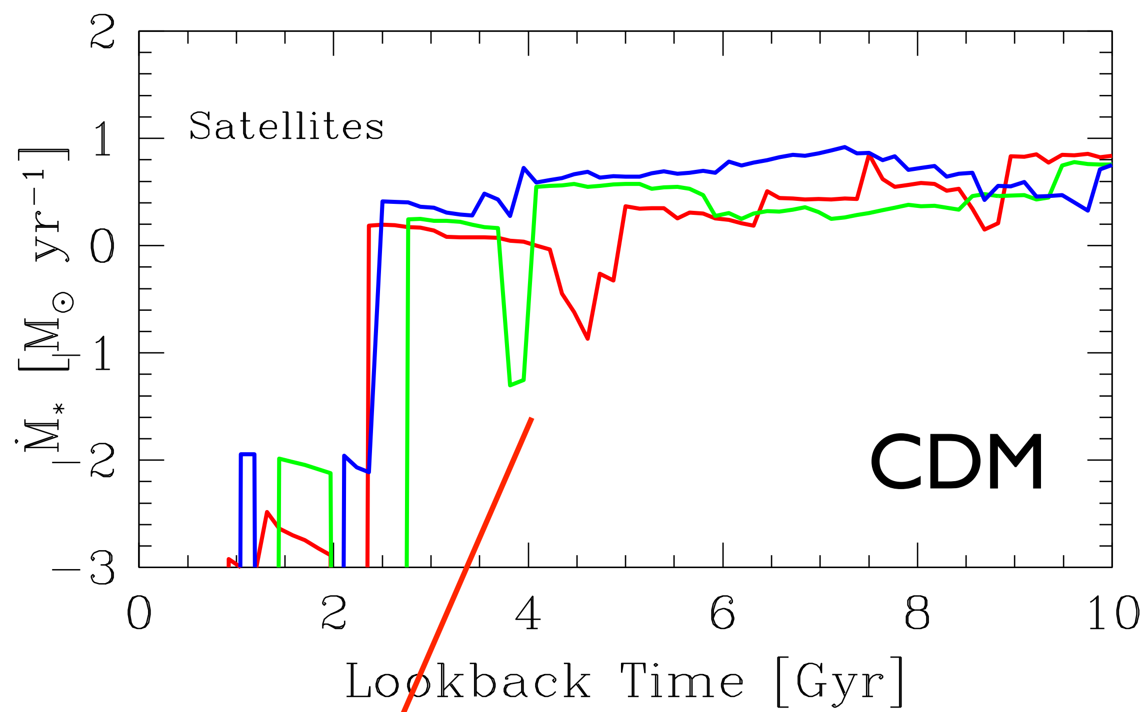

Passive Satellites in CDM at low redshift

- Cold gas converted into stars at high z
- Hot gas stripped when they were incorporated into larger DM haloesNo further star formation

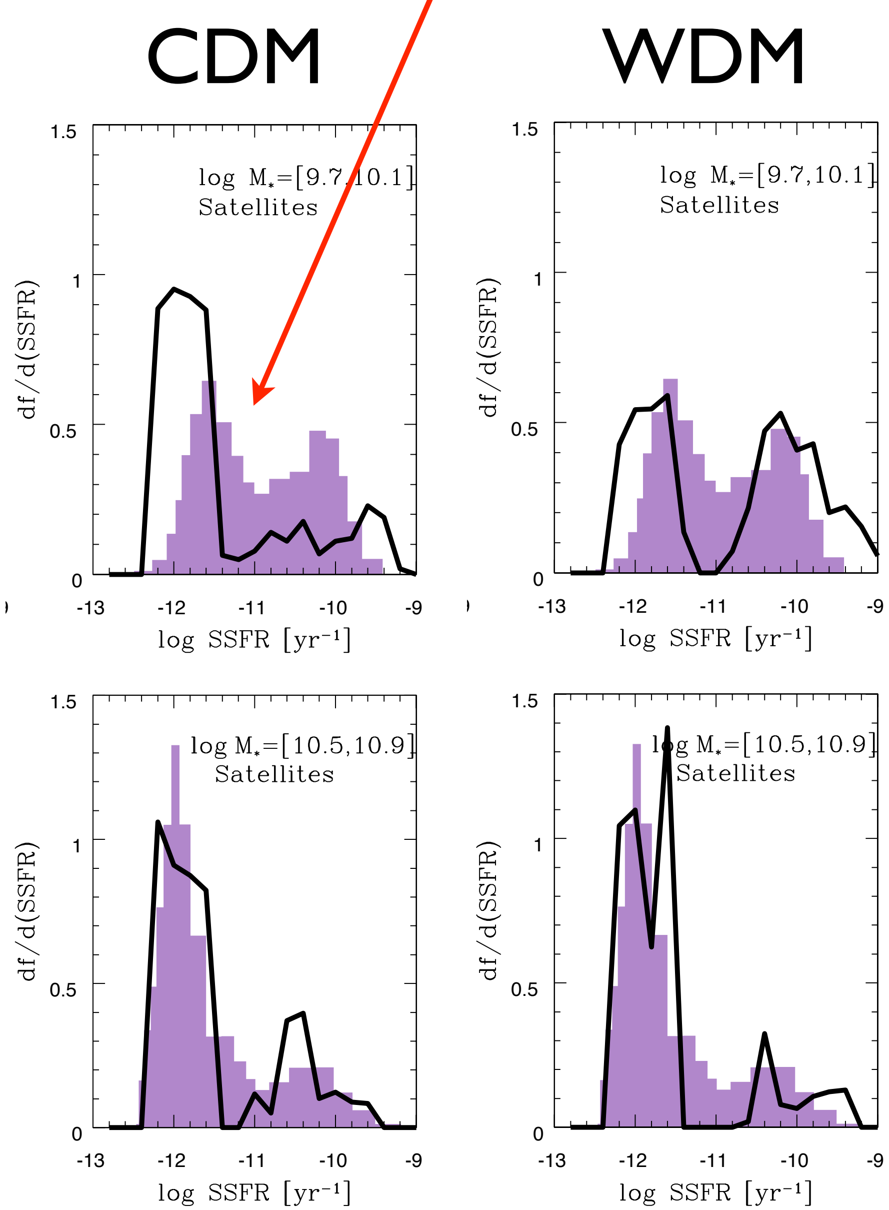

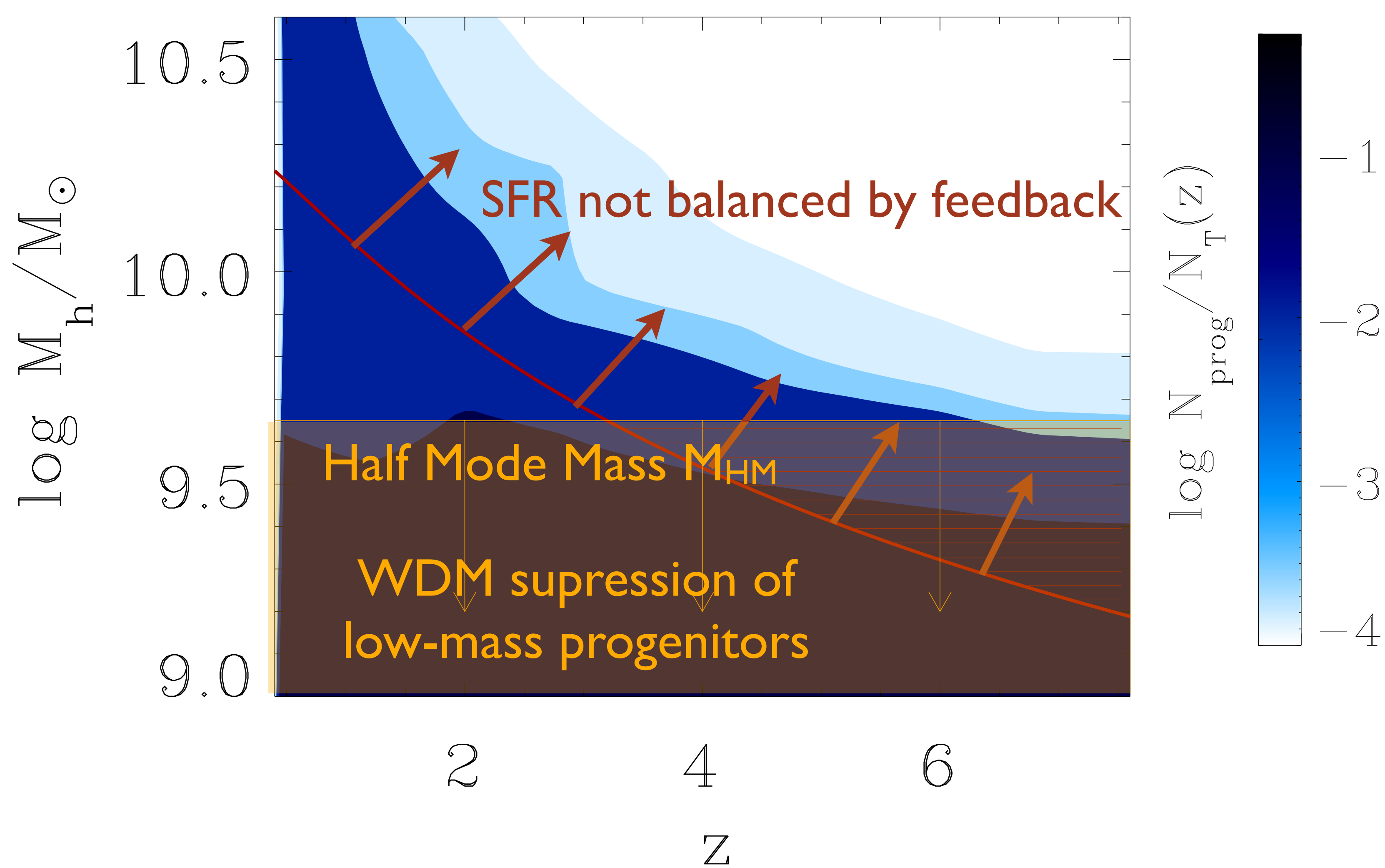

Star Formation histories of satellites in WDM

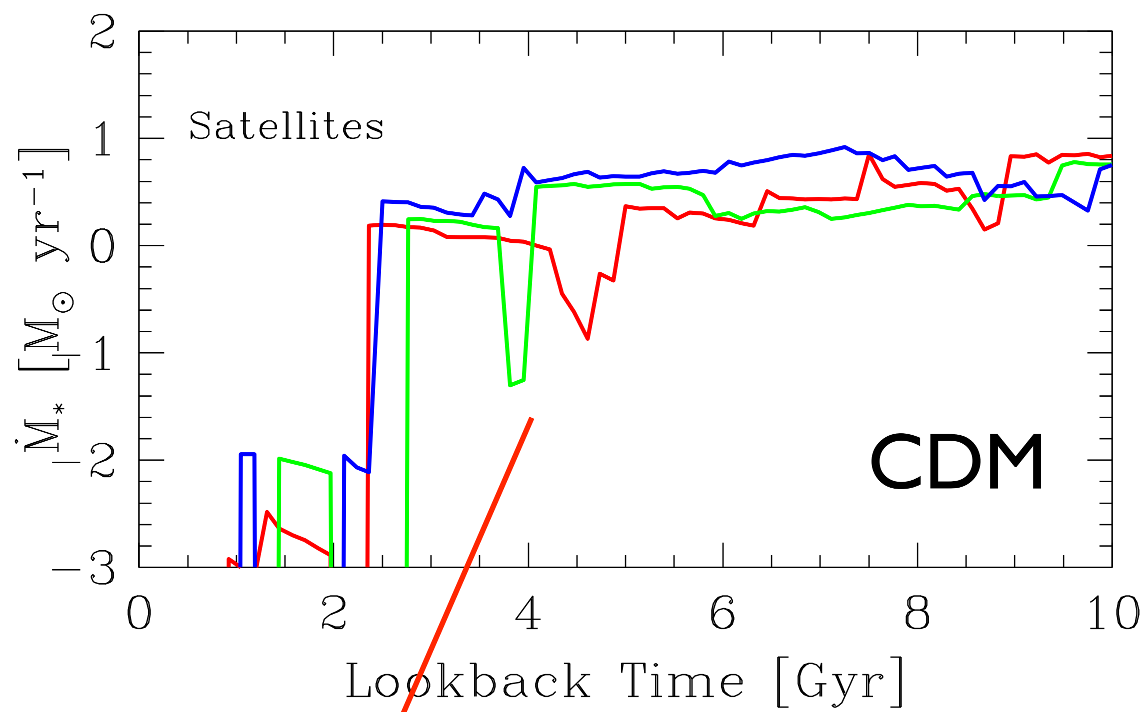

Passive Satellites in CDM at low redshift

- Cold gas converted into stars at high z
- Hot gas stripped when they were incorporated into larger DM haloesNo further star formation

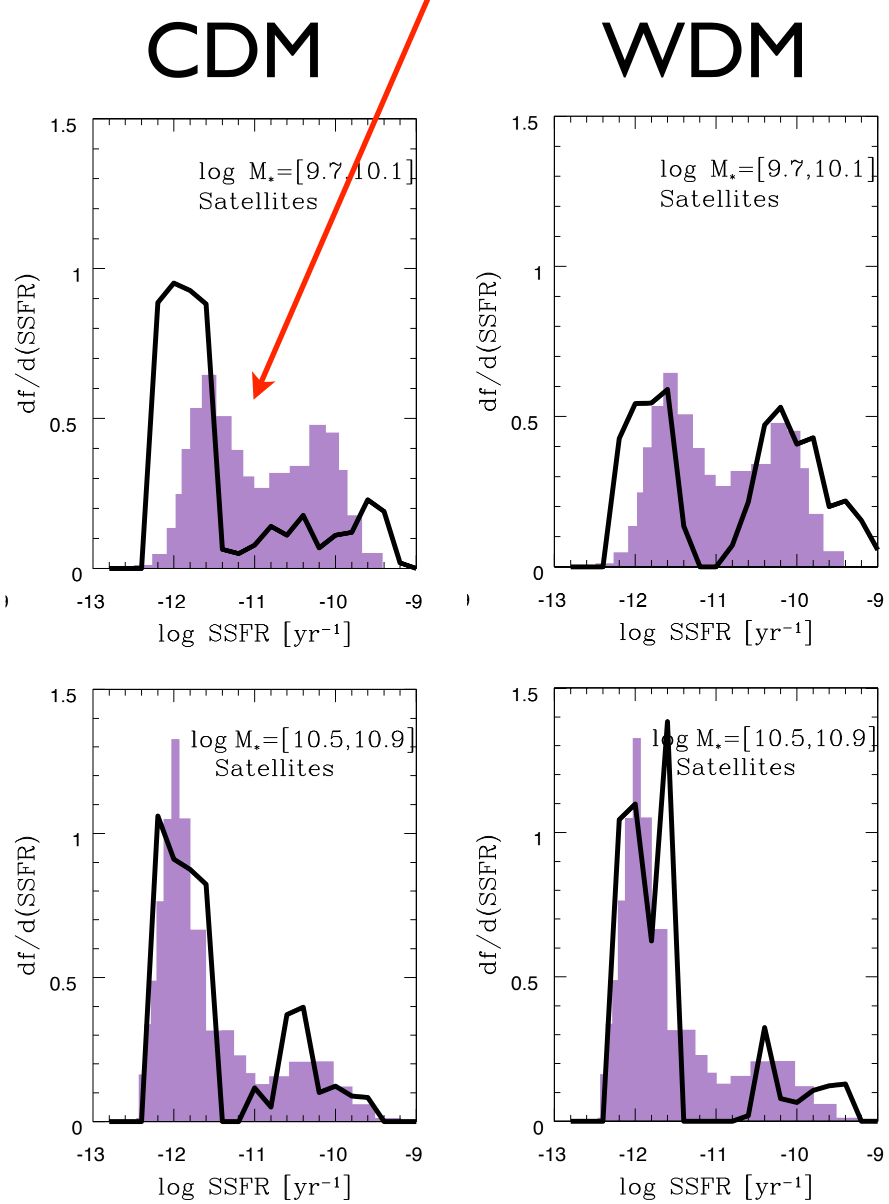

Reduction in the number of progenitors with high SFR at high redshifts

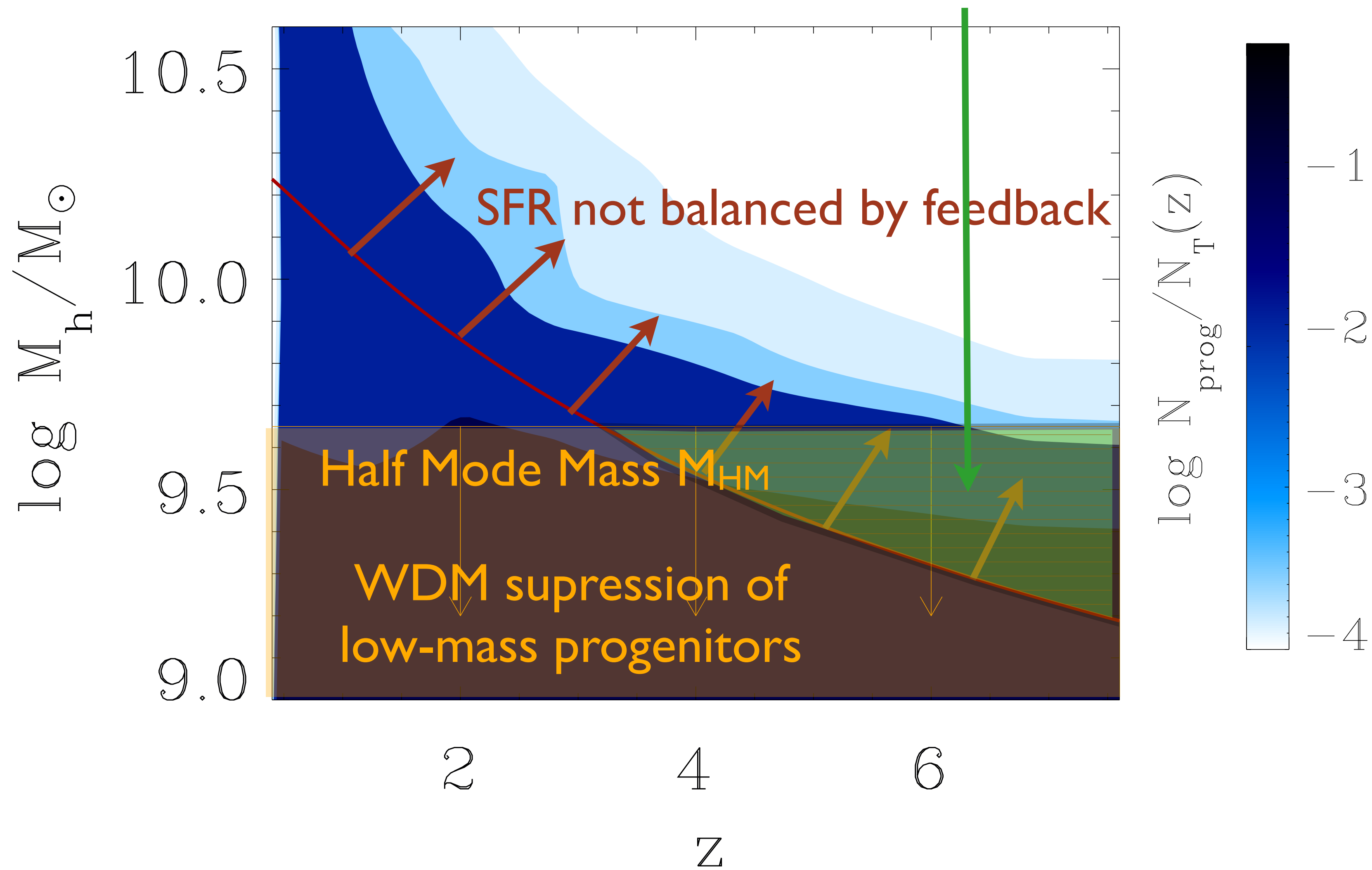

Growth of Stellar Mass for Satellite Galaxies

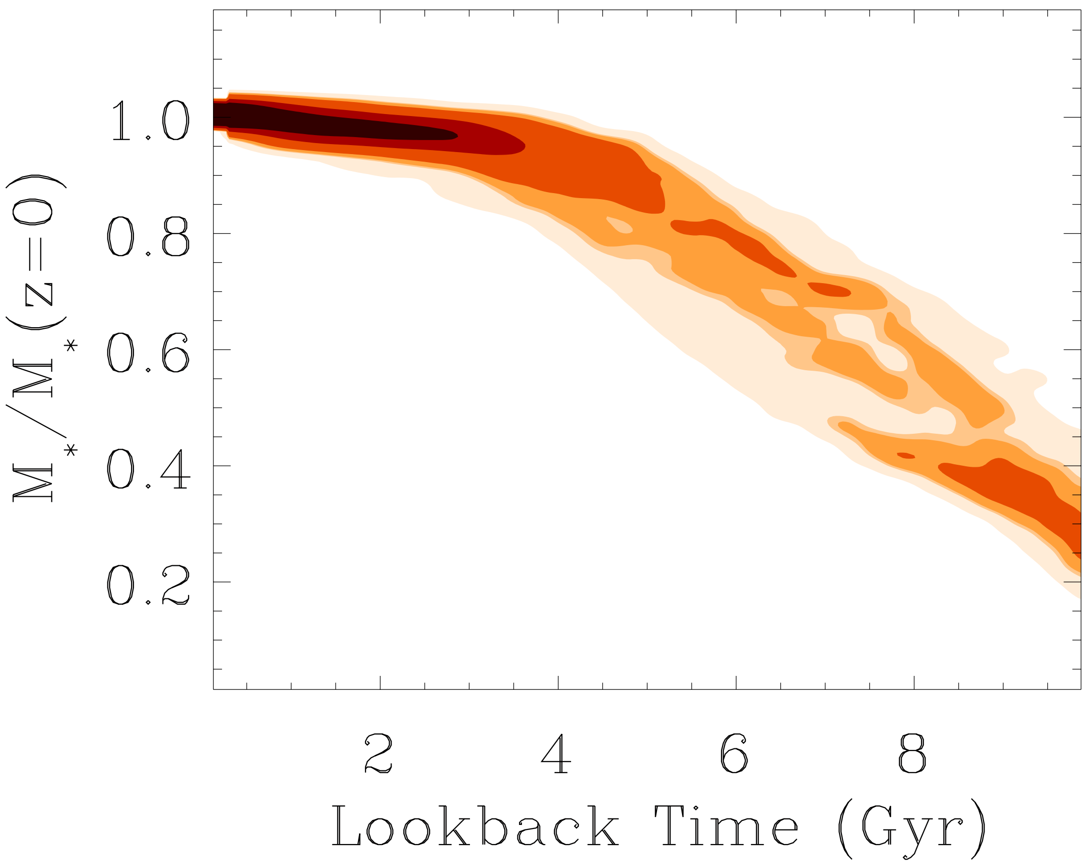

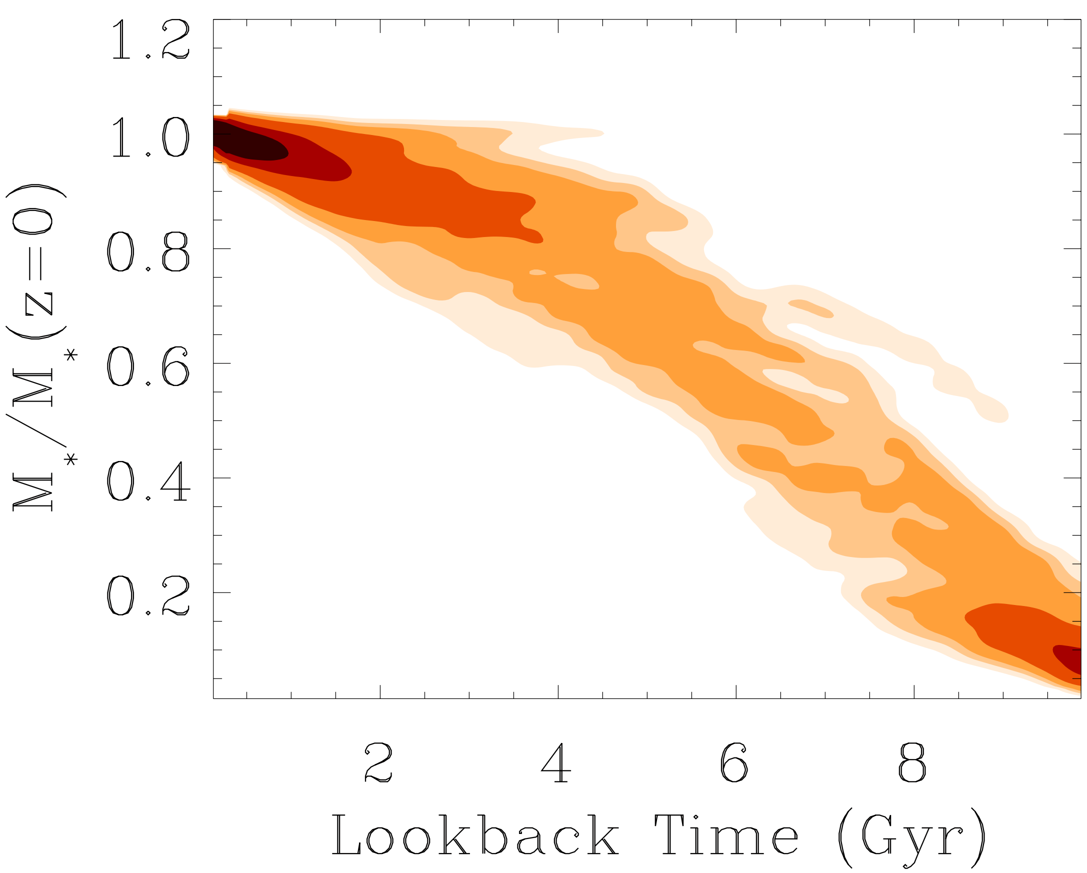

The suppression of progenitors of satellite galaxies with high SFR (those characterized by ineffective feedback) yields Slower growth of stella mass in WDM

Growth of Stellar Mass for Satellite Galaxies

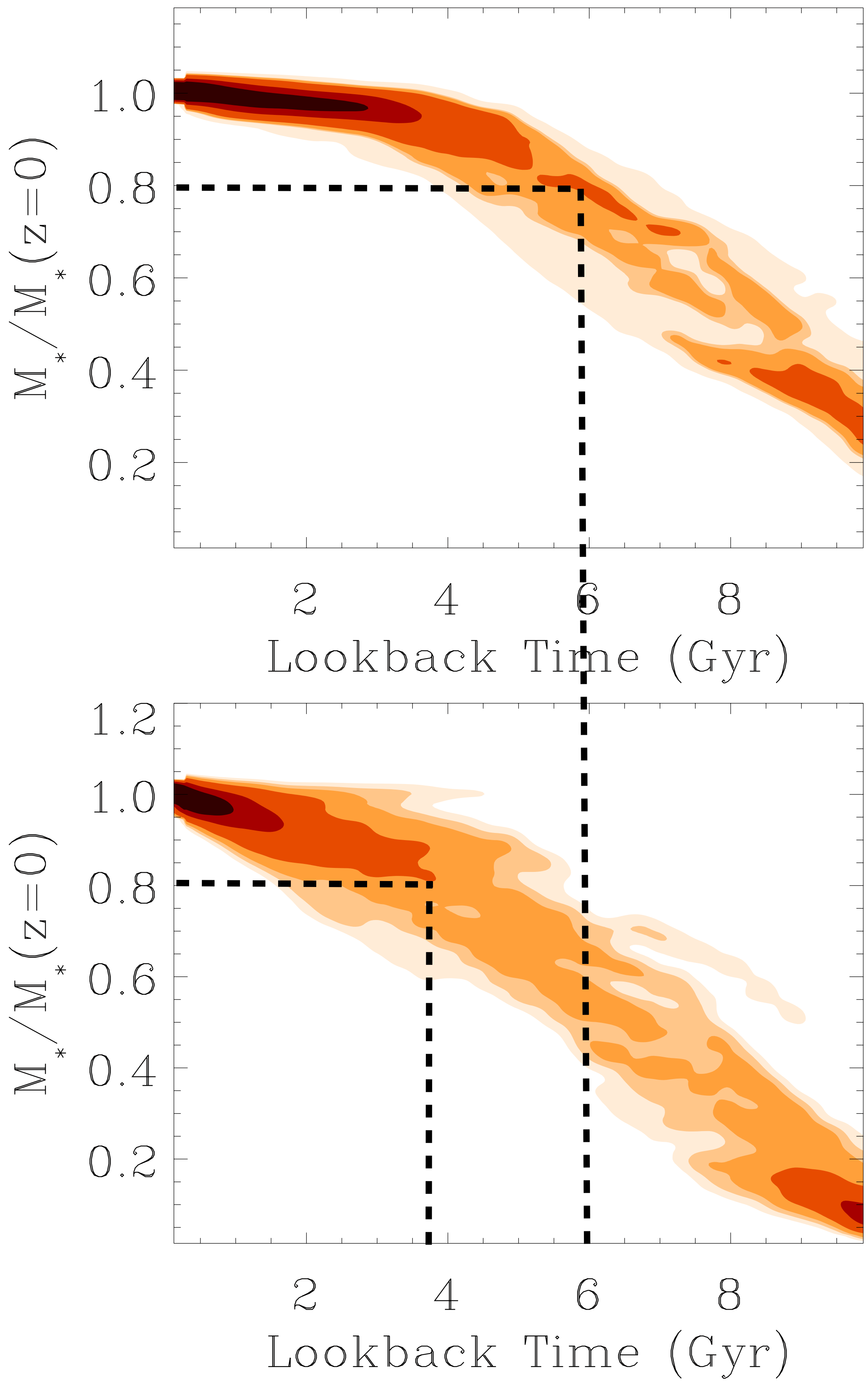

The suppression of progenitors of satellite galaxies with high SFR (those characterized by ineffective feedback) yields Slower growth of stella mass in WDM

CDM: 80 % of mass formed 6 Gyr ago
WDM: 80 % of mass formed 4 Gyr ago

Approx. delay ~ 2 Gyr

Fraction of Quiescent Satellite Galaxies

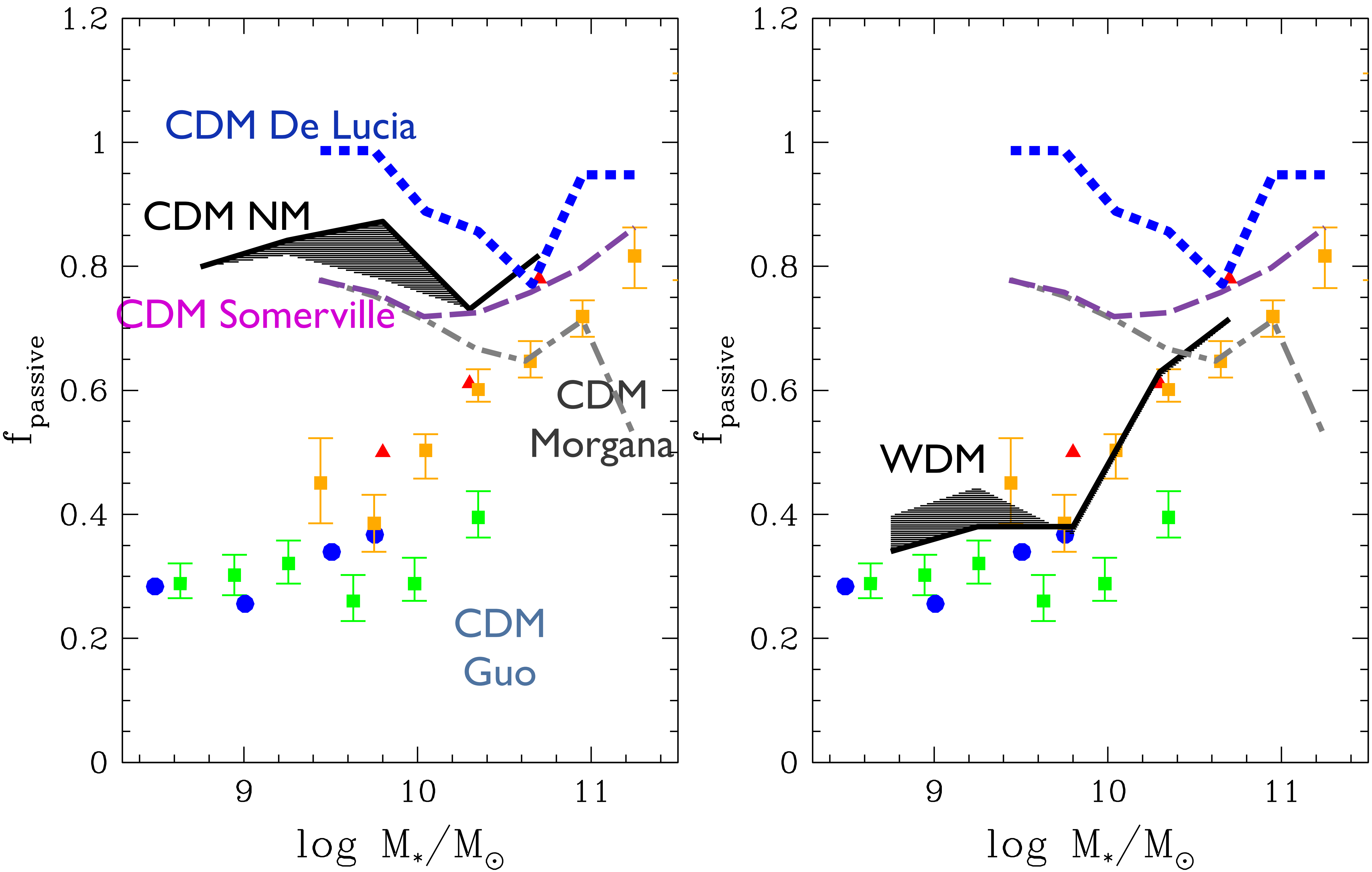

The Age of stellar populations in low-mass galaxies

CDM predicts early collapse of a huge number of low-mass halos, which remain isolated at later times retaining the early-formed stellar populations; as a result, CDM-based SAMs generally provide flat age-mass relations (Fontanot et al. 2009; Pasquali et al. 2010; De Lucia & Borgani 2012).

Increasing the stellar feedback worsen the problem

Early SF: WDM induces delay in star formation, affects small-mass objects(see, e.g., Angulo et al. 2013)

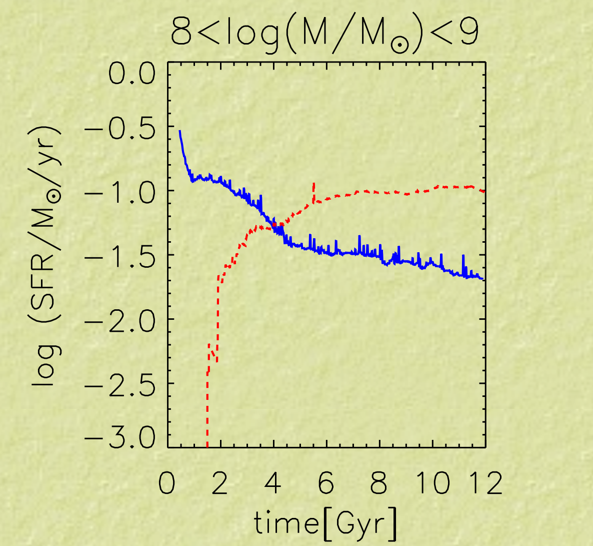

$$Age(t_0) = \frac{\int_0^{t_0} (t_0 - t)\, \psi(t)\, dt}{\int_0^{t_0} \psi(t)\, dt}$$

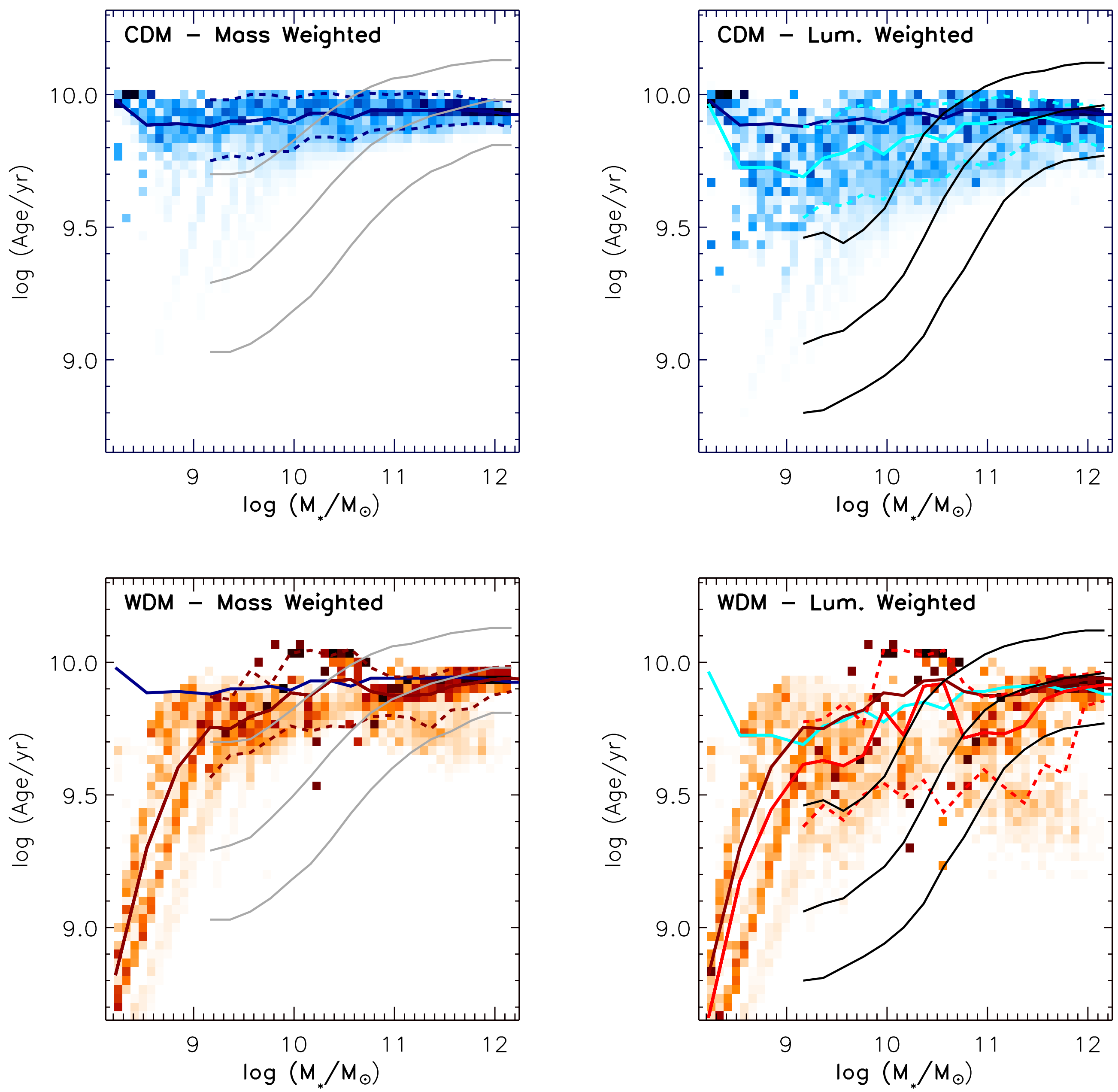

Calura, NM, Gallazzi 2014

The upper, the middle and the lower grey (black) curves represent the 16th, the 50th (median) and the 84th percentiles of the observed distribution in mass-(light-)weighted stellar age (Gallazzi et al. 2008)

Future Prospects

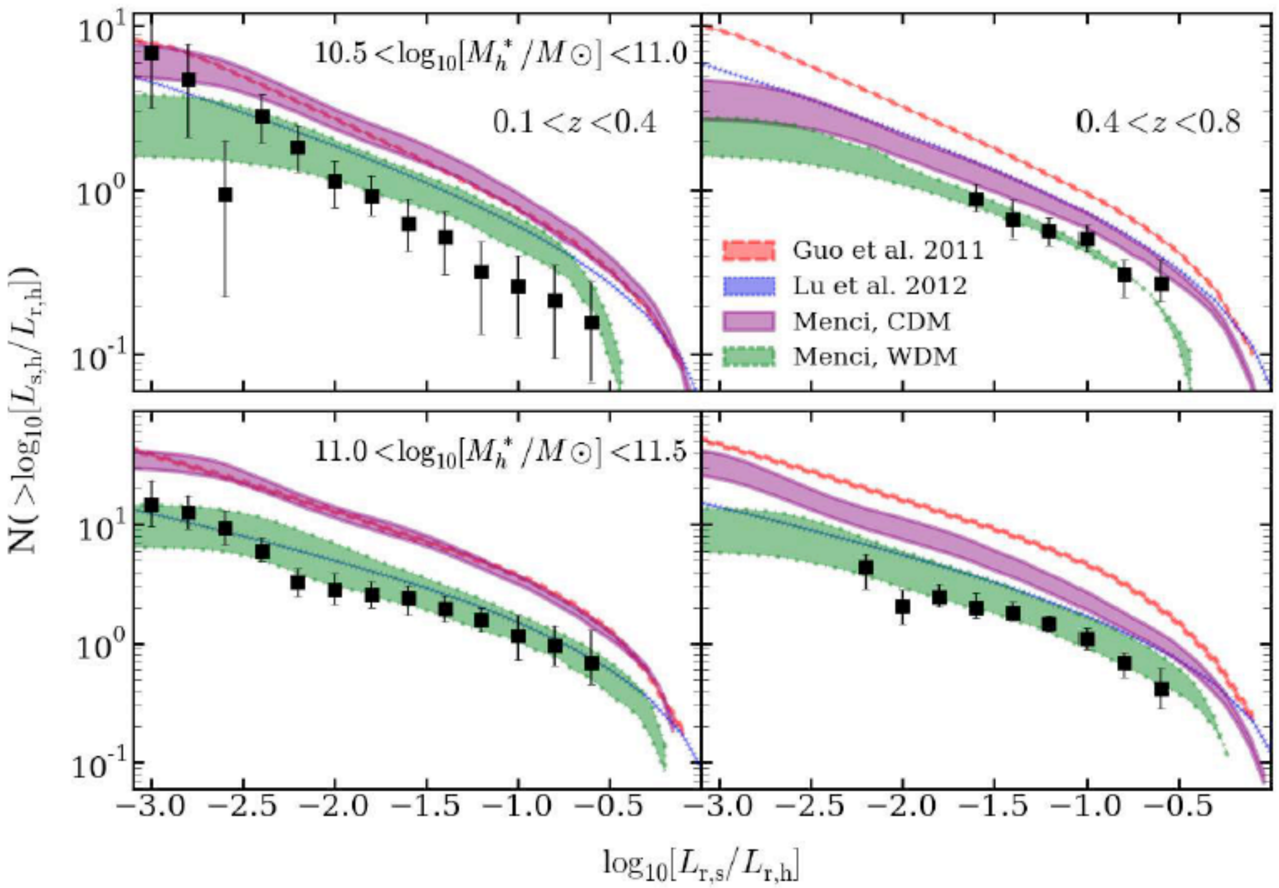

To reduce the number of predicted satellites CDM models have to maximize feedback effects

This results into red colors (suppressed star formation) in satellite galaxies

Near Future: breaking the degeneracy between feedback and DM models

Extend the field satellite luminosity function down by 2 magn using HST data (10000 times fainter than their hosts at z<1.5.

Reliably measure the satellite colors

Constraining the WDM candidate mass through the abundance of low-mass galaxies

Schultz et al. 2014

Use abundance matching at the bright end of the the high-z luminosity functions to compute L-M_h relation.

Comparing the observed and the predicted densities of faint galaxies they derive a lower mass limit m_X>1 keV

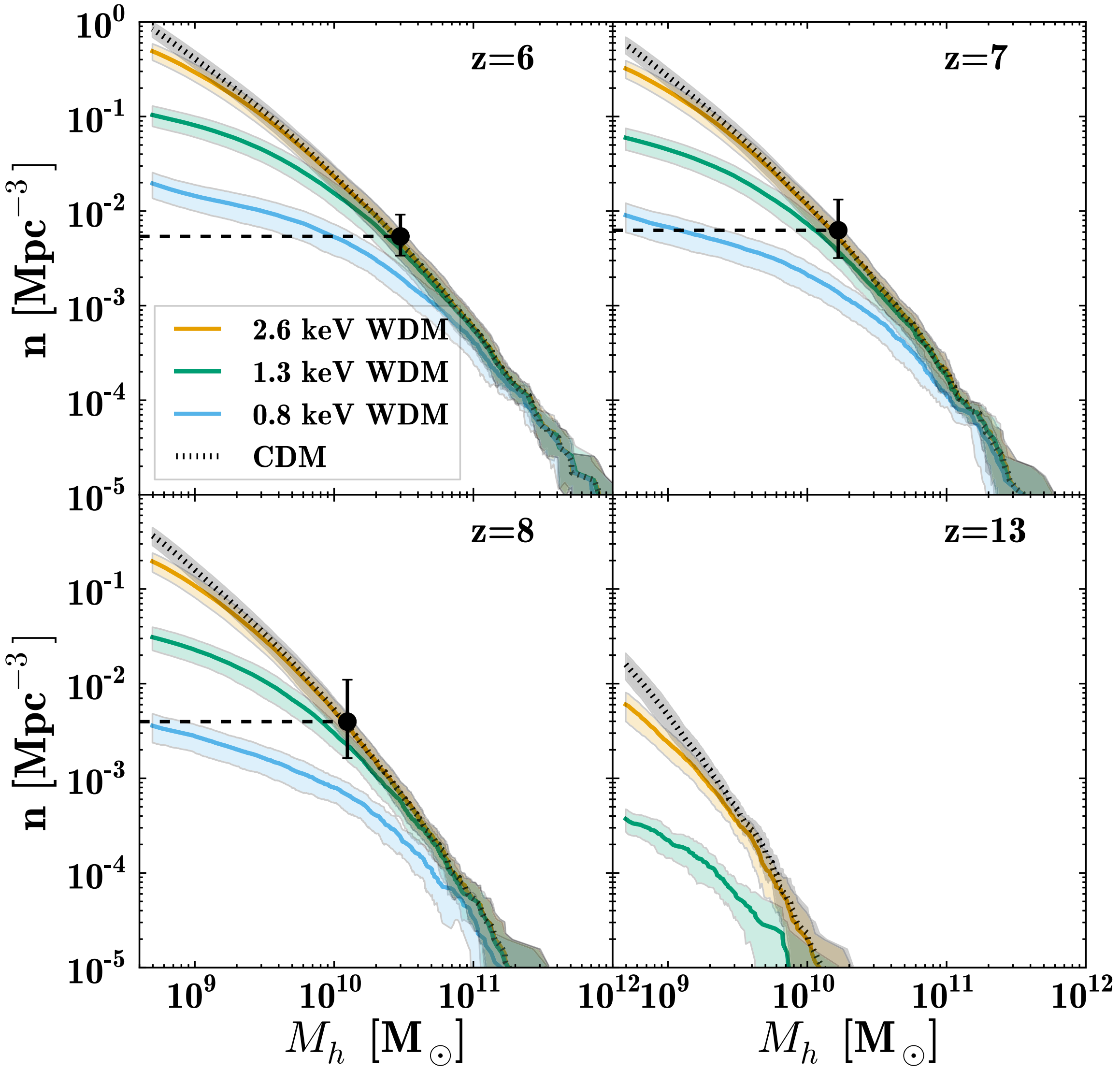

Constraining the WDM candidate mass through the abundance of low-mass galaxies

Schultz et al. 2014
Use abundance matching at the bright end of the the high-z luminosity functions to compute L-M_h relation.

Comparing the observed and the predicted densities of faint galaxies they derive a lower mass limit m_X>1 keV

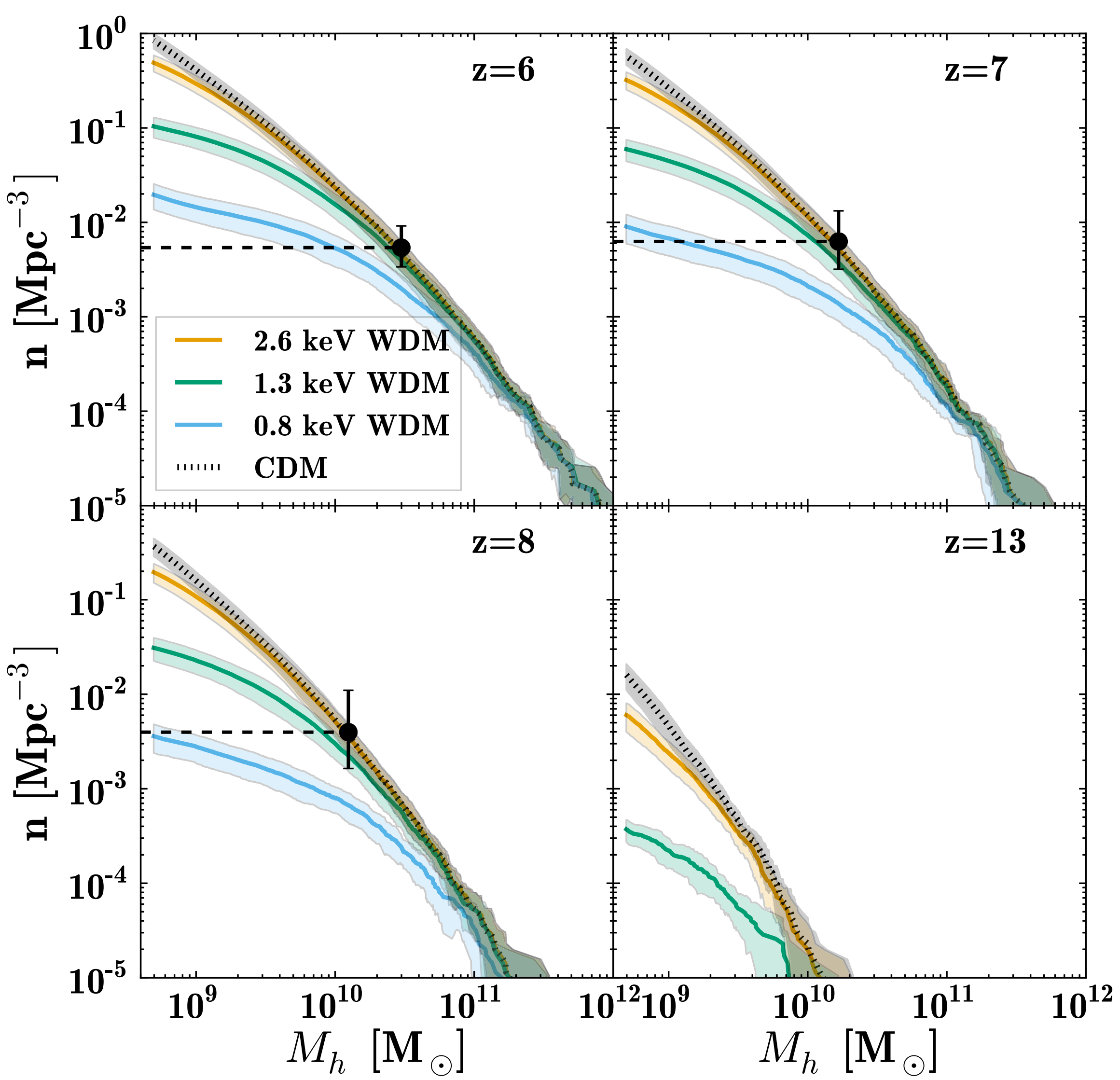

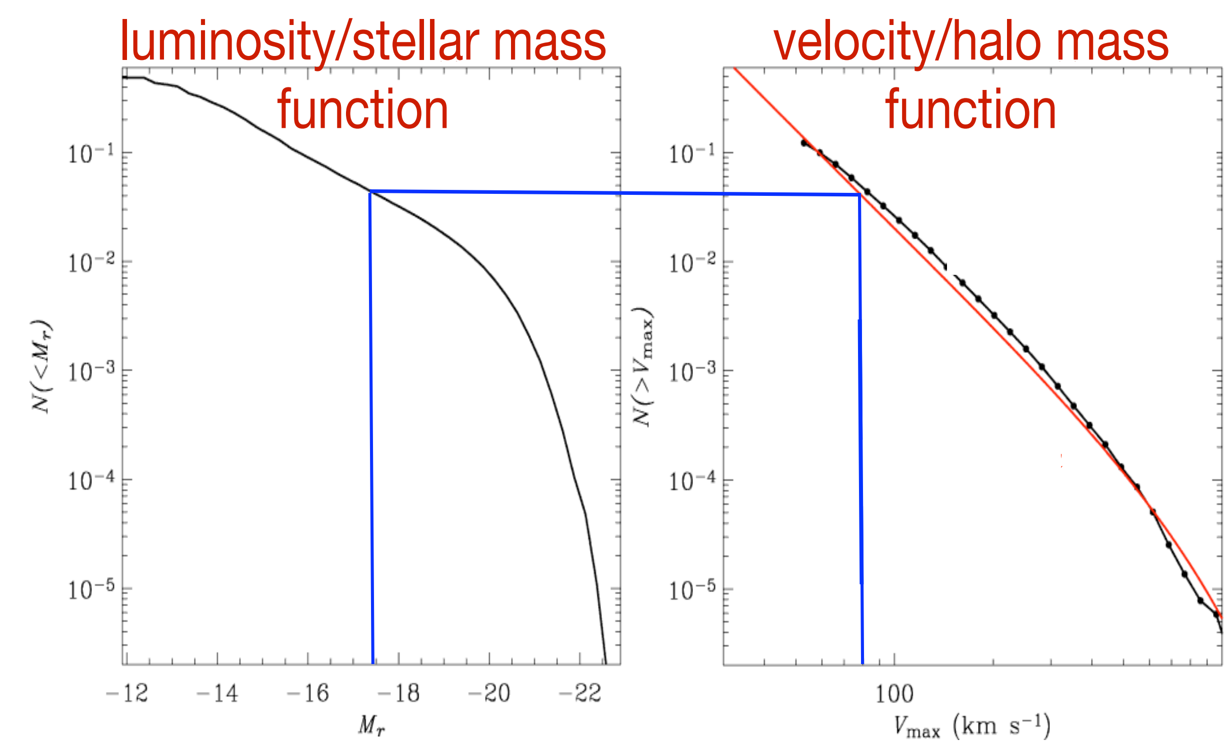

Constraining the WDM candidate mass through the abundance of low-mass galaxies

Schultz et al. 2014

Use abundance matching at the bright end of the the high-z luminosity functions to compute L-M_h relation.

Comparing the observed and the predicted densities of faint galaxies they derive a lower mass limit m_X>1 keV

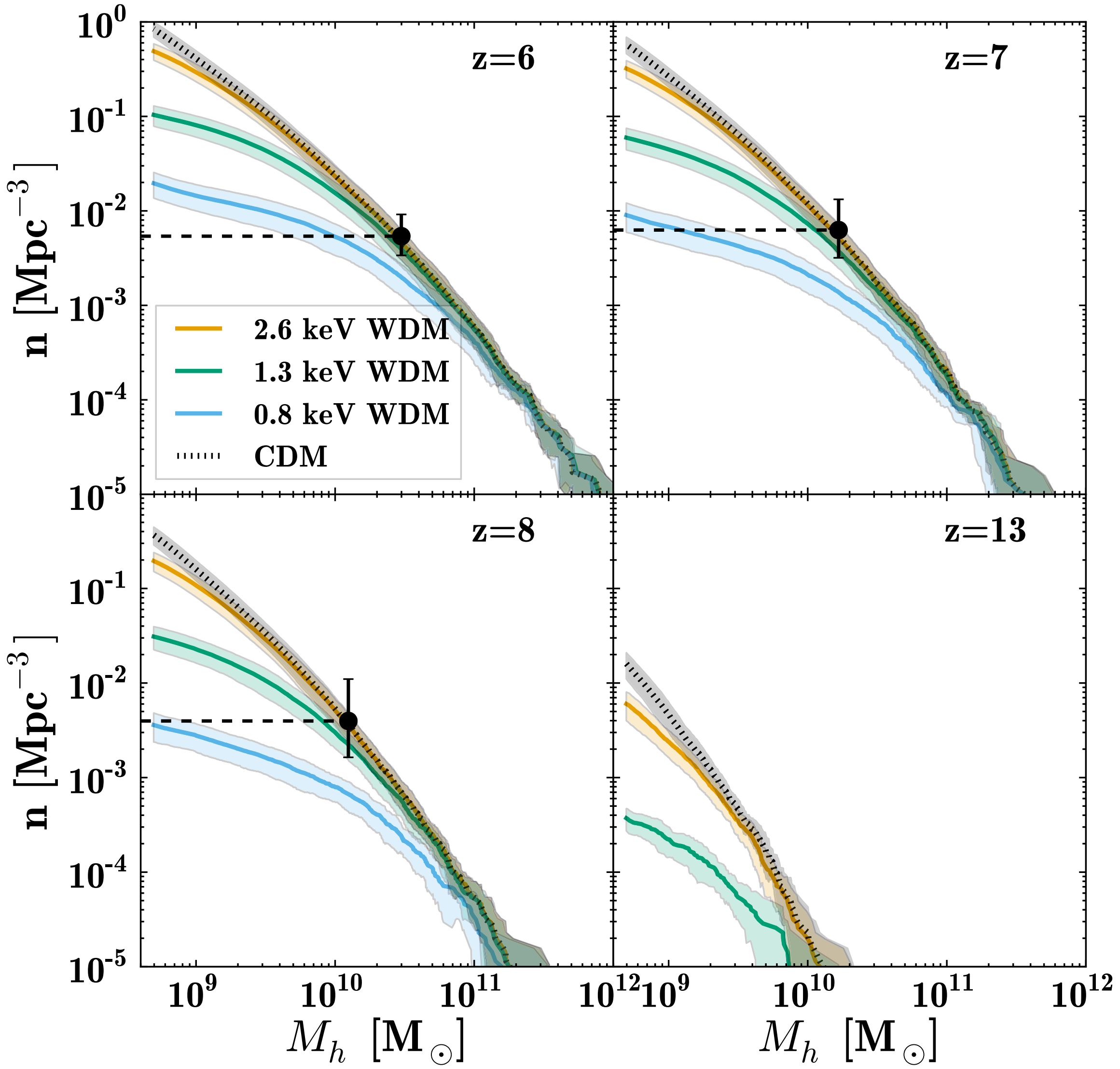

A different approach
focus on lower redshift but deeper observations

THE ASTROPHYSICAL JOURNAL, 780:143 (14pp), 2014 January 10 ALAVI ET AL.

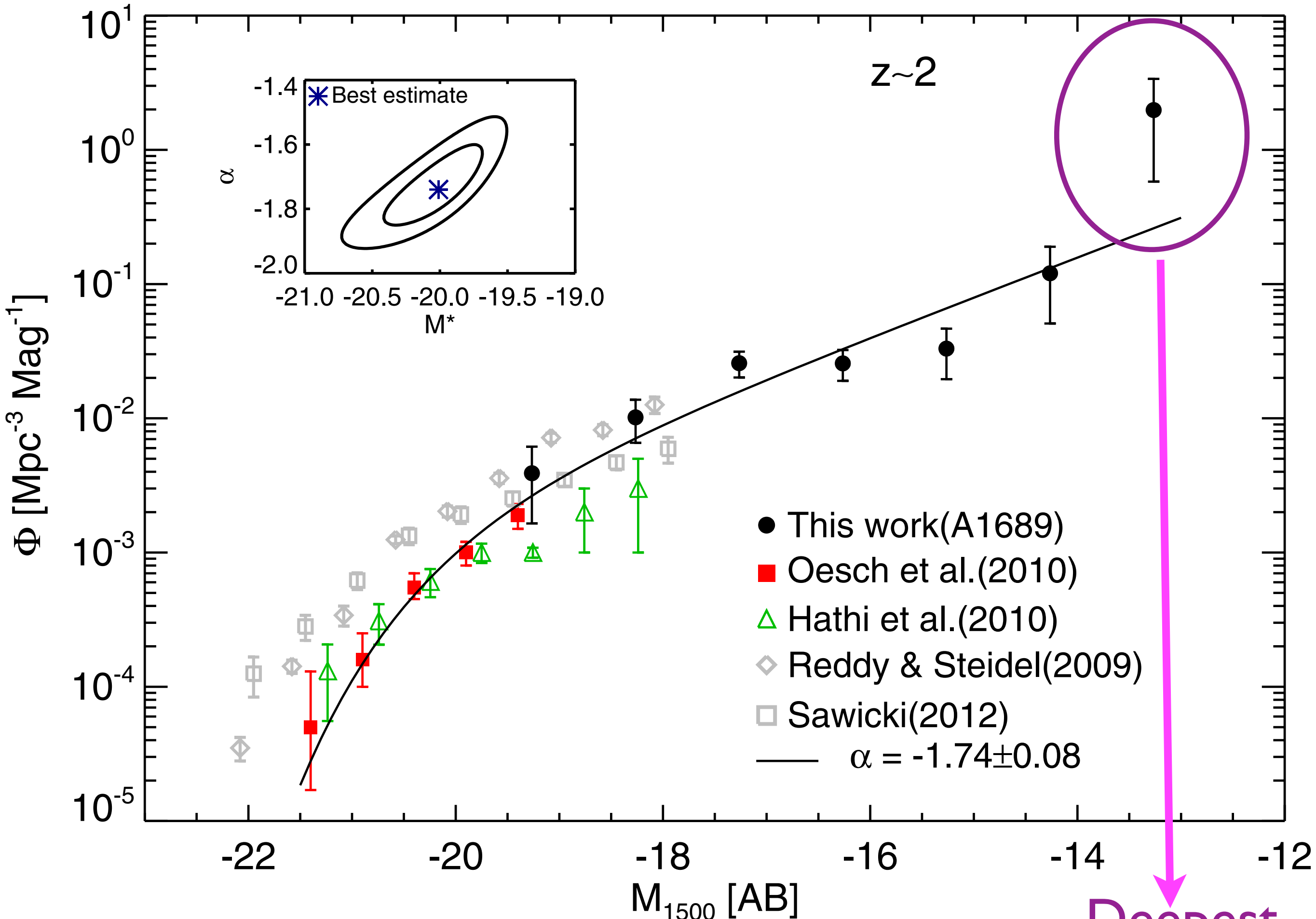

Deepest Luminosity Function measured so far

To connect M_{1500} to DM mass M

1) UV luminosity is directly linked to SFR

log SFR=-0.4(M_{UV}+18.6-9.97 E_{B-V}) $M_{\odot}$/yr

Deep ultraviolet imaging of the lensing cluster A1689 with the WFC3/UVIS camera on *Hubble Space Telescope* in the F275W (30 orbits) and F336W (4 orbits) filters.
Identify z ~ 2 star-forming galaxies via their Lyman break. Because of the unprecedented depth of the images and the large magnification provided by the lensing cluster, we detect galaxies 100× fainter than previous surveys at this redshift.

Constraining m_X through ultra-deep LF of lensed galaxies

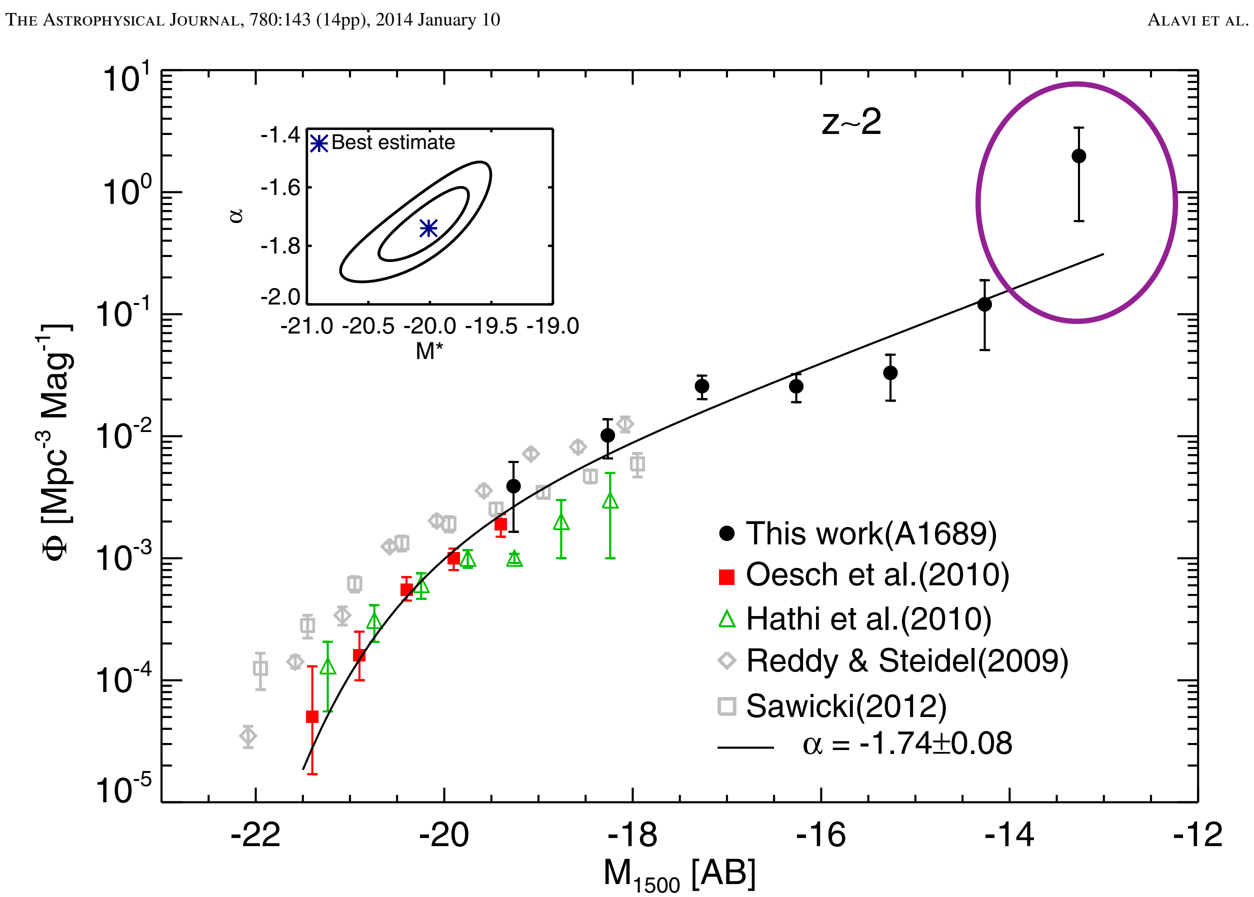

To connect M_{1500} to DM mass M

1) UV luminosity is directly linked to SFR

$\log SFR = -0.4(M_{UV} + 18.6 - 9.97\, E_{B-V})\ M_\odot/yr$

2) $SFR = M_{gas}/\tau_*$

3) $\log M/M_\odot = -0.4(M_{UV} + 18.6) + 8 - \eta$

4) $\eta = \dfrac{M_*}{M}\,\dfrac{M}{M_*}\,\dfrac{10^8\ yrs}{\tau_*}$

Constraining m_X through ultra-deep LF of lensed galaxies

NM, Sanchez, Castellano, Grazian 2015

Santini et al. 2014

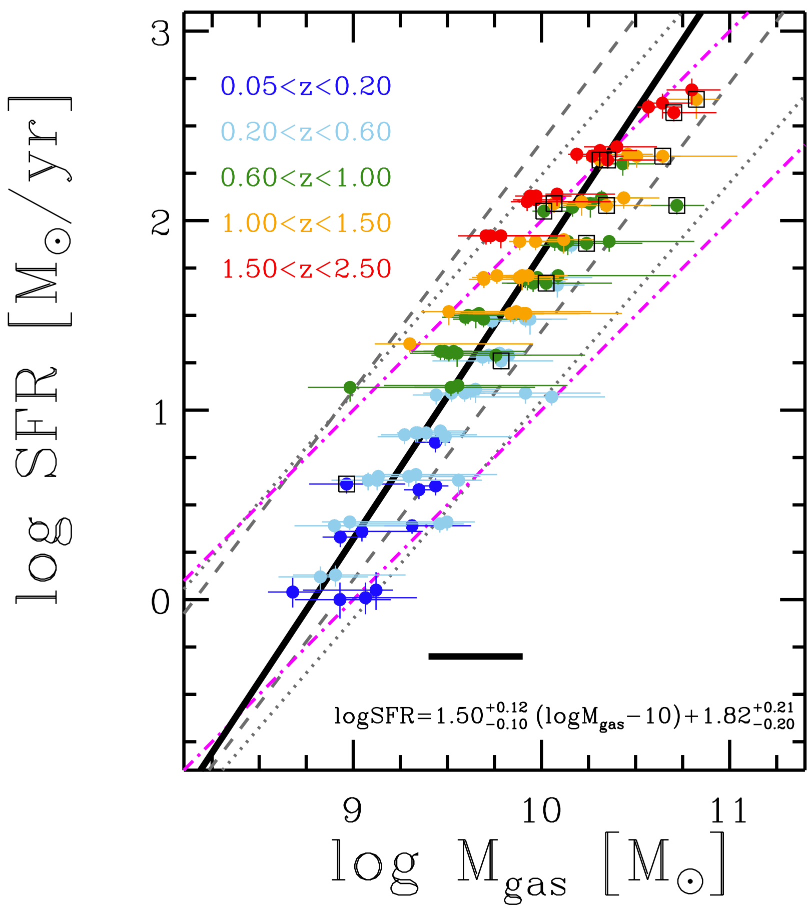

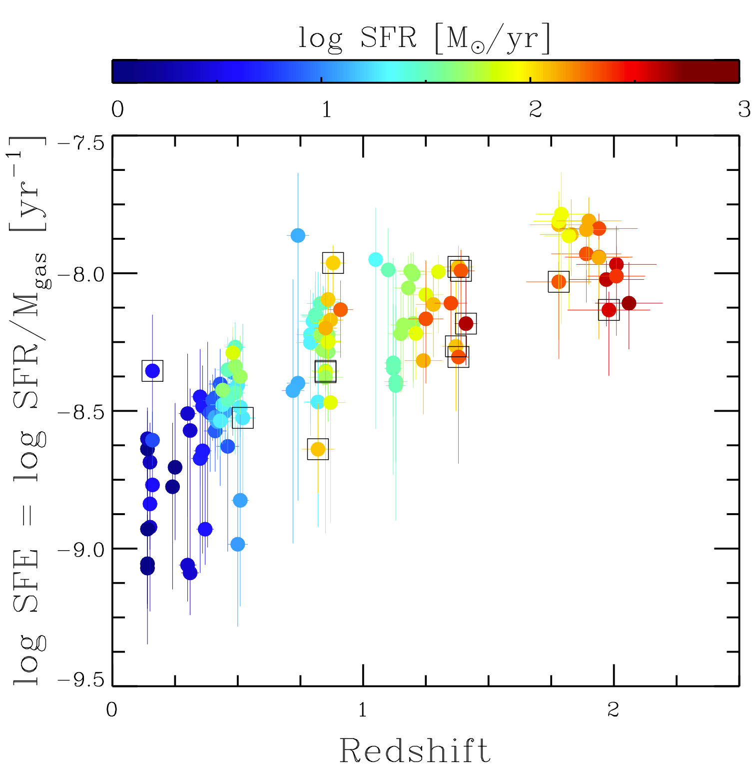

The slope of the SFR - M_{gas} relation yields the gas-to-star conversion timescale at z=2

$\tau_* = 3\ 10^7 - 2\ 10^8$ yrs

To connect M_{1500} to DM mass M

1) UV luminosity is directly linked to SFR

$\log SFR = -0.4(M_{UV} + 18.6 - 9.97\ E_{B-V})\ M_\odot/yr$

2) $SFR = M_{gas}/\tau_*$

Constraining m_X through ultra-deep LF of lensed galaxies

To connect M_{1500} to DM mass M

1) UV luminosity is directly linked to SFR
   $\log SFR = -0.4(M_{UV} + 18.6 - 9.97\, E_{B-V})\ M_\odot/yr$

2) $SFR = M_{gas}/\tau_*$

3) $\log M/M_\odot = -0.4(M_{UV} + 18.6) + 8 - \eta$

4) $\eta = \frac{M_*}{M} \frac{M_{gas}}{M_*} \frac{10^8\,yrs}{\tau_*}$

$\eta \rightarrow$ efficiency of SF for give DM mass (L/M ratios)

Constraining m_X through ultra-deep LF of lensed galaxies

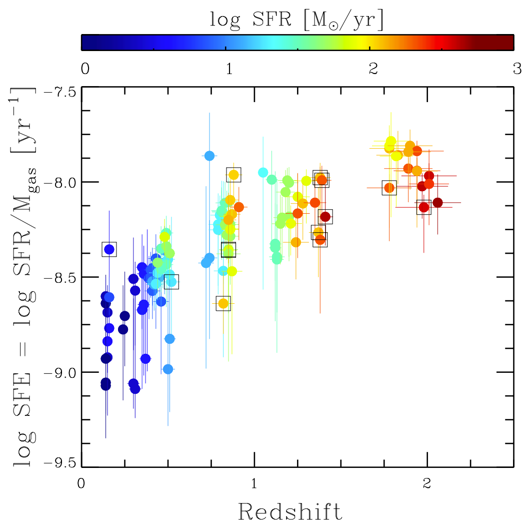

conversion timescale at z=2

$\tau_* = 3\ 10^7 - 2\ 10^8$ yrs

Daddi 2010; Santini et al. 2014;

To connect M_{1500} to DM mass M

1) UV luminosity is directly linked to SFR

$\log SFR = -0.4(M_{UV} + 18.6 - 9.97\ E_{B-V})\ M_\odot/yr$

2) $SFR = M_{gas}/\tau_*$

3) $\log M/M_\odot = -0.4(M_{UV} + 18.6) + 8 - \eta$

4) $\eta = \frac{M_*}{M} \frac{M_{gas}}{M_*} \frac{10^8\ yrs}{\tau_*}$

Constraining m_X through ultra-deep LF of lensed galaxies

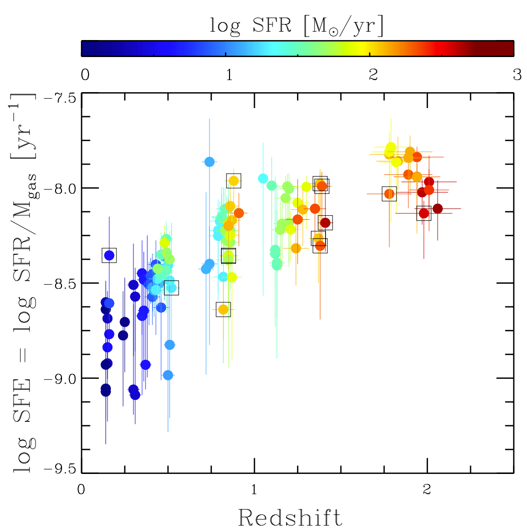

conversion timescale at z=2

$\tau_* = 3\ 10^7 - 2\ 10^8$ yrs

Daddi 2010; Santini et al. 2014;

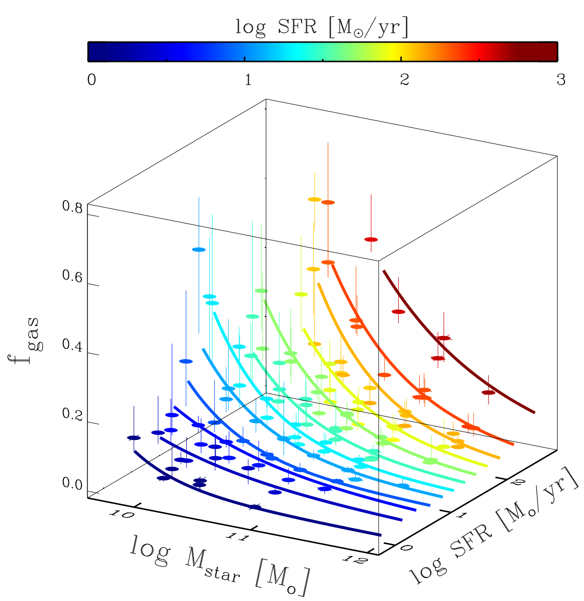

For Dwarf galaxies

fgas=0.2-0.6

Tacconi et al. 2013; Conselicei et al. 20143; Santini et al. 2014; Silverman et al. 2015

To connect M_{1500} to DM mass M

1) UV luminosity is directly linked to SFR

$\log SFR = -0.4(M_{UV} + 18.6 - 9.97\ E_{B-V})\ M_\odot/yr$

2) $SFR = M_{gas}/\tau_*$

3) $\log M/M_\odot = -0.4(M_{UV} + 18.6) + 8 - \eta$

4) $\eta = \frac{M_*}{M} \frac{M_{gas}}{M_*} \frac{10^8\ yrs}{\tau_*}$

Constraining mx through ultra-deep LF of lensed galaxies

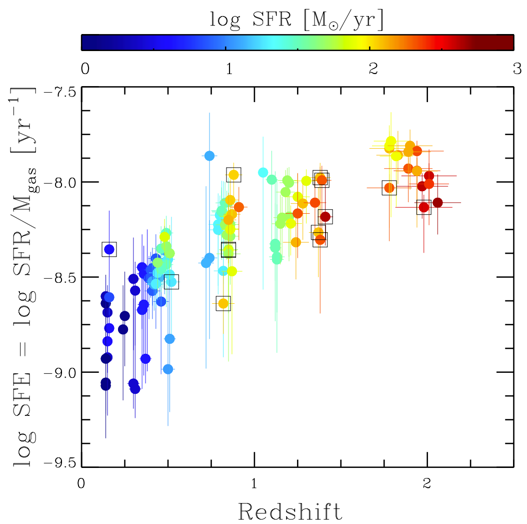

conversion timescale at z=2

$\tau_* = 3\ 10^7 - 2\ 10^8$ yrs

Daddi 2010; Santini et al. 2014;

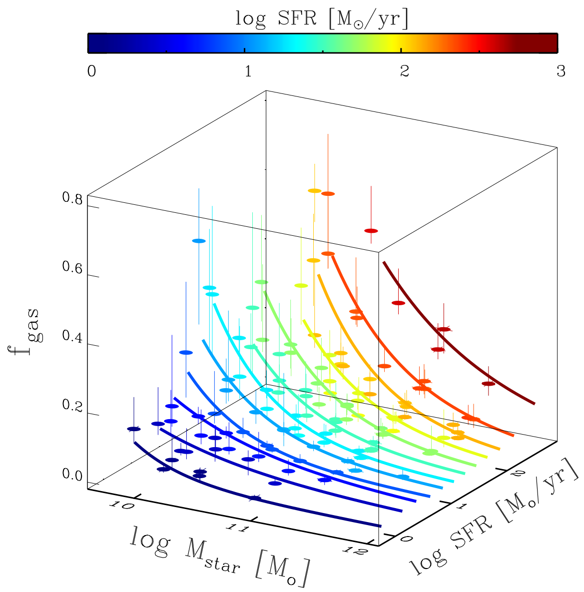

For Dwarf galaxies

fgas=0.2-0.6

Tacconi et al. 2013; Conselicei et al. 20143; Santini et al. 2014; Silverman et al. 2015

To connect M_{1500} to DM mass M

1) UV luminosity is directly linked to SFR

$\log SFR = -0.4(M_{UV} + 18.6 - 9.97\ E_{B-V})\ M_\odot/yr$

2) $SFR = M_{gas}/\tau_*$

3) $\log M/M_\odot = -0.4(M_{UV} + 18.6) + 8 - \eta$

4) $\eta = \dfrac{M_*}{M}\ \dfrac{M_{gas}}{M_*}\ \dfrac{10^8\ yrs}{\tau_*}$

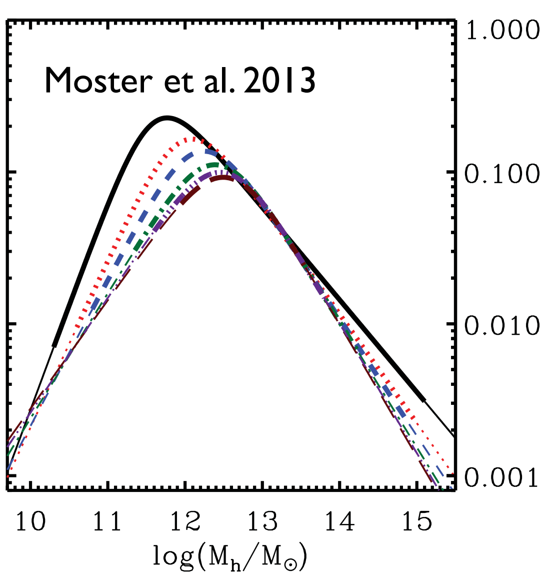

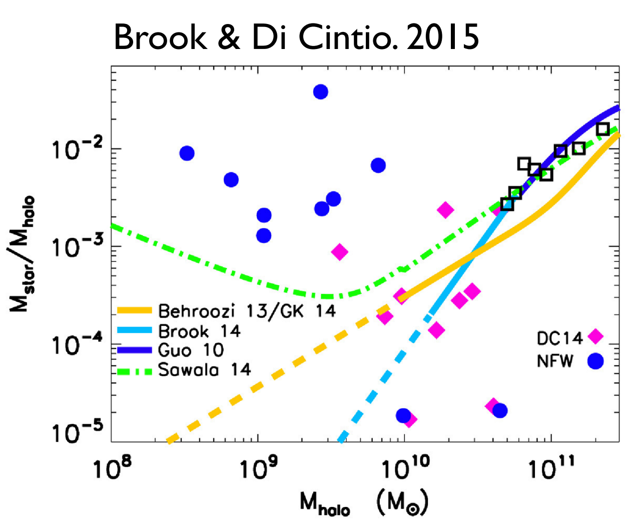

log M*/M range from

-3.5 (inefficient SF)

to

-1.5 (very efficient SF)

Constraining mx through ultra-deep LF of lensed galaxies

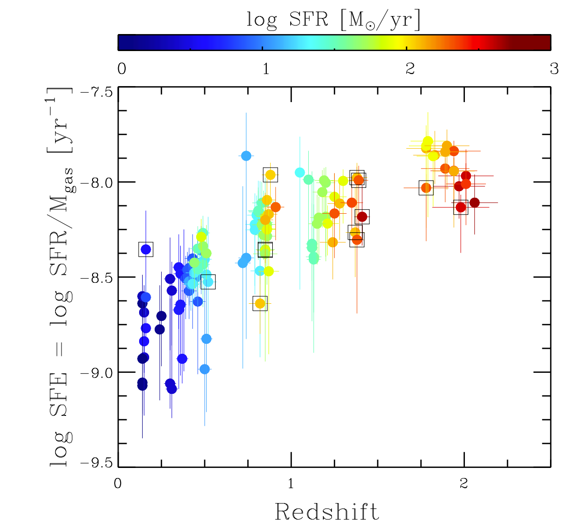

conversion timescale at z=2

$\tau_* = 3\ 10^7 - 2\ 10^8$ yrs

Daddi 2010; Santini et al. 2014;

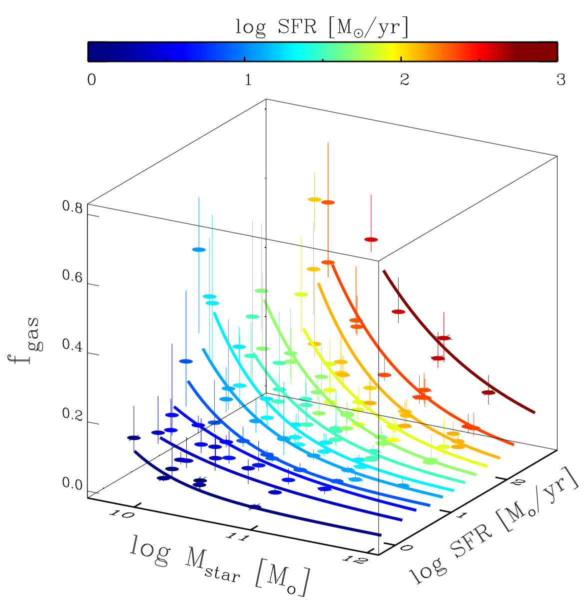

For Dwarf galaxies

fgas=0.2-0.6

Tacconi et al. 2013; Conselicei et al. 20143; Santini et al. 2014; Silverman et al. 2015

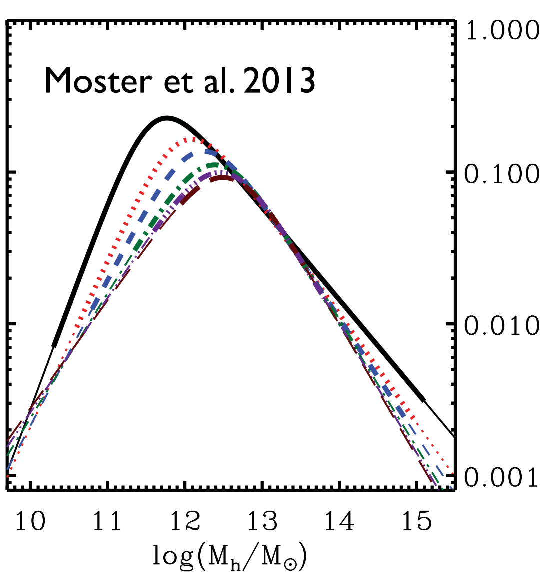

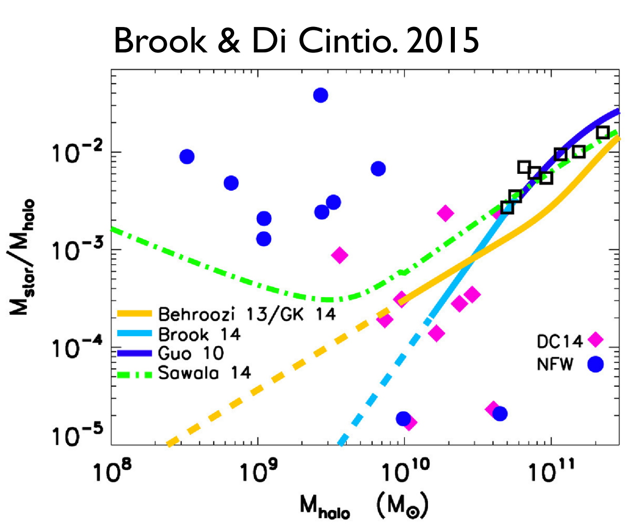

To connect M_{1500} to DM mass M

1) UV luminosity is directly linked to SFR

$\log SFR = -0.4(M_{UV} + 18.6 - 9.97\ E_{B-V})\ M_\odot/yr$

2) $SFR = M_{gas}/\tau_*$

3) $\log M/M_\odot = -0.4(M_{UV} + 18.6) + 8 - \eta$

4) $\eta = \dfrac{M_*}{M}\ \dfrac{M_{gas}}{M_*}\ \dfrac{10^8\ yrs}{\tau_*}$

5) we consider the whole range

$\log \eta = -3.8 - 1.2$

log M*/M range from

-3.5 (inefficient SF)

to

-1.5 (very efficient SF)

Constraining m_X through ultra-deep LF of lensed galaxies

NM, Sanchez, Castellano, Grazian 2015

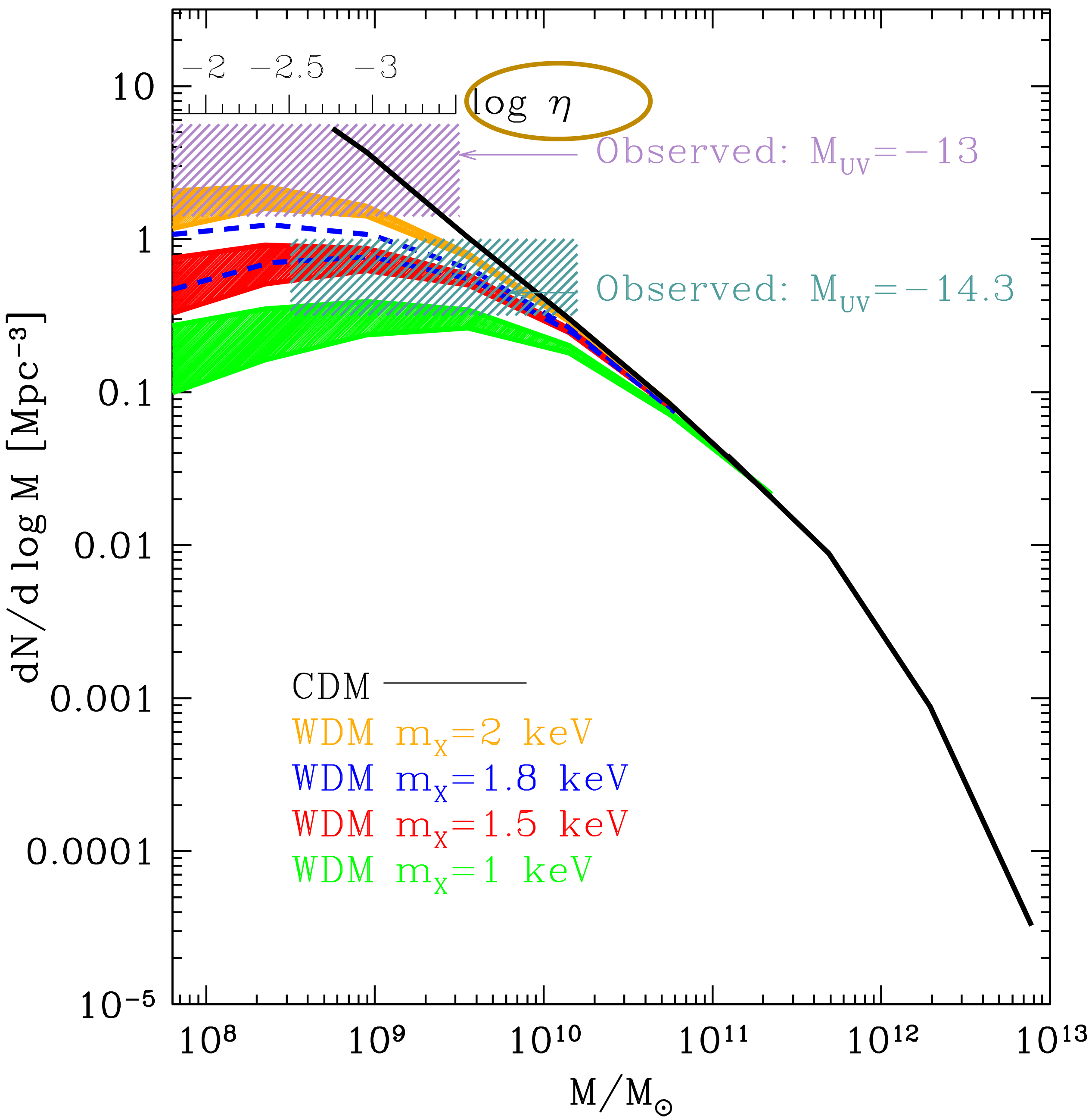

To connect M_{1500} to DM mass M

1) UV luminosity is directly linked to SFR
$\log SFR=-0.4(M_{UV}+18.6-9.97\ E_{B-V})\ M_\odot/yr$

2) $SFR=M_{gas}/\tau_*$

3) $\log M/M_\odot = -0.4(M_{UV}+18.6) + 8 - \eta$

4) $\eta = \frac{M_*}{M}\ \frac{M_{gas}}{M_*}\ \frac{10^8\ yrs}{\tau_*}$

5) we consider the whole range
$\log \eta = -3.8 - 1.2$

All uncertainties due to baryonic physics are parametrized by η
robust constraints

Constraining m_X through ultra-deep LF of lensed galaxies

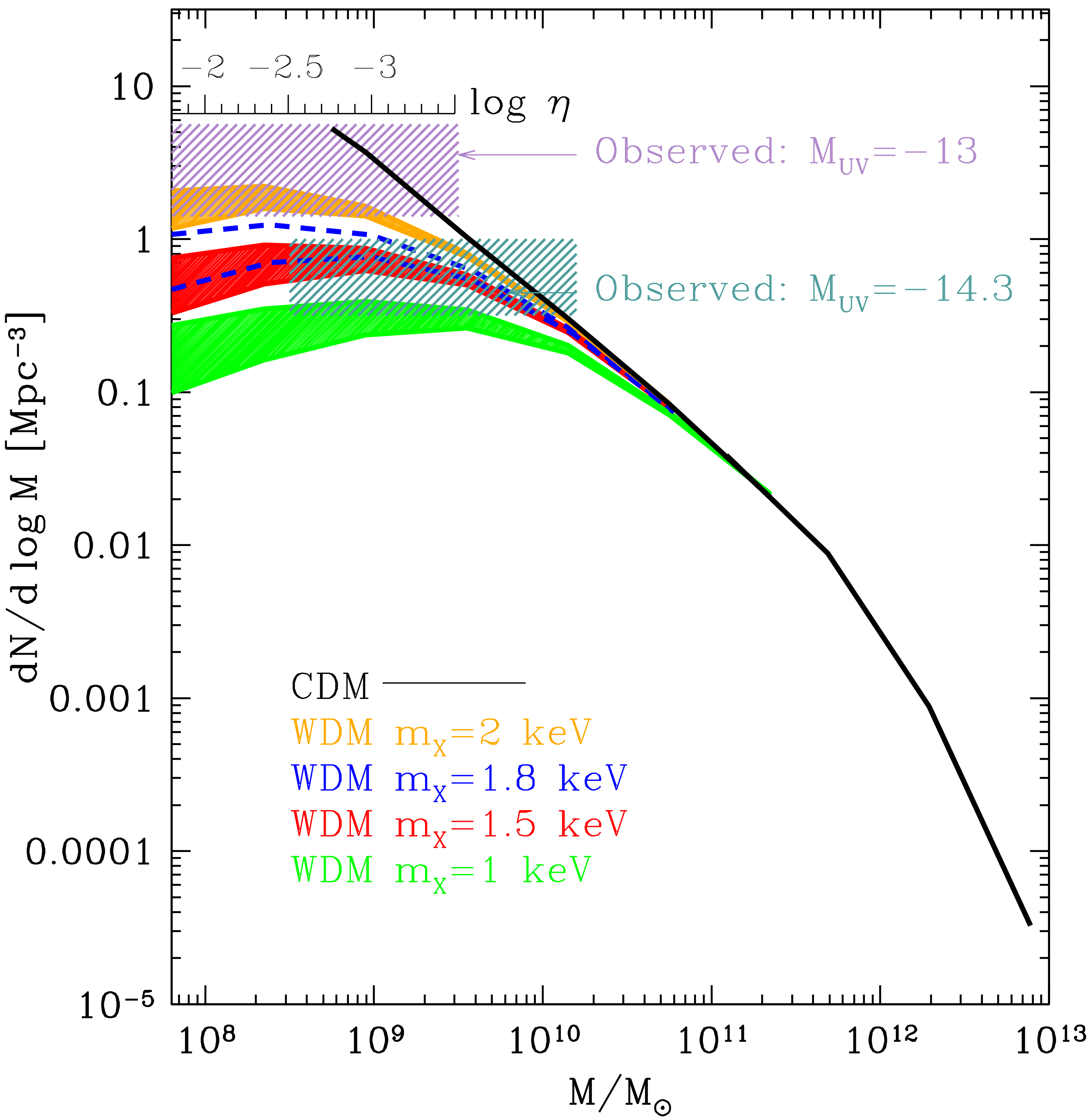

m_X>1.8 keV (thermal relic mass)

lower m_X do not provide the observed abundance. Note: baryonic processes can make the LF flatter but not steeper !

The result is robust with respect to

The effect of baryonic processes included in η. Observations probe the mass function in the mass range around the half-mode mass where the DM mass functions are characterized by a maximum value.

The modeling of residual DM dispersion velocities. Their would yield a sharper decrease of the mass function at small masses (see, e.g., Benson et al. 2013), thus yielding tighter constraints.

The kind of DM clumps hosting the UV emitting galaxies. In fact, the upper boundaries of the solid filled regions correspond to predictions including also proto-halos.

The possible effects of UV background and reionization. Such effects would further suppress the abundance of galaxies in low-mass halos (Sawala et al. 2015).

CDM requires low η
i.e., low star formation efficiency.
Compares critically with
observed M*-Mhalo relations

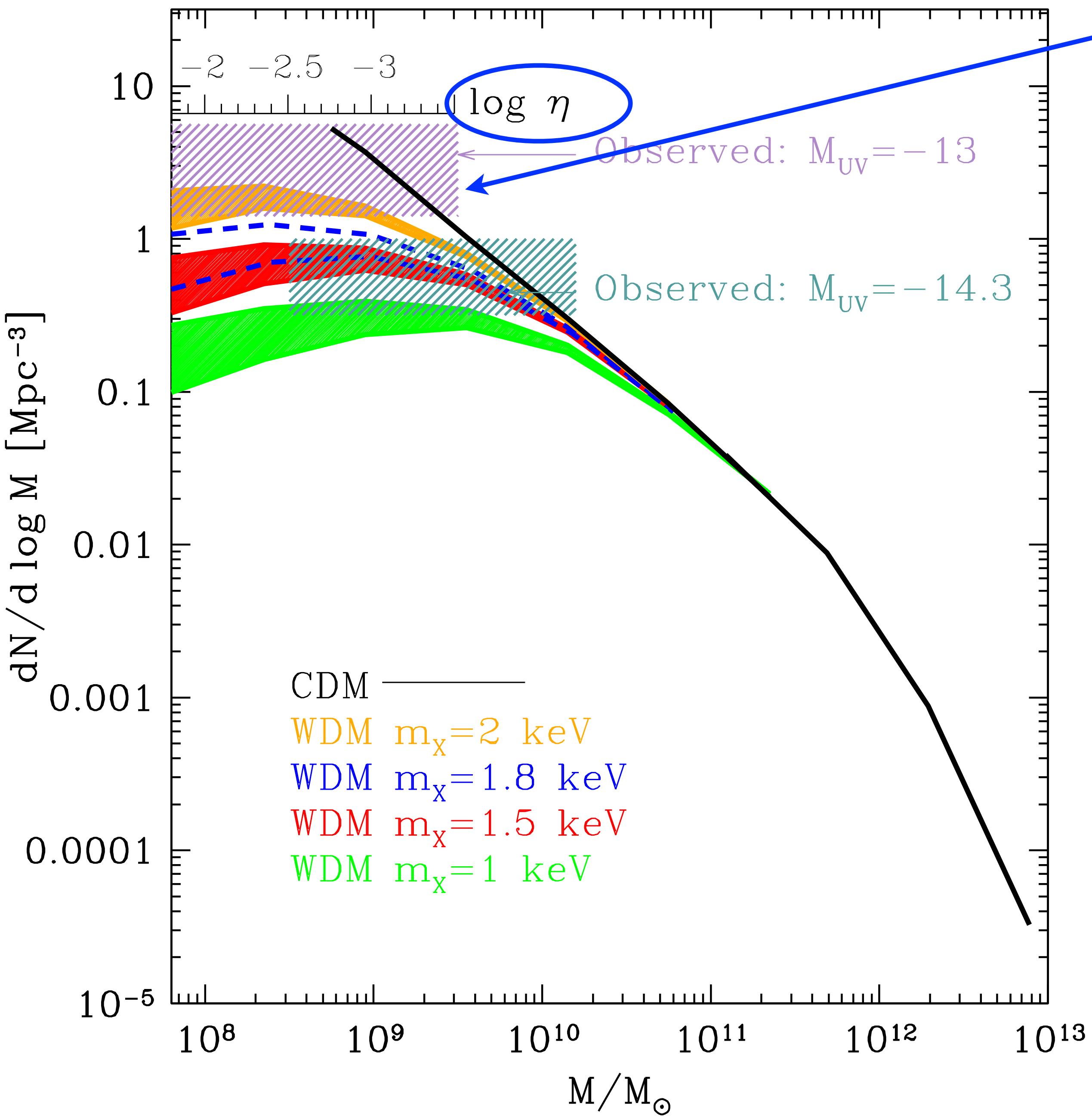

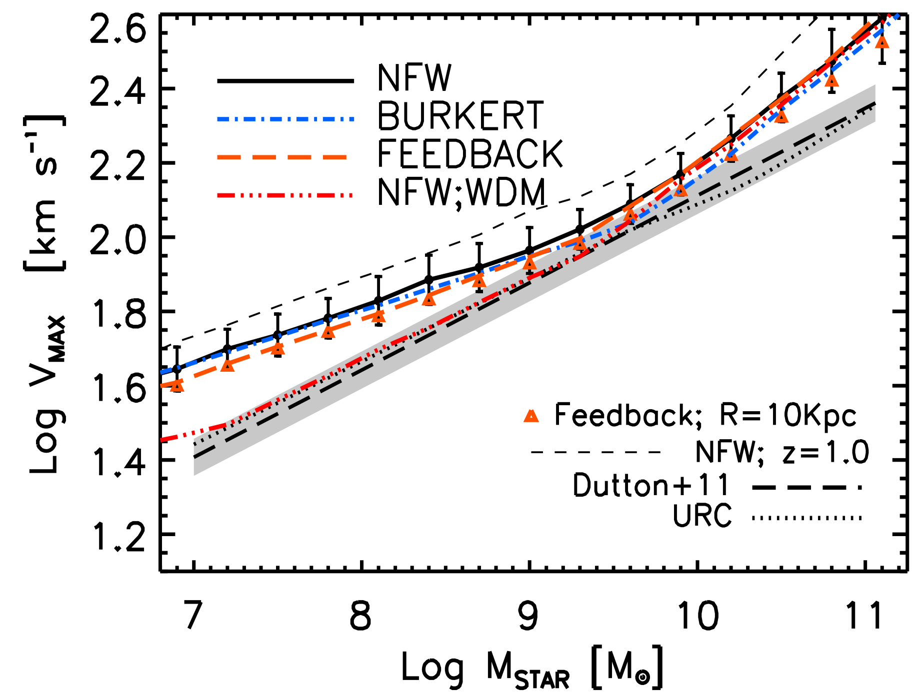

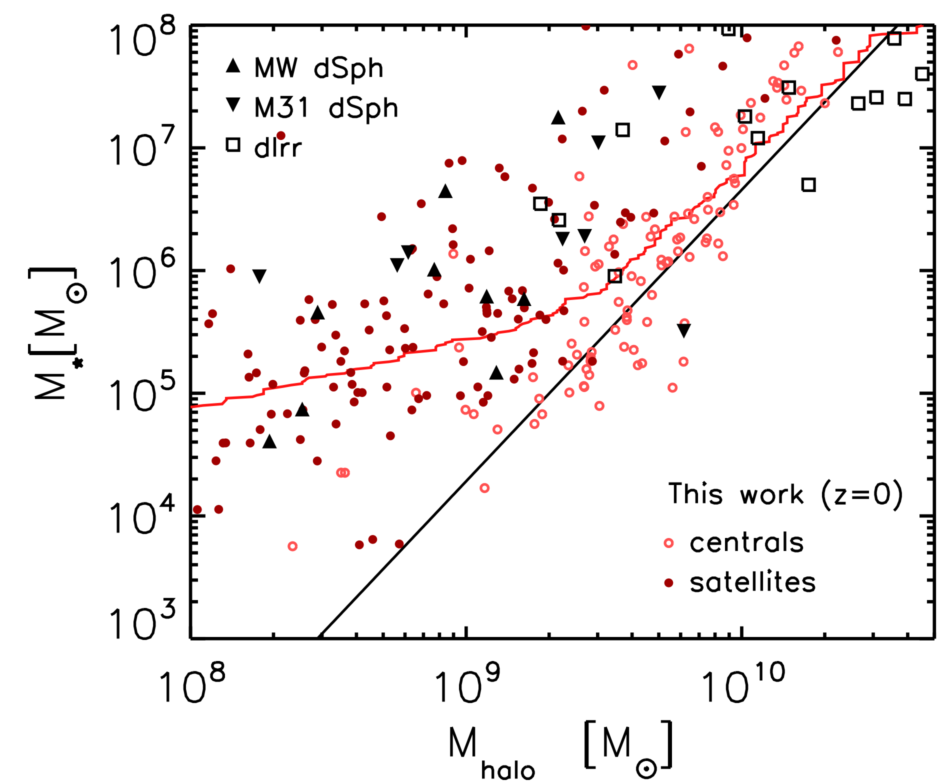

Constraining the m_X mass through the abundance of galaxies with M_{UV}=-13 at z=2-4

The Frontier Fields Goals

Using Director's Discretionary (DD) observing time, HST is undertaking a revolutionary deep field observing program to peer deeper into the Universe than ever before and provide a first glimpse of JWST's universe.

These Frontier Fields will combine the power of HST with the natural gravitational telescopes of high-magnification clusters of galaxies. Using both the Wide Field Camera 3 and Advanced Camera for Surveys in parallel, HST will produce the deepest observations of clusters and their lensed galaxies ever obtained, and the second-deepest observations of blank fields (located near the clusters). These images will reveal distant galaxy populations ~10-100 times fainter than any previously observed, improve our statistical understanding of galaxies during the epoch of reionization, and provide unprecedented measurements of the dark matter within massive clusters.

This program is based upon the 2012 recommendations from the Hubble Deep Fields Initiative Science Working group: SWG Report 2012

Six Frontier Fields

Cluster Name	z	Cluster		Parallel Field	
		RA	Dec	RA	Dec
Year 1:					
Abell 2744	0.308	00:14:21.2	-30:23:50.1	00:13:53.6	-30:22:54.3
MACSJ0416.1-2403	0.396	04:16:08.9	-24:04:28.7	04:16:33.1	-24:06:48.7
Year 2:					
MACSJ0717.5+3745	0.545	07:17:34.0	+37:44:49.0	07:17:17.0	+37:49:47.3
MACSJ1149.5+2223	0.543	11:49:36.3	+22:23:58.1	11:49:40.5	+22:18:02.3
Year 3:					
Abell S1063 (RXCJ2248.7-4431)	0.348	22:48:44.4	-44:31:48.5	22:49:17.7	-44:32:43.8
Abell 370	0.375	02:39:52.9	-01:34:36.5	02:40:13.4	-01:37:32.8

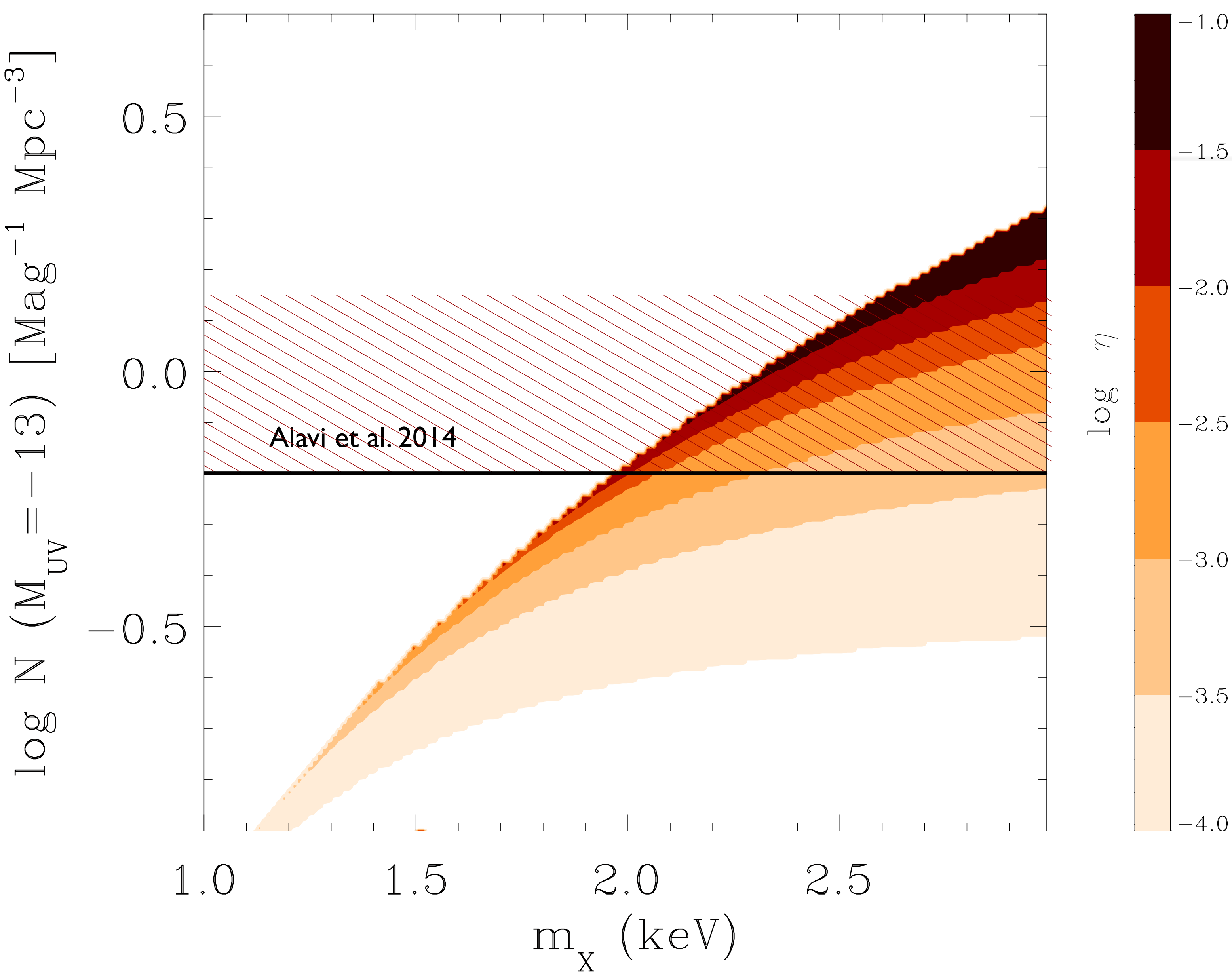

in the limit m_X>>1 keV (CDM) small star formation efficiencies η~-3 are required to match the observed abundance of galaxies with M_{UV}=-13

for m_X~2.5 keV (corresponding to sterile neutrino masses $m_{sterile}$~7 keV) a wide range of -2.5< η < -1.5 is consistent with the observed abundance of galaxies with M_{UV}=-13

LSB galaxies in Virgo (Giallongo et al. 2015)

TABLE 1
LSB CATALOG IN THE VIRGO-XMMUJ1230 FIELD

ID	LSB Label	RA	DEC	R	μ_0	n^a	M_R^b	r^c (arcsec)	r (pc)^c	b/a	$R-Z$
6490	A	187.3919684	+13.7704609	21.86	24.91	0.92	-9.24	3.07	246	0.7	0.00
6043	B	187.6635951	+13.7391869	20.38	24.54	0.70	-10.79	4.48	359	0.7	0.31
5833	C	187.5879561	+13.7058350	21.59	26.23	0.55	-9.56	4.37	350	0.9	-0.23
5143	D	187.5483601	+13.6914967	18.30	24.01	0.67	-12.87	7.99	639	0.9	0.44
4739	E	187.3814266	+13.6619273	18.75	23.49	0.72	-12.42	5.71	457	0.7	0.35
4367	F	187.3863203	+13.6222745	21.93	24.54	0.88	-9.25	2.73	218	0.6	0.20
3516	G	187.6600347	+13.6196001	18.05	24.25	0.62	-13.12	10.43	835	0.7	0.11
3214	H	187.6224577	+13.5565951	21.14	25.11	0.57	-10.03	3.14	251	0.9	0.39
2245	J	187.4138959	+13.5075398	21.24	25.53	0.69	-9.93	4.19	335	0.8	0.11
2001	K	187.7070994	+13.5053537	19.07	25.79	0.44	-12.11	10.68	855	0.9	-0.30
2003	L	187.7244716	+13.4939191	21.89	26.12	0.30	-9.28	3.05	244	0.9	0.02

[a] Sérsic index
[b] Absloute magnitudes computed adopting an average distance modulus for Virgo $\Delta M = 31.1$ (Mei et al. (2007)), an average galactic absorption of -0.07.
[c] Scale radius from the Sersic profile fitting. An angular scale of 80 pc arcsec^{-1} has been adopted.

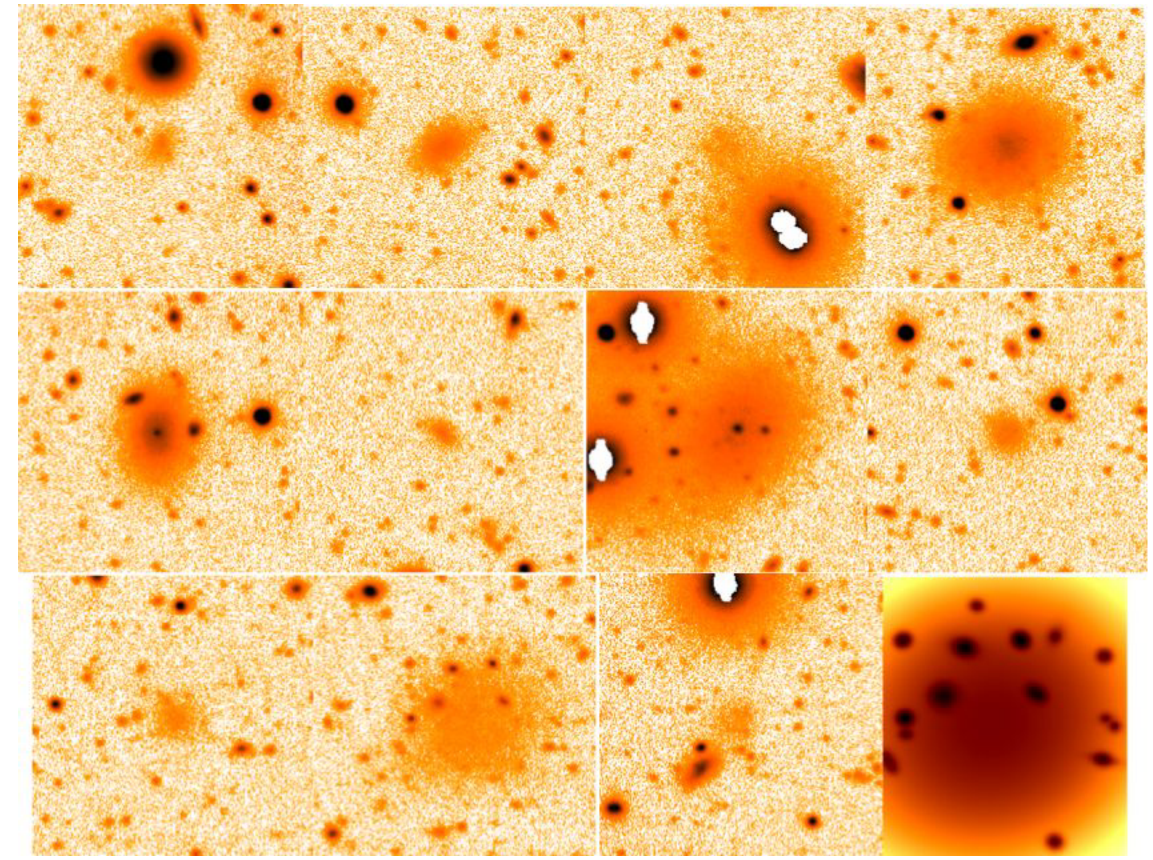

FIG. 2.— Selected LSB dwarfs in the Virgo-xmmuj1230 field; the box size of each image is $\simeq 57$ arcsec. The sequence from the t the bottom follows the list in Table 1. The last box on the bottom right show a zoomed image of the Galfit best fit model of the LS "K". All the small background sources expected within the LSB halo have been fitted separately.

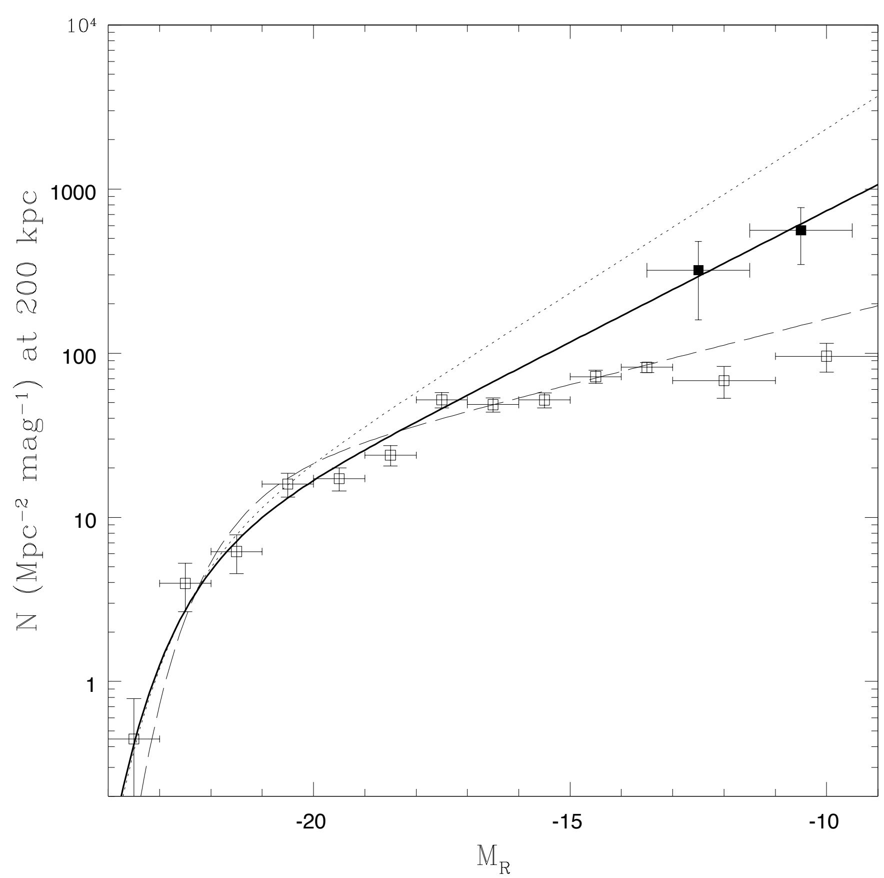

FIG. 3.— Virgo projected luminosity function normalized at 200 kpc. Filled squares are from the present sample after conversion from AB to the Vega magnitude system by $R(Vega) - R(AB) = -0.26$. Empty squares are from Trentham & Tully (2002) in the Vega system. The continuous curve represents a Schechter shape with slope $\alpha \sim -1.4$ and $M^* \sim -22.3$. Two faint slopes $\alpha \sim -1.2, -1.5$ are also shown for comparison (dashed and dotted, respectively).

Steep LF N(L) ~ L$^{-1.4}$

Compute sub-haloes mass function N(M)~M$^{-\alpha dm}$
measure α_{DM} for different WDM mass

$\propto$

Compute N(L) for different L/M ratios
i.e., reasonable values of β (assuming L~M$^{\beta}$)

Compare with observed slope

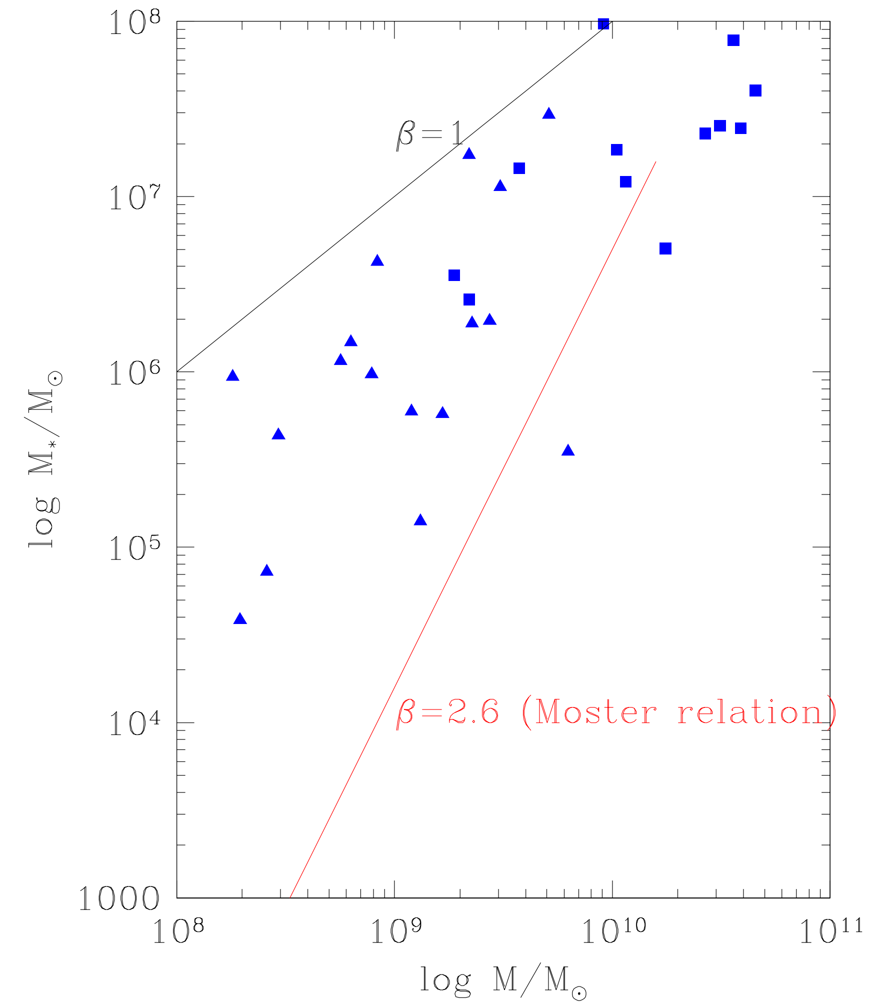

$$L \propto M^{\beta}$$

$$L/M \propto M^{\beta-1}$$

$$N(M) \propto M^{-\alpha_{dm}} \rightarrow N(L) \propto L^{-\alpha}$$

$$\alpha = \frac{1-\alpha_{DM}-\beta}{\beta}$$

E.g. α=2, β=1 $\longrightarrow$ $N(L) \propto L^{-3/2}$

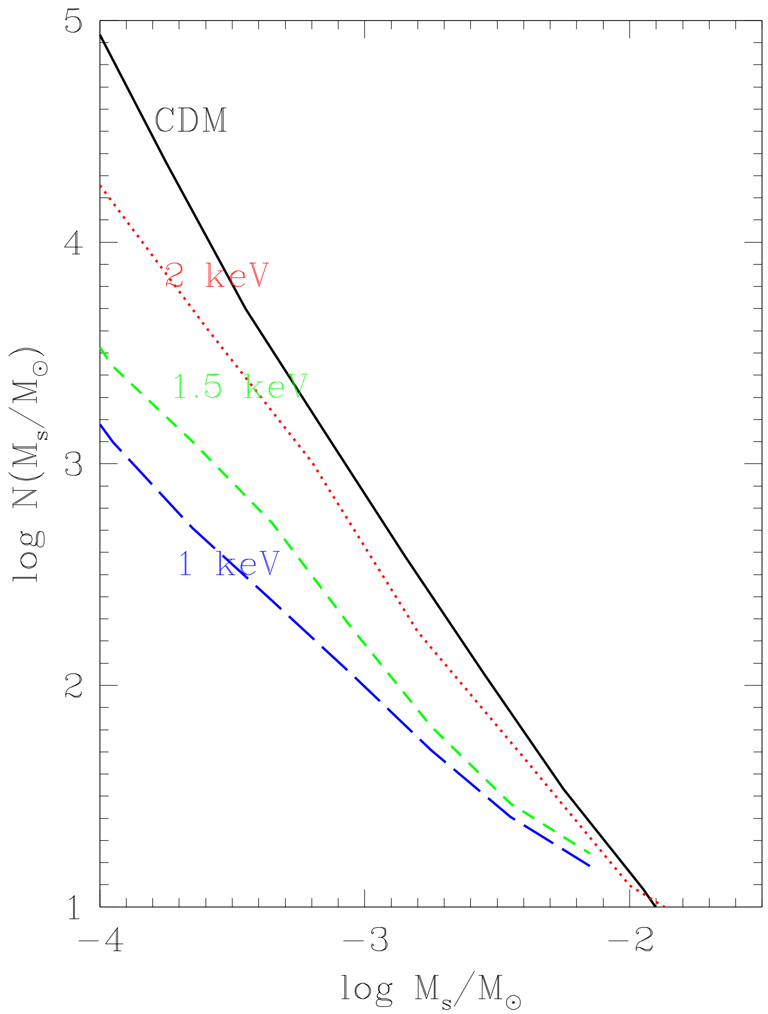

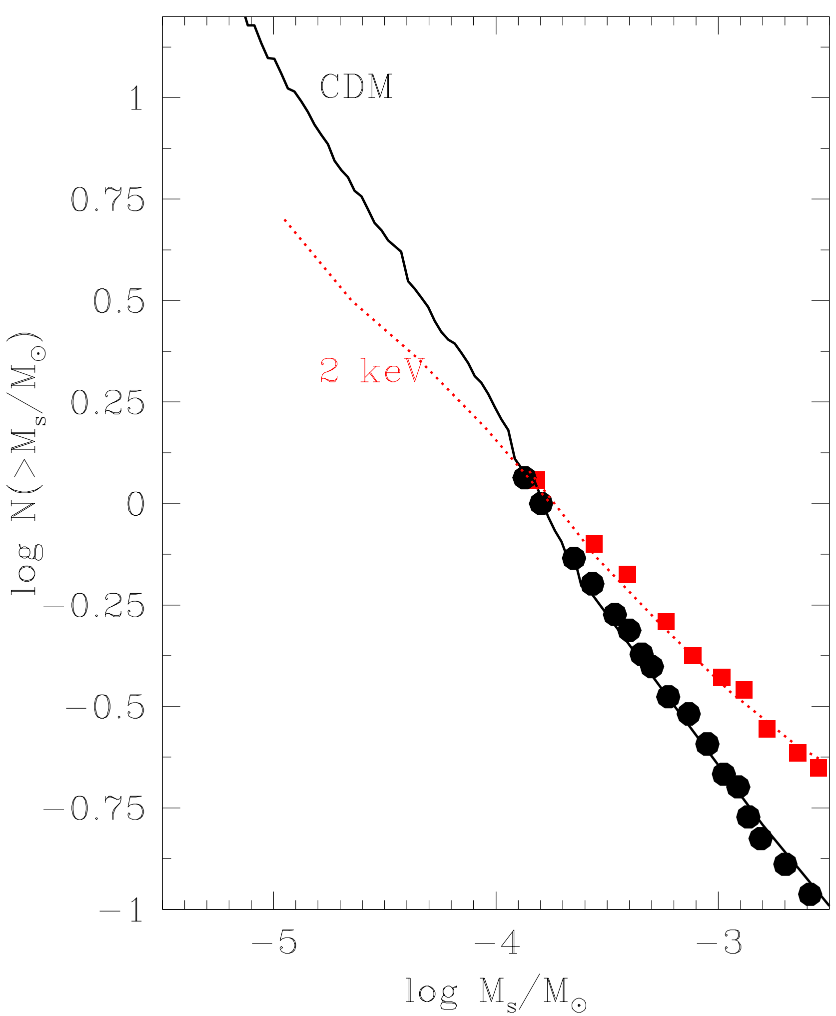

$\alpha(m_{X=}1\ \text{keV})=1.2$

$\alpha(m_{X=}1.5\ \text{keV})=1.4$

$\alpha(m_{X=}2\ \text{keV})=1.6$

αCDM=1.8

In the CDM and
m_X=2keV case
we can test the results
against N-body results
(but extend to much
smaller satellite masses)

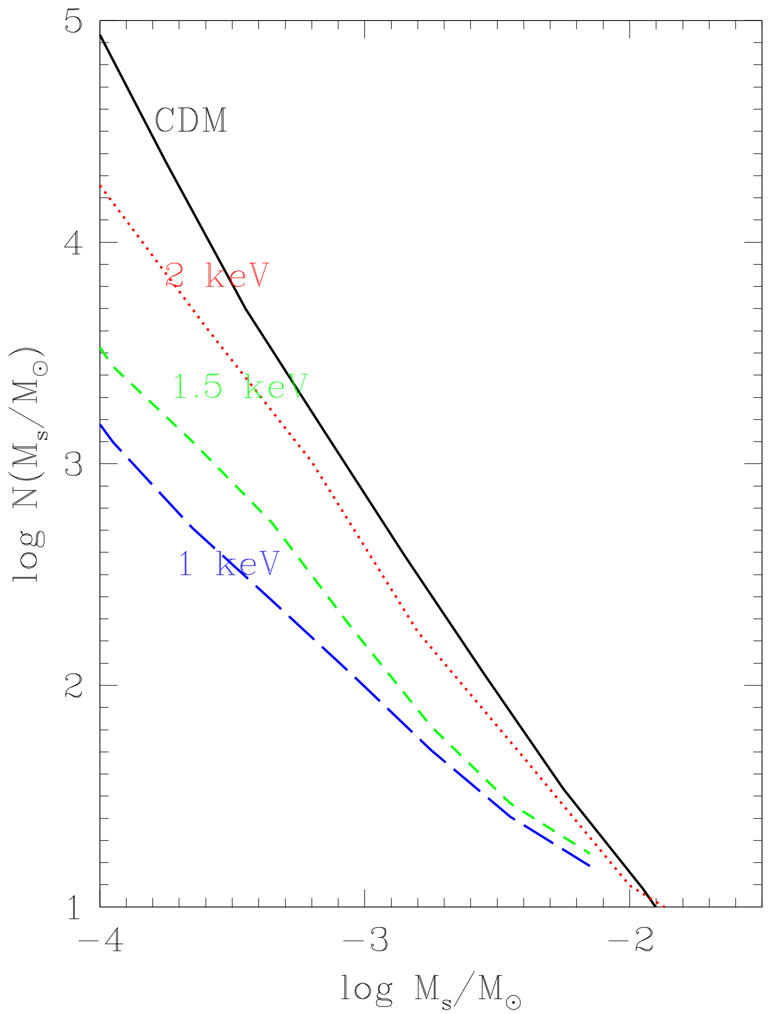

$\alpha(m_{X=}1\ \text{keV})=1.2$

$\alpha(m_{X=}1.5\ \text{keV})=1.4$

$\alpha(m_{X=}2\ \text{keV})=1.6$

$\alpha\text{CDM}=1.8$

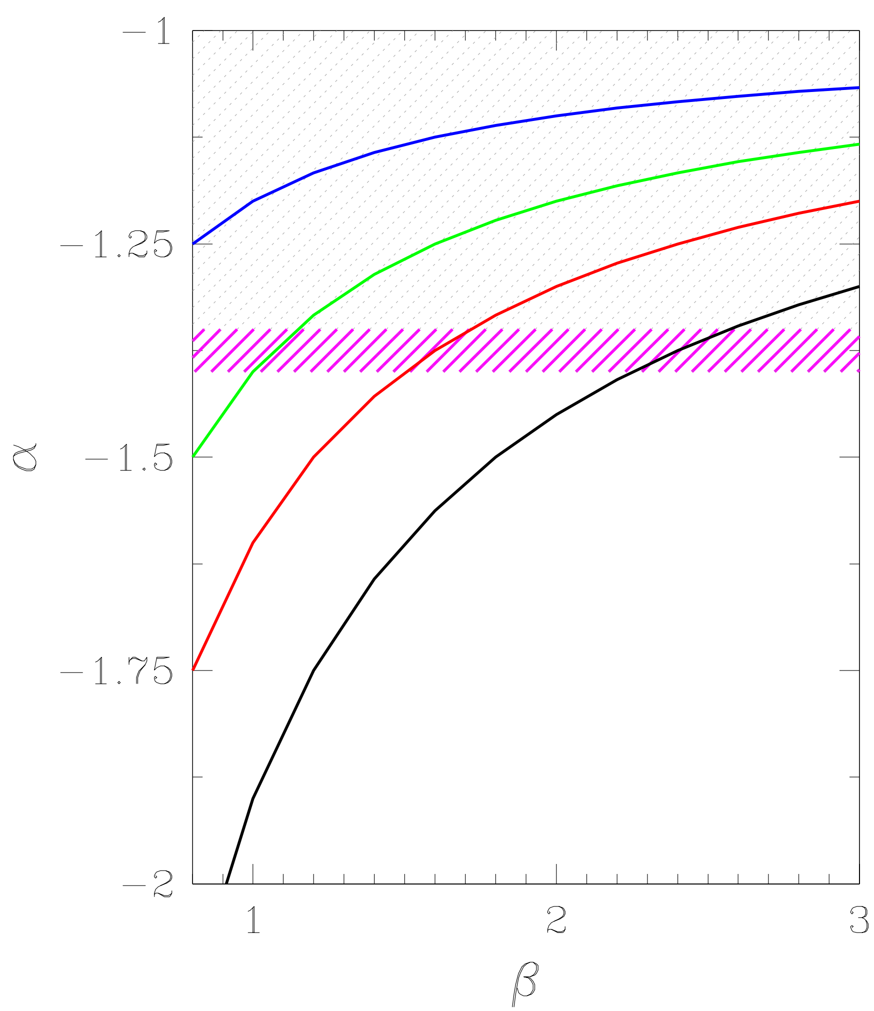

slope of N(L) is too flat in the $m_{X=}1$ kev and $m_{X=}1.5$ keV cases for any $1<\beta<3$

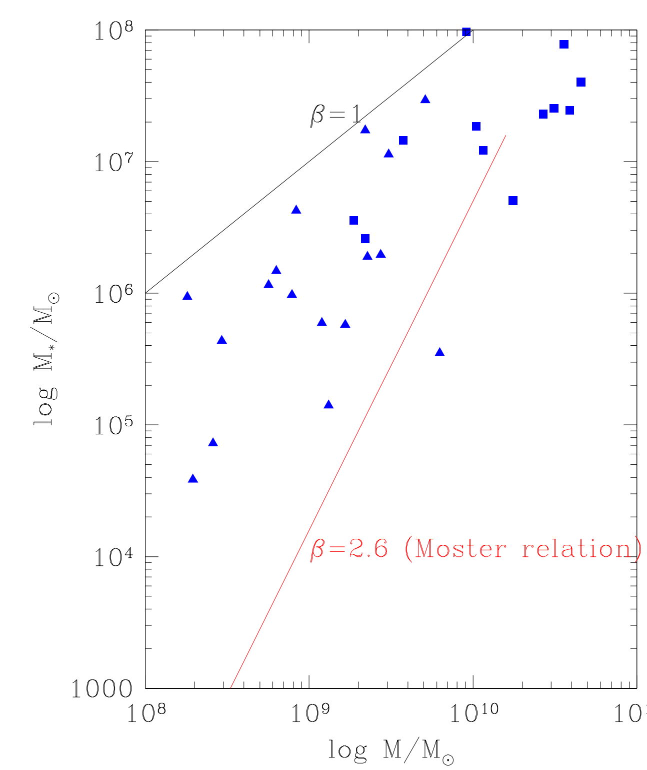

CDM would require $\beta \sim 2.5$ unfavoured by data

Conclusions

WDM galaxy formation models provides a solution to several critical issues:
- density profiles (also at high-z)
- abundance of low-mass/low-luminosity galaxies even at $z \gtrsim 2$
- luminosity function of AGNs (low-luminosity $L < 10^{43}$ erg) at $z \gtrsim 2$
- luminosity function of satellites (large surveys)
- M_*-M_h relation
- Satellite colors (i.e., star formation histories of low-mass galaxies)

Constraints on WDM particle mass
- From MW satellites (but subject to halo-to-halo variance)
- From galaxy luminosity functions/counts
  a) high-redshift (but present observations still not deep enough: constrain $m_X > 1$ keV
  b) lower redshift, ultra-deep (down to $M_{UV} \approx -10$) UV luminosity function $m_X > 1.8$ keV

Summary

The mass of DM particles has a major impact on galaxy formation
(suppression of small-scale perturbations due to free-streaming)
CDM is the limit of M_{fs}<< masses of cosmological interest

CDM problems on small scales:

- cusps + number of satellite galaxies
- abundance of low-mass (faint) galaxies at low and high redhsifts
- fraction of quiescent satellites
- V_{max}-M_* relation

Baryonic physics can hardly solve all the problems

Galaxy formation in WDM cosmology is a viable solution
if the spectrum is like that corresponding to a thermal relic DM with $m \lessapprox 2$ keV
(analogous to that corresponding to sterile neutrino produced according to
Dodelson & Widrow with m_ν<8 keV)

There is a tension with current limits from high-z structure (Lyman-a forest)

Summary

The mass of DM particles has a major impact on galaxy formation
(suppression of small-scale perturbations due to free-streaming)
CDM is the limit of $M_{fs} <<$ masses of cosmological interest

CDM problems on small scales:
- cusps + number of satellite galaxies
- abundance of low-mass (faint) galaxies at low and high redhsifts
- fraction of quiescent satellites
- V_{max}-M_* relation

Baryonic physics can hardly solve all the problems

Galaxy formation in WDM cosmology is a viable solution
if the spectrum is like that corresponding to a thermal relic DM with $m \lessapprox 2$ keV
(analogous to that corresponding to sterile neutrino produced according to Dodelson & Widrow with $m_\nu < 8$ keV)

There is a tension with current limits from high-z structure (Lyman-a forest)

Summary

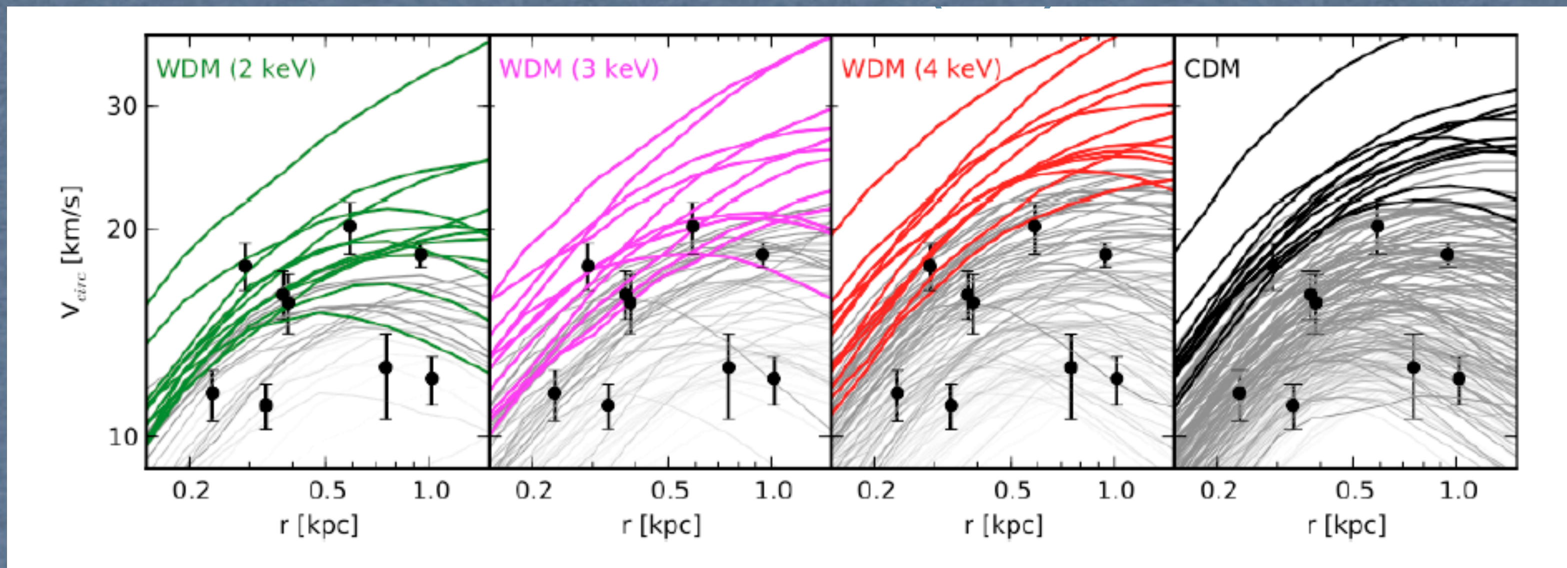

s

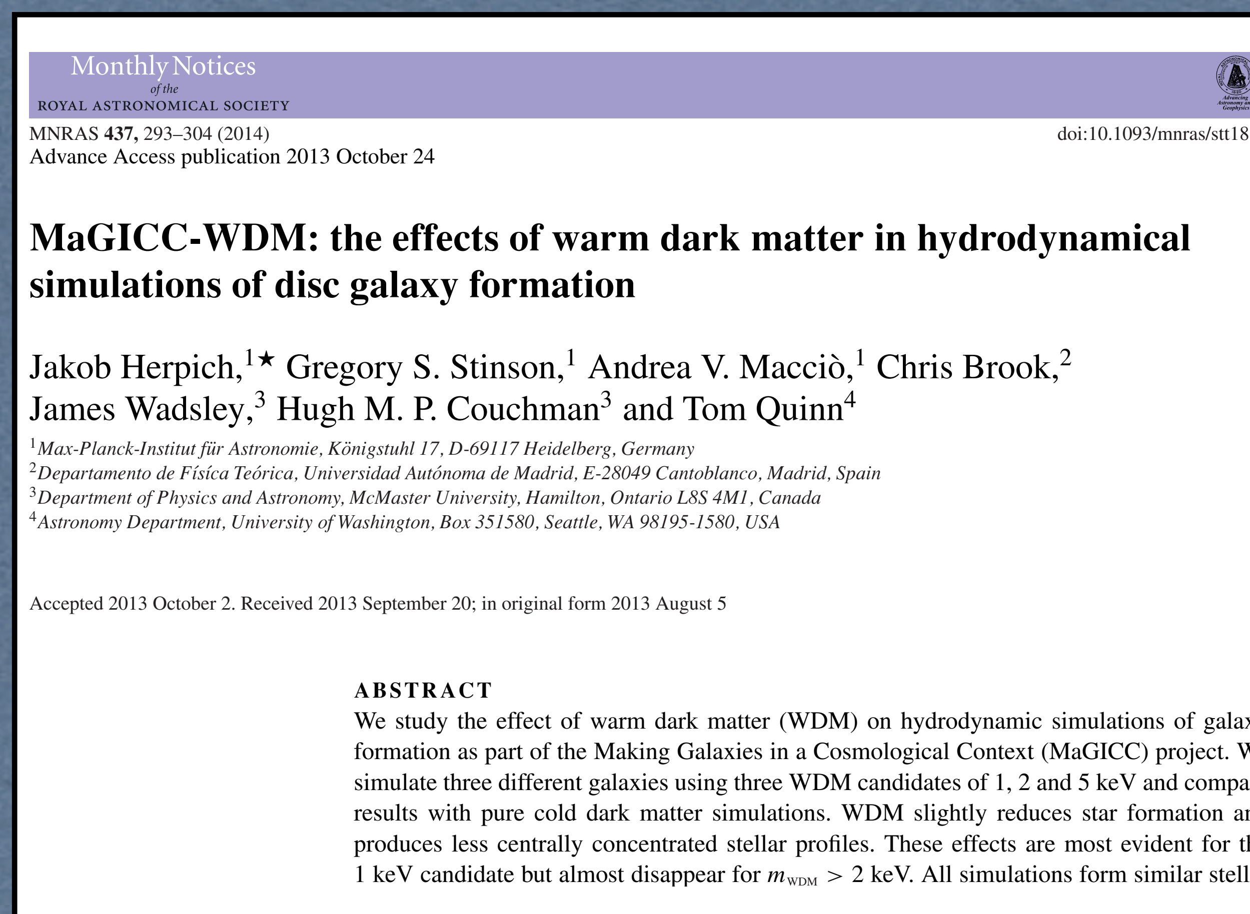

Monthly Notices of the Royal Astronomical Society
MNRAS **437**, 293–304 (2014) doi:10.1093/mnras/stt188
Advance Access publication 2013 October 24

MaGICC-WDM: the effects of warm dark matter in hydrodynamical simulations of disc galaxy formation

Jakob Herpich,[1★] Gregory S. Stinson,[1] Andrea V. Macciò,[1] Chris Brook,[2] James Wadsley,[3] Hugh M. P. Couchman[3] and Tom Quinn[4]

[1] Max-Planck-Institut für Astronomie, Königstuhl 17, D-69117 Heidelberg, Germany
[2] Departamento de Física Teórica, Universidad Autónoma de Madrid, E-28049 Cantoblanco, Madrid, Spain
[3] Department of Physics and Astronomy, McMaster University, Hamilton, Ontario L8S 4M1, Canada
[4] Astronomy Department, University of Washington, Box 351580, Seattle, WA 98195-1580, USA

Accepted 2013 October 2. Received 2013 September 20; in original form 2013 August 5

ABSTRACT
We study the effect of warm dark matter (WDM) on hydrodynamic simulations of galaxy formation as part of the Making Galaxies in a Cosmological Context (MaGICC) project. We simulate three different galaxies using three WDM candidates of 1, 2 and 5 keV and compare results with pure cold dark matter simulations. WDM slightly reduces star formation and produces less centrally concentrated stellar profiles. These effects are most evident for the 1 keV candidate but almost disappear for $m_{\rm WDM} > 2$ keV. All simulations form similar stella

ith $m \lesssim 2$ keV
ording to

n-a forest)

Summary

The mass of DM particles has a major impact on galaxy formation
(suppression of small-scale perturbations due to free-streaming)
CDM is the limit of $M_{fs} \ll$ masses of cosmological interest

CDM problems on small scales:

- cusps + number of satellite galaxies
- abundance of low-mass (faint) galaxies at low and high redhsifts
- fraction of quiescent satellites
- V_{max}-M_* relation

Baryonic physics can hardly solve all the problems

Galaxy formation in WDM cosmology is a viable solution
if the spectrum is like that corresponding to a thermal relic DM with $m \lesssim 2$ keV
(analogous to that corresponding to sterile neutrino produced according to
Dodelson & Widrow with $m_\nu < 8$ keV)

There is a tension with current limits from high-z structure (Lyman-a forest)